

Springer Earth System Sciences

Matías C. Ghiglione *Editor*

Geodynamic Evolution of the Southernmost Andes

Connections with the Scotia Arc

 Springer

Springer Earth System Sciences

Series editors

Philippe Blondel, Bath, UK

Eric Guilyardi, Paris, France

Jorge Rabassa, Ushuaia, Argentina

Clive Horwood, Chichester, UK

More information about this series at <http://www.springer.com/series/10178>

Matías C. Ghiglione
Editor

Geodynamic Evolution of the Southernmost Andes

Connections with the Scotia Arc

 Springer

Editor

Matías C. Ghiglione
National Council of Argentina (CONICET)
Universidad de Buenos Aires
Buenos Aires
Argentina

ISSN 2197-9596

Springer Earth System Sciences

ISBN 978-3-319-39725-2

DOI 10.1007/978-3-319-39727-6

ISSN 2197-960X (electronic)

ISBN 978-3-319-39727-6 (eBook)

Library of Congress Control Number: 2016941068

© Springer International Publishing Switzerland 2016

This work is subject to copyright. All rights are reserved by the Publisher, whether the whole or part of the material is concerned, specifically the rights of translation, reprinting, reuse of illustrations, recitation, broadcasting, reproduction on microfilms or in any other physical way, and transmission or information storage and retrieval, electronic adaptation, computer software, or by similar or dissimilar methodology now known or hereafter developed.

The use of general descriptive names, registered names, trademarks, service marks, etc. in this publication does not imply, even in the absence of a specific statement, that such names are exempt from the relevant protective laws and regulations and therefore free for general use.

The publisher, the authors and the editors are safe to assume that the advice and information in this book are believed to be true and accurate at the date of publication. Neither the publisher nor the authors or the editors give a warranty, express or implied, with respect to the material contained herein or for any errors or omissions that may have been made.

Printed on acid-free paper

This Springer imprint is published by Springer Nature

The registered company is Springer International Publishing AG Switzerland

Foreword

This new volume of the “Springer Earth System Science” deals with the attractive Southernmost Andes–Antarctica connection issue, which has called the attention of several generations of field geologists, geophysicists, and oceanologists. A new generation of researchers, but already experienced young scientists, is presenting the results of several years of investigation in these remote regions of very difficult access. It is interesting to compare the early work on land of Katz (1964)¹ and the studies of Dalziel et al. (1974)² in the Rocas Verdes marginal basin and the Scotia Arc, to see how much we have advanced in the knowledge and the timing of the tectonic processes. This book will be a milestone for understanding the new connections of the Patagonian–Fuegian Andes with the Scotia Arc and related areas.

Special attention should be paid to the work of Matías C. Ghiglione and coworkers, who is based on an extensive and detailed fieldwork. His research started in the Tierra del Fuego Island during his Ph.D. thesis (1999–2003), to continue in the Patagonian Andes of Argentina and Chile over the last years. As a result of this extensive fieldwork, together with available industrial seismic lines, he has proposed new details and processes on the geodynamic evolution of the southernmost Andes and its relation with subsidence and sedimentation in the Argentine continental margin.

The progress in the knowledge of the metamorphic conditions (pressure, temperature, and timing), the geochemical characteristics, and age of the metamorphic complexes is another piece of new data that allow setting thoughtful paleogeographic schemes for the Paleozoic and Mesozoic evolutions. Calderon and coworkers present new solid hypotheses, which will deserve further research and consideration.

¹Katz HR (1964) Some new concepts on geosynclinal development and mountain building at the southern end of South America. XXII Intern Geol Congr, India, Proceedings 4:242–255.

²Dalziel IWD, De Wit MF, Palmer KF (1974) Fossil marginal basin in the southern Andes. *Nature* 250:291–294.

Most of the Andes have evidence in recent years of important variations in the present and old subduction geometries of the Benioff zones. The Southernmost Andes is not an exception, and the data presented by González Guillot show firm evidence of these variations based on petrological and spatial changes in the magmatic front through time.

The review of the Scotia arc development, at different time windows, and their connections with the Patagonian–Fuegian Andes through time, profits of the comprehensive experience of Graeme Eagles on this subject. The different schemes of Eagles show didactically and rigorously fine details on the processes involved in this complex evolution.

Seismicity in the southernmost South America and its complex relation with the geodynamic context of the Scotia Arc is an important but little understood topic. Sue and Ghiglione undertake this subject from the view of brittle deformation, fault kinematics, and related seismicity, to elucidate deformation pattern in the southernmost Andes and surrounding southern oceans.

The analysis of the Patagonian Orocline, a classic problem of the last 50 years in the Southernmost Andes since the early proposal of Warren Carey, clearly shows that the continental margin bend is not a proper orocline. Several paleomagnetic studies have shown the complexity of this evolution and how rotations vary on time and space through the orogen. The proposal of Marco Maffione, based on the new and old paleomagnetic and structural data, for changing the Patagonian Orocline to a Patagonian Arc, deserves attention. This is not just a change in the denomination, if not an identification of previous paleogeography and further modifications, which could be a clue to the final understanding of this important feature.

As a final remark, I want to express that the reading of this book brought to my memory nice scenes of navigation in the small zodiacs, landing in abrupt fjords, and walking in wet pit plains, which arouse my envy to these young researchers that can continue to enjoy these beautiful landscapes, even under the rain and intense snowfall, but full of excellent geology. Congratulations to the authors and especially to the editor for the initiative and for the robust final product obtained.

Victor A. Ramos
Emeritus Professor
Universidad de Buenos Aires

Contents

An Introduction to the Geodynamic Evolution of the Southernmost Andes: Connections with the Scotia Arc.	1
Matías C. Ghiglione	
Tectonic Evolution of Paleozoic and Mesozoic Andean Metamorphic Complexes and the Rocas Verdes Ophiolites in Southern Patagonia.	7
Mauricio Calderón, Francisco Hervé, Francisco Fuentes, Julie C. Fosdick, Fernando Sepúlveda and Gonzalo Galaz	
Magmatic Evolution of the Southernmost Andes and Its Relation with Subduction Processes.	37
Mauricio González Guillot	
Tectonic Reconstructions of the Southernmost Andes and the Scotia Sea During the Opening of the Drake Passage	75
Graeme Eagles	
The Relation Between Neogene Denudation of the Southernmost Andes and Sedimentation in the Offshore Argentine and Malvinas Basins During the Opening of the Drake Passage	109
Matías C. Ghiglione, Christian Sue, Miguel E. Ramos, Jonathan E. Tobal and Rocío E. Gallardo	
Wrenching Tectonism in the Southernmost Andes and the Scotia Sea Constrained from Fault Kinematic and Seismotectonic Overviews.	137
Christian Sue and Matías C. Ghiglione	
Kinematic Evolution of the Southern Andean Orogenic Arc	173
Marco Maffione	
Index	201

Contributors

Mauricio Calderón Carrera de Geología, Universidad Andres Bello, Santiago, Chile

Graeme Eagles Helmholtz Centre for Marine and Polar Research, Alfred Wegener Institute, Bremerhaven, Germany

Julie C. Fosdick Department of Geological Sciences, Indiana University, Bloomington, USA

Francisco Fuentes Carrera de Geología, Universidad Andres Bello, Santiago, Chile

Gonzalo Galaz Departamento de Geología Regional, Instituto de Geología, Universidad nacional Autónoma de México, México D.F., México

Rocío E. Gallardo Departamento de Ciencias Geológicas, Instituto de Estudios Andinos “Don Pablo Groeber” CONICET, FCEN—Universidad de Buenos Aires, Buenos Aires, Argentina

Matías C. Ghiglione Departamento de Ciencias Geológicas, Instituto de Estudios Andinos “Don Pablo Groeber” CONICET, FCEN—Universidad de Buenos Aires, Buenos Aires, Argentina

Mauricio González Guillot Centro Austral de Investigaciones Científicas CADIC-CONICET, and Instituto de Ciencias Polares, Ambiente y Recursos Naturales, Universidad Nacional de Tierra del Fuego, Tierra del Fuego, Ushuaia, Argentina

Francisco Hervé Carrera de Geología, Universidad Andres Bello, Santiago, Chile; Departamento de Geología, Universidad de Chile, Santiago, Chile

Marco Maffione Department of Earth Sciences, Utrecht University, Utrecht, The Netherlands

Miguel E. Ramos Departamento de Ciencias Geológicas, Instituto de Estudios Andinos “Don Pablo Groeber” CONICET, FCEN—Universidad de Buenos Aires, Buenos Aires, Argentina

Fernando Sepúlveda Servicio Nacional de Geología y Minería, Santiago, Chile

Christian Sue Bourgogne Franche-Comté University, Laboratoire Chrono-environnement, Besançon, France

Jonathan E. Tobal Departamento de Ciencias Geológicas, Instituto de Estudios Andinos “Don Pablo Groeber” CONICET, FCEN—Universidad de Buenos Aires, Buenos Aires, Argentina

An Introduction to the Geodynamic Evolution of the Southernmost Andes: Connections with the Scotia Arc

Matías C. Ghiglione

1 Introduction

The backbone of this book is the analysis of the relation between the tectonic evolution of the Southernmost Andes and its southern neighbors: Antarctica and the Scotia Sea. The Southernmost Andes comprise the southern bent of the Andean mountains, where they progressively change their strike from the N–S-oriented Southern Patagonian Andes to the E–W-trending Fuegian Andes (Fig. 1). These Andean segments and their corresponding basement, sedimentary basins, magmatic rocks, and batholithic belts are linked, even if sometimes elusively, to the evolution of the Antarctic Peninsula and of the islands spread in the Southern ocean.

The Scotia Sea separating South America and the Antarctic Peninsula (Fig. 1) is only ~30 Myr old, very young, considering a joint geological history of the Southernmost Andes, Patagonia, and Antarctica than can be traced back to late Paleozoic times (i.e., 300 Myr or more). Analysis of marine geophysical data in the Scotia Sea (cf. Eagles et al. 2006) and geological data from Tierra del Fuego (Ghiglione et al. 2008) demonstrate that the disconnection of South America and Antarctica started at about 50 Ma. However, oceanic spreading producing the final opening of the Drake Passage, and the consequent strike-slip movements along the North and South Scotia ridges (Fig. 1), occurred just since the Oligocene. Therefore, there is a joint history of Antarctica and South America that was shattered by the opening of the Scotia Sea; the remaining pieces of the puzzle, how can

M.C. Ghiglione (✉)

Departamento de Ciencias Geológicas, Instituto de Estudios Andinos “Don Pablo Groeber”
CONICET, FCEN—Universidad de Buenos Aires, Buenos Aires, Argentina
e-mail: matias@gl.fcen.uba.ar

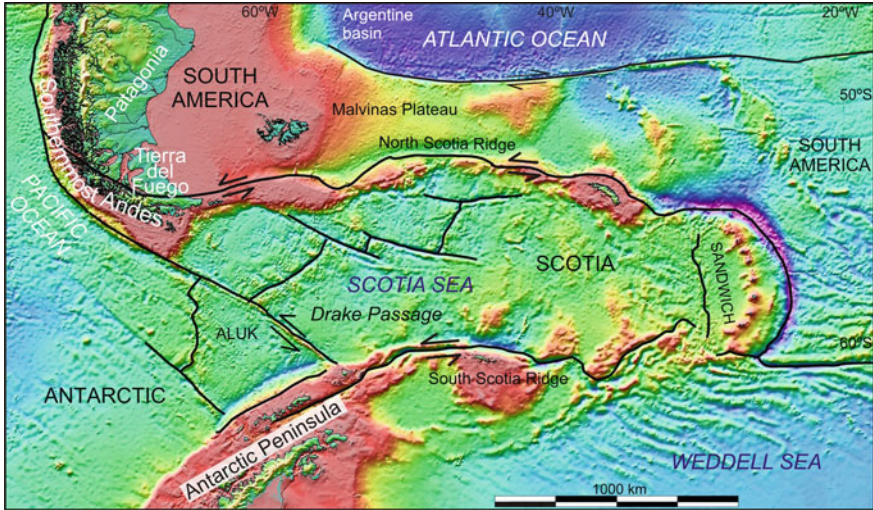


Fig. 1 Major tectonic plates (*black uppercase letters*) and some other geological and geographical features studied in this book, enclosing the Southernmost Andes, Scotia Sea, and the Antarctic Peninsula region

they fit together, and how were they separated from each other are the subjects of this book.

The overview presents state-of-the-art reviews intended for all scientist and professionals, as well as PhD and Master students working in the region. Since each chapter presents the necessary background and a historical appraisal, it is anticipated to be a useful tool for interested readers trying to understand the main geodynamic framework and debates of the Southernmost Andes–Scotia Arc region.

The following chapters summarize the works and thoughts of young Earth Science researchers that have worked on the geological and geophysical exploration of the region for over the last two decades. Each of the main authors have all finish their PhD's around 10 years ago on a number of multidisciplinary subjects in the region and since then have keep conducting field works, sampling, and analyzing the area. Multiple point of views and methods are therefore presented to address update summaries of new and long-lasting debates, including the complex evolution of the Rocas Verdes marginal basin (Dalziel et al. 1974) and the Patagonian Batholith (Katz 1964), plate kinematic reconstructions, and fault kinematics of the southern South America–Scotia Sea region, paleomagnetism and kinematics of the *Patagonian Orocline* (Carey 1958), orogenic growth in the Southernmost Andes and basin dynamics. The impact of the studied data in a number of global topics, such as the Paleozoic geodynamic context of Patagonia and Antarctica within the *Terra Australis* orogen (*sensu* Cawood 2005), the Eocene–Oligocene global climatic change, offshore sedimentation in the Atlantic platform, active seismicity, kinematics of deformation along the North and South Scotia ridges, and the opening of the Drake Passage, is also addressed.

The authors started from scratch exhaustive data compilations and present them in tables and summary figures. It should be highlighted the consistency and coherence of the data, although most information in the region is scarce and scattered due to the remoteness of islands and fiords, in a polar context of weather conditions that are bearable only in the summer months. Indeed, the compiled information is the product of multiple campaigns over 30 years, data collected with several methods, different logistics, and multiple countries involved. After they were filtered for modern requisites and compiled in regional databases, they are, however, very consistent and stress the thoughtfulness of the referenced researchers.

Therefore, one of the main outputs of this book is the presentation of extensive synthetic databases and their thoughtful analysis. The tectonic history of the Southernmost Andes, and their rich and complex relation with their southern neighbors is, however, too big to be left without personal views and perceptions. The following chapters present not only a review of theories and databases, but they address new perspectives, and potential paradigms that will lead the future research on the region.

2 Book Structure

The backbone used to structure the book is a chronological order of studied topics that are also arranged in a comprehensible way to understand the context. However, each chapter addresses the necessary background to understand the analyzed subjects and methodologies. The following chapters start with the evolution of Paleozoic and Mesozoic metamorphic complexes (second chapter), and the Mesozoic–Cenozoic magmatic evolution of the Patagonian and Fuegian batholiths (third chapter) that constitute the basement of the region. The book continues with Cenozoic plate kinematic reconstructions from geological, marine, and satellite geophysical data (fourth chapter), the late Cenozoic foreland basin dynamics and sediment dispersal during the opening of the Drake Passage (fifth chapter) and a seismotectonic overview (sixth chapter), to finally present a disquisition about the kinematic evolution of the Patagonian Orocline (seventh chapter).

Calderón et al. (2016) summarize the tectonic and magmatic evolution of Paleozoic and Mesozoic metamorphic complexes in southern Patagonia and the Rocas Verdes ophiolites in the second chapter, on the base of combined petrological, geochemical, and geochronological datasets. This chapter explains the evolution of magmatic belts, marginal basins, and continental fragments that once formed part of the peripheral realm of southwestern Gondwanan and gives details on their connections with the Antarctic Peninsula. These authors revisit the evolution of the Rocas Verdes basin, explaining its relation with the Patagonian and Fuegian batholiths and the Magallanes–Austral basin, and present schematic reconstructions of its Jurassic to Cretaceous tectonic evolution. Additionally, the

possibility that the Antarctic Peninsula was located west of the present margin of southern Patagonia (cf. Jokat et al. 2003) is also addressed.

The Jurassic through Miocene episodic magmatic growth of the main arc and rear arc magmatic suites in the Southernmost Andes is discussed in the third chapter by Guillot (2016). This author presents a detailed and updated report of field features, lithology, geochemistry and age of the Fuegian Batholith and satellite plutons, and a thoughtful comparison among the different plutonic suites. An account of variations in the composition of magmas and shifts in the position of the volcanic front in the Patagonian–Fuegian batholiths are shown in sketches and maps, and are associated to fluctuating subduction parameters. The peculiar tectonic setting that affected the magmatic arc construction includes the opening and closure of the Rocas Verdes marginal basin and oroclinal bending in the latest Cretaceous–Paleogene. A mid-Cretaceous slab-flattening event, which caused a cratonward migration of the volcanic front, the widening of the arc, and inception of potassic magmatism in the rear arc is also proposed.

In the fourth chapter, Eagles (2016) reviews geological data exposed around the Scotia Sea margins, and the patterns of fracture zones and magnetic reversal isochrons from marine and satellite geophysical data. This author reviews what can be interpreted of the plate tectonic history of the region by using these resources and presents a detailed and quantitative approach to its plate kinematics. A set of tectonic reconstructions of the Southernmost Andes and the Scotia Sea during the opening of the Drake Passage from 6 to 50 Ma are shown in this fourth chapter. Additionally, main changes in the plate tectonic configuration and in the geodynamic setting are related to deformation and kinematics in the Southernmost Andes. This author presents an overview and debate of pre-Scotia times in which the established proximity of South Georgia to Tierra del Fuego in Early Cretaceous times is disputed.

Ghiglione et al. (2016) present in the fifth chapter an overview of Neogene orogenic growth and denudation in the Southernmost Andes, and related sediment dispersal in the Magallanes–Austral–Malvinas foreland basin during the opening of the Drake Passage. These authors propose that great volumes of sediments produced by Miocene–Pliocene denudation of the cordillera bypassed Patagonia and reached the Argentinean continental margin, where they were accommodated in thick sequences with high sedimentation rates. The evidence summarized in this fifth chapter shows a sequence of geodynamic events and paleogeographic changes leading to that output, including the approximation and collision of the Chile Ridge against the Pacific margin, the dynamic uplift of extra-Andean Patagonia, and the propagation of Antarctic waters masses into the Argentine Basin after the deepening of the Drake Passage.

In the sixth chapter, Sue and Ghiglione (2016) present a synthesis of the fault system associated with major fault zones in the Southernmost Andes and the Scotia Sea and review the available kinematic databases from fault slip data and GPS-measured deformation. These authors establish a current stress pattern stable since Oligocene times, reflecting that the global left-lateral motion between Antarctica and South America plate is the main driving force for the entire area.

Discrepancies between long-term and short-term slip velocities along the Magallanes–Fagnano fault system are also evaluated, suggesting a complex mechanics that makes calculating a recurrence time history for the characteristic earthquakes difficult.

The seventh and final chapter by Maffione (2016) gives an structural and paleomagnetic account of the regional-scale curvature developed in the Patagonian–Fuegian Andes, namely Patagonian Orocline (Carey 1958). In this chapter, a historical, and comprehensive review of the up-to-date paleomagnetic, structural, and magnetic fabric data is presented, together with a discussion on current models and future challenges. This author propose that the orogenic curvature of the Southernmost Andes does not specifically fit in any of the classic definitions of curved mountain belts, and it rather represents a “hybrid” curved belt. For this reason, the more generic term of “Patagonian Arc” is introduced, to signify a slip-partitioning mechanism along preexisting faults that controlled the kinematic evolution of the bent.

References

- Calderón M, Hervé F, Fuentes F, Fosdick JC, Sepúlveda F, Galaz G (2016) Tectonic evolution of Paleozoic and Mesozoic andean metamorphic complexes and the Rocas Verdes ophiolites in southern Patagonia. In: Ghiglione MC (ed) *Geodynamic Evolution of the Southernmost Andes*. Springer Earth System Sciences, pp 7–36
- Carey SW (1958) The tectonic approach to continental drift. *Continental drift: a symposium*. Hobart. Geology Department, University of Tasmania, Tasmania, pp 177–355
- Cawood PA (2005) Terra Australis orogen: Rodinia breakup and development of the pacific and Iapetus margins of Gondwana during the Neoproterozoic and Paleozoic. *Earth-Sci Rev* 69:249–279
- Dalziel IWD, De Wit MF, Palmer KF (1974) Fossil marginal basin in the southern Andes. *Nature* 250:291–294
- Eagles G (2016) Tectonic reconstructions of the Southernmost Andes and the Scotia Sea during the opening of the Drake Passage. In: Ghiglione MC (ed) *Geodynamic Evolution of the Southernmost Andes*. Springer Earth System Sciences, pp 75–108
- Eagles G, Livermore RA, Morris P (2006) Small basins in the Scotia Sea: The Eo-cene drake passage gateway. *Earth Planet Sci Lett* 242:343
- Ghiglione MC, Yagupsky D, Ghidella M, Ramos VA (2008) Continental stretching preceding the opening of the Drake Passage: evidence from Tierra del Fuego. *Geology* 36:643–646
- Ghiglione MC, Sue C, Ramos ME, Tobal JE, Gallardo RE (2016) The relation between neogene denudation of the Southernmost Andes and sedimentation in the offshore Argentine and Malvinas basins during the opening of the Drake Passage. In: Ghiglione MC (ed) *Geodynamic Evolution of the Southernmost Andes*. Springer Earth System Sciences, pp 109–135
- Guillot MG (2016) Magmatic evolution of the southernmost Andes and its relation with subduction processes. In: Ghiglione MC (ed) *Geodynamic Evolution of the Southernmost Andes*. Springer Earth System Sciences, pp 37–74
- Jokat W, Boebel T, König M, Meyer U (2003) Timing and geometry of early Gondwana breakup. *J Geophys Res* 108:2428
- Katz HR (1964) Some new concepts on geosynclinal development and mountain building at the southern end of South America. *XXII Intern Geol Congr India Proc* 4:242–255

- Maffione M (2016) Kinematic evolution of the Southern Andean orogenic arc. In: Ghiglione MC (ed) Geodynamic Evolution of the Southernmost Andes. Springer Earth System Sciences, pp 173–200
- Sue C, Ghiglione MC (2016) Wrenching tectonism in the Southernmost Andes and the Scotia Sea constrained from fault kinematic and seismotectonic overviews. In: Ghiglione MC (ed) Geodynamic Evolution of the Southernmost Andes. Springer Earth System Sciences, pp 137–171

Tectonic Evolution of Paleozoic and Mesozoic Andean Metamorphic Complexes and the Rocas Verdes Ophiolites in Southern Patagonia

Mauricio Calderón, Francisco Hervé, Francisco Fuentes,
Julie C. Fosdick, Fernando Sepúlveda and Gonzalo Galaz

Abstract The petrology and geochronology of Paleozoic and Mesozoic metamorphic and ophiolitic complexes in southern Patagonia constrain the evolution of magmatic belts, marginal basins, and continental fragments that once formed part of the peripheral realm of the southwestern Gondwanan margin. The upper Paleozoic metasedimentary rocks exposed along the eastern slopes of the Andean ranges contain prominent zircon components of Devonian and earliest Carboniferous age. These strata were deposited in marine basins fed by sediment derived from almost coeval felsic magmatic belts and recycled units with Ordovician and Cambrian components; some of which have been identified to the east, in Argentina. Permian to Triassic metasedimentary complexes, mainly exposed along the western slope of the Southern Patagonian Andes and in the Antarctic Peninsula, show conspicuous peaks of Permian detrital zircons with sparse older age components, supporting their deposition near active magmatic belts in a convergent margin setting. It is proposed that rapid northward migration of Gondwana (between 330 and 270 Ma) promoted crustal extension and the establishment of an arc and back-arc marginal basin configuration during the Permian. Subsequent closure of the marginal basins occurred during the Late Triassic–Early Jurassic Chonide orogeny. Middle Jurassic fragmentation of Gondwana involved continental extension, synrift silicic and bimodal magmatism, and seafloor-spreading, leading to the oceanic-type Late

M. Calderón (✉) · F. Hervé · F. Fuentes
Carrera de Geología, Universidad Andres Bello, Sazie 2119, Santiago, Chile
e-mail: mcaldera@gmail.com

F. Hervé
Departamento de Geología, Universidad de Chile, Plaza Ercilla 803, Santiago, Chile

J.C. Fosdick
Department of Geological Sciences, Indiana University, 1001 East 10th Street,
Bloomington, USA

F. Sepúlveda
Servicio Nacional de Geología y Minería, Av. Santa María 0104, Santiago, Chile

G. Galaz
Departamento de Geología Regional, Instituto de Geología, Universidad nacional Autónoma de México, México D.F. 04510, México

Jurassic to Early Cretaceous Rocas Verdes basin. Once the Antarctic Peninsula microplate migrated southward, subduction was re-established in southern Patagonia in Early Cretaceous time, involving processes of subduction erosion and high-*P/T* metamorphism in the forearc region. The Rocas Verdes basin started to close in the latest Early Cretaceous involving underthrusting and subduction of its oceanic seafloor. These convergent processes culminated with the Late Cretaceous Patagonian and Fuegian orogeny involving the tectonic emplacement of ophiolitic complexes, collision of drifted crustal slivers against the continent, and development of the Magallanes–Austral foreland basin.

Keywords Metamorphic complexes · Rocas Verdes ophiolites · Patagonian Andes · Fuegian Andes · Antarctic Peninsula · Magallanes–Austral basin

1 Introduction

The southernmost edge of South America, hereafter referred to as southern Patagonia, encompasses igneous and metamorphic complexes that represent one interconnected assemblage of diachronous magmatic belts and accretionary complexes that once formed part of the southwestern margin of Gondwana (Hervé et al. 2003; Pankhurst et al. 2003; Eagles 2016), also known as the Terra Australis Orogen (Cawood 2005). Some of these units composed the continental basement, in which the Upper Jurassic to Lower Cretaceous Rocas Verdes marginal basin was developed (Katz 1964; Dalziel et al. 1974; Suárez and Pettigrew 1976; Dalziel 1981; Stern and de Wit 2003; Calderón et al. 2007a), following the onset of Gondwana fragmentation in Middle Jurassic times (Bruhn et al. 1978; Pankhurst et al. 2000). Today, the rift and oceanic-type seafloor remnants of the Rocas Verdes basin are preserved as discontinuous belts of supracrustal bimodal igneous suites and ophiolitic complexes tectonically juxtaposed onto the cratonic margin of southern Patagonia during the late Mesozoic Andean orogeny (Dott et al. 1977; Dalziel 1981; Cunningham 1994; Stern and de Wit 2003; Calderón et al. 2013) (Fig. 1).

The intricate internal architecture of metamorphic and ophiolitic complexes, coupled with the lack of fossil records in complexly deformed metasedimentary rocks, has fostered the development and application of several analytical techniques (geochemistry, geothermobarometry, igneous and detrital U–Pb zircon geochronology, low-temperature thermochronology) to resolve temporal and genetic relationships among them and provide an improved framework for paleogeographic analysis. The understanding of these complexes has been further established with the combination of U–Pb SHRIMP (Sensitive High-Resolution Ion Microprobe) geochronology and Lu–Hf isotopic data for individual zircon grains, providing timing of formation and sediment deposition and the nature of host magmas and provenance areas (Hervé et al. 2003, 2010a, b; Pankhurst et al. 2003; Augustsson et al. 2006; Augustsson and Bahlburg 2008; Fanning et al. 2011; Castillo et al. 2015). Furthermore, the geological evolution of some of these

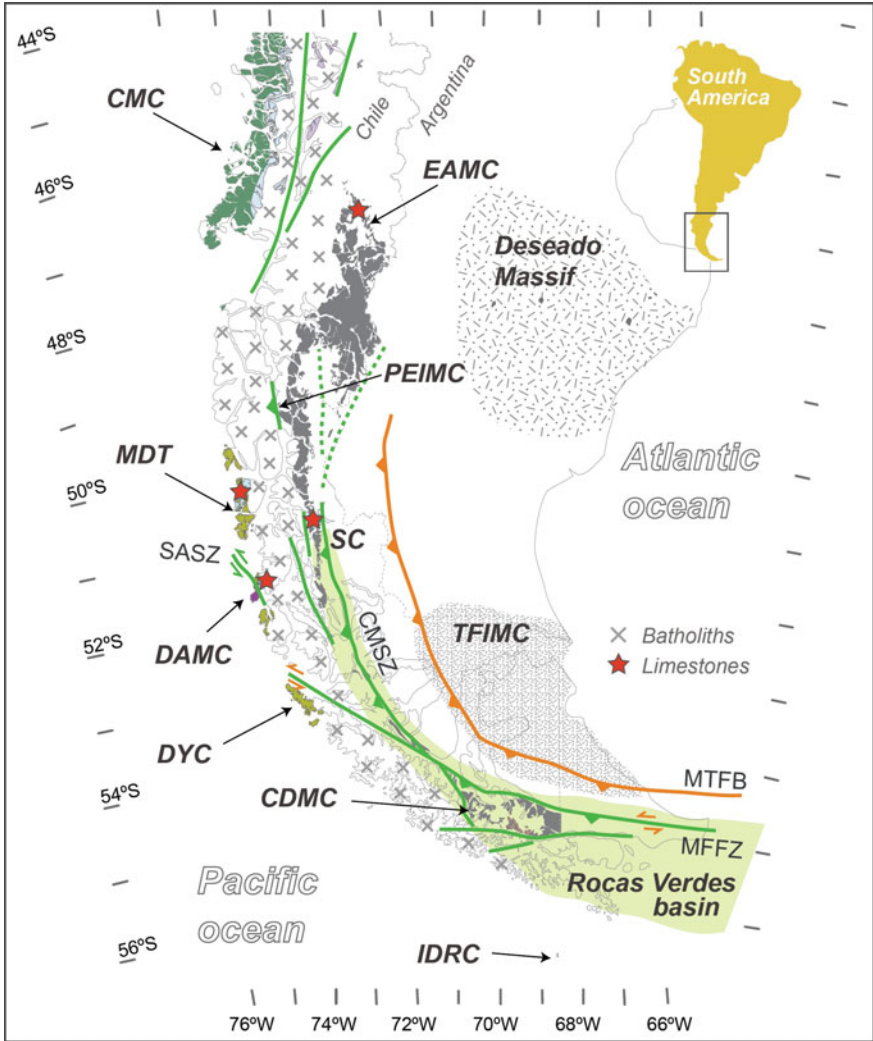


Fig. 1 Geological sketch map of the Paleozoic and Mesozoic igneous and metamorphic complexes in southern South America (after Sernageomin 2003). The contour of the Rocas Verdes basin ophiolites and related volcanic and sedimentary rocks is illustrated. Major fault zones are illustrated. Abbreviations of geological units are: CDMC Cordillera Darwin Metamorphic Complex; CMC Chonos Metamorphic Complex; DAMC Diego de Almagro Metamorphic Complex; DC Denaro Complex; DRMC Diego Ramirez Metamorphic Complex; NYC Duque de York Complex; EAMC Eastern Andean Metamorphic Complex; MDT Madre de Dios Terrane; MRMC Main Range Metamorphic Complex; PEIMC Puerto Edén Igneous and Metamorphic Complex; SC Staines Complex; TL Tarlton Limestones; TFIMC Tierra del Fuego Igneous and Metamorphic Complex. Abbreviations of major fault zones are: CMSZ Canal de las Montañas Shear Zone, MFFZ Magallanes-Fagnano fault zone, MTFB Magallanes Thrust and Fold Belt; SASZ Seno Arcabuz Shear Zone

complexes has been proposed using determinations of metamorphic pressure (P)–temperature (T) conditions and low-temperature thermochronology (Willner et al. 2000, 2004, 2009; Ramírez-Sánchez et al. 2005; Calderón et al. 2007b, 2012; Sepúlveda et al. 2008; Maloney et al. 2011).

In light of already-published data from heterochronous petrotectonic assemblages, the paleogeographic evolution of the continental margin of southern Patagonia is discussed in terms of shared geodynamic scenarios, such as the emplacement of magmatic belts (arc and/or rifts) and related sedimentary basins on older basement complexes, and development of oceanic-type marginal basins above subduction zones. The possibility that the Antarctic Peninsula was located west of the present margin of southern Patagonia (cf. Jokat et al. 2003; Hervé et al. 2006) is also addressed.

2 Igneous and Metamorphic Complexes of Patagonia and Tierra del Fuego

The Southern Patagonian and Fuegian Andes are a relatively low-elevation mountain belt made up in part by the upper Paleozoic to Mesozoic metamorphic complexes and by Jurassic to Cretaceous supra-subduction zone ophiolitic complexes of the Rocas Verdes basin. Most of the metamorphic and ophiolitic complexes crop out west and east of the continuous Mesozoic to Cenozoic Patagonian Batholith (Hervé et al. 1984, 2007a; Pankhurst et al. 1999; Guillot 2016) with portions of continental basement rocks buried beneath the Jurassic volcanoclastic deposits of the Chon Aike Silicic Large Igneous Province and younger sedimentary infill of the Magallanes–Austral basin (Pankhurst et al. 2003; Hervé et al. 2008) (Fig. 1). The older continental rocks in southern Patagonia are in the Deseado Massif area (Pankhurst et al. 2003) and below the Jurassic to Cenozoic strata in southern Patagonia and Tierra del Fuego (Söllner et al. 2000; Hervé et al. 2010a). In this section, we present a summarized description of metamorphic and ophiolitic complexes, detailing lithologies, U–Pb zircon geochronology, metamorphic characteristics, and geodynamic significance.

Two main divisions are recognized and employed to arrange the descriptions: Upper Paleozoic to Mesozoic **Andean metamorphic complexes** (Sect. 2.1) and **Ophiolitic complexes of the Rocas Verdes basin** from Jurassic to Cretaceous supra-subduction zone (Sect. 2.2). The **Mesozoic Mylonitic Belts** of the Seno Arcabuz (SASZ) and Canal de las Montañas (CMSZ) shear zones acting as main tectonic boundaries (Figs. 1 and 2) are described separately (Sect. 2.3).

2.1 Andean Metamorphic Complexes

The Andean metamorphic complexes are mainly composed by polydeformed metasedimentary rocks, local bodies of limestone, and metamorphosed mafic rocks. Deformation and metamorphism precludes conventional stratigraphic logging and preservation of biostratigraphic records. However, U–Pb SHRIMP geochronology of detrital zircon grains in different metasedimentary rocks provides constraints on the timing of sediment deposition of their protoliths and their possible

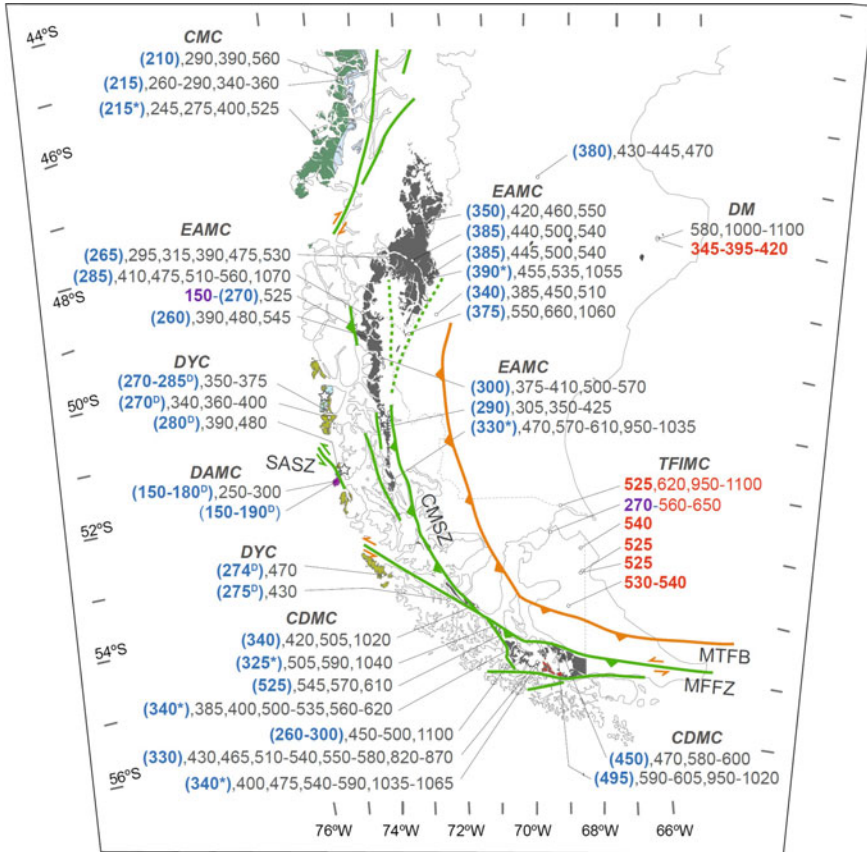


Fig. 2 Geological sketch map with published SHRIMP U–Pb zircon ages (Ma). In metamorphic rocks, the detrital zircon ages in parenthesis (blue) are the youngest obtained detrital age calculated with 3 zircon grains that can be interpreted as maximum sedimentation ages (asterisks indicate the age of 1 or 2 grains); older ages indicate principal provenance grouping of zircons. In situ crystallization ages in plutonic and gneissic rocks are indicated in red; older ages indicate inherited crustal components involved during their formation. Ages in purple correspond to the metamorphic age obtained in zircon overgrowths from migmatitic gneisses. For a detailed analysis of the data, reference should be made to the original papers (Hervé et al. 2003, 2010a, b; Pankhurst et al. 2003; Augustsson et al. 2006; Augustsson and Bahlburg 2008; Permuy Vidal et al. 2014; Malkowski et al. 2015; Castillo et al. 2015). Abbreviations are the same than those in Fig. 1

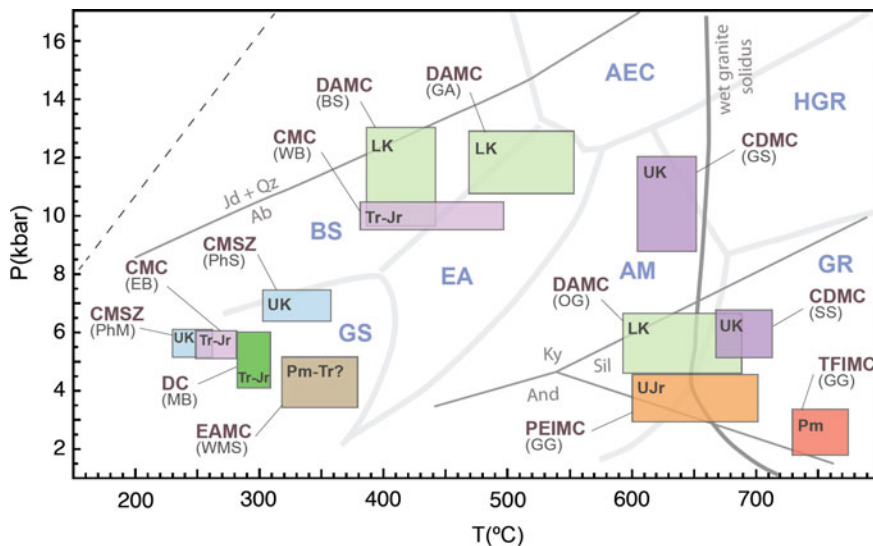


Fig. 3 Pressure–temperature diagram showing metamorphic conditions calculated in metamorphic rocks and the age of metamorphism. The overview of general metamorphic facies, stability field of andalusite-sillimanite-kyanite and wet granite solidus are also shown (Spear et al. 1999; Ernst 2009). For a detailed analysis of the data, reference should be made to the original papers (Ramírez-Sánchez et al. 2005; Calderón et al. 2007b, 2012; Willner et al. 2000, 2004, 2009; Sepúlveda et al. 2008; Hervé et al. 2010a; Maloney et al. 2011). Metamorphic facies abbreviations are: *GS* greenschist; *BS* blueschist; *EA* epidote amphibolite; *AM* amphibolite; *GR* sillimanite-granulite; *HGR* kyanite-granulite; *AEC* amphibolite-eclogite. Abbreviations are the same than those in Fig. 1

paleogeographic settings. The compilation of U–Pb detrital and igneous zircon ages of igneous and metamorphic complexes is shown in Fig. 2. A P–T diagram indicating the P–T conditions and age of metamorphism rocks belonging to different metamorphic complexes is illustrated in Fig. 3. Here, we describe the igneous and metamorphic complexes from the oldest to the youngest.

2.1.1 Tierra del Fuego Igneous and Metamorphic Complex (TFIMC)

The TFIMC corresponds to the Fuegian basement of the Magallanes–Austral basin (Söllner et al. 2000; Pankhurst et al. 2003; Hervé et al. 2010a), buried beneath km-thick successions of Jurassic volcanoclastic and younger sedimentary strata. This complex is dominated by foliated peraluminous biotite granitoids, and some containing cordierite and garnet, variably transformed to orthogneisses. Gneisses are predominately composed by coarse-grained aggregates of quartz, plagioclase, and K-feldspar, separated by finer bands of deformed and partly chloritized green biotite. The attitude of the foliation is difficult to determine, but is usually at high angles to the core length, suggesting that a low-dipping foliation is predominant. Some of the gneisses contain the mineral assemblage cordierite-sillimanite-garnet-biotite-plagioclase-orthoclase-quartz.

The plutonic zircon age spectra in samples of this complex (Hervé et al. 2010a) display: (1) a Cambrian igneous component (525–540 Ma); (2) a Cambrian migmatitic gneiss with peaks of inherited zircons at ~950–1100 and 560–650 Ma; and (3) a Permian high-grade anatectic event (of ~270 Ma) recorded in metamorphic zircon overgrowths on precursor rocks with noticeable Cambrian zircon components. The P–T metamorphic conditions calculated in the Permian cordierite-sillimanite-garnet migmatitic gneisses varies between 2–3 kbar and 730–770 °C, respectively (Fig. 3).

The oldest rocks in the TFIMC can be related to the sedimentary source of phyllitic metasedimentary rocks at Dos Hermanos locality (Deseado Massif, Fig. 1) characterized by a younger peak of ~565 Ma in detrital zircons (Pankhurst et al. 2003). Meanwhile, the Permian age for the upper crustal anatexis in the TFIMC is comparable with the age of high-grade metamorphism (~260 Ma) in gneisses located at Adie inlet (eastern margin of Antarctic Peninsula), formed from precursor metasedimentary rocks with Cambrian ages (Millar et al. 2002). These indicate similar and contemporaneous crustal anatectic processes in southern Patagonia and western Antarctic Peninsula (Hervé et al. 2010a).

2.1.2 Eastern Andean Metamorphic Complex (EAMC)

The EAMC includes the previously defined Cochrane and Lago General Carrera units (Lagally 1975) as well as the Staines Complex at the latitude of Puerto Natales (Forsythe and Allen 1980). Metamorphic complexes located in the Andean range consist mainly of polydeformed turbiditic successions, with minor limestone bodies and metabasites. The EAMC has been correlated with other units in Argentina such as the Devonian to lower Carboniferous Bahía de la Lancha and Río Lácteo Formations, and the Cerro-Negro mica schists (Permuy Vidal et al. 2014).

On the basis of detrital zircon U–Pb analyses (Hervé et al. 2003; Augustsson et al. 2006; Augustsson and Bahlburg 2008), the EAMC includes sedimentary components deposited between the late Devonian and the early Carboniferous (eastern domain), as well as younger turbidites deposited during the Permian and Triassic (western domain) (Fig. 2). Metamorphosed turbidites from the eastern domain shows Ordovician, Devonian, and early Carboniferous peaks of detrital zircons, and the western domain shows peaks of Permian zircons with variable proportions of Carboniferous, Devonian, Ordovician, and Cambrian grains.

Provenance studies based on petrographic and geochemical data (Hervé et al. 1998; Faúndez et al. 2002; Ramírez-Sánchez 2002; Augustsson and Bahlburg 2003; Lacassie 2003) suggest that turbidites of the eastern domain record deposition in a passive continental margin and were derived from a cratonic source, which possibly had undergone a complex and extended sedimentary recycling history. However, Augustsson and Bahlburg (2008) suggested that the eastern domain was fed from metasedimentary country rocks of an evolving magmatic arc. In contrast, detrital zircon U–Pb ages in the sedimentary protoliths of the Cerro Negro schists yield a statistically well-defined Devonian maximum depositional age (of ~380 Ma),

supporting a forearc setting for its deposition (Permuy Vidal et al. 2014). The detrital zircon spectra, occurrence of metaplutonic lithic fragments, detrital biotite, and the major element composition of the metasedimentary strata of the western domain indicate that the basin probably was fed from the arc proper and their country rocks (Augustsson and Bahlburg 2008). Potential sedimentary source areas for the Ordovician, Devonian, and early Carboniferous detrital zircons in the eastern domain are located to the east, in the Deseado Massif, and in northern Patagonia (Figs. 1 and 2) (Pankhurst et al. 2003, 2006; Moreira et al. 2013).

Potential sources of Permian detritus for the western domain are the plutonic complexes in the northern Patagonia interpreted as the result of voluminous and widespread silicic plutonism and volcanism linked to break-off of the subducted plate between the Deseado Massif and northern Patagonia (Fig. 1) (Pankhurst et al. 2006). Magmatic belts of Permian and Triassic age are not known at present in southern Patagonia, with the exception of punctual Permian migmatites and granites described in the TFIMC (Hervé et al. 2010a). Similarly, Permian and Triassic granitoids crop out sporadically along the Antarctic Peninsula, and many of them are peraluminous (Millar et al. 2002).

The metamorphic grade of the EAMC is in the greenschist facies or lower, and higher-grade rocks occur only in the contact aureoles of Mesozoic to Cenozoic intrusions (Ramírez-Sánchez 2002; Calderón 2000; Valdés 2005). P–T calculations in low-grade metapelites of the EAMC (Cochrane unit), consisting of quartz, albite, and white mica, yielded P–T conditions of 4 ± 1.2 kbar and 300–390 °C (Fig. 3). The rocks of this complex were affected by a Permian metamorphic event (Thomson and Hervé 2002; Augustsson et al. 2006) under lower P/T metamorphic conditions than those that are typical of subduction accretionary complexes (Hervé et al. 1998; Ramírez-Sánchez et al. 2005). At the Puerto Edén area, the EAMC underwent Late Jurassic low P/T amphibolite facies metamorphism and anatexis (Watters 1964; Calderón 2000; Hervé et al. 2003).

2.1.3 Cordillera Darwin Metamorphic Complex (CDMC)

The CDMC consists of metasedimentary, metaplutonic and metavolcanic units, of supposed late Paleozoic to early Mesozoic age, which have a unique late Mesozoic metamorphic imprint among the metamorphic basement complexes of the Southern Patagonian and Fuegian Andes, which is characterized by the generation of biotite, staurolite, kyanite, and sillimanite zones (Nelson et al. 1980; Hervé et al. 1981a; Kohn et al. 1995; Klepeis et al. 2010). The main lithologies of this complex are: (1) pelitic schists with quartz, plagioclase, muscovite, biotite, chlorite, garnet, staurolite, ilmenite, kyanite, and sillimanite (fibrolite); (2) metabasites with garnet, plagioclase, hornblende, biotite, chlorite, quartz, epidote, titanite, and ilmenite; (3) garnet-bearing orthogneisses; and (4) quartz-mica schists generated by dynamic metamorphism of precursor Jurassic silicic volcanoclastic rocks (cf. Hervé et al. 2010b; Klepeis et al. 2010; Maloney et al. 2011).

The detrital zircon U–Pb age spectra in most metasedimentary rocks of the CDMC are characterized by Mississippian peaks (~ 330 – 340 Ma) with variable proportions of Devonian, Ordovician, Cambrian, and Neo- to Meso-proterozoic components (Fig. 2) (Hervé et al. 2010b). These age peak signatures are comparable with detrital zircon patterns from the eastern domain of the EAMC. The paucity of Cambrian detrital zircons indicates that the TFIMC was not the main source of detritus for the protolith of the CDMC, suggesting the existence of a pre-Jurassic suture zone between both metamorphic complexes (Hervé et al. 2010b).

Metamorphic P–T conditions determined by Maloney et al. (2011) in garnet-bearing schists constrain a P–T path dominated by decompression from 12 to 9 kbar at ~ 620 °C (Fig. 3), culminating with staurolite and kyanite growth at 75 Ma (U–Th–Pb in situ dating of monazite). Additionally, these authors indicate that late contact aureoles developed adjacent to granite intrusions include sillimanite-bearing migmatites formed at P of 6 kbar and at T higher than 670 °C. The metamorphic petrology and field relationships are consistent with processes of continent-ward underthrusting, imbrications, and crustal thickening during the closure of the Rocas Verdes basin (Klepeis et al. 2010) with later exhumation controlled by thrusting (Maloney et al. 2011) that is an alternative to the model that considers the CDMC as an extensionally exhumed metamorphic core complex (Dalziel and Brown 1989; Kohn et al. 1993).

2.1.4 Madre de Dios Terrane (MDT)

The MDT is composed of three tectonically interleaved lithostratigraphic units: the Tarlton Limestone, the Denaro, and the Duque de York complexes (Forsythe and Mpodozis 1979, 1983). The Tarlton Limestone (TL) is a massive pelagic limestone body that was deposited in an oceanic carbonate platform during late Carboniferous–early Permian times (Douglass and Nestell 1976) overlying a broadly contemporaneous (Ling et al. 1985) oceanic substrate (the Denaro Complex). The Denaro Complex (DC) represents the oceanic floor composed of pillow basalts with enriched (E) and normal (N) mid-oceanic ridge basalts (MORB) geochemical signatures, radiolarian and Mn- and Fe-bearing cherts probably representing an oceanic ridge environment distal from the continental influence of Gondwanaland. This exotic terrane was later accreted to the continental margin during the early Mesozoic. The metabasalts of the DC preserve relic igneous phases, augite, and chromite and comprise metamorphic mineral assemblages of the pumpellyite-actinolite facies consisting of albite, chlorite, epidote, pumpellyite, stilpnomelane, titanite, garnet (grandite), white mica (phengite), actinolite, titanomagnetite, and quartz (Sepúlveda 2004; Sepúlveda et al. 2008). Peak metamorphic conditions of ~ 290 – 310 °C and 4–6 kbar (Fig. 3) were estimated by Willner et al. (2009). These authors suggest that the Madre de Dios Accretionary Complex was frontally accreted in a subduction zone environment.

The Duque de York Complex (DYC) is a turbiditic succession, which was deposited unconformably over the TL and the DC when they reached the vicinity of

the continental margin (Forsythe and Mpodozis 1979, 1983). The DYC includes palynomorphs of Permian age (Sepúlveda et al. 2010), as well as radiolarian cherts which indicate an early Permian deposition age (Quezada 2010). Metapelites exhibit porphyroblasts of cordierite and biotite in contact with the batholith (Parra 2015).

Detrital zircon U–Pb age data from rocks of the DYC show a dominant peak of Permian zircons (~270–290 Ma) (Hervé et al. 2003; Sepúlveda et al. 2010; Castillo et al. 2015), consistent with the biostratigraphic age. These rocks also comprise subordinate Carboniferous and Ordovician zircon populations, the latter becoming an important contribution in the southernmost outcrops of this unit (e.g., Desolation Island, Castillo et al. 2015). Combination of petrographic and geochemical analyses in rocks of the DYC (Lacassie 2003) indicates that this unit was derived from a geochemically intermediate igneous source, interpreted to have originated on a deeply dissected continental magmatic arc. The DYC basin was probably adjacent to the continental crust of Gondwanaland, in an active margin tectonic setting (Faúndez et al. 2002; Lacassie et al. 2006). Zircon fission track data indicate that the DYC (and probably the TL and DC units) was metamorphosed before or during the earliest Jurassic under low-grade metamorphic conditions (Thomson and Hervé 2002).

2.1.5 Chonos Metamorphic Complex (CMC)

The CMC consists predominantly of metaturbidites (Pimpirev et al. 1999), with more restricted occurrences of metabasites and metacherts. The CMC has a Late Triassic depositional age, as indicated by fossil fauna (Fang et al. 1998) and by detrital zircon SHRIMP U–Pb age determinations (Hervé and Fanning 2000). The complex was differentiated into two north–south-trending belts by Hervé et al. (1981b). The eastern belt has well-preserved primary sedimentary and volcanic structures, which are progressively obliterated when passing into the more pervasively deformed and recrystallized western belt rocks. Detrital zircons show characteristic peaks of the Upper Triassic detrital zircons with variable proportions of Permian, Carboniferous, Devonian, and Cambrian components (Hervé et al. 2003)

The lithologies of this complex correspond to psammopelitic rocks in the eastern belt with detrital quartz, plagioclase, K-feldspar, and muscovite in a very fine matrix consisting of quartz, albite, illite, chlorite (clinochlore), and white mica (muscovite and phengite). Accessory phases are titanite, rutile, zircon, tourmaline, apatite, and epidote. Metabasites with relict pillow structures and subophitic textures display mineral assemblages of quartz, albite, amphibole (actinolite), pumpellyite, chlorite, stilpnomelane, titanite, epidote, and veinlets of phengitic white mica. Meta-ironstones, usually interleaved with tectonic lenses of metachert, are dark finely banded carbonate rocks consisting of siderite, chlorite, and graphite. The metamorphic mineral assemblage of metapsammopelitic schists in the western belt consists of quartz, albite, white mica (generally phengite), chlorite, titanite, graphite with epidote, calcite, tourmaline, and Fe–Ti oxides as common accessory phases. Foliated metabasites or greenschists are

made up by amphibole (magnesium-hornblende), epidote, quartz, albite, titanite, ilmenite, and rare apatite. Exceptional garnet-bearing metabasites also occur. Meta-ironstone in the western belt consists of rocks formed by quartz-rich bands with abundant stilpnomelane and subordinate chlorite, amphibole, calcite, and white mica. Willner et al. (2000) resolved that maximum P–T conditions are 4.5–6 kbar and 250–280 °C for the eastern belt and 8–10 kbar and 380–550 °C for the western belt (EB and WB, respectively, in Fig. 3).

2.1.6 Puerto Edén Igneous and Metamorphic Complex (PEIMC)

The PEIMC consists of medium- to high-grade metamorphic rocks, migmatites, and plutonic rocks. Schists are composed of quartz, muscovite, plagioclase, biotite, pinnitized cordierite, andalusite (some with inclusions of staurolite), sillimanite, and K-feldspar. Accessory minerals are tourmaline, zircon, apatite, corundum, graphite, and Fe–Ti oxides. Also occur medium- to coarse-grained leucocratic gneisses, sillimanite gneisses, and stromatitic migmatites. Metamorphic assemblages, textural relations, and geothermobarometry suggest a low P/T and nearly isobaric metamorphic and partial melting event (~600–700 °C and 3–4.5 kbar) superimposed on the greenschist facies metamorphic rocks of the EAMC (Calderón 2006; Calderón et al. 2007b).

Metamorphic overgrowths on zircons in sillimanite paragneisses record a Late Jurassic (~150 Ma) age taken as evidence of local gneiss formation under in situ anatexis conditions during the emplacement of the Jurassic components of the South Patagonian Batholith (Hervé et al. 2003) formed during continental rifting in a supra-subduction setting (Calderón et al. 2007b).

2.1.7 Diego de Almagro Metamorphic Complex (DAMC)

The DAMC is composed of two subunits of differing metamorphic imprints, one composed of garnet amphibolites and blueschists, and the other of quartz-mica schists and an orthogneiss. The contact between them has not been observed in the field. SHRIMP U–Pb ages in zircons from the orthogneiss and a quartz-rich spessartine-bearing schist interleaved in the blueschists (Hervé and Fanning 2003) have yielded Middle Jurassic ages that are interpreted as the crystallization age of their igneous forerunners, a muscovite-garnet-bearing granite and a rhyolitic rock. This complex is in tectonic contact (Forsythe 1981, 1982) with the DYC along the mid-crustal sinistral strike-slip Seno Arcabuz shear zone (Olivares et al. 2003; Willner et al. 2004).

Quartz-rich mica schist and a mylonitized granite contain Late Jurassic zircons of ~166 and 170 Ma, respectively (Hervé and Fanning 2003). According to these authors, these rocks were metamorphosed during the Cretaceous in a subduction zone environment, which developed blueschist assemblages in metabasalts interleaved with the mica schist.

The mineralogy of the DAMC metamorphic rocks is well described by Willner et al. (2004) and Hyppolito (2010). The amphibolites consist of Ca-amphibole (hornblende and actinolite), epidote, chlorite, albite, quartz, phengite, titanite, and subordinate garnet (partially altered to chlorite), calcite, ilmenite, apatite, and pyrite. Orthogneisses and schists within the Seno Arcabuz shear zone consist of quartz, plagioclase, muscovite, biotite, apatite, and tourmaline. Hypidioblastic garnet with helicitic inclusion trails of graphite, biotite, and white mica occur in the schists. These rocks were overprinted by discrete shear band cleavage with newly grown quartz, phengite, chlorite, stilpnomelane, epidote, and albite. Amphibolites in the shear zone consist of hornblende, quartz, plagioclase, epidote, and titanite. Willner et al. (2004) established a converging P–T path followed by blueschists (initially crystallized at 9.5–13.5 kbar and 380–450 °C) and amphibolites (first crystallized at 11.2–13.2 kbar and 460–565 °C) into the P–T space defined between 6.3–9.6 kbar and 320–385 °C, respectively (Fig. 3). Orthogneisses crystallized first at 4.9–6.5 kbar and 580–690 °C and their retrograde phengite, chlorite, and stilpnomelane assemblage crystallized at a minimum pressure of ~5.7 kbar at 300 °C. The high P/T metamorphism in the rocks of the DAMC developed in a subduction zone during the Cretaceous (Hervé et al. 1999; Willner et al. 2004).

2.1.8 Diego Ramírez Metamorphic Complex (DRMC)

The DRMC is located in the Diego Ramírez Island, in the southern extreme of South America, and consists of pillow basalts and metasedimentary rocks that form a crush mélange (Wilson et al. 1989) with glaucophane-bearing metamorphic assemblages. A Middle Jurassic Rb–Sr whole-rock errorchron in the metasedimentary rocks (Davidson et al. 1989) suggests that these rocks can be correlated with those of the DAMC. Both complexes are envisaged as the remnants of mafic oceanic floor developed in a Jurassic marginal basin located between southern Patagonia and Antarctic Peninsula (Hervé and Fanning 2003).

2.2 Rocas Verdes Ophiolitic Complexes

The Rocas Verdes ophiolitic complexes preserve an incomplete “ophiolite pseudostratigraphy” (lacking the ultramafic rocks) and are particularly well suited for examining the tectonic and petrological transition from rift to back-arc basin evolution and subsequent closure and orogeny in the Southern Patagonian Andes. The rocks are foliated and metamorphosed in a discontinuous way; most parts of the large complexes preserve original textures and structures with characteristic secondary mineralogy of non-deformative seafloor hydrothermal metamorphism (Stern et al. 1976; Elthon and Stern 1978; Allen 1982; Calderón 2006; Avendaño 2008; Prades 2008; Calderón et al. 2013). In this section, the lithological, geochronological, geochemical, and isotopic information of the main ophiolitic complexes is presented. The location and geochronological data of ophiolitic complexes and

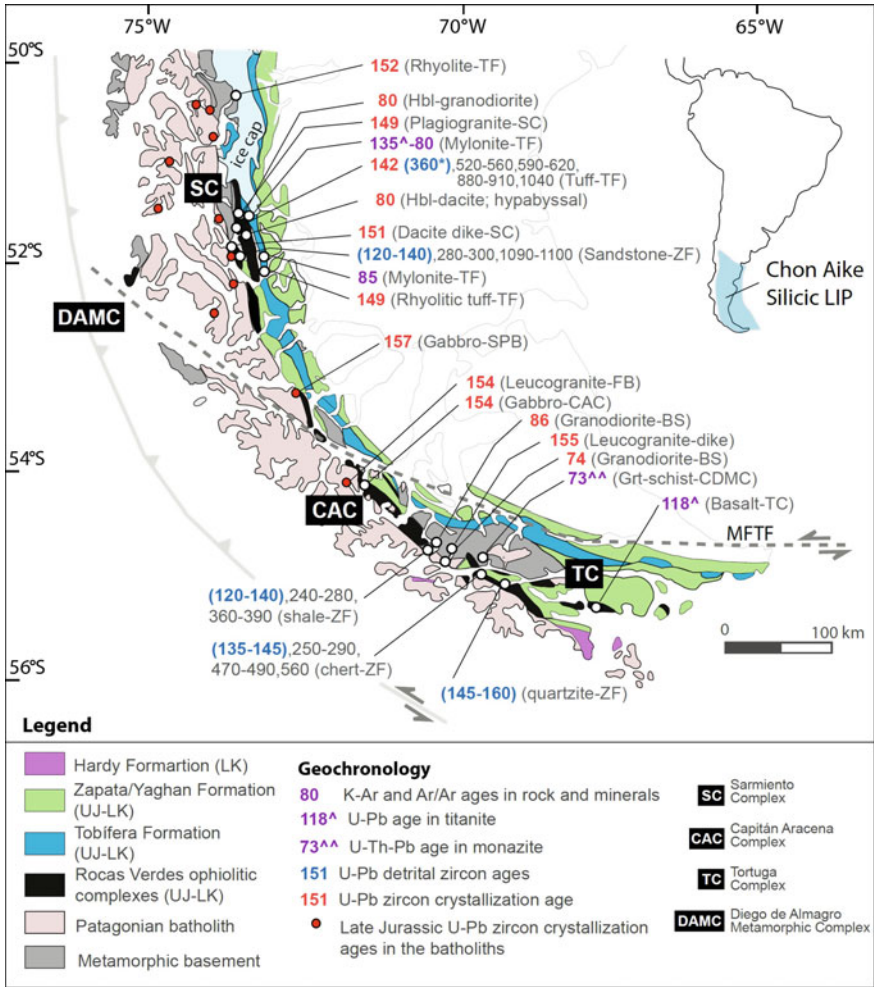


Fig. 4 Geological sketch map of Paleozoic and Mesozoic lithostratigraphic units in the Southernmost Andes of South America, including the Rocas Verdes ophiolites, folded and sheared volcanic and sedimentary successions of the Tobifera, Zapata, Yahgán Formations, the Patagonian and Fuegian batholiths, and metamorphic complexes. In sedimentary rocks, detrital zircon ages in parenthesis (blue) are the youngest obtained detrital age grains (*asterisks* indicate the age of 1 or 2 grains); older ages indicate principal provenance grouping of zircons. In situ crystallization ages in volcanic and plutonic rocks are indicated in red. Ages in purple correspond to the metamorphic age obtained by several methods as indicated in the figure. For a detailed analysis of the data, reference should be made to the original papers (Hervé et al. 2007a; Klepeis et al. 2010; Maloney et al. 2011; Calderón et al. 2007a, 2012, 2013). Abbreviations are: CAC Capitán Aracena Complex; DAMC Diego de Almagro Metamorphic Complex; SC Sarmiento Complex; TC Tortuga Complex

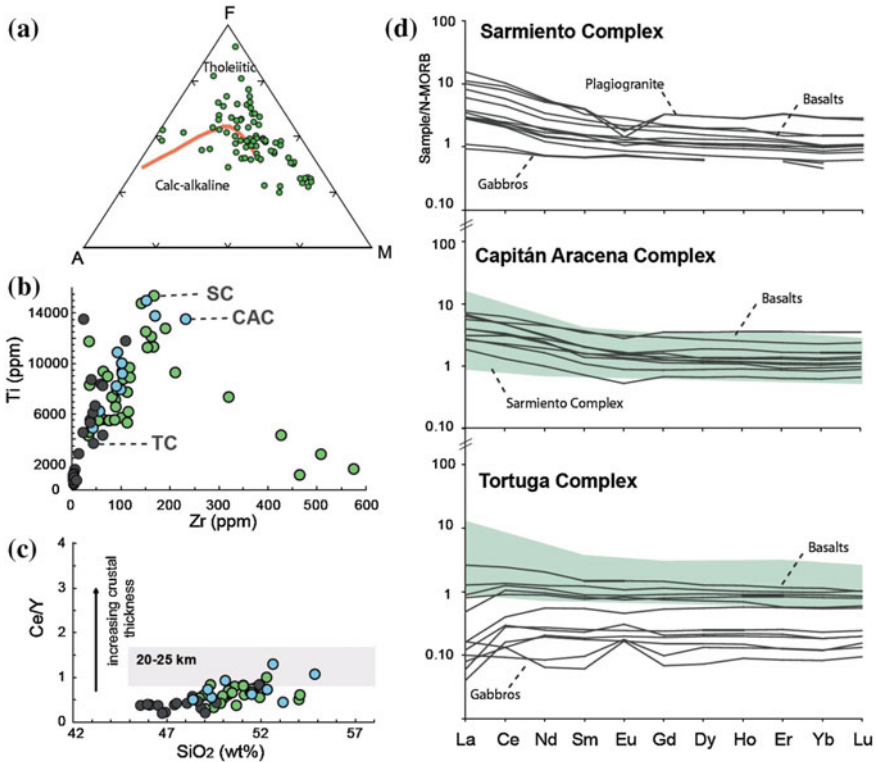


Fig. 5 Geochemical and petrological features of pillow basalts, basaltic dikes, diabases, and gabbroic rocks of the different Rocas Verdes ophiolitic complexes shown in diagrams. **a** AFM, **b** Ti versus Zr, **c** Ce/Y versus SiO₂ [values of crustal thickness are from Mantle and Collins (2008)]. **d** Normal mid-ocean ridge basalt (N-MORB) normalized Rare Earth Element diagram of the ophiolitic complexes of the Rocas Verdes basin, using Sun and McDonough (1989) normalization values. For a detailed analysis of the geochemical data, reference should be made to the original papers (Stern 1979, 1980; Saunders et al. 1979; Fildani and Hessler 2005; Calderón et al. 2013)

related granitic rocks are presented in Fig. 4. The available major and trace element geochemical composition and Nd-isotopic data for the ophiolitic rocks and other geological units in the region are illustrated in Figs. 5 and 6.

2.2.1 Sarmiento Complex (SC)

The Sarmiento Complex occurs in a north–south-trending 10- to 20-km-wide belt bound by the Canal de las Montañas Shear Zone in the east. Three main lithological units are distinguished (Calderón et al. 2007c): a thick mafic extrusive layer of pillow basalts and breccias with intercalations of radiolarian chert; a mafic–felsic

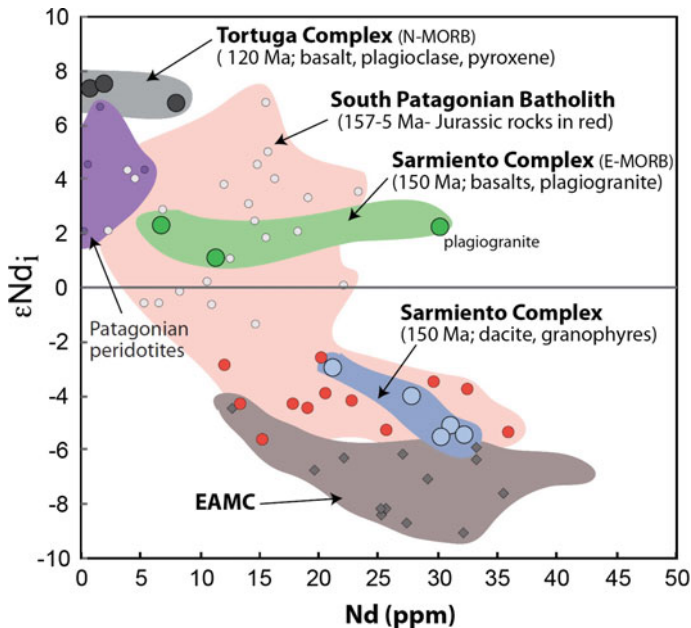


Fig. 6 Comparison of ϵNd_t versus Nd values of: igneous rocks from the Sarmiento and Tortuga ophiolitic complexes, and the South Patagonian Batholith; metasedimentary rocks, schists, and gneisses of the Eastern Andean Metamorphic Complex (EAMC); and peridotite xenoliths in extra Andean Patagonia (Stern 1991; Augustsson and Bahlburg 2003; Schilling et al. 2005; Hervé et al. 2007a; Calderón et al. 2007c). Noticeable are the similarities between felsic rocks of bimodal association in the Sarmiento Complex and Jurassic granites of the batholith, indicating the involvement of crustal components during their formation. It is also obvious the cogenetic origin between the basalts and plagiogranites, the last as product of extreme fractional crystallization

extrusive layer consisting predominantly of layers of pillow basalts, including intercalations of rhyolitic tuffs, hyaloclastites, and rhyolitic and dacitic dikes, which is in turn cut by mafic intrusive bodies; and a mafic–felsic intrusive layer consisting mainly of medium-grained granophyre cut by fine-grained gabbro and late sub-horizontal plagiogranite dikes. The base of this unit is composed of metagabbro and amphibolite. These rocks are exposed in two north–south-trending steeply dipping thrust sheets located in the central and western portions of the Sarmiento Cordillera (Allen 1982; Calderón et al. 2007a; Rapalini et al. 2008).

A dacite dyke crosscutting pillow-basalt successions and a plagiogranite dyke in sheeted dikes of the basal Sarmiento Complex contain ~ 150 Ma zircon crystals, indicating that mafic submarine volcanism had started prior to or during the Late Jurassic (Calderón et al. 2007a). The neighbor silicic pyroclastic rocks of the Tobifera Formation, intercalated with synrift deposits along fault-bounded grabens within Paleozoic metasedimentary rocks, were dated at 148 and 142 Ma, and thus coeval with ophiolitic magmatism. A fine-grained sandstone layer between the hemipelagic shales of the Zapata Formation located at c. 1000 m above its

depositional contact over pillow basalts reveals 12 ages between 132 and 143 Ma (a prominent peak that constrains an apparent maximum depositional age) and a Permian population (260–300 Ma) defined by four grains. Pre-tectonic grains of titanite from phyllonites of the basal and low-grade metamorphic sole of the Sarmiento Complex yielded a SHRIMP U–Pb mean crystallization age of roughly 135 Ma that probably constrain the age of seafloor-like metamorphism in the back-arc setting (Calderón et al. 2013).

2.2.2 Capitán Aracena Complex (CAC)

To the south of and in the middle portion of the main trace of the Magallanes–Fagnano Fault Zone, the CAC crops out in a northwest–southeast-trending 20-km-wide belt located at the northeast of Cordillera Darwin (Prades 2008). It forms a body elongated in a southeast–northwest direction that is thrust northward over metasedimentary rocks of the Yahgán Formation (Otzen 1987). The rocks are associated with diverse granitoid bodies that intrude them and with rhyolitic rocks of the Tobífera Formation.

Basaltic pillow lavas are occasionally cut by mafic dikes and preserve primary variolitic, amygdaloidal, porphyritic, and glomerophytic textures. The fine-grained seriate, intersertal, microgranular, and ophitic textures are characteristic in mafic dikes. There are also short tracts of green aphanitic foliated rocks, as their occasional intense foliation appears in the field to be mafic dike complexes. Coarse-grained gabbros were observed at several localities and, at some of these, were close to pillow basalts with no apparent discontinuity between them.

A medium-grained gabbro collected 100 m below pillow basalts having no discontinuity with the underlying rocks yielded a weighted mean age of ~154 Ma (Calderón et al. 2013). A similar age of ~155 Ma was obtained in a leucogranite intruded by ophiolitic mafic dikes. Both indicate that the early rifting stage of the Rocas Verdes basin development at the latitudes of the CAC was accompanied by bimodal magmatism.

2.2.3 Tortuga Complex

The Tortuga ophiolite is exposed in an east–west-trending 20-km-wide belt extending from the southwestern part of the Isla Navarino to the region south of the Canal Beagle. The southern border of the ophiolite is in fault contact with a tightly folded and weakly foliated package of turbiditic rocks. To the north, the possible depositional contact between the Tortuga ophiolite and the sedimentary rocks is obscured by subsequent thrust-fold deformation and earliest Late Cretaceous magmatism (Hervé et al. 1984). The Tortuga Complex is remarkable for its exceptional exposures of mafic oceanic-like crustal pseudostratigraphy, which grades upward from cumulate gabbros to pillow and sheet-flow basalts (Godoy 1978; Stern 1979).

The extrusive unit of the Tortuga ophiolite consists of a more than 2000-m-thick succession of submarine volcanic rocks, including massive and pillowed basalts, volcanic breccias, hyaloclastites, and intercalated horizons of chert and siltstones. The basalts bear plagioclase and clinopyroxene, and some contain subordinate pseudomorphs after discernible primary orthopyroxene and olivine. Pillow basalts preserve a fine-grained variolitic texture, with skeletal plagioclase laths and fans of dendritic clinopyroxene. Massive lava flows, or diabase sills, with characteristic columnar structures have medium-grained ophitic and variolitic textures of plagioclase intergrown with pyroxene granules. Massive diabase screens within a 1-km-thick level of sheeted dikes consist of medium-grained plagioclase and clinopyroxene and orthopyroxene and have ophitic, subophitic, and intergranular textures. The exposed base of the Tortuga ophiolite consists of an igneous complex made up of slightly altered massive and layered gabbros, most of which are two pyroxene and olivine gabbros, leucogabbros, and clinopyroxene troctolites intruded by dikes of basalt and fine diabase with chilled margins.

A cherty layer directly overlying pillow basalts yielded two dominant groups of zircon ages, about 136 and 143 Ma (that constrains an apparent maximum depositional age), with subordinate zircon grains of Permian, Cambrian, and latest Neoproterozoic ages (Calderón et al. 2013).

U–Pb LA-MC-ICP-MS in situ analyses in titanite, which is in association with amphibole, epidote, chlorite, plagioclase, and quartz in veins within the margins of pillow basalts yielded an Aptian mean crystallization age of ~118 Ma (Calderón et al. 2013). This can be interpreted as the age of greenschist facies seafloor metamorphism in the back-arc basin.

2.2.4 Geochemistry and Nd-Isotope Compositions

The mafic rocks of the Rocas Verdes basin ophiolites crystallized from tholeiitic magmas that are characterized by increasing Ti contents during the early stages of differentiation followed by decreasing contents in the later stages because of fractionation of magnetite (Fig. 5) (Stern 1979, 1980; Miller et al. 1994; Calderón et al. 2013). Geochemistry is also compatible with the concept of a thinned crust resulting from extension in a rift or back-arc environment.

Rare Earth Elements (REE) diagrams normalized to the composition of normal mid-oceanic ridge basalts show the similarity between the Sarmiento and the Capitán Aracena complexes; these are more enriched in large-ion lithophile elements than is the Tortuga Complex, which suggests that the former have a greater affinity with E-MORB magma. In the Tortuga Complex, mafic rocks crystallized from N-MORB magma probably generated by decompression melting of the sub-back-arc mantle and record the most advanced evolutionary stage of the Rocas Verdes basin opening to a mid-ocean ridge-type setting (cf., Saunders et al. 1979; Stern 1979; Calderón et al. 2013). The contrasting affinities of E- and N-type MORB compositions are also suggested by the Nd-isotopic compositions of mafic rocks of the Sarmiento and Tortuga complexes (Fig. 6) (Stern 1991; Calderón et al.

2007c). These features reflect that mantle-derived tholeiitic magmas were generated by melting of progressively more depleted sources during the interplay between back-arc mantle convection and the release of stress across the continental plate boundary (Stern and de Wit 2003).

2.3 *Mesozoic Mylonitic Belts*

2.3.1 *Seno Arcabuz Shear Zone (SASZ)*

The SASZ is a NNW-trending low-grade mylonitic belt that juxtaposes different structural levels at Isla Diego de Almagro (DAMC and DYC) and record two deformation events (Olivares et al. 2003): an early mylonitic foliation, and a late low-strain foliation originated by folding of the older fabric. Ductile deformation and sinistral-reverse kinematic indicators are typical of transpressional shear zones. According to the syntectonic mineralogy, deformation occurred at greenschist metamorphic grade. Zircon fission track ages from rocks of the SASZ are of ~ 65 Ma and record the end of shearing that juxtaposed all rocks in the middle crust (Willner et al. 2004).

2.3.2 *Canal de las Montañas Shear Zone (CMSZ)*

The CMSZ is a low-grade mylonite belt generated from felsic ignimbritic, pelitic and basaltic protoliths of the Upper Jurassic–Lower Cretaceous Rocas Verdes basin, interpreted as the metamorphic sole thrust of the Sarmiento Complex (Calderón et al. 2012). Highly strained rocks of the CMSZ display a reverse, continent-ward tectonic transport, with a minor dextral component of shearing. Transitional pumpellyite–actinolite and the upper greenschist facies metamorphic conditions at ~ 5 – 6 kbar and 230 – 260 °C indicate that the primary shearing event occurred in a subduction zone setting. In situ $40\text{Ar}/39\text{Ar}$ laserprobe chronology yielded ages of ~ 85 Ma on syntectonic phengite.

3 Discussion

In this section, we summarize the Paleozoic and Mesozoic tectonic and magmatic evolution of Southern Patagonian Andes based on the combined petrological, geochemical, and geochronological datasets described herein. Our tectonic synthesis is considered within the paleogeographic context provided by the PLATES program (The University of Texas Institute for Geophysics) in which the southwestern continental margin of Gondwana was nearly WNW-trending until Triassic time.

In these models, three discrete episodes of rapid drifting of the Gondwanan margin occurred between 420 – 390 Ma (to the south), 390 – 360 Ma (to the west),

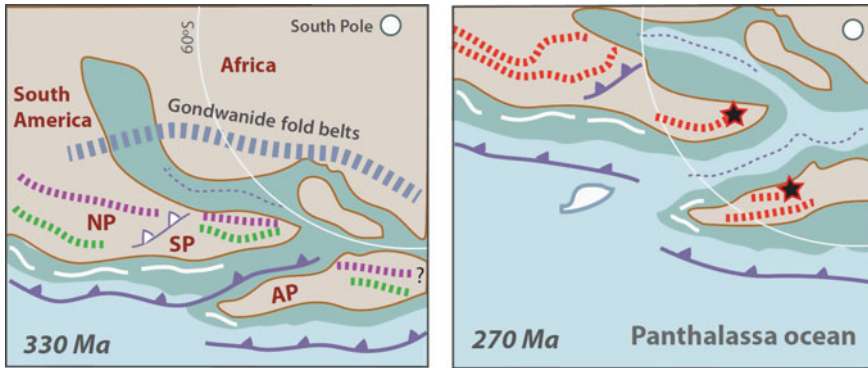
and 330–300 Ma (to the north). These changes, attributed to underlying mantle dynamics and changes in the configuration of tectonic plates, were likely a major control on the tectonic evolution of the continental margin and sediment routing of clastic detritus shed into marginal basins, as reflected by detrital zircon provenance data discussed below (Fig. 2). Additionally, we revisit the tectonic evolution of the Rocas Verdes basin in light of new geochronology and petrology of different supracrustal units (ophiolites, metamorphic complexes, mylonite belts) metamorphosed under different P–T conditions, at different times.

3.1 *Devonian-Carboniferous*

The occurrence of lower Devonian and Mississippian plutonic rocks in the Deseado Massif and the southward migration of Gondwana (420–390 Ma) suggest that subduction processes operated along the continental margin before the accretion of the Antarctic Peninsula to southern Patagonia (Fig. 7). However, given the persisting lack of information about the tectonic setting in which these magmatic rocks have formed, we prefer to conservatively refer to them as magmatic belts associated with either to subduction-related magmatic arcs or to volcanic rift zones.

Detrital zircon U–Pb geochronology of turbidite protoliths to the upper Paleozoic metamorphic rocks of the eastern domain of the EAMC and the CDMC points to the existence of Cambrian, Ordovician, Devonian, and Carboniferous magmatic belts in southern Patagonia and/or neighboring continental areas that have since been removed or buried (cf. Hervé et al. 2003, 2010a; Augustsson et al. 2006; Augustsson and Bahlburg 2008). Most of the Cambrian, Devonian, and Carboniferous igneous and metamorphic rocks are found in the Deseado Massif and in the TFIMC. However, detrital zircons of Ordovician age are recovered from some of these rocks and no evidence of plutonic/volcanic complexes of this age is known in southern Patagonia (Fig. 2). Plutonic complexes of Ordovician age crop out in the North Patagonian Massif (Pankhurst et al. 2006) and the evidence of a similar belt possibly concealed in southern Patagonia is indirectly provided by Middle Ordovician granitic cobbles in basal clastic successions of the Jurassic Tobifera Formation (to the north of the CDMC; Hervé et al. 2010b) and within conglomerates of the Permian Golondrina Basin, east of the Deseado Massif (Fig. 1) (Pankhurst et al. 2003).

According to paleogeographic models, the Antarctic Peninsula microplate transited from east to west, parallel to the westward drift of Gondwana (390–360 Ma) until the microplate became attached to the south part of southern Patagonia in the Mid-Carboniferous (Fig. 7) (cf. Ramos 2010). Bell and Suarez (2000) suggested that the main deformation and metamorphic events in the eastern belt of the EAMC occurred in pre-late Carboniferous times probably resulting from microplate interactions, rather than forearc accretion. A reasonable scenario that we consider is that, during the middle–late Devonian, a transform boundary was established along the continental margin with episodic magmatism and transpressional deformation in precursor basins.



Legend







- 
Subaerial Permian magmatic belts
 North Papagonia (NP): post-collisional
 South Patagonia (SP): rift and/or back-arc
 Antarctic Peninsula (AP): rift, back-arc and volcanic arc
 (purple: Ordovician; green: Devonian and Carboniferous)
- 
Turbiditic deposits and local limestones
 (protolith of the EAMC and CDMC (passive margin);
 NYC (backarc and forearc basins))
- 
Mid ocean spreading centers
- 
Oceanic terranes (DC and TL)
- 
Permian (270 Ma) low P/T migmatites
 (Punta Baja-Adie Inlet)
- 
Inferred Mid-Carboniferous suture zone

Fig. 7 Schematic reconstructions of the late Mississippian to early Permian paleogeographic and tectonic evolution of Gondwana margin at southern South America based on the geodynamic significance of Paleozoic metamorphic and igneous complexes in southern Patagonian and Antarctic Peninsula. The location of Antarctic Peninsula is based on paleogeographic maps of the Institute for Geophysics, The University of Texas at Austin

3.2 Permian-Triassic

Detrital zircon U–Pb geochronology of metasedimentary rocks of the western belt of the EAMC and the NYC indicates that their sedimentary protoliths contain predominantly Permian zircons and subordinate older grains. A wide variety of detrital components are recognized in the western belt of the EAMC, with zircons of Cambrian, Ordovician, Devonian, and Pennsylvanian ages. In contrast, the Duque de York Complex (NYC) yields a dominant peak of Permian zircons (~270–280 Ma; Hervé et al. 2003; Fanning et al. 2011; Castillo et al. 2015) with minor but discernable peaks of zircons with Devonian age and few Ordovician grains (Fig. 2). Cambrian components, such as those igneous rocks in the TFIMC

and detrital components in the EAMC and CDMC, are absent. This detrital signature is consistent with a depositional setting of the DYC far from the influence of Cambrian basement rocks and tectonic evolution and recycling of Patagonian Andes metasedimentary complexes.

The Trinity Peninsula Group (TPG) in the northern Antarctic Peninsula yields a similar detrital zircon U–Pb age distribution compared to the DYC, but with the addition of pronounced Ordovician zircon populations (Hervé et al. 2006; Barbeau et al. 2010; Bradshaw et al. 2012; Castillo et al. 2015). Cobbles of Ordovician and Devonian igneous rocks are also found in Permo-Carboniferous conglomerates of the TPG (Bradshaw et al. 2012) suggesting that hidden magmatic belts, such as those identified in Patagonia, were proximal to the TPG (Fig. 7). Amphibolite-grade metamorphic rocks in Antarctic Peninsula were formed during episodic events of Ordovician, Permian, and Triassic metamorphism linked to tectono-magmatic activity in this block (cf. Pankhurst et al. 2003; Wendt et al. 2008; Riley et al. 2012).

Provenance analyses in turbidites of the DYC and TPG suggest deposition in forearc basins of the Gondwana convergent margin (Faúndez et al. 2002; Lacassie et al. 2006; Castillo et al. 2015), despite lack of known bedrock exposures of Permian igneous sources. In contrast, previous workers postulate that Permo-Triassic turbidites in Antarctic Peninsula were also deposited in a passive margin environment and/or within back-arc basins (cf. Burton-Johnson and Riley 2015). Taking this into consideration, we propose that the apparent southward jump of the magmatic activity in the region was related to the fast northward drift of the supercontinent at ~ 330 Ma that promoted the relative retreat of the continental margin and crustal extension in the supra-subduction setting with the consequent establishment of an arc and back-arc basin configuration during the Permian and Early Triassic (Fig. 7). Such as in retreating convergent margins (e.g., the modern western Pacific), contemporaneous development of passive margins, back-arc, and forearc basins are present, and this complex setting may help elucidate the variety of sedimentary environments interpreted for the western belt of the EAMC, the DYC, and the TPG. Afterward, the marginal basins were closed during the Late Triassic–Early Jurassic Chonide orogeny. Dalziel et al. (2000) proposed that this orogenic event was related to subduction of buoyant oceanic lithosphere that induced shallow flat subduction of the downgoing lithosphere.

3.3 *Jurassic-Cretaceous*

During the initial stage of Gondwana breakup, continental extension was accompanied by synrift silicic and bimodal magmatism and oceanic-type spreading in the overriding and attenuated continental crust (cf. Bruhn et al. 1978; Pankhurst et al. 2000; Stern and de Wit 2003). Paleogeographic models show that at the end of the Triassic, the southwestern Gondwana margin was NW-trending at that at 180 Ma Antarctic Peninsula was detached from southern Patagonia resulting in the

development of marginal basins separating both continental blocks, and the emplacement of the Upper Jurassic—Lower Cretaceous Rocas Verdes basin in southern Patagonia (Dalziel 1981).

During the incipient stages of the Rocas Verdes basin evolution (Fig. 8), repetitive injection of mantle-derived mafic magmas triggered high-grade metamorphism, anatexis, and granite magma generation at mid- to upper crustal levels, resulting in the generation of bimodal magmatic associations and granites (Calderón et al. 2007a, b, c). Granophyres and dacitic dikes in the Sarmiento Complex are isotopically similar to the Upper Jurassic granitoids in the South Patagonian Batholith (Fig. 6) and thus probably represent the earliest components of the composite batholith that formed during the early rifting phase of the Rocas Verdes basin evolution, in a supra-subduction setting.

The back-arc stage of the Rocas Verdes basin started once the Antarctic Peninsula microplate was translated southward in Early Cretaceous time, and subduction was re-established along the margin of southern Patagonia. Subduction activity is recorded in blueschist and epidote-amphibolite facies metamorphic rocks of the DAMC (Fig. 5), involving processes of subduction erosion and high-P/T metamorphism of the forearc segment (Willner et al. 2004). These processes were coeval with the greater extension and ocean ridge-type magmatism in the back-arc basin suggesting that both domains, the forearc and back-arc, were tectonically decoupled.

The Rocas Verdes basin started to close at the end of the Early Cretaceous (Aptian–Albian), involving underthrusting and subduction of its oceanic seafloor until Late Cretaceous time (Calderón et al. 2013), coeval with the early development of the Magallanes–Austral foreland basin signaled by distal turbiditic deposits in the sedimentary record (Fildani et al. 2003; Fosdick et al. 2011). A subduction environment for the closure of the Rocas Verdes basin has been determined in felsic schists and mylonites of the CMSZ (Hervé et al. 2007b; Calderón et al. 2012). These processes culminated with collision or accretion of the drifted magmatic arc and/or peripheral crustal blocks against the continent (Cunningham 1995; Kohn et al. 1995; Klepeis et al. 2010; Fosdick et al. 2011; Maloney et al. 2011; Calderón et al. 2012, 2013; Betka et al. 2015; Guillot 2016), in part recorded in high-P and high-T metamorphic rocks of the CDMC.

Lithospheric shortening, thickening, and resulting thrust-loading of the retroarc Patagonian fold and thrust belt caused deepening of the Magallanes–Austral foreland basin during the Late Cretaceous. The sedimentary infill of the Magallanes–Austral basin records additional detrital geochronological evidence of lower Paleozoic magmatic arc activity (Fildani and Hessler 2005; Barbeau et al. 2009; Romans et al. 2010; Fosdick et al. 2015), although variable deformation and exhumation across the magmatic arc and hinterland have obscured much of the Paleozoic outcrop record.

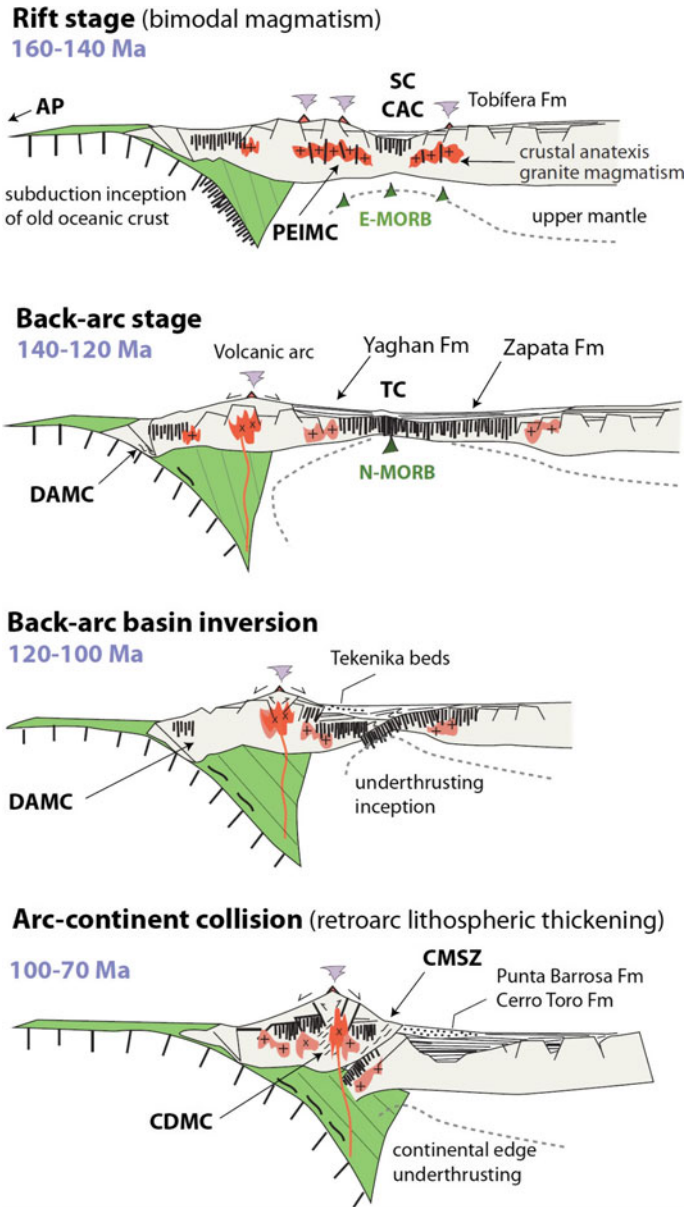


Fig. 8 Schematic reconstructions of the Jurassic to Cretaceous tectonic evolution of the Rocas Verdes basin after Calderón et al. (2013). The time span coincides with the relative separation of Antarctic Peninsula from South America. Abbreviations of metamorphic and ophiolitic complexes are presented in the caption of Figs. 1 and 4

4 Conclusions

The southern edge of South America records a complex Phanerozoic geological history related to global changes in plate configuration, including several episodes of magmatism related to crustal extension or contraction in a supra-subduction setting. Because older basins and sedimentary successions are overprinted by younger tectonic events, much of the history must be deduced from combined petrological and geochronological studies and the application of actualistic plate tectonic models and paleotectonic reconstruction models. We propose that extensional fault zones and spreading ridges, developed during breakup and/or dispersion of peripheral microplates, can evolve to transform zones, and vice versa. The closure of basins, formed within such zones of crustal weakness, causes internal deformation of the basin in-fill and formation of low- or medium-grade metamorphic complexes, with well-defined, frequently tectonically reactivated margins. Whether these zones host voluminous injections of mantle-derived magmas during continental extension, processes will contribute to the lateral growth of the continental crust and reworking via anatexis and generation of granitic magmas. An integrated four-dimensional analysis of igneous and metamorphic complexes, including ophiolites and batholiths, is necessary for more complete understanding of the entire geological evolution of the Patagonian and Antarctic regions.

Acknowledgements This contribution was supported by the CONICYT Anillo Antártico Projects (ARTG-04 and ACT-105) and by the FONDECYT projects to FH (1980741, 1010412, 7010412, 1050431) and to MC (11075000, 1161818), which allowed the study of the Patagonian Andes in recent years. Captains Conrado Alvarez, Gilles Rigaud, and Hugo Cárdenas in their boats Penguin, Foam, Explorador, Morgane, Chonos, and Marypaz II took us safely to remote areas. C. Mark Fanning has guided the SHRIMP U–Pb zircon age determinations and participated in most field campaigns. Valuable discussions and fieldwork with Elisa Ramirez, Cecilia Herrera, Augusto Rapalini, Umberto Cordani, Hans Massonne, Cristóbal Ramirez de Arellano, Bob Pankhurst, Andrea Fildani, and Brian Romans are greatly acknowledged.

References

- Allen RB (1982) Geología de la Cordillera Sarmiento, Andes Patagónicos, entre los 51°00' y 52° 15' Lat. S, Magallanes, Chile. Servicio Nacional de Geología y Minería, Boletín 38:1–46
- Augustsson C, Bahlburg H (2003) Active or passive continental margin? Geochemical and Nd isotope constraints of metasediments in the backstop of a pre-Andean accretionary wedge in southernmost Chile (46°30'–48°30'S). *Geol Soc London Spec Publ* 208:253–268
- Augustsson C, Münker C, Bahlburg H, Fanning CM (2006) Provenance of late Palaeozoic metasediments of the SW South American Gondwana margin: a combined U–Pb and Hf-isotope study of single detrital zircons. *Geol Soc London* 163:983–995
- Augustsson C, Bahlburg H (2008) Provenance of late Palaeozoic metasediments of the Patagonian proto-Pacific margin (southernmost Chile and Argentina). *Int J Earth Sc* 97:71–88
- Avendaño V (2008) Petrología del Complejo Ofiolítico Tortuga, Magallanes Chile: evidencias de un metamorfismo Cretácico Inferior. Graduation thesis, Departamento de Geología, Universidad de Chile, 128 p

- Barbeau DL, Olivero EB, Swanson-Hysell NL, Zahid KM, Murray KE, Gehrels GE (2009) Detrital-zircon geochronology of the eastern Magallanes foreland basin: implications for Eocene kinematics of the northern Scotia Arc and Drake Passage. *Earth Planet Sc Lett* 284:489–503
- Barbeau DL, Davis JT, Murray KE, Valencia V, Gehrels GE, Zahid KM, Gombosi J (2010) Detrital-zircon geochronology of the metasedimentary rocks of northwestern Graham Land. *Antarctic Sci* 22:65–78
- Betka P, Klepeis K, Mosher S (2015) Along-strike variation in crustal shortening and kinematic evolution of the base of a retroarc fold and thrust belt: Magallanes, Chile 53°S–54°S. *Geol Soc Am Bull* B31130-1
- Bradshaw JD, Vaughan APM, Millar IL, Flowerdew MJ, Trouw RAJ, Fanning CM, Whitehouse MJ (2012) Permo-Carboniferous conglomerates in the Trinity Peninsula Group at View Point, Antarctic Peninsula: sedimentology, geochronology and isotope evidence for provenance and tectonic setting in Gondwana. *Geol Mag* 149(4):626–644
- Bruhn RL, Stern CR, de Wit MJ (1978) Field and geochemical data bearing on the development of a Mesozoic volcano-tectonic rift zone and back-arc basin in southernmost South America. *Earth Planet Sci Lett* 41:32–46
- Burton-Johnson A, Riley TR (2015) Autochthonous v. accreted terrane development of continental margins: a revised in situ tectonic history of the Antarctic Peninsula. *Geol Soc London* 172:822–835
- Calderón M (2000) Metamorfismo de contacto en el margen oriental del batolito Sur-Patagónico (48°–50°30'S), Magallanes, Chile. Graduation thesis, Departamento de Geología, Universidad de Chile, 70 pp
- Calderón M (2006) Petrogenesis and tectonic evolution of Late Jurassic bimodal magmatic suites (Sarmiento Complex) and migmatites (Puerto Edén Igneous Metamorphic Complex) in the Southern Patagonian Andes, Chile. Doctoral thesis, Universidad de Chile, Santiago
- Calderón M, Fildani A, Hervé F, Fanning CM, Weislogel A, Cordani U (2007a) Late Jurassic bimodal magmatism in the northern seafloor remnant of the Rocas Verdes basin, Southern Patagonian Andes. *Geol Soc London* 164:1011–1022
- Calderón M, Hervé F, Massonne H-J, Tassinari CG, Pankhurst RJ, Godoy E, Theye T (2007b) Petrogenesis of the Puerto Eden Igneous and Metamorphic Complex, Magallanes, Chile: late Jurassic anatexis of meta-greywackes and granitoid magma genesis. *Lithos* 93:17–38
- Calderón M, Hervé F, Cordani U, Massonne H-J (2007c) Crust-Mantle interactions and the generation of silicic melts: insights from the Sarmiento Complex, southern Patagonian Andes. *Rev Geol Chile* 34:249–275
- Calderón M, Fosdick JC, Warren C, Massonne H-J, Fanning CM, Fadel Cury L, Schwanethal J, Fonseca PE, Galaz G, Gaytán D, Hervé F (2012) The low-grade Canal de las Montañas Shear Zone and its role on the tectonic emplacement of the Sarmiento Ophiolitic Complex and Late Cretaceous Patagonian Andes orogeny, Chile. *Tectonophysics* 524–525:165–185
- Calderón M, Prades CF, Hervé F, Avendaño V, Fanning CM, Massonne H-J, Theye T, Simonetti A (2013) Petrological vestiges of Late Jurassic-Early Cretaceous transition from rift to back-arc basin in southernmost Chile: new age and geochemical data from the Capitán Aracena, Carlos III and Tortuga Ophiolitic complexes. *Geoch J* 47:201–217
- Castillo P, Fanning CM, Hervé F, Lacassie JP (2015) Characterisation and tracing of Permian magmatism in the south-western segment of the Gondwana margin; U–Pb age, Lu–Hf and O isotopic compositions of detrital zircons from metasedimentary complexes of northern Antarctic Peninsula and western Patagonia. *Gondwana Res* (in press)
- Cawood PA (2005) Terra Australis Orogen: Rodinia breakup and development of the Pacific and Iapetus margins of Gondwana during the Neoproterozoic and Paleozoic. *Earth Sci Rev* 69:249–279
- Cunningham WD (1994) Uplifted ophiolitic rocks on Isla Gordon, southernmost Chile: implications for the closure history of the Rocas Verdes marginal basin and the tectonic evolution of the Beagle Channel region. *J South Am Earth Sci* 7:135–147

- Cunningham WD (1995) Orogenesis at the southern tip of the Americas: the structural evolution of the Cordillera Darwin metamorphic complex, southernmost Chile. *Tectonophysics* 244:197–229
- Dalziel IWD, de Wit MJ, Palmer KF (1974) Fossil marginal basin in the southern Andes. *Nature* 250:291–294
- Dalziel IWD (1981) Back-arc extension in the southern Andes: a review and critical reappraisal. *Philos T Roy Soc A* 300:319–335
- Dalziel IWD, Brown RL (1989) Tectonic denudation of the Darwin metamorphic core complex in the Andes of Tierra del Fuego, southernmost Chile: implications for Cordilleran orogenesis. *Geology* 17:699–703
- Dalziel IWD, Lawver LA, Murphy JB (2000) Plumes, orogenesis, and supercontinental fragmentation. *Earth Planet Sci Lett* 178:1–11
- Davidson J, Mpodozis C, Godoy E, Hervé F, Muñoz N (1989) Jurassic accretion of a high buoyancy guyot in southernmost South America: the Diego Ramírez Islands. *Rev Geol Chile* 16:247–251
- Dott RH, Winn RD, de Wit MJ, Bruhn RL (1977) Tectonic and sedimentary significance of Cretaceous Tekenika Beds of Tierra del Fuego. *Nature* 266:620–622
- Douglass RC, Nestell MK (1976) Late Paleozoic foraminifera from Southern Chile. *US Geological Survey Special Paper* 858, 49 pp
- Eagles G (2016) Tectonic reconstructions of the southernmost Andes and the Scotia Sea during the opening of the Drake Passage. In: Ghiglione MC (ed) *Geodynamic Evolution of the Southernmost Andes*. Springer Earth System Sciences, pp 75–108
- Elthon D, Stern CR (1978) Metamorphic petrology of the Sarmiento ophiolite complex, Chile. *Geology* 6:464–468
- Ernst WG (2009) Subduction-zone metamorphism, calc-alkaline magmatism, and convergent-margin crustal evolution. *Gondwana Res* 18:8–16
- Fang Z, Boucot A, Covacevich V, Hervé F (1998) Discovery of late Triassic fossils in the Chonos Metamorphic Complex, southern Chile. *Rev Geol Chile* 25:165–173
- Fanning CM, Hervé F, Pankhurst RJ, Rapela CW, Kleiman LE, Yaxley GM, Cas-tillo P (2011) Lu–Hf isotope evidence for the provenance of Permian detritus in accretionary complexes of western Patagonia and the northern Antarctic Peninsula region. *J South Am Earth Sci* 32:485–496
- Faúndez V, Hervé F, Lacassie JP (2002) Provenance studies of prelate Jurassic metaturbidite successions of the Patagonian Andes, southern Chile. *N Z J Geol Geophys* 45:411–425
- Fildani A, Hessler AM (2005) Stratigraphic record across a retroarc basin inversion: Rocas Verdes–Magallanes basin, Patagonian Andes, Chile. *Geol Soc Am Bull* 117:1596–1614
- Fildani A, Cope TD, Graham SA, Wooden JL (2003) Initiation of the Magallanes foreland basin: timing of the southernmost Patagonian Andes orogeny revised by detrital zircon provenance analysis. *Geology* 31:1081–1084
- Forsythe R (1981) Geological investigations of pre-Late Jurassic terranes in the Southernmost Andes. *Doctoral thesis, Columbia University*, 298 pp
- Forsythe R (1982) The late Paleozoic and early Mesozoic evolution of southern South America: a plate tectonic interpretation. *Geol Soc London* 139:671–682
- Forsythe R, Allen RB (1980) The basement rocks of Península Staines, Región XII, Province of Última Esperanza, Chile. *Rev Geol Chile* 10:3–15
- Forsythe RD, Mpodozis C (1979) El Archipiélago de Madre de Dios, Patagonia Occidental, Magallanes: rasgos generales de la estratigrafía y estructura del basamento pre-Jurásico Superior. *Rev Geol Chile* 7:13–29
- Forsythe RD, Mpodozis C (1983) Geología del Basamento pre-Jurásico Superior en el Archipiélago Madre de Dios, Magallanes, Chile. *Servicio Nacional de Geología y Minería, Boletín* 39, 63 p
- Fosdick JC, Romans BW, Fildani A, Bernhardt A, Calderón M, Graham SA (2011) Kinematic evolution of the Patagonian retroarc fold-thrust belt and Magallanes foreland basin, Chile and Argentina, 51°30'S. *Geol Soc Am Bull* 123:1679–1698

- Fosdick JC, Grove M, Graham SA, Hourigan JK, Lovera O, Romans BW (2015) Detrital thermochronologic record of foreland burial heating, sedimentary provenance, and orogenesis in Patagonia. *Basin Res* 27:546–572
- Godoy E (1978) Observaciones en el Complejo Ofiolítico de Isla Milne Edwards-Cerro Tortuga (Isla Navarino) Magallanes-Chile. VII Congreso Geológico Argentino, Neuquén, Actas, II:625–636
- Guillot MG (2016) Magmatic evolution of the southernmost Andes and its relation with subduction processes. In: Ghiglione MC (ed) *Geodynamic Evolution of the Southernmost Andes*. Springer Earth System Sciences, pp 37–74
- Hervé F, Fanning CM (2000) Late Triassic zircons in meta-turbidites of the Chonos Metamorphic Complex, southern Chile. *Rev Geol Chile* 28:91–104
- Hervé F, Fanning CM (2003) Early Cretaceous subduction of continental crust at the Diego de Almagro archipelago, Southern Chile. *Episodes* 26:285–289
- Hervé F, Nelson E, Kawashita K, Suárez M (1981a) New isotopic ages and the timing of orogenic events in the Cordillera Darwin, southernmost Chilean Andes. *Earth Planet Sci Lett* 55:257–265
- Hervé F, Mpodozis C, Davidson J, Godoy E (1981b) Observaciones estructurales y petrográficas en el basamento metamórfico del Archipiélago de los Chonos entre el Canal King y el Canal Ninualac, Aisén. *Rev Geol Chile* 13(14):3–16
- Hervé M, Suárez M, Puig A (1984) The Patagonian batholith S of Tierra del Fuego, Chile: timing and tectonic implications. *Geol Soc London* 141:909–917
- Hervé F, Aguirre L, Godoy E, Massonne H-J, Morata D, Pankhurst RJ, Ramírez E, Sepúlveda V, Willner A (1998) Nuevos antecedentes acerca de la edad y las condiciones P-T de los Complejos Metamórficos en Aysén, Chile. X Congreso Latinoamericano de Geología, Buenos Aires, II:134–137
- Hervé F, Prior D, López G, Ramos VA, Rapalini A, Thomson S, Lacassie JP, Fanning CM (1999) Mesozoic blueschists from Diego de Almagro, Southern Chile. II South American Symposium on Isotope Geology, Córdoba, Actas, (Extended Abstract):318–321
- Hervé F, Fanning CM, Pankhurst RJ (2003) Detrital zircon age patterns and provenance in the metamorphic complexes of Southern Chile. *J South Am Earth Sci* 16(107):123
- Hervé F, Miller H, Pimpirev C (2006) Patagonia-Antarctica connections before Gondwana break-up. In: Fütterer DK, Dmaske D, Kleinschmidt G, Miller H, Tessensohn F (eds) *Antarctica: contributions to global earth sciences*. Springer, Berlin, Heidelberg, New York, pp 217–228
- Hervé F, Pankhurst RJ, Fanning CM, Calderón M, Yaxley GM (2007a) The South Patagonian batholith: 150 my of granite magmatism on a plate margin. *Lithos* 97:373–394
- Hervé F, Massonne H-J, Calderón M, Theye T (2007b) Metamorphic PT conditions of Late Jurassic rhyolites in the Magallanes fold and thrust belt, Patagonian Andes, Chile. *J Iberian Geol* 33:5–16
- Hervé F, Calderón M, Faundez V (2008) The metamorphic complexes of the Patagonian and Fueguian Andes. *Geol Acta* 6:43–53
- Hervé F, Calderón M, Fanning CM, Kraus S, Pankhurst RJ (2010a) SHRIMP chronology of the Magallanes basin basement, Tierra del Fuego: Cambrian plutonism and Permian high-grade metamorphism. *Andean Geology* 37(2):253–275
- Hervé F, Fanning CM, Pankhurst RJ, Mpodozis C, Klepeis K, Calderón M, Thomson SN (2010b) Detrital zircon SHRIMP U–Pb age study of the Cordillera Darwin Metamorphic Complex of Tierra del Fuego: sedimentary sources and implications for the evolution of the Pacific margin of Gondwana. *Geol Soc London* 167:555–568
- Hyppolito T (2010) Termobarometria, evolução tectono-metamórfica, e geoquímica de xistos azuis, rochas eclogíticas e litotipos associados da ilha Diego de Almagro, Patagônia Chilena. Master Thesis, Instituto de Geociências, Universidade de São Paulo, São Paulo.
- Jokat W, Boebel T, König M, Meyer U (2003) Timing and geometry of early Gondwana breakup. *J Geophys Res* 108:2428

- Katz HR (1964) Some new concepts on geosynclinal development and mountain building at the southern end of South America. In: Proceedings of 22nd international geological congress, India New Delhi. vol 4, pp 242–255
- Klepeis K, Betka P, Clarke G, Fanning CM, Hervé F, Rojas L, Mpodozois C, Thomson SN (2010) Continental underthrusting and obduction during the Cretaceous closure of the Rocas Verdes rift basin, Cordillera Darwin, Patagonian Andes. *Tectonics* 29:TC3014
- Kohn MJ, Spear F, Dalziel IWD (1993) Metamorphic P–T paths from Cordillera Darwin, a core complex in Tierra del Fuego, Chile. *J Petrol* 34:519–542
- Kohn MJ, Spear FS, Harrison TM, Dalziel IWD (1995) 40Ar/39Ar geochronology and P–T–t paths from the Cordillera Darwin Metamorphic Complex, Tierra del Fuego, Chile. *J Metam Geol* 13:251–270
- Lacassie JP (2003) Estudio de la Proveniencia Sedimentaria de los Complejos Metamórficos de los Andes Patagónicos (46°–51°S), mediante la aplicación de redes neuronales e isótopos estables. Doctoral thesis, Universidad de Chile, 119 pp
- Lacassie JP, Hervé F, Roser B (2006) Sedimentary provenance study of the post–Early Permian to pre–early cretaceous metasedimentary duque de York Complex, Chile. *Rev Geol Chile* 33:199–219
- Lagally U (1975) Geologische Untersuchungen im Gebiet Lake General Carrera - Lake Cochrane, Prov. Aysen/Chile unter besonderer Berücksichtigung des Grundgebirges und seiner tektonik. Doctoral thesis, Universität München, 143 pp
- Ling HY, Forsythe RD, Douglass CR (1985) Late Paleozoic microfaunas from southernmost Chile and their relation to Gondwanaland forearc development. *Geology* 13:357–360
- Malkowski MA, Grove M, Graham SA (2015) Unzipping the Patagonian Andes—Long-lived influence of rifting history on foreland basin evolution. *Lithosphere*. doi:10.1130/L489.1
- Maloney KT, Clarke GL, Klepeis KA, Fanning CM, Wang W (2011) Crustal growth during back–arc closure: cretaceous exhumation history of Cordillera Darwin, southern Patagonia. *J Metam Geol* 29:649–672
- Mantle GW, Collins WJ (2008) Quantifying crustal thickness variations in evolving orogens: correlation between arc basalt composition and Moho depth. *Geology* 36:87–90
- Millar IL, Pankhurst RJ, Fanning CM (2002) Basement chronology of the Antarctic Peninsula: recurrent magmatism and anatexis in the Palaeozoic Gondwana margin. *Geol Soc London* 159:145–157
- Miller CA, Barton M, Hanson R, Flemming T (1994) An Early Cretaceous volcanic arc–marginal basin transition zone, Peninsula Hardy, southernmost Chile. *J Volc Geoth Res* 63:33–58
- Moreira P, Fernández R, Hervé F, Fanning CM, Schalamuk IA (2013) Detrital zircons U–Pb SHRIMP ages and provenance of La Modesta Formation, Patagonia Argentina. *J South Am Earth Sci* 47:32–46
- Nelson E, Dalziel IWD, Milnes AG (1980) Structural geology of the Cordillera Darwin: collision style orogenesis in the southernmost Chilean Andes. *Eclogae Geologicae Helveticae* 73:727–751
- Olivares B, Cembrano J, Hervé F, López G, Prior D (2003) Geometría y cinemática de la Zona de Cizalle Seno Arcahué, Andes patagónicos, Chile. *Rev Geol Chile* 30:39–52
- Otzen G (1987) Geología Regional de la isla Capitán Aracena y Clarence, Magallanes, Chile. Informe Técnico ENAP (inédit report)
- Pankhurst RJ, Weaver SD, Hervé F, Larrondo P (1999) Mesozoic–Cenozoic evolution of the North Patagonian Batholith in Aysén, Southern Chile. *Geol Soc London* 156:673–694
- Pankhurst RJ, Riley TR, Fanning CM, Kelley SP (2000) Episodic silicic volcanism in Patagonia and the Antarctic Peninsula: Chronology of magmatism associated with the break-up of Gondwana. *J Petrol* 41:603–625
- Pankhurst RJ, Rapela CW, Loske WP, Márquez M, Fanning CM (2003) Chronological study of the pre-Permian basement rocks of southern Patagonia. *J South Am Earth Sci* 16:27–44
- Pankhurst RJ, Rapela CW, Fanning CM, Márquez M (2006) Gondwanide continental collision and the origin of Patagonia. *Earth Sci Rev* 76:235–257

- Parra F (2015) Análisis de proveniencia y ambiente de sedimentación de las unidades sedimentarias de la isla Diego de Almagro (51°30'S). Graduation thesis, Departamento de Geología, Universidad de Chile, 85 pp
- Permuy Vidal C, Moreira P, Guido DM, Fanning CM (2014) Linkages between the southern Patagonia pre-Permian basements: new insights from detrital zircons U-Pb SHRIMP ages from the Cerro Negro District. *Geol Acta* 12:137–150
- Pimpirev C, Miller H, Hervé F (1999) Preliminary results on the lithofacies and palaeoenvironmental interpretation of the Paleozoic turbidite sequence in Chonos Archipiélago, Southern Chile. *Comunicaciones* 48–49:3–12
- Prades CF (2008) Petrología y metamorfismo de las rocas basálticas en la isla Capitán Aracena, isla Carlos III y Estero La Pera, Region de Magallanes, Chile. Graduation thesis, Departamento de Geología, Universidad de Chile, 135 p
- Quezada A (2010) Proveniencia sedimentaria y ambiente deposicional de unidades atribuidas a los complejos Duque de York y Denaro, Patagonia XII Región, Chile. Graduation thesis, Departamento de Geología, Universidad de Chile, 126 pp
- Ramírez-Sánchez E (2002) Geotermobarometría en metapelitas de complejos metamórficos de Aysen, Chile. Doctoral thesis, Universidad de Chile, 143 pp
- Ramírez-Sánchez E, Hervé F, Kelm U, Sassi R (2005) P–T conditions of metapelites from metamorphic complexes in Aysen, Chile. *J South Am Earth Sci* 19:373–386
- Ramos V (2010) The Grenville-age basement of the Andes. *J South Am Earth Sci* 29:77–91
- Rapalini AE, Calderón M, Singer S, Hervé F, Cordani U (2008) Tectonic implications of a paleomagnetic study of the Sarmiento Ophiolitic Complex, southern Chile. *Tectonophysics* 452:29–41
- Riley TR, Flowerdew MJ, Whitehouse MJ (2012) U–Pb ion-microprobe zircon geochronology from the basement inliers of eastern Graham Land, Antarctic Peninsula. *Geol Soc London* 169:381–393
- Romans BW, Fildani A, Graham SA, Hubbard SM, Covault JA (2010) Importance of predecessor basin history on sedimentary fill of a retroarc foreland basin: provenance analysis of the Cretaceous Magallanes basin, Chile (50°52'S). *Basin Res* 22:640–658
- Saunders AD, Tarney J, Stern CR, Dalziel IWD (1979) Geochemistry of Mesozoic marginal basin floor igneous rocks from southern Chile. *Geol Soc Am Bull* 90:237–258
- Schilling M, Conceição RV, Mallmann G, Koester E, Kawashita K, Hervé F, Mo-rata D, Motoki A (2005) Spinel-facies mantle xenoliths from Cerro Redondo, Argentine Patagonia: petrographic, geochemical, and isotopic evidence of interaction between xenoliths and host basalt. *Lithos* 82:485–502
- Sepúlveda FA (2004) Metamorfismo de bajo grado en rocas del Complejo Denaro, archipiélago Madre de Dios, XII Región. Graduation thesis, Departamento de Geología, Universidad de Chile, 49 pp
- Sepúlveda FA, Hervé F, Calderón M, Lacassie JP (2008) Petrology of igneous and metamorphic units from the allochthonous Madre de Dios Terrane, Magallanes, Chile. *Gondwana Res* 13:238–249
- Sepúlveda FA, Palma-Heldt S, Hervé F, Fanning CM (2010) Permian depositional age of metaturbidites of the Duque de York Complex, southern Chile: U-Pb SHRIMP data and palynology. *Andean Geol* 37:375–397
- Sernageomin (2003) Mapa Geológico de Chile: versión digital. publicación geológica digital, No. 4, 2003. CDRom, versión 1.0, 2003. Base Geológica escala 1:1.000.000. Gobierno de Chile, Servicio Nacional de Geología y Minería, Subdirección Nacional de Geología
- Söllner F, Miller H, Hervé M (2000) An Early Cambrian granodiorite age from the pre-Andean basement of Tierra del Fuego (Chile): the missing link between South America and Antarctica? *J South Am Earth Sci* 13:163–177
- Spear FS, Kohn MJ, Cheney JT (1999) P–T paths from anatexis pelites. *Contrib Miner Petrol* 134:17–32
- Stern CR (1979) Open and closed system igneous fractionation within two Chilean ophiolites and the tectonic implications. *Contrib Miner Petrol* 68:243–258

- Stern CR (1980) Geochemistry of Chilean ophiolites: evidence for the compositional evolution of the mantle source of back-arc basin basalts. *J Geophys Res* 85:955–966
- Stern CR (1991) Isotopic composition of Late Jurassic and Early Cretaceous mafic igneous rocks from the Southernmost Andes: implications for sub-Andean mantle. *Rev Geol Chile* 18:15–23
- Stern CR, de Wit MJ (2003) Rocas Verdes ophiolites, southernmost South America: remnants of progressive stages of development on oceanic-type crust in a continental margin back-arc basin. In: Dilek Y, Robinson PT (eds) *Ophiolites in earth history*, vol 218, pp 1–19 (Geol Soc London Sp Pub)
- Stern CR, de Wit MJ, Lawrence JR (1976) Igneous and metamorphic processes associated with formation of Chilean ophiolites and their implications for ocean floor metamorphism, seismic layering and magnetism. *J Geophys Res* 81:4370–4380
- Suárez M, Pettigrew TH (1976) An upper Mesozoic Island-arc-back-arc system in the southern Andes and South Georgia. *Geol Mag* 113:305–328
- Sun S, McDonough W (1989) Chemical and isotopic systematics of oceanic basalts: implications for mantle composition and processes. *Geol Soc London Spec Publ* 42:313–345
- Thomson SN, Hervé F (2002) New time constraints for the age of metamorphism at the ancestral Pacific Gondwana margin of Southern Chile. *Rev Geol Chile* 29:255–271
- Valdés A (2005) Petrología de la aureola metamórfica de contacto del plutón monzogranítico Río Murta, XI región de Aysén, Chile. Graduation thesis, Universidad de Concepción, 143 pp
- Watters W (1964) Geological work at Puerto Edén, Wellington Island, southern Chile. *Transac Roy Soc NZ (Geology)* 2:155–168
- Wendt AS, Vaughan APM, Tate A (2008) Metamorphic rocks in the Antarctic Peninsula region. *Geol Mag* 145:655–676
- Willner A, Hervé F, Massonne H-J (2000) Mineral chemistry and pressure–temperature evolution of two contrasting high-pressure–low-temperature belts in the Chonos Archipelago, Southern Chile. *J Petrol* 4:309–330
- Willner AP, Hervé F, Thomson SN, Massonne H-J (2004) Converging PT-paths of Mesozoic HP-LT metamorphic units (Diego de Almagro Island, Southern Chile, 51°30'S): evidence for juxtaposition during late shortening of an active continental margin. *Miner Petrol* 81:43–84
- Willner AP, Sepúlveda FA, Hervé F, Massonne H-J, Sudo M (2009) Conditions and timing of pumpellyite–actinolite-facies metamorphism in the Early Mesozoic frontal accretionary prism of the Madre de Dios Archipelago (Latitude 50°20'S; Southern Chile). *J Petrol* 50:2127–2155
- Wilson TJ, Hanson RE, Grunow AM (1989) Multistage melange formation within an accretionary complex, Diego Ramírez Islands, Southern Chile. *Geology* 17:11–14

Magmatic Evolution of the Southernmost Andes and Its Relation with Subduction Processes

Mauricio González Guillot

Abstract The magmatic arc in the southernmost Andes is represented by the Fuegian Batholith and satellite plutons, plus minor volcanic and volcanoclastic sequences. Magmatism was active from the Late Jurassic to the Miocene in response to subduction of the Pacific plates beneath South America. The batholith was constructed episodically and includes a calc-alkaline trench-side arc and shoshonitic rear-arc suites. The oldest components are minor S-like granitoids; recent volcanism is very scarce. The volcanic front shifted, and the composition of magmas changed several times due to a variable subduction configuration. Major tectonic events included the opening and closure of the Rocas Verdes marginal basin in the Jurassic–Cretaceous and oroclinal bending during the latest Cretaceous–Paleogene. A well-established slab shallowing event initiated in the mid-Cretaceous, causing a cratonward migration of the volcanic front, the widening of the arc, and inception of potassic magmatism in the rear-arc. This event was associated with marginal basin inversion, regional peak metamorphism, and orogenic deformation. Different timing and position of rear-arc suites with respect to the volcanic front in the Fuegian and Southern Patagonian Andes may have been influenced by differential development of the marginal basin, which was wider to the south. The vanishing of magmatism in the Miocene may have responded to highly oblique convergence plus buoyant subduction.

Keywords Fuegian Batholith · Patagonian Batholith · Trench-side arc · Rear-arc · Subduction parameters · Fuegian Andes · Rocas Verdes basin

M.G. Guillot (✉)
Centro Austral de Investigaciones Científicas CADIC-CONICET,
and Instituto de Ciencias Polares, Ambiente y Recursos Naturales,
Universidad Nacional de Tierra del Fuego, Tierra del Fuego, Ushuaia, Argentina
e-mail: g_guillot@cadic-conicet.gob.ar

1 Introduction

The Fuegian Andes constitutes the segment of the Andean Cordillera that runs east–west at the southernmost tip of South America (Fig. 1). The Mesozoic–Cenozoic magmatic arc that forms part of this belt encompasses several suites related to subduction of the Pacific plates beneath South America.

The main arc is composed of calc-alkaline plutons that make up the bulk of the Fuegian Batholith, along with volcanic rocks of the Hardy and Packsaddle Formations (Fig. 1) (Hervé et al. 1984; Puig et al. 1984; Suárez et al. 1985; Miller et al. 1994). To the rear-arc in Tierra del Fuego, small isolated, shoshonitic plutons crop out, grouped in the Fuegian Potassic Magmatism (FPM) (González Guillot et al. 2009), and other minor high-K, calc-alkaline hypabyssal intrusions, the Ushuaia Peninsula Andesites (UPA) (González Guillot et al. 2011). The main arc and rear-arc units represent magmas generated in a trench-side and back-arc side, respectively, similar to those formed in dual volcanic chains (c.f. Tatsumi and Eggins 1995).

The construction of the batholithic backbone was episodic in both the Fuegian and Patagonian Andes (e.g., Hervé et al. 2007a, 1984). However, while magmatism on the latter remained approximately on the same general axis (Hervé et al. 2007a), the Fuegian Batholith is wider and registers a more evident shift of the volcanic front during time (Hervé et al. 1984) as a consequence of changing subduction parameters. For instance, in the mid-Cretaceous, an episode of slab flattening took place (Stern et al. 1991; Stern and De Wit 2003; González Guillot et al. 2009, 2011) which produced a landward migration of the calc-alkaline volcanic front and the inception of potassic, rear-arc magmatism (Fig. 1). This process was associated with crustal deformation during the closure of the Rocas Verdes marginal basin (e.g., Dalziel et al. 1974; Stern et al. 1991). Accordingly, Folguera and Ramos (2011) proposed that events of slab flattening and steepening of the subducted plate have been repetitive along discrete sectors in the southernmost Andes since the last 100 Myr.

Hence, the Fuegian Andes provides an excellent scenario to study across-arc chemical and temporal variations of magmatic rocks in continental arc settings, from calc-alkaline units at the volcanic front, to potassic plutons at the farthest rear-arc. It has the additional attribute of a marginal basin developed during the early stages of arc construction. However, no thorough research on the evolution of arc magmatism has been done so far in this segment of the Andes, mainly because of the remoteness and inaccessibility of the region.

Fig. 1 Regional geological map of Tierra del Fuego and South Patagonia. Abbreviations: *MFFS* ► Magallanes–Fagnano fault system, *FTB* fold and thrust belt front, *B* Burney volcano, *C* Cook volcano, *PA* Punta Arenas, *P* Porvenir, *RG* Río Grande, *U* Ushuaia. The numbers refer to rear-arc intrusions: 1 and 2 UPA at Ushuaia Peninsula and Trapecio Hill, respectively, 3–6 FPM plutons: Ushuaia (3), Moat (4), Jeu-Jepén (5), and Kranck (6). 7 corresponds to a monzonitic pluton correlated with the FPM. *Sources* Hervé et al. (1984), Suárez et al. (1985), Sernageomin (2003), Olivero and Malumián (2007), González Guillot et al. (2009), Anguita (2010), Klepeis et al. (2010), and McAtamney et al. (2011). The *black dots* and *white squares* and *diamonds* are from Hervé et al. (2007a)

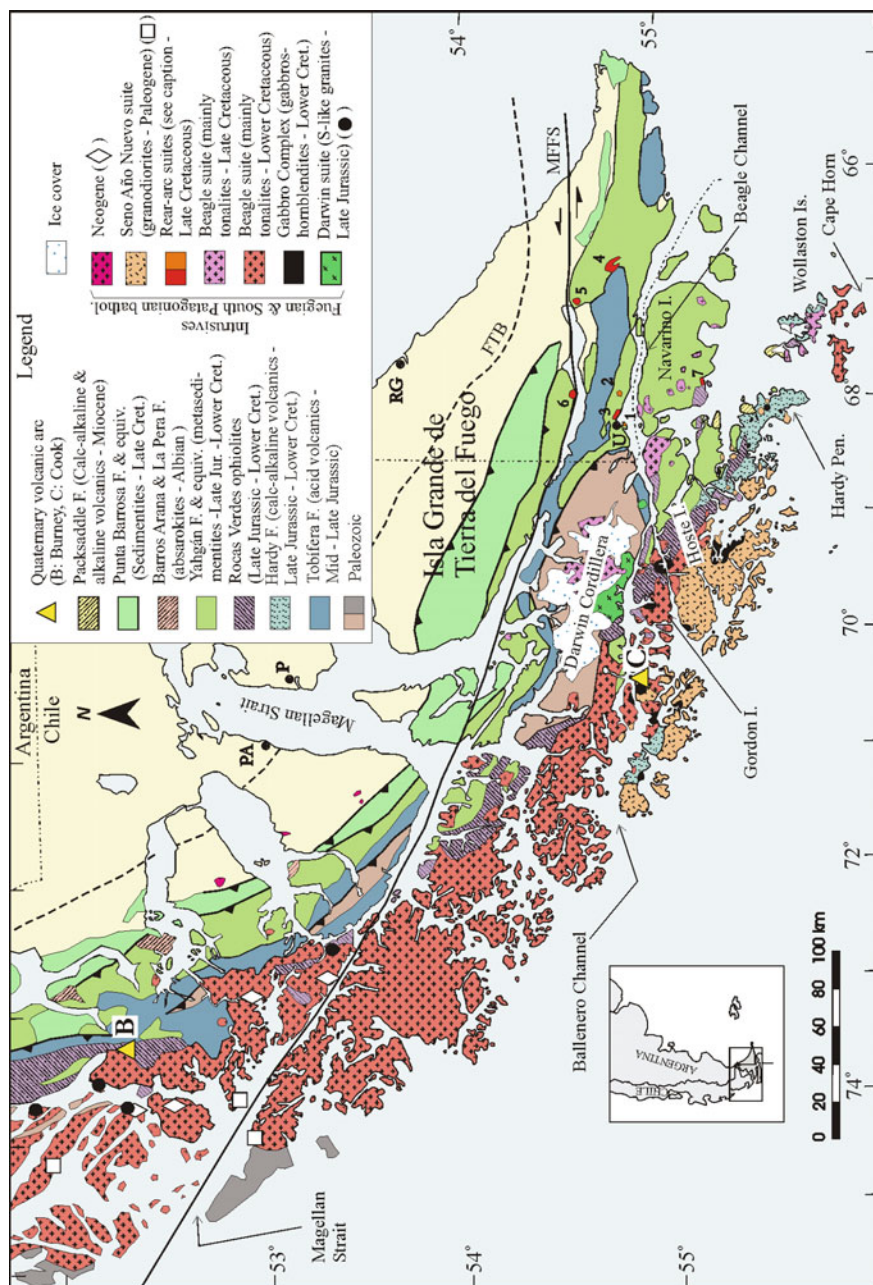


Table 1 List of abbreviations used in the text

FB	Fuegian Batholith
MPF	Fuegian Potassic Magmatism
PB	Patagonian Batholith
SPB	Southern Patagonian Batholith
UPA	Ushuaia Peninsula Andesites

This paper reviews the major geological and geochemical features of the Fuegian Batholith and satellite plutons, compares them with the Southern Patagonian Batholith, and discusses some of the implications of changing subduction parameters and marginal basin inversion to magma genesis, emplacement, and differentiation. Additionally, new interpretations on the timing and tectonic setting during rear-arc magmatism are provided, in light of the new U/Pb zircon ages available. The abbreviations used in this chapter are listed in Table 1.

2 Regional Geology

The southernmost Andes are characterized by several magmatic episodes occurred since mid-Mesozoic times (see Fig. 1 for location of lithological units). Remnants of a conspicuous bimodal volcanic province are present in the surface and sub-surface between Patagonia and the Antarctic Peninsula, the Chon Aike–West Antarctica large igneous province (Pankhurst et al. 1998). The volcanic rocks are mainly rhyolites and basalts, but flows of intermediate composition are also present. In Tierra del Fuego, this magmatism is represented by the Upper Jurassic–Lower Cretaceous Tobifera or Lemaire Formation and includes effusive, pyroclastic, and epiclastic facies (Bruhn et al. 1978; Hanson and Wilson 1991; Olivero and Malumián 2007; González Guillot et al. 2016). This volcanic event represents the culmination of widespread extensional deformation that began in the Late Triassic or Early Jurassic and led to the formation of a number of basins in southern South America and ultimately to the fragmentation of Gondwana (Kay et al. 1989).

The extension led to the development of the ensialic, Upper Jurassic–Lower Cretaceous Rocas Verdes marginal basin, floored by oceanic-type mafic rocks, along a narrow strip bordering the continental margin between 51°S and 56°S (Dalziel et al. 1974; Suárez 1977b; Saunders et al. 1979; Stern 1979, 1980; Stern and De Wit 2003; Calderón et al. 2007, 2016). Remnants of the Rocas Verdes basin are also found in South Georgia Island (Alabaster and Storey 1990; Storey and Alabaster 1991; Mukasa and Dalziel 1996), although a direct correlation with the southernmost Andes is motive of debate (see Eagles 2016 for a discussion on the subject). Further to the south, the oceanic floor may have been linked to the Weddell Sea (de Wit 1977; Grunow 1993; Mukasa and Dalziel 1996; Barker 2001).

The magmatic arc is represented by the Patagonian and Fuegian batholiths and the Hardy Formation volcanics (Suárez et al. 1985; Miller et al. 1994; Hervé et al. 2007a). Other scarce volcanic units in Tierra del Fuego, the Miocene Packsaddle

Formation and the Recent Cook deposits, are also related to subduction (Puig et al. 1984; Suárez et al. 1985). The Packsaddle volcanics include calc-alkaline (21 Ma) and alkaline (18 Ma) terms.

The Hardy Formation consists of Upper Jurassic–Lower Cretaceous pyroclastic and volcanoclastic rocks and lavas of calc-alkaline affinity (Suárez et al. 1985; Miller et al. 1994). Toward the back-arc, this unit interfingers with the contemporaneous Yahgán Formation (Fig. 1), which represents the volcanoclastic infill of the marginal basin (Suárez and Pettigrew 1976). Northward, the Yahgán Formation is laterally replaced by black mudstones of the Beauvoir-La Paciencia Formations (Olivero and Martinioni 2001; Olivero and Malumián 2007).

The PB extends from 39°S to 56°S and is usually subdivided into three segments: the North Patagonian Batholith, north of 46°30'S, the Southern Patagonian Batholith (SPB, 46°30'–53°00'S), and the Fuegian Batholith (FB), south of 53°S. The FB and SPB were emplaced episodically between 157 and 15 Ma (Halpern 1973; Hervé et al. 1984, 2007a; Suárez et al. 1985, 1986; Bruce et al. 1991; Martin et al. 2001), while the locus of magmatism changed many times during its construction.

The closure of the marginal basin encompassed crustal deformation, peak regional metamorphism, and uplift (Dalziel et al. 1974; Dott et al. 1977; Bruhn 1979; Hervé et al. 1981; Nelson 1982; Dalziel 1986; Cunningham 1995). Several authors (e.g., Gealey 1980; Nelson et al. 1980; Dalziel 1981; Cunningham 1995; Kraemer 2003; Fildani and Hessler 2005; Galaz et al. 2005; Hervé et al. 2007b) suggested, and recently Klepeis et al. (2010) and Maloney et al. (2011) emphasized, a model of basin inversion by underthrusting of the leading edge of the continent under the magmatic arc, while subduction of the proto-Pacific margin under South America was still active. This occurred prior to 86 Ma in Cordillera Darwin (Klepeis et al. 2010) or 80 Ma at 52°S (Calderón et al. 2012).

Deformation and landward propagation of the Andean fold and thrust belt were mainly controlled by thrusting in a compressional regime (Klepeis 1994a; Klepeis et al. 2010; Maloney et al. 2011; Likerman et al. 2013); although alternative interpretations hold a transpressional closure of the Rocas Verdes basin during a period of oblique convergence, with partitioned strike-slip component localized along the Canal Beagle (Cunningham 1993, 1995; Ghiglione and Ramos 2005).

The ~90° bending of the southernmost Andes was attributed either to true oroclinal rotation (*Patagonian Orocline* sensu Carey 1955) initiated in the Late Cretaceous (Cunningham et al. 1991; Kraemer 2003; Rapalini et al. 2015), or to an original curved orogen (Diraison et al. 2000), or to a progressive arc initiated by rotation during the closure of the Rocas Verdes basin and culminated mainly as a primary arc during the final stages of orogenic deformation (Ghiglione and Cristallini 2007; Poblete et al. 2014; Torres Carbonell et al. 2014; Maffione et al. 2010, 2015).

In the late Paleogene, convergence in the southernmost Andes declined and sinistral strike-slip and oblique-slip faulting dominated (Cunningham 1993, 1995; Klepeis 1994b; Klepeis and Austin 1997; Diraison et al. 2000; Ghiglione and Ramos 2005; Gombosi et al. 2009; Klepeis et al. 2010). Wrenching initiated along

the Canal Beagle and in the Neogene shifted northward to the Magallanes–Fagnano fault system (Fig. 1) (e.g., Klepeis 1994b; Menichetti et al. 2008). This transition coincides with the formation of the South America–Scotia transform boundary (Lodolo et al. 2003; Rossello 2005; Eagles 2016). Associated with this change in plate boundary configuration, magmatism in the arc vanished during the Neogene in Tierra del Fuego, reappearing only as minor manifestations in the Quaternary. The present volcanic arc is composed of six Quaternary volcanoes, all of them but the southernmost one, located to the east of the batholith (Fig. 1) (Puig et al. 1984; Stern and Kilian 1996). According to Rubio et al. (2000), subduction between 52°S and 57°S is still active or has recently ceased and is highly oblique, with a relative convergence rate of 1.3 mm/a (Pelayo and Wiens 1989).

3 The Fuegian Batholith and Satellite Plutons

The FB is a multiple intrusion dominated by granodiorites and tonalities (Kranck 1932; Suárez 1977a; Hervé et al. 1984; Suárez et al. 1985; Nelson et al. 1988). It can be divided into (i) the S-like granitoids of Cordillera Darwin (Sect. 3.1), (ii) the I-type calc-alkaline plutons of the main arc (Sect. 3.2), and (iii) the shoshonitic and other potassic intrusions of the rear-arc (Sect. 3.3).

3.1 *The Jurassic S-like Granitoids*

These granitoids are grouped in the Darwin suite, which is dominated by orthogneisses intruded in Paleozoic basement rocks and Mesozoic cover sequences on the continental flank of the batholith in the Fuegian and Patagonian Andes (Nelson et al. 1980; Hervé et al. 1981a, 2007a) (Fig. 1). The orthogneisses consist of biotite granites, granodiorites, and quartz monzonites, with minor garnet, muscovite, and amphibole. Myrmekite and accessory allanite are also common. The rocks range from weakly foliated to mylonitic and are intruded by mafic dykes of the ophiolitic suite and the undeformed Beagle suite granitoids (Nelson et al. 1980). Associated amphibole gabbros provide the suite a bimodal nature (Hervé et al. 2007a).

The granites are Upper Jurassic, with U/Pb zircon ages of 164–153 Ma (Mukasa and Dalziel 1996; Klepeis et al. 2010) and an initial $^{87}\text{Sr}/^{86}\text{Sr}$ ratio of 0.7087 (Hervé et al. 1981). In the SPB, these plutons were dated in 157–144 Ma, with initial $^{87}\text{Sr}/^{86}\text{Sr}$ ratios of 0.7068–0.7092 and negative ϵNdt values of -4.2 to -7.0 (Hervé et al. 2007a). The age and isotopic composition suggest that they are the plutonic equivalents of the voluminous Tobífera rhyolites (Bruhn et al. 1978; Hervé et al. 1981, 2007a).

The silicic (76 % SiO_2), low CaO (0.6 %) and Sr (11–58 ppm), and peraluminous nature of the orthogneisses, together with their high initial $^{87}\text{Sr}/^{86}\text{Sr}$ ratios, are compatible with an origin either by (i) anatexis of the lower crust triggered by the

heat provided from under-plated mantle-derived basalts or by (ii) crustal contamination of I-type magmas (Bruhn et al. 1978; Nelson et al. 1980; Suárez et al. 1990; Hervé et al. 2007a). According to Suárez et al. (1990), they are somewhat intermediate in their nature between true S-type and I-type granites generated in an extensional setting during fragmentation of Gondwana, adjacent to a subduction zone. Furthermore, the rhyolites of the Tobífera Formation are high K_2O , calc-alkaline, and peraluminous, a distinctive feature of rhyolites of extensional environments involving anatexis of continental crust (Gust et al. 1985).

3.2 *The Main Arc*

Included here are the I-type, calc-alkaline plutons that form the bulk of the batholith. These plutons, along with the Hardy Formation and Packsaddle volcanics, represent the trench-side suites of the magmatic arc.

3.2.1 **Lithology**

The plutons south of Canal Beagle were divided into three different suites considering age, petrography, fabric, and contact relationships with the hosting rock (Fig. 1) (Hervé et al. 1984; Suárez et al. 1985): (i) a Gabbroic assemblage (Lower Cretaceous), (ii) the Beagle suite (Lower to Upper Cretaceous), and (iii) the Seno Año Nuevo suite (Paleogene).

The Gabbroic assemblage was separated from other suites rather arbitrarily to group gabbros, gabbronorites, diorites, and hornblendites exposed as relicts within later granitoids. They form bodies of up to 30 km² scattered along the FB. Contact relationships with other granitoids indicate that they are older in all cases. The suite consists mainly of hornblende gabbro, exhibits cumulate textures, and shows no penetrative foliation, although mylonitic structures are occasionally found. The mineralogy includes combinations of labradorite, hornblende, clinopyroxene, orthopyroxene, and rare olivine and biotite (Figs. 2 and 3).

These rocks have yielded hornblende K/Ar ages from 141 to 103 Ma, i.e., embracing the pre-tectonic to syntectonic stages of the Late Cretaceous Andean orogeny (Hervé et al. 1984). Basic synplutonic dykes and inclusions in the Beagle granitoids, interpreted as part of the Gabbroic assemblage, would extend this basic magmatism to the Late Cretaceous.

The Beagle suite dominates the FB (Fig. 1) and consists of tonalites and granodiorites, with minor quartz monzodiorites and quartz diorites (Fig. 4a). Except at Wollaston Islands, the granitoids show synmagmatic penetrative foliation formed during emplacement. Mineral composition is andesine, alkali feldspar, quartz, hornblende (8 %), and biotite (7 %) (Fig. 2). Clinopyroxene is extremely scarce and appears mantled by hornblende. Accessory phases are apatite, titanite, opaque, zircon, and allanite.

Fig. 2 Mafic mineral composition of trench-side arc and rear-arc suites in Tierra del Fuego (Suárez et al. 1985; González Guillot 2009; González Guillot et al. 2012). *UP* Ushuaia pluton, *MP* Moat pluton, *JJP* Jeu-Jepén pluton, *KP* Kranck pluton, *GA* Gabbroic assemblage, *BS* Beagle suite, *SAN* Seno Año Nuevo suite

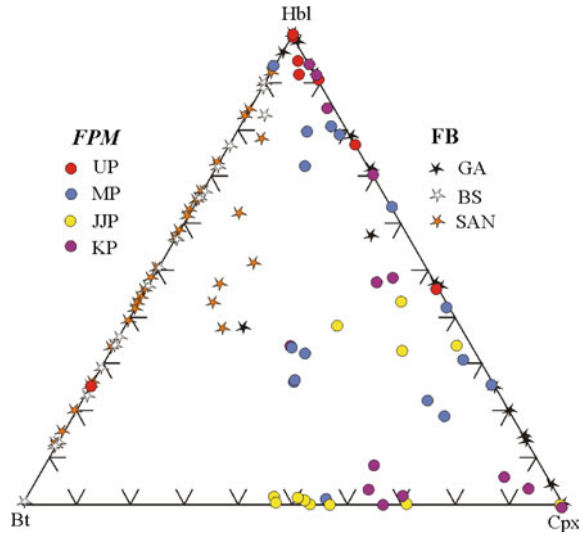
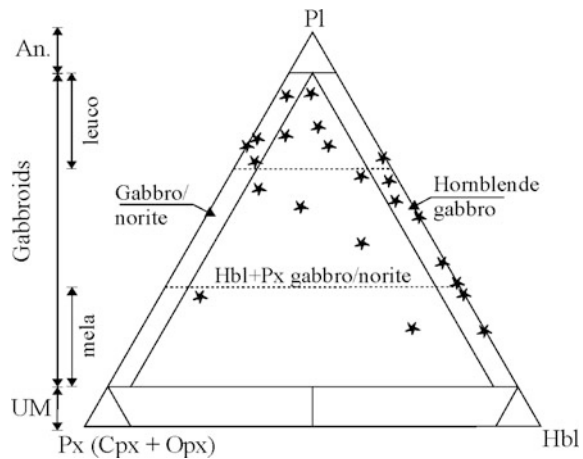


Fig. 3 Modal composition of the Gabbroic assemblage (Suárez et al. 1985)



K/Ar and Rb/Sr mineral ages, and scarce $^{40}\text{Ar}/^{39}\text{Ar}$ and U/Pb ages range between 117 and 74 Ma (Halpern and Rex 1972; Halpern 1973; Hervé et al. 1984; Suárez et al. 1985, 1986; Mukasa et al. 1988; Kohn et al. 1995; Klepeis et al. 2010; McAtamney et al. 2011). Lower and Upper Cretaceous plutons are concentrated to the south and north of the FB, respectively (Fig. 1).

The Seno Año Nuevo suite is exposed along the Pacific side of the batholith (Fig. 1). The plutons are non-foliated and range from quartz diorites to granites, with tonalite, granodiorite, and quartz monzodiorites as the most common lithologies (Fig. 4a). They are petrographically comparable with the Beagle suite, but somewhat more K-feldspar-rich (Fig. 2) and younger. K/Ar and Rb/Sr mineral ages are in the range 60–34 Ma (Hervé et al. 1984; Suárez et al. 1985).

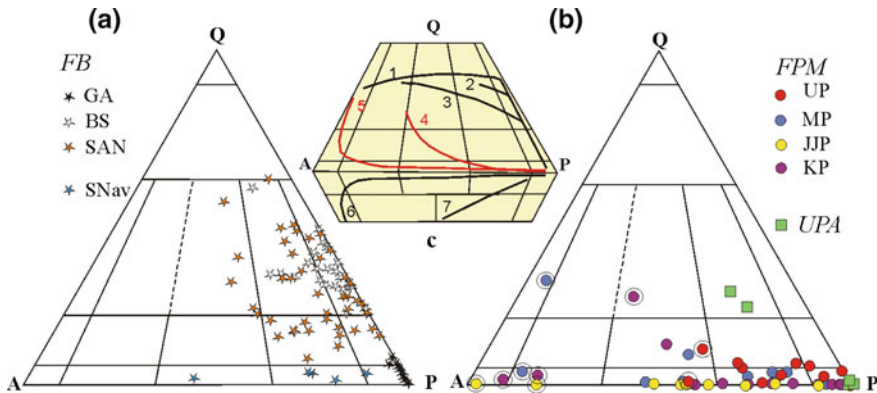


Fig. 4 Modal composition of trench-side arc and rear-arc. **a** Gabbroic assemblage (*GA*), Beagle (*BS*), and Seno Año Nuevo (*SAN*) suites (Suárez et al. 1985) and a monzonitic pluton of south Navarino Island (*SNav*) (Katz and Watters 1966). **b** FPM plutons (*UP* Ushuaia, *MP* Moat, *JJP* Jeu-Jepén, *KP* Kranck) (González Guillot 2009; González Guillot et al. 2012), and *UPA* (González Guillot et al. 2011). The encircled samples in the FPM correspond to late-stage veins. **c** Magmatic trends of Lameyre (1987), Lameyre and Bowden (1982), and Lameyre and Bonin (1991): 1 tholeiitic, 2 calc-alkaline tonalitic-trondhjemitic, 3 calc-alkaline granodioritic, 4 monzonitic, 5 alkaline (silica-undersaturated), 6 alkaline (silica-undersaturated), and 7 alkaline (silica strongly undersaturated)

3.2.2 Geochemistry

The geochemical data of the FB are scarce and restricted to major elements (Suárez 1977a; Suárez et al. 1985) and to an incomplete suite of trace elements obtained ~40 years ago by means of XRF (Suárez 1977a).

The three suites described are subalkaline (Fig. 5a) and metaluminous, typical of Cordilleran batholiths. The Beagle and Seno Año Nuevo suites define medium- to high-K, calc-alkaline trends, whereas the Gabbroic assemblage has a more ambiguous composition, straddling the low-K tholeiitic and medium-K dividing line (Fig. 6). The K_2O/Na_2O ratio varies on average from 0.24 (Gabbroic assemblage), through 0.35 (Beagle) to 0.59 (Seno Año Nuevo) (Table 2). Suárez et al. (1985) indicated the Gabbroic assemblage represents an immature stage of the arc and that the other two suites are progressively more evolved.

Trace elements normalized to MORB show serrated patterns characteristic of arc magmas, with high large ion lithophile element (LILE) content relative to N-MORB, K and Sr peaks, and Nb troughs (Fig. 7). The LILE/HFSE (high-field-strength elements) ratios are relatively high, with Rb/Zr averaging 0.34 (Table 2). LREE are enriched with respect to chondrite and Y, with La_N/Y_N of 1.81–14.35 (Table 2).

The Hardy Formation This unit represents the volcanic counterpart of the Mesozoic arc. The lavas range from basalt to dacite, with medium-K, calc-alkaline geochemistry (Figs. 5a and 6) (Suárez et al. 1985; Miller et al. 1994). Normalized

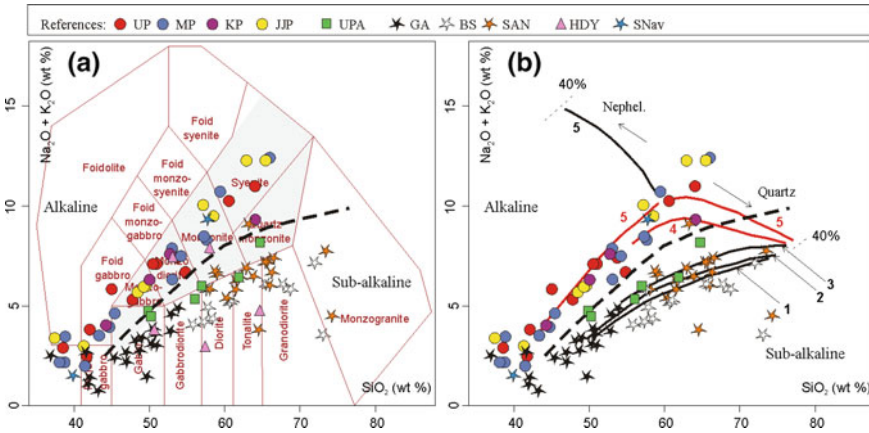


Fig. 5 Total alkali silica (*TAS*) diagrams for the *FB* and satellite plutons. **a** Trench-side arc suites (*FB* and Hardy Fm (*HDY*); Suárez et al. 1985 and Miller et al. 1994, respectively), and rear-arc suites (*FPM*; Acevedo et al. 2002; González Guillot 2009; González Guillot et al. 2012; and UPA plus a monzonitic pluton of south Navarino Island (*SNav*); González Guillot et al. 2011 and Kranck 1932, respectively). Fields of Middlemost (1991), the shading marks the mildly alkaline (transalkali) field. Alkaline and subalkaline divide of Miyashiro (1978). **b** The same diagram with trends of Lameyre (1987) and Lameyre and Bonin (1991): 1 calc-alkaline tonalitic-trondhjemitic, 2 tholeiitic, 3 calc-alkaline granodioritic, 4 monzonitic, and 5 alkaline. Normative *Q* and *Ne* contents are indicated. Same references as in Fig. 4

Fig. 6 K_2O versus SiO_2 diagram for the *FB* and satellite plutons. Division lines of Rickwood (1989). Same references as in Fig. 4

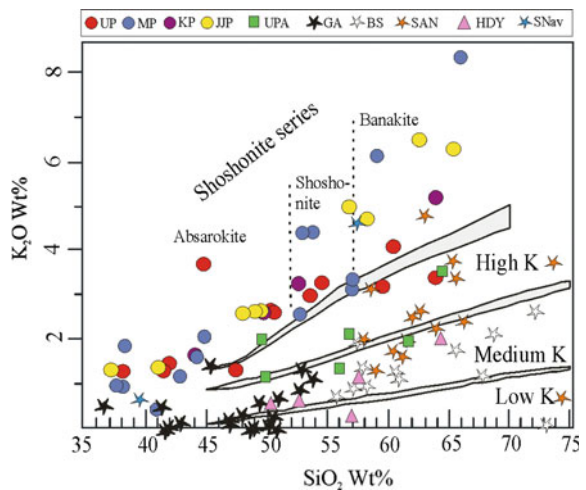


Table 2 Summarized chemical composition and ratios of trench-side arc and rear-arc suites

Suite	GA		BS*		SAN		Hardy		UPA		FPM	
	Range	Aver. (n)	Range	Aver. (n)	Range	Aver. (n)	Range	Aver. (n)	Range	Aver. (n)	Range	Aver. (n)
SiO ₂	36.7–56.7	47.4(19)	48.4–73.1	62.1(40)	54.4–74.2	62.8(18)	50.5–64.5	56.6(5)	49.8–64.6	56.6(6)	37.2–65.86	50.44(37)
K ₂ O/N ₂ O	0.00–1.32	0.24(19)	0.02–1.09	0.44(40)	0.17–1.07	0.59(18)	0.10–0.76	0.26(5)	0.33–0.74	0.50(7)	0.25–1.78	0.82(39)
K ₂ **	0.58	–	0.76	1.00	–	–	–	0.38	–	1.46	–	3.04
Rb/Zr	–	–	0.05–0.70	0.34(28)	–	–	0.02–0.38	0.21(5)	0.29–0.81	0.49(6)	0.20–1.73	0.92(30)
L _{AN} /Y _N ***	–	–	1.85–14.31	6.50(28)	–	–	1.79–3.79	2.75(5)	5.51–23.07	12.25(6)	1.49–14.46	7.19(30)
L _{AN} /Y _{N(G1)} ***	–	–	–	4.92	–	–	–	2.37	–	6.93	–	7.46
Th	–	–	2.00–28.00	8.61(28)	–	–	0.60–6.60	3.06(5)	7.40–23.00	12.96(7)	0.30–21.60	7.39(32)
Th/La	–	–	0.11–0.80	0.41(28)	–	–	0.10–0.44	0.26(5)	0.32–0.49	0.42(6)	0.04–0.62	0.27(30)
Ce/Pb	–	–	0.77–14.50	3.66(28)	–	–	3.96–7.82	5.38(5)	5.61–9.71	8.20(5)	4.72–47.00	22.02(16)
Pb/Th	–	–	0.50–3.00	1.49(28)	–	–	0.94–4.33	2.03(5)	0.43–0.68	0.60(5)	0.19–5.33	1.15(16)

GA Gabbroic assemblage, BS Beagle suite, SAN Seno Año Nuevo suite (Suárez et al. 1985), Data of Hardy Fm from Miller et al. (1994)

FPM Fuegian Potassic Magmatism (Acevedo et al. 2002; González Guillot 2009; González Guillot et al. 2012)

UPA Ushuaia Peninsula Andesites (Acevedo et al. 2002; González Guillot et al. 2011)

*Includes data from Suárez (1977a)

**K₂O at 51 % SiO₂ from linear regression lines

***Norm. factors: CI chondrite (Taylor and McLennan 1985)

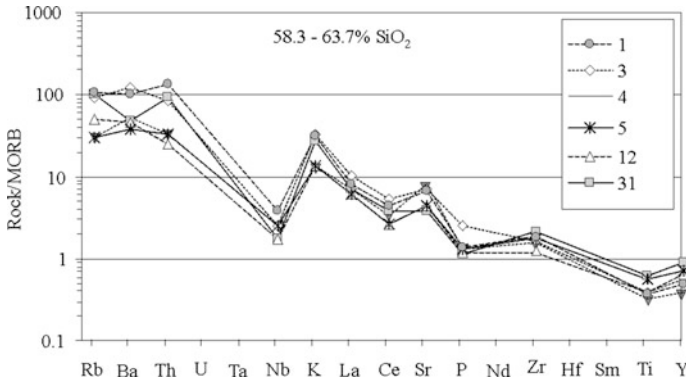


Fig. 7 Normalized trace multielement diagram of the FB (Beagle suite, Suárez 1977a). Normalization factors from Sun and McDonough (1989)

trace element plots display patterns typical of magmatic arcs, such as enrichment in LILE relative to N-MORB and negative HFSE anomalies relative to LILE, P, and LREE. Chondrite normalized data indicate moderate LREE enrichment (Table 2). Fossils in the volcanoclastic sequences indicate a Tithonian–Valanginian age (Suárez et al. 1985), whereas intercalated rhyolite intrusions yielded ages of 120 and 107 Ma (U/Pb zircon and $^{40}\text{Ar}/^{39}\text{Ar}$ in hornblende, respectively) (Miller et al. 1994).

3.3 The Rear-Arc

The rear-arc in Tierra del Fuego is composed of isolated plutons with mildly alkaline, potassic composition, the Fuegian Potassic Magmatism (FPM) (González Guillot et al. 2009), and other minor intrusions of high-K, calc-alkaline composition, the Ushuaia Peninsula Andesites (González Guillot et al. 2011). Both suites appear as scattered intrusions north of Canal Beagle, east of Cordillera Darwin, separated from the rest of the batholith (Fig. 1). Other potassic units within the axis of the FB and in the Southern Patagonian Andes may be related to the FPM and are briefly described below.

3.3.1 The Fuegian Potassic Magmatism (FPM)

Field Features and Lithology

This suite is composed of four small (25-3 km²), composite plutons (Ushuaia, Moat, Jeu-Jepén, and Kranck) (Fig. 1), each one encompassing a broad lithological spectrum from ultramafic to felsic facies (Figs. 4b and 8). Lithologies include clinopyroxenites, hornblendites, gabbros, diorites, monzogabbros, monzodiorites,

monzonites, syenites, and alkali feldspar syenites. Quartz varieties of the mafic to felsic facies may be present in some plutons, as well as late lamprophyre dykes.

Pyroxenites and hornblendites are abundant in the Ushuaia and Moat plutons, where they form massive bodies or autoliths in more felsic rocks. Contrarily, in the Jeu-Jepén and Kranck plutons, they are scarce, restricted only to small (decameter scale) lenses and clusters of autoliths. Associated pegmatitic veins or pockets of anorthosite–gabbro and thin aplitic dykes of meladorite/malagabbro are common.

Gabbros, diorites, monzogabbros, and monzodiorites form also massive bodies and show variable textures (granular, cumular, porphyritic, traquitic). Hornblende or biotite are almost absent in these lithologies in Jeu-Jepén and Ushuaia plutons, respectively. The other plutons may contain pyroxene–hornblende, pyroxene–biotite, and/or pyroxene–hornblende–biotite varieties (Fig. 2).

Monzonites form massive bodies and minor dykes in all but the Ushuaia pluton. Late-stage magmatic pulses are rectilinear to anastomosing veins and veinlets, and breccia infill of syenite and K-feldspar syenite (Fig. 4b), or monzonite in the Ushuaia pluton.

Scarce veinlets of alkali feldspar granite and monzogranite occur in the Moat and Kranck plutons, respectively (Fig. 4b). The Ushuaia and Jeu-Jepén plutons also contain border facies of quartz monzodiorite and tonalite with biotite + garnet \pm fibrolite, which appear to be hybrids between dioritic or monzodioritic magmas and anatectic melts from the country metapelites (Fig. 8) (González Guillot and Acevedo 2009).

Crosscut relationships indicate a general temporal trend of emplacement and crystallization from the ultramafic, through mafic to felsic facies and finally lamprophyres, accompanied by progressive changes in mineral composition, e.g., an increase in Ab content in plagioclase and Fe content in mafic minerals, consistent with magmatic differentiation processes.

Igneous layering between ultramafic and mafic facies is common, and accompanied by igneous foliation parallel to it. Evidences of mingling between mafic and ultramafic facies are also present. Additionally, the Ushuaia pluton shows concentric compositional zonation with a pyroxenite core and more evolved lithologies toward the margins (Fig. 8). This and other features, including positive anomalies in platinum group elements, led González Guillot and Schalamuk (2009) to compare it to Alaskan-type complexes.

The suite lacks metamorphism and penetrative deformation.

Age

There is a large variability in the ages reported for the FPM, even from a single pluton, depending on the lithologies sampled and the methods employed. The most reliable ages are U/Pb zircon ages from the Ushuaia and Jeu-Jepén plutons, a late-stage felsic dyke of 75 ± 2 Ma (Barbeau et al. 2009) and a monzonite of 72 ± 0.8 Ma (Cerrodo et al. 2011a), respectively. These are consistent with

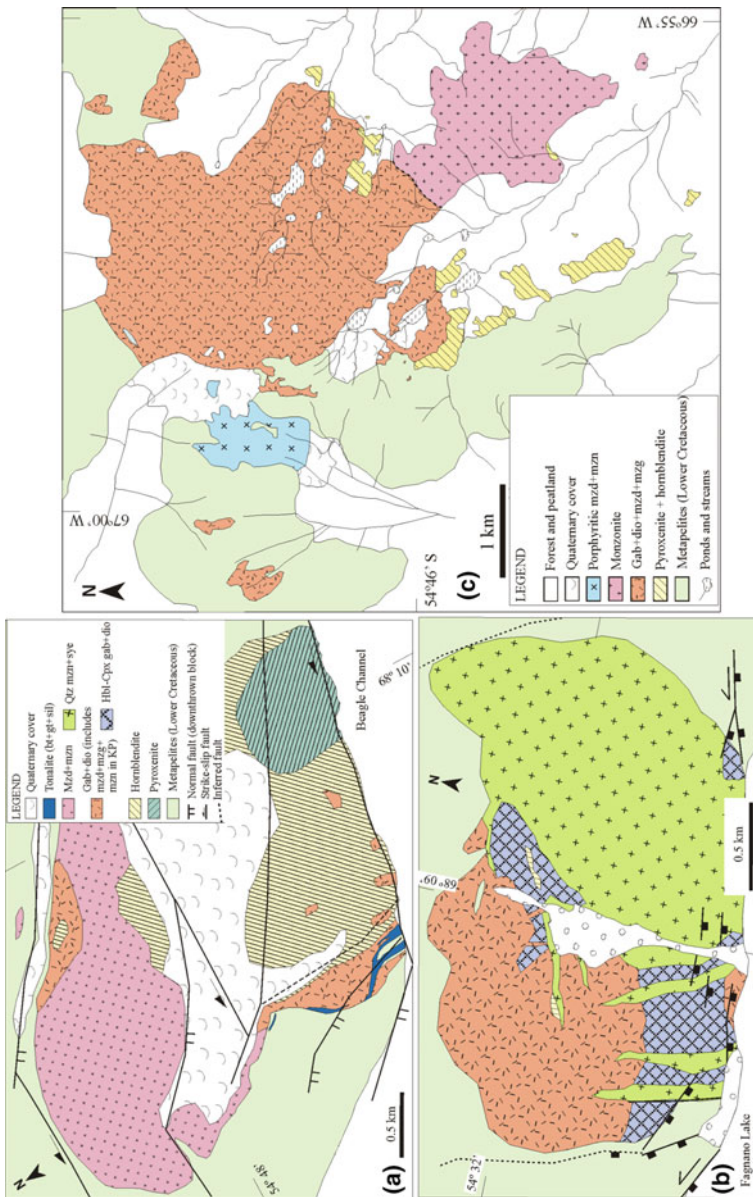


Fig. 8 Geological maps of FPM plutons. **a** Ushuaia pluton (modified from González Guillot 2009). **b** Kranck pluton (modified from González Guillot et al. 2012). **c** Moat pluton (modified from González Guillot et al. 2009)

unpublished U/Pb zircon ages of mafic to felsic facies from the Ushuaia and Kranck plutons in the range of 78–68 Ma (M. Martins Pimentel, pers. com.).

Older lower-resolution results extend this magmatism to the Early Cretaceous. These are K/Ar ages (hornblende or whole rock) from the Ushuaia, Jeu-Jepén, and Kranck plutons in the range of 113–93 Ma (Acevedo et al. 2000, 2002; Peroni et al. 2009; Cerredo et al. 2011b), or a Rb/Sr isochron age of 115 ± 3 Ma in the Moat pluton (González Guillot et al. 2009). Since the plutons lack penetrative subsolidus fabric and metamorphism, they should postdate the main Andean phase occurred prior to 86 Ma (see Section “Regional Geology”). Consequently, all the K/Ar and Rb/Sr ages must be erroneous.

Geochemistry

All plutons show a mildly alkaline (transalkali) trend in a TAS diagram (Fig. 5a) and have high-K₂O contents, the samples occupying the shoshonitic field on a K₂O–SiO₂ plot (Fig. 6). The K₂O/Na₂O ratio is high, ≥ 0.6 in most samples and ≥ 1 in rocks with silica content $>55\%$ (Table 2). The content in TiO₂ is low ($<1.4\%$), except in ultramafics with Ti-magnetite and ilmenite cumulates. These are typical chemical characteristics that distinguish the shoshonitic magma series (Morrison 1980).

Trace elements normalized to MORB show the characteristic serrated pattern of arc magmas, with high LILE content, K and Sr spikes, and troughs in Nb and Ta (Fig. 9). LILE/HFSE ratios are high, with Rb/Zr from 0.4 to 1.7 in most samples (Table 2). Rare earth elements (REE) normalized to chondrite show enrichment of LREE (light) relative to HREE (heavy) and a rather horizontal trajectory of the latter (Fig. 10). La/Yb varies from 8.4 to 27.8, except in the ultramafic rocks, which show a strong depletion in LREE, a trend that diminishes gradually toward the most evolved rocks.

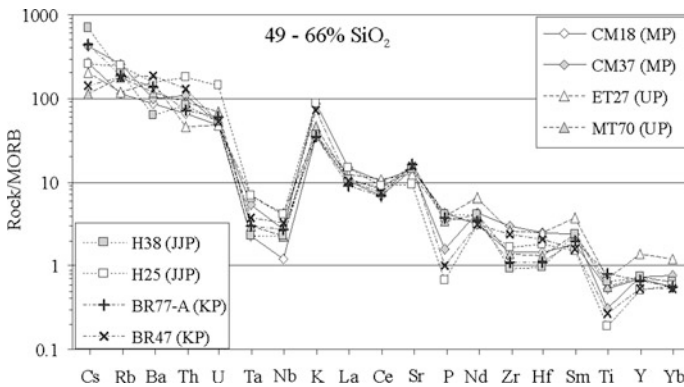


Fig. 9 Normalized trace multi-element diagram of the FPM (González Guillot 2009; González Guillot et al. 2012). Normalization factors from Sun and McDonough (1989)

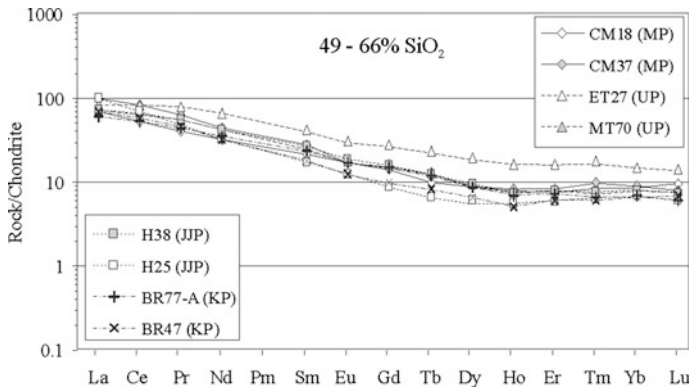


Fig. 10 Normalized REE patterns of the FPM (González Guillot 2009; González Guillot et al. 2012). Normalization factors from Taylor and McLennan (1985)

The suite is typically I-type, metaluminous, except the biotite–garnet–fibrolite border facies, which are peraluminous.

The monzonites of Navarino Island Kranck (1932) and Katz and Watters (1966) described scarce plutons composed of gabbro to monzonite in southern Navarino Island (Fig. 1). Chemically, they show mildly alkaline and shoshonitic trends in the TAS and K_2O – SiO_2 diagrams, respectively (Figs. 5a and 6). Their petrography and chemistry are similar to that of the FPM. Additionally, some hornblendites with mildly alkaline composition from Gordon Island (Fig. 1), of 110–106 Ma (K/Ar in hornblende, Suárez et al. 1985), may also be included in the FPM (Figs. 5a and 6).

The absarokites of Barros Arana and La Pera Formations These are rear-arc units that crop out to the east of the SPB (Fig. 1). They consist of a sequence of mafic dykes, lavas, and volcanoclastic breccias occurring within the sedimentary infill of the Rocas Verdes basin (Soffia 1988; Stern et al. 1991) and formed before the Andean deformation, in the late or post-Albian (Stern et al. 1991; Mpodozis et al. 2007). The geochemistry indicates that they were originated by subduction (Stern et al. 1991; Prades 2008; Anguita 2010). The age of the Barros Arana Formation is 104 Ma (hornblende K/Ar, Stern et al. 1991), whereas the maximum age of the La Pera Formation is estimated as 102 Ma (detrital zircon, Mpodozis 2006). The fossil content in the Erezcano and Canal Bertrand Formations, where the basalts intercalate, confirms an Albian age (Fuenzalida and Covacevich 1988; Castelli et al. 1992). The remarkable characteristic of these units is the high total alkalis, K_2O , LILE, and LREE contents and high LILE/HFSE and LREE/HREE ratios, typical of the mafic members of the shoshonite association (absarokites). In these respects, they are equivalent to the FPM, although the absarokites are older and less radiogenic in terms of $^{143}Nd/^{144}Nd$ and $^{87}Sr/^{86}Sr$ ratios. The differences in isotopic composition may be due to a greater time of residence within the crust of the FPM magmas, in comparison with the basalts, related to the mode of emplacement (intrusive vs. extrusive, respectively) and the tectonic regime (see Sect. 5) (González Guillot et al. 2009).

3.3.2 The Ushuaia Peninsula Andesites (UPA)

The UPA consist of hypabyssal intrusions intruded in Lower Cretaceous units that crop out mainly in the Ushuaia Peninsula, the type locality, and on the top of the Trapecio Hill (Fig. 1). At Rodríguez Hill, 4 km to the north of Kranck pluton, strongly altered lamprophyric and andesitic dykes are present, dated in 104 Ma (K/Ar whole rock), which trend N–S, i.e., orthogonal to the Andean structures (Martinioni et al. 1999). Dykes similar in composition, orientation, and position toward the rear-arc were reported at 52°S and dated in 79 Ma ($^{40}\text{Ar}/^{39}\text{Ar}$ on hornblende, Calderón et al. 2012).

Field Features and Lithology

Irregular sheet-like intrusions and plugs crop out at both the Ushuaia Peninsula and Trapecio Hill, ranging 0.1–10 m thick (Fig. 11). The rocks have no metamorphism, are undeformed, and crosscut the slaty cleavage and folding of the country rock. Depending on the composition and texture, they vary among quartz meladiorites, granodiorites, andesites, dacites, and lamprophyres (Fig. 4b) (González Guillot et al. 2011).

The quartz meladiorites form dykes or small apophysis of dark-colored rocks (M > 50 %) with (hornblende) megacrystic to seriate texture. The granodiorites form thin dykes and breccia infill crosscutting quartz meladiorites. The andesites and dacites form dykes and sills of variable thickness, from few millimeters up to 10 m wide, and cut all the other lithologies. They are light-colored (M 5–20 %) and have subvolcanic textures (porphyritic, seriate, and microgranular), with parts showing autobreccia texture. They bear enclaves of hornblendite. All the sequence is cut by 10–30-cm-thick lamprophyre dykes (Fig. 11).

Age

K/Ar data from the Ushuaia Peninsula yielded an age range of 104–77 Ma (Ramos et al. 1986; Acevedo et al. 2002; Elsztain 2004; Peroni et al. 2009). The youngest ages correspond to a “granitic porphyry” (Ramos et al. 1986) and two lamprophyre dykes (Elsztain 2004) that yielded ~ 77 and ~ 88 Ma, respectively. These younger ages are roughly coincident with a U/Pb zircon age of 83 ± 0.93 Ma from an andesite sill on that locality (unpublished, M. Martins Pimentel, pers. com.) and indicate the rocks are post-tectonic, in agreement with the lack of metamorphism and penetrative deformation. The more reliable U/Pb age also evidences that the UPA is older than the plutons of the FPM, contrarily to what was previously suggested based on the available K/Ar ages (González Guillot et al. 2011).

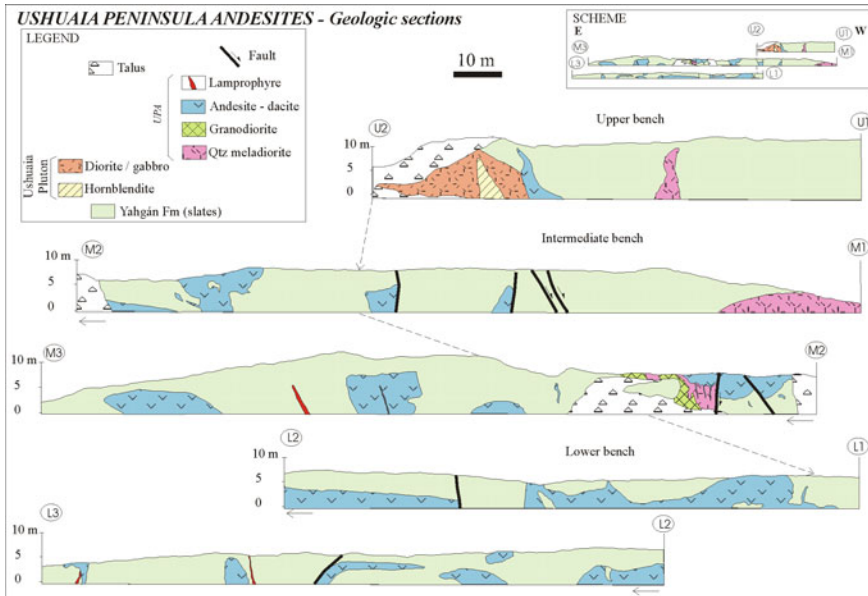


Fig. 11 Geological profiles of the UPA from a quarry at Ushuaia Peninsula. Modified from González Guillot et al. (2011)

Geochemistry

The UPA is subalkaline, metaluminous (A/CNK from 0.66 to 1.02), characterized by a calc-alkaline trend with medium to high- K_2O content (Figs. 5a and 6). The K_2O/Na_2O ratio varies from 0.34 to 0.74 (Table 2).

Normalized trace element plots (Fig. 12) show a typical serrate pattern, with Nb, Ta, and Ti troughs, K and Sr spikes, and high LILE/HFSE ratios, that characterizes subduction-related magmas. Total abundances of LILE and HFSE are high, especially Ba (505–1434 ppm), Sr (752–1351 ppm), Rb (38–89 ppm), Nb (7–13 ppm), Ta (0.5–1.1 ppm), and Th (7–23 ppm). All (except Rb) show good positive correlation with SiO_2 .

The REE normalized to chondrite show a steep arrangement of LREE and a roughly flat to concave pattern of HREE (Fig. 13) as is typical of subduction-related rocks with significant hornblende fractionation. High LREE and slightly depleted HREE cause a high LREE/HREE ratio, with La/Yb ranging from 11 to 38. The Sm/Yb ratio varies between 2.2 and 3.1.

The low HREE (1.26–1.73 ppm Yb) and Y (9.0–18.9 ppm) contents of the UPA and the high LREE/HREE are similar to magnesian andesites from western Aleutians (Yogodzinski et al. 1994, 1995). The high LILE and HFSE contents, and the low HREE contents and U/Th (0.18–0.30) and Ba/Th (36–116) ratios,

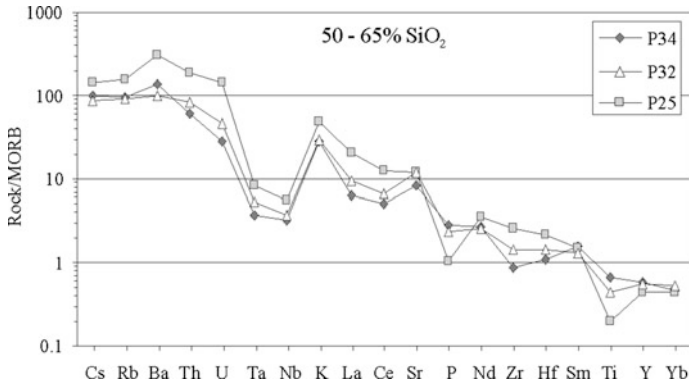


Fig. 12 Normalized trace multielement diagram of the UPA (González Guillot et al. 2011). Normalization factors from Sun and McDonough (1989)

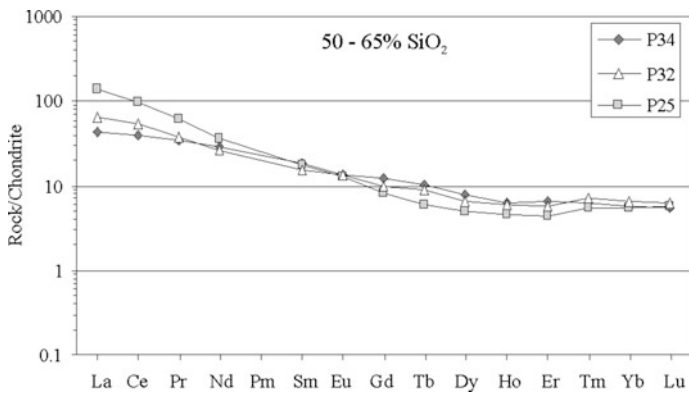


Fig. 13 Chondrite normalized REE patterns of the UPA (González Guillot et al. 2011). Normalization factors from Taylor and McLennan (1985)

especially, resemble also the northern lavas of the Holocene Austral Volcanic Zone (AVZ) in the Andes (49°S–54°S), which is considered a typical example of adakitic magmatism (Stern and Kilian 1996). This chemical signature of the UPA is interpreted as caused by contribution to the mantle source either of (i) subducted sediment partial melts, generated in the garnet stability field, or (ii) of partial melts of the top of the subducted basaltic crust (González Guillot et al. 2011).

3.4 Comparison Among the Different Plutonic Suites

Following the modal criteria of Lameyre and Bowden (1982), Lameyre (1987), and Lameyre and Bonin (1991) (Fig. 4), the suites of the FB define a calc-alkaline

tonalitic–trondhjemitic trend (Beagle suite) and a calc-alkaline tonalitic–trondhjemitic to granodioritic trend (Seno Año Nuevo suite), whereas the Gabbroic assemblage could be defined either as tholeiitic or calc-alkaline. On the other hand, the rear-arc suites define a silica-saturated alkaline trend and to a lesser extent a monzonitic trend (FPM) and a calc-alkaline granodioritic trend (UPA). The Jurassic S-like granitoids correspond to the granitoids of crustal origin.

These compositional trends were also distinguished previously using geochemical parameters (Fig. 5a). On the other hand, the Hardy Formation does not follow a clear trend in Fig. 5a, with samples straddling the subalkaline–alkaline divide, although its medium-K, calc-alkaline composition is depicted in the K_2O – SiO_2 diagram (Fig. 6). The distinction of these trends may be improved by comparison with the compilations of Lameyre (1987) and Lameyre and Bonin (1991) (Fig. 5b). The mildly alkaline trend of the FPM follows a silica-saturated alkaline trend, although few samples divert to a monzonitic trend (equivalent to the volcanic shoshonitic associations, c.f. Pagel and Leterrier 1980) (curves 5 and 4 in Fig. 5b, respectively). The plutons of southern Navarino Island and some hornblendites of the Gabbroic assemblage also show a silica-saturated alkaline trend. These and the FPM have K_2O contents typical of the shoshonite series, whereas the main of the FB and the Hardy Formation show lower K_2O content, which increases with time from the low to the high- K_2O fields in the K_2O – SiO_2 diagram (Fig. 6). The composition of the UPA straddles the divide between medium- and high- K_2O calc-alkaline fields.

Monzonitic series, as defined by Lameyre and Bowden (1982) and Lameyre and Bonin (1991), include gabbros, diorites, monzogabbros, monzodiorites, monzonites, quartz monzonites, monzogranites, and scarce syenogranites. On the other hand, the silica-saturated alkaline series are bimodal, since they lack the intermediate lithologies, and are dominated by the granitic end members. This bimodal character is not present in the FPM, nor is there an abundance of felsic end members (actually intermediate members dominate). Thus, it follows that the silica-saturated alkaline trend of the FPM is merely a transitional variation of the monzonitic trend.

Trace elements provide more differences between the trench-side arc and rear-arc units. The FPM has higher LILE and P, compared to the calc-alkaline batholith (Fig. 14). Additionally, it also shows higher LILE/HFSE (e.g., Rb/Zr 0.57–3.28) and La_N/Y_N (3.62–14.65) ratios compared to the FB (Rb/Zr 0.23–0.60, La_N/Y_N 4.54–10.39) (Table 2).

4 Spatial and Temporal Distribution of Magmatic Suites

Figure 15 summarizes the information given in Sects. 3.1–3.4. It evidences that magmatism in the Fuegian Andes was episodic and that the batholith grew incrementally, including the rear-arc intrusions. In Tierra del Fuego, the magmatic suites are arranged with an ESE–WNW orientation, and trends progressively become more N–S toward the north, parallel to the present trench (Fig. 1). The oldest FB

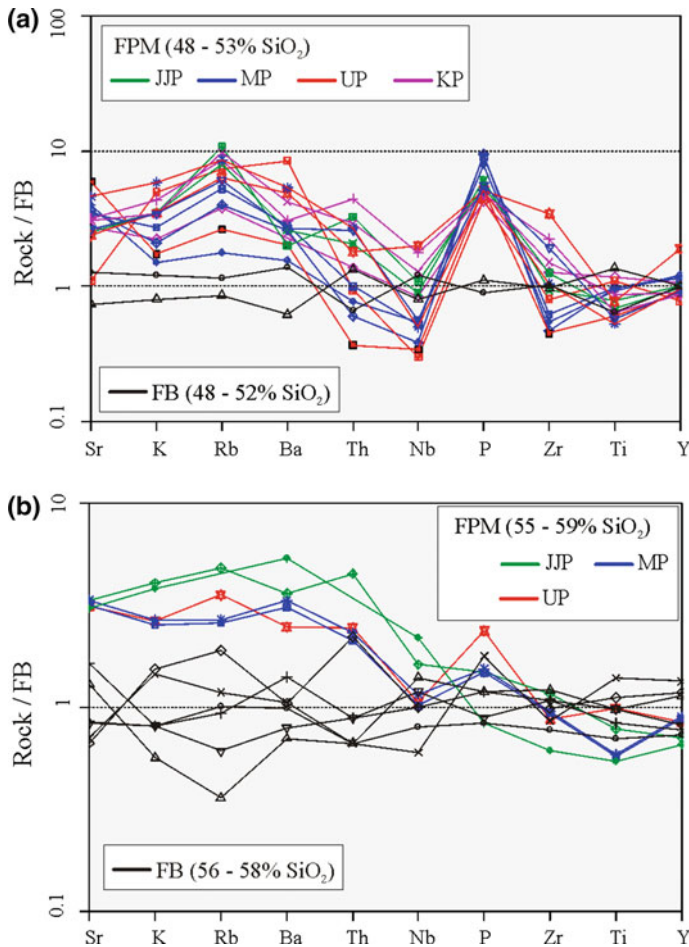


Fig. 14 Trace multielement diagram of the FPM (González Guillot 2009; González Guillot et al. 2012) and FB (Suárez 1977a), normalized to the average of the samples of the FB in each case. Abbreviations as in Fig. 2. **a** Basic samples. **b** Intermediate samples

plutons were emplaced along the cratonic margin of the batholith during the Late Jurassic (Fig. 15). Afterward, a first oceanward shift in the volcanic front is documented, as Lower Cretaceous plutons and volcanics outcrop toward the Pacific side (Fig. 15) (Suárez et al. 1985, 1986; Miller et al. 1994; Hervé et al. 2007a). During the Late Cretaceous, magmatism of the Beagle suite shifted cratonward (Fig. 15), since Upper Cretaceous plutons crop out to the NNE of the Lower Cretaceous ones. Additionally, there seems to be a decrease in ages from south to north of the Canal Beagle, as most plutons to the south have ages in the range 98–80 Ma (Halpern 1973; Hervé et al. 1984; Suárez et al. 1986; Kohn et al. 1995; Mukasa and Dalziel 1996), whereas ages in Cordillera Darwin range from 86 to

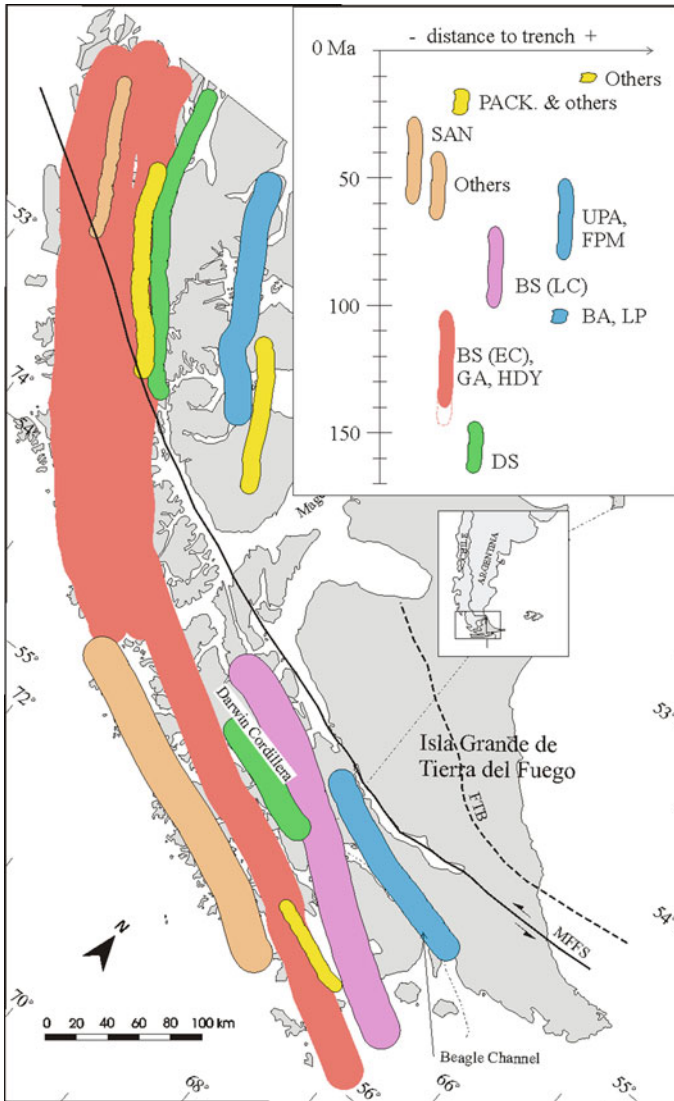


Fig. 15 Simplified map showing the geographic distribution of trench-side arc and rear-arc suites in Tierra del Fuego and Southern Patagonia. The inset emphasizes the time distribution and relative distance to the paleo-trench. Data from Hervé et al. (1984, 2007a), Suárez et al. (1985, 1986), Stern et al. (1991), Miller et al. (1994), Klepeis et al. (2010), Barbeau et al. (2009), and Cerredo et al. (2011a), this review. *DS* Darwin suite, *EC* Early Cretaceous, *LC* Late Cretaceous, *BA* Barros Arana Fm, *LP* La Pera Fm, *PACK* Packsaddle Fm. Others refer to unnamed plutons in the SPB. Other abbreviations as in Table 1 and Figs. 1, 2 and 5

73 Ma (Mukasa and Dalziel 1996; Klepeis et al. 2010; McAtamney et al. 2011). Rear-arc intrusions in Tierra del Fuego are coeval with the Beagle suite in Cordillera Darwin, while the northernmost plutons of the MPF are slightly younger.

Thus, a progressive cratonward migration of the volcanic front is registered in the southernmost Andes, which started in the mid-Cretaceous associated with the closure of the marginal basin (Stern et al. 1991) and culminated in the latest Cretaceous (Fig. 15).

During emplacement of the 60–34 Ma Seno Año Nuevo suite and the Miocene Packsaddle volcanics, the calc-alkaline volcanic front in Tierra del Fuego shifted back to the Pacific side (Fig. 15) and remained there up to its culmination in the Miocene, except for the small Recent Cook volcano eruptions (Hervé et al. 1984; Puig et al. 1984) (Fig. 1).

Contrarily, in the Southern Patagonian Andes, the Late Cretaceous to Miocene volcanic front remained in a steady position (Fig. 15) (Hervé et al. 2007a). After a period of magmatic quiescence between 40 and 25 Ma, Miocene magmatism was abundant in the core of the SPB (Hervé et al. 2007a), together with rear-arc satellite bodies up to 70 km to the east (Fig. 15) (Michael 1991; Sánchez et al. 2006; Ramos et al. 2004; Hervé et al. 2007a; Michel et al. 2008; Ramírez de Arellano et al. 2012).

Concerning the Upper Cretaceous suites, the following question arises: Why is the potassic magmatism (both UPA and MPF) absent in Cordillera Darwin, while it reappears at 52°–53°S? The fact that potassic magmatism took place cratonward of the marginal basin at its northern and southern ends, associated with its closure, leaves the possibility of occurrence all along its length. Coeval plutons of the Beagle suite in Cordillera Darwin were intruded at pressures close to 6 kbar (Maloney et al. 2011), while the MPF plutons were emplaced at 2–4 kbar (González Guillot et al. 2009). Thus, one possibility for the absence of potassic plutons at Cordillera Darwin is that they should have emplaced at higher levels and then eroded away. Figure 15 shows that the axis of the rear-arc actually passes through the northern flank of Cordillera Darwin, where low-grade metamorphic sequences crop out, which are equivalent to those to the east where the FPM is emplaced. This implies, alternatively, that potassic plutons may be present in that northern flank awaiting to be discovered.

4.1 Across-Arc Compositional Variations

There follows below a more detailed comparison of the plutonic suites that helps to elucidate the geometry of the subduction zone for the Cretaceous. Nevertheless, it is not easy to compare trace elements for the FB and rear-arc suites because there is a mixture of 40-year-old XRF and recent ICP-ES and ICP-MS results, and the complete spectrum of trace elements and REE for the former unit was not obtained.

The landward shift in the volcanic front in the mid-Cretaceous encompassed (i) the widening of the arc, broadly from 50 to 90 km in the Early Cretaceous to 80–120 km in the Late Cretaceous (Fig. 15), and (ii) progressive changes of magma

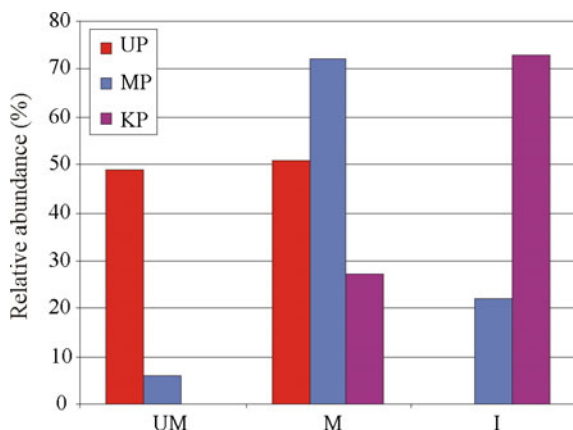
composition away from the trench (Figs. 1, 2, 3, 4, 5, 6, 7, 8, 9, 10, 11, 12, 13, 14 and 15).

Both potassic suites of the rear-arc appear to represent the plutonic equivalents of a second volcanic front in what are known in modern arcs as dual volcanic chains, located above relatively low angle-subducting slabs (Marsh 1979; Tatsumi and Eggins 1995). Secondary volcanic chains are characterized by small magma volume, lower normative quartz, greater amounts of hydrous phases, and higher concentrations of incompatible elements, compared to trench-side chains (Tatsumi and Eggins 1995; Tatsumi 2003). This is related to smaller fluid flux into the magma source region (Tatsumi and Eggins 1995; Tatsumi and Kogiso 1997). Together with magma generation and segregation at greater depths beneath the rear-arc (Tatsumi et al. 1983), the less H₂O supply is translated as less percentage of partial melting (Gill 1981; Sakuyama and Nesbitt 1986). Alternatively, different metasomatic agents to the mantle wedge have been proposed for trench-side arc and rear-arc magmas, low-temperature hydrous fluids versus slab (sediment and/or basalt) melts, or supercritical fluids, respectively (Stern 1991; Kay and Mpodozis 2002; Morris and Ryan 2003; Kimura et al. 2010; Hanyu et al. 2012). Another variable in continental settings is crustal and/or subcontinental mantle contamination/assimilation of rear-arc magmas as they traverse thicker lithosphere.

Further inspection of the Cretaceous suites in the Fuegian Andes reveals not only differences between trench-side and rear-arc plutons, but also systematic changes within the rear-arc with distance to the paleo-trench (González Guillot 2009; González Guillot et al. 2012).

There is an increase in the relative abundance of felsic rocks (monzonite, syenite, and K-feldspar syenite) relative to mafic (monzodiorite, monzogabbro, diorite, and gabbro) and ultramafic rocks (hornblendite and pyroxenite). The ultramafic:mafic:felsic ratio varies from 49:51:0 in the Ushuaia pluton, through 6:72:22 in the Moat pluton to 0:27:73 in the Kranck pluton (Fig. 16), which is similar to that in the Jeu-Jepén pluton. This do not correspond to different level of exposure of the plutons, since two of them, one in the south (Ushuaia) and other in the north

Fig. 16 Relative abundance of ultramafic (UM), mafic (M), and intermediate (I) lithologies in three FPM plutons, based on the maps of Fig. 8. Abbreviations as in Fig. 2. See text for more detail



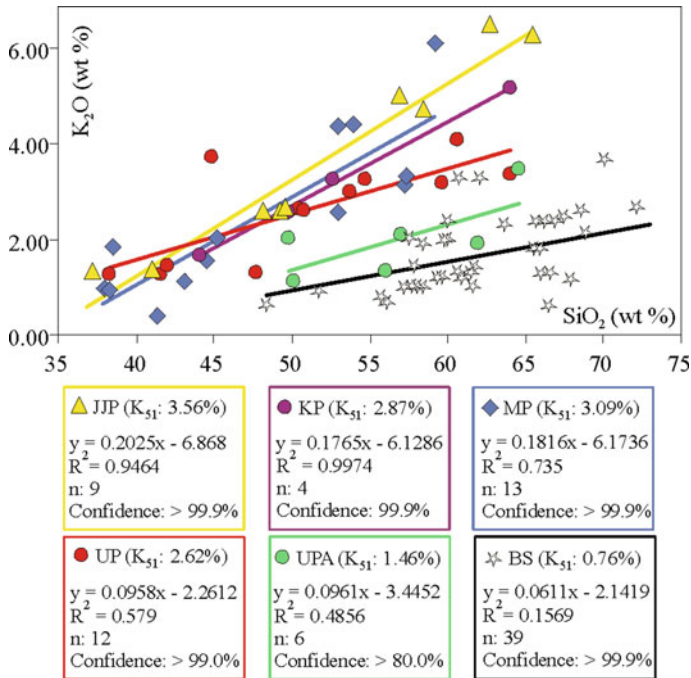


Fig. 17 K_2O versus SiO_2 diagram with linear regression curves for FPM (JJP, KP, MP, UP), UPA and FB (Beagle suite). Same references as in Fig. 2 and Table 1. Equations and statistical parameters are provided, along with the K_{51} values for each suite. See text for further detail

(Jeu-Jepén), are exposed at or near roof level. Additionally, there is a concomitant progressive increase in K-feldspar in the most differentiated facies, as late-stage veins consist of monzonite in the Ushuaia pluton, syenite in the Moat pluton, and K-feldspar syenite in Kranck and Jeu-Jepén plutons (Fig. 4b).

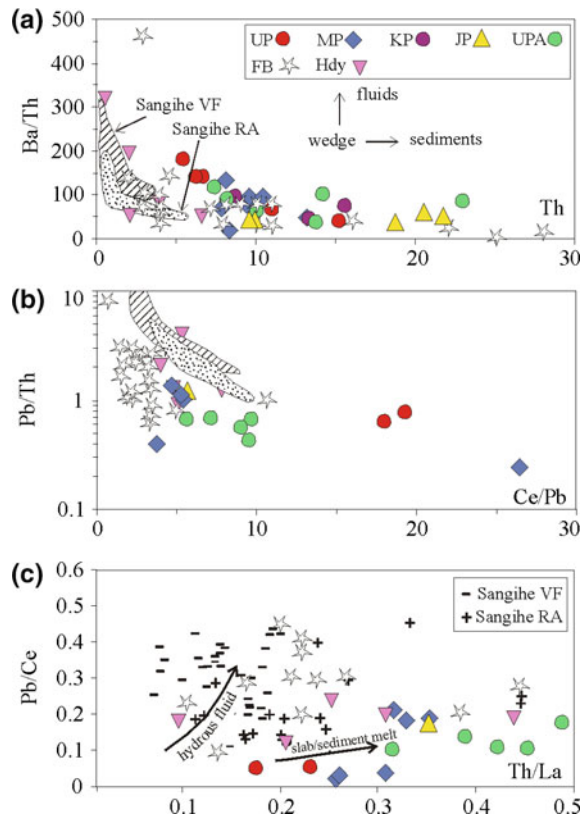
The K_2O content for a given silica value also increases with distance to the paleo-trench (Fig. 17). The K_{51} values (K_2O wt% at 51 wt% SiO_2 calculated from linear regressions in Fig. 17, Tatsumi and Eggins 1995) for both rear-arc suites are greater than 1.46 %, above the lower limit of most back-arc-side volcanoes worldwide (1.2 %, Tatsumi and Eggins 1995), whereas the K_{51} value for the coeval Beagle suite is 0.76 % (Fig. 17; Table 2). The rate of increasing K_2O with silica also increases northward, as the slopes of the regression lines are progressively steeper. Additionally, LREE enrichment and HREE depletion, among many other chemical parameters, have been documented in rear-arc magmas in numerous arcs (see review in Tatsumi and Eggins 1995). Since no HREE are available for the FB, Y is used instead, which has similar behavior in magmatic systems (Rollinson 1993). The La_N/Y_N ratio (normalized to CI chondrite of Taylor and McLennan 1985) for a given silica content (51 %) varies from 4.92 in the FB (Beagle suite), to 6.03 in the Ushuaia pluton up to 9.29 in the Jeu-Jepén pluton (Table 2). The La_N/Y_{N51} in the UPA is 6.93, similar to the average in the MPF, although the ratios for

greater silica values are the highest, consistent with an addition of subducted sediment partial melts to the source region (González Guillot et al. 2011, see below).

Higher Ba/Th, Pb/Th, and Pb/Ce ratios and lower Th contents and Th/La ratios in the volcanic front relative to the rear-arc are believed to be indicators of addition of slab-derived fluid to the mantle source because Ba and Pb are more fluid mobile, whereas Th, La, and Ce are relatively compatible in melts but not in hydrous fluids (Stern and Kilian 1996; Hawkesworth et al. 1997; Elliott et al. 1997; Johnson and Plank 1999; Pearce et al. 2005; Kimura et al. 2010). The variation in these values from volcanic front to rear-arc is continuous rather than abrupt and reflects a change in the composition of the slab component as the slab depth increases.

In Tierra del Fuego, from the volcanic front (Beagle suite and Hardy Formation) toward the rear-arc (UPA and FPM), there is a general increase in Th content and in Ce/Pb and Th/La ratios (Fig. 18), whereas Pb/Th ratios are similar to higher in the volcanic front with respect to the rear-arc suites (Fig. 18b). On the other hand, Ba/Th ratios are roughly similar in the Fuegian and Patagonian batholiths and the rear-arc suites, but some Hardy Formation samples show the highest ratios.

Fig. 18 Th versus Ba/Th (a), Ce/Pb versus Pb/Th (b), and Th/La versus Pb/Ce (c) of trench-side arc (FB and Hdy) and rear-arc suites (FPM and UPA) in Tierra del Fuego. Data from Suárez (1977a), Miller et al. (1994), González Guillot (2009), and González Guillot et al. (2011, 2012). For comparison, data of the Sangihe volcanic front and rear-arc (Indonesia) are presented (Hanyu et al. 2012)



Comparing the two rear-arc units, the UPA have greater Th contents and Th/La ratios, and lower Pb/Th ratios than the FPM (Fig. 18; Table 2).

The geochemical variability shown above is consistent with a mantle wedge metasomatized by fluids beneath the volcanic front and by subducted sediment (or basalt) melts, generated in the garnet stability field, in the zone where the UPA generated (González Guillot et al. 2011). The farther-from-the-trench suite (FPM), however, has a somewhat intermediate composition in these variables between the UPA and the FB (Fig. 18), although it shows the largest K and other LILE enrichments (Table 2). It appears then that the FPM is formed in a mantle source metasomatized by fluids, but by lower degrees of partial melting.

5 Tectonic Setting During Arc Construction

The oceanward shift of the volcanic front after emplacement of the Darwin suite (Fig. 15) can be related to the opening and widening of the Rocas Verdes basin that initiated in the latest Jurassic, which split the magmatic arc during steepening of the subducting slab (Fig. 19a–b) (e.g., Miller et al. 1994; Hervé et al. 2007a).

The geochemical signature of UPA, FPM and the Barros Arana and La Pera shoshonites is typical of rear-arc magmatism, consistent with north–northeastward subduction of the proto-Pacific plate (González Guillot et al. 2012). This is in contrast with another interpretation that assumes that the Late Cretaceous magmatism was related to southward subduction of the marginal basin oceanic floor (Mpodozis and Rojas 2006; Klepeis et al. 2010).

Thus, in the mid- and Late Cretaceous, a subduction shallowing and ensuing cratonward shift in the volcanic front took place during marginal basin closure (Fig. 19c) (Stern et al. 1991; Stern and De Wit 2003; González Guillot et al. 2011). The resulting compression produced shortening by means of continental underthrusting and obduction of the oceanic floor (e.g., Cunningham 1995; Kraemer 2003), enhancing the migration of the volcanic front. The process did not reach a mature state as in other segments of the Andes (e.g., the flat Pampean subduction zone, Barazangi and Isacks 1976); however, a brief magmatic gap between 68 and 60 Ma existed in Tierra del Fuego (Fig. 15). A later shift of the volcanic front toward the Pacific at 60 Ma in Tierra del Fuego (Fig. 15), plus the preservation of remnants of the Jurassic accretionary prism (Davidson et al. 1989), suggests that subduction erosion was not significant during the Cretaceous. However, the increase in relative convergence and plate coupling inherent to slab shallowing may have facilitated sediment supply to the magma source of the UPA (González Guillot et al. 2011).

Rear-arc potassic magmatism was diachronous, around 104 Ma (pre-tectonic) at 52°–53°S and 83–68 Ma (post-tectonic) at 55°S. Additionally, rear-arc magmas extruded ~35–40 km landward of the contemporaneous trench-side plutons in the Southern Patagonian Andes, whereas there is not such a spatial hiatus in Tierra del Fuego. Instead, there is a progression in age and composition, from medium-K,

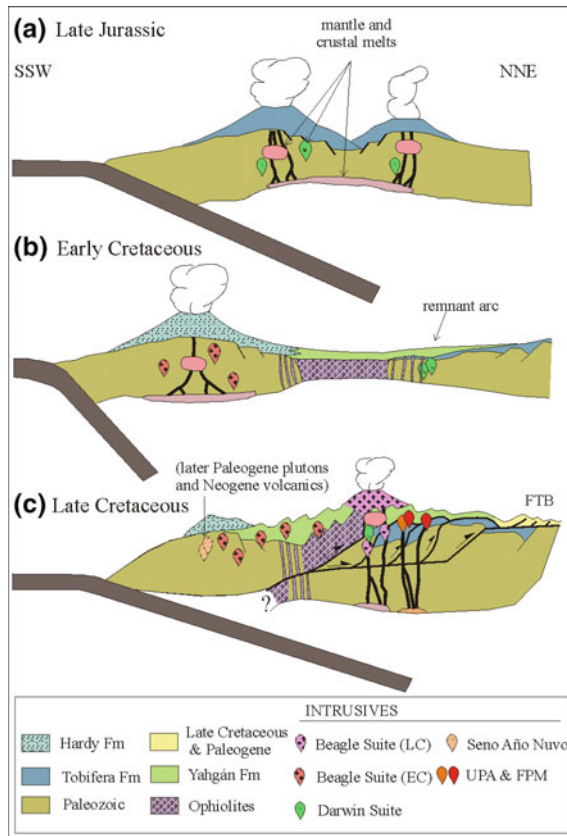


Fig. 19 Sketches showing models for the tectonomagmatic evolution of the Pacific margin of Tierra del Fuego from the latest Jurassic to the Late Cretaceous. **a** Subduction-related magmatism in an extensional arc. Generation of mantle and crustal melts to form the Darwin suite intrusions and Tobifera volcanics. **b** Slab steepening derived in slab rollback and full extension that splits the arc and develops the Rocas Verdes marginal basin. Most Darwin suite plutons remain in the remnant arc. Calc-alkaline magmatism continues in the frontal arc. **c** A slab flattening event produces inversion of the marginal basin and orogenic shortening. Magmatism shifts landward, and rear-arc potassic magmatism takes place. The position of the subsequent Paleogene and Neogene magmatism is indicated. *Sources* Stern et al. (1991), Miller et al. (1994), Hervé et al. (2007a), González Guillot et al. (2009, 2011), Klepeis et al. (2010) and Torres Carbonell and Dimieri (2013)

through high-K, to shoshonitic (Figs. 6 and 15), from the trench-side arc to the rear-arc. These constraints indicate that rear-arc magmatism in the Southern Patagonian Andes occurred shortly after the initiation of flattening, whereas it occurred long afterward at 55°S. A possible cause of this delay may be connected to a wider marginal basin in Tierra del Fuego with respect to Southern Patagonia (e.g., Stern and De Wit 2003; Kraemer 2003).

Based on the lack of radiogenic isotopic compositions, Stern et al. (1991) proposed that the Barros Arana basalts did not interact with crustal basement, as was the case of coeval plutons in the PB. These authors assumed that the rear-arc was still under extension during lava extrusion, while compressional deformation may have already begun to the west. On the other hand, the FPM was emplaced under a state of stress neutral to compressional, after the metamorphic climax. Extreme differentiation as occurred in this suite is possible in closed systems, isolated from continuous injections of fresh magma and from tapping of differentiated products through eruptive vents (Stern 1979). The slab flattening event initiated tens of million years before provides the conditions for a locked subduction system, consistent with a compressional setting.

The evidence indicates that both rear-arc shoshonitic suites were emplaced in different tectonic settings, leading to the opposite mode of occurrence: extrusive versus intrusive, and chemical and lithological compositions. Morrison (1980) concluded that shoshonitic rocks are associated with arc deformation during the termination of subduction or during flipping of the subduction zone. It seems that the Barros Arana and La Pera absarokites represent an early manifestation of subduction flattening (Stern et al. 1991), whereas the FPM and UPA represent the culmination of that phase.

From the latest Cretaceous on, a more obvious decoupling in the position of the volcanic front occurs between the FB and SPB. After the culmination of rear-arc magmatism, an important plate reconfiguration gave way to voluminous Paleogene plutonism toward the trench in Tierra del Fuego (Seno Año Nuevo, Fig. 15). The process took ~ 8 Myr from 68 Ma (the youngest rear-arc pluton) to 60 Ma (the oldest Paleogene pluton). However, Paleogene plutonism is scarce and occurs roughly at the central axis of the batholith in the Southern Patagonian Andes (Fig. 15) (Hervé et al. 2007a), implying a less dramatic change in the subduction parameters. The magmatic gap there occurred between 75 and 67 Ma (Hervé et al. 2007a).

Additionally, while Paleogene and Neogene magmatism remained at a stable position in the Fuegian Andes (Puig et al. 1984), Neogene plutons at 52°S – 53°S are more widely distributed and extended to the east (Fig. 15). This manifests a renewed flattening and cratonward migration of magmatic activity in the Southern Patagonian Andes (e.g., Espinoza et al. 2007; Folguera and Ramos 2011; Ramírez de Arellano et al. 2012).

The Paleogene retreat of the volcanic front in Tierra del Fuego may be related to highly oblique convergence—opposed to a quasi-orthogonal convergence to the north—(Eagles and Scott 2014; Eagles 2016), rather than to steepening of the subducted plate. These conditions also controlled the Neogene contrasting evolution of magmatism on both segments. This should be taken into account for further research concerning whether or not the bend in the southernmost Andes is a true orocline, possibly initiated after ~ 70 Ma (cf. Maffione 2016; Rapalini et al. 2015).

According to Eagles and Scott (2014), the absence of calc-alkaline magmatism after the Seno Año Nuevo suite might be related to the approach of the Farallon/Nazca–Phoenix ridge to the trench at ~ 30 Ma and the subduction of

young, volatile-poor, buoyant oceanic lithosphere (Breitsprecher and Thorkelson 2009). After a hiatus, calc-alkaline volcanism resumed briefly at Peninsula Hardy (Packsaddle Fm) in earliest Miocene times, before ceasing again until recently (Puig et al. 1984). Subduction of the Nazca–Phoenix ridge at ~ 20 Ma led to the alkaline term of the Packsaddle Fm associated with slab window processes (Breitsprecher and Thorkelson 2009; Eagles et al. 2009).

6 Conclusions

The magmatic arc in Tierra del Fuego occurred as a response of northward subduction (present coordinates) of the proto-Pacific plate under South America. It grew episodically from the Late Jurassic to the Miocene. The FB is the most voluminous constituent of the arc, followed by volcanic and volcanoclastic components and minor rear-arc intrusions. The volcanic front shifted, and the composition of magmas changed several times during arc construction. The oldest components of the FB are Upper Jurassic S-like granitoids and hornblende gabbros. They occur at the northern margin of the batholith. In the latest Jurassic–Early Cretaceous, magmatism shifted to the Pacific side of the archipelago as a consequence of the opening and widening of the Rocas Verdes marginal basin, according to some authors linked to a steepening of the slab and trench rollback (e.g., Miller et al. 1994).

A slab flattening event in the mid-Cretaceous derived in the inversion of the marginal basin, peak metamorphism, and orogenesis. This caused a cratonward migration of the volcanic front, the widening of the arc, and inception of potassic magmatism in the rear-arc (Stern et al. 1991; González Guillot et al. 2011). There is a progressive change in age and composition of Cretaceous plutons toward the continent in Tierra del Fuego, from medium-K, calc-alkaline, through high-K, calc-alkaline to shoshonitic. Shoshonitic magmatism in the rear-arc in Tierra del Fuego was partly coeval with calc-alkaline magmatism in the trench-side arc, although the former includes the youngest components of the Late Cretaceous arc. Besides, there is no spatial hiatus between coeval trench-side arc and rear-arc suites. Contrarily, in the Southern Patagonian Andes shoshonitic rear-arc magmatism occurred ~ 20 Myr before than in the Fuegian Andes and ~ 40 km landward of the contemporaneous calc-alkaline plutons. Therefore, shoshonitic magmatism represents the initial stages of flattening in Patagonia and its culmination in Tierra del Fuego.

After ~ 8 Myr of no magmatic activity in Tierra del Fuego, between 68 and 60 Ma, magmatism shifted back to the Pacific side of the archipelago and remained there until its culmination.

Decoupling in the locus, timing and composition of magmatism between the Fuegian and Southern Patagonian Andes from the mid-Cretaceous, but especially from the Paleogene onward, may be related to differential development of the

marginal basin and probably to oroclinal bending in the latest Cretaceous–Paleogene. This conclusion agrees with structural models that consider the oroclinal anticlockwise rotation of the Fuegian Andes with respect to the Patagonian Andes, in a context where the Rocas Verdes basin was significantly wider to the south (Kraemer 2003) and is consistent with highly oblique subduction since the Paleogene (Eagles and Scott 2014).

Acknowledgments My special thanks to Márcio Martins Pimentel (Brasilia University) for providing the geochronological data commented in this review. I also appreciate Mónica Escayola and Daniel Acevedo’s comments and field assistance during my Ph.D. research; part of the latter has been included in this chapter. Mara Uría helped with translation into English.

References

- Acevedo RD, Roig CE, Linares E, Oстера HA, Valín-Alberdi ML, Queiroga-Mafra JM (2000) La intrusión plutónica del Cerro Jeu-Jepén. Isla Grande de Tierra del Fuego, República Argentina. *Cadernos do Laboratorio Xeolóxico de Laxe* 25:357–359
- Acevedo RD, Linares E, Oстера HA, Valín-Alberdi ML (2002) La Hornblendita Ushuaia (Tierra del Fuego): Geoquímica y Geocronología. *Rev Asoc Geol Argentina* 57(2):133–142
- Alabaster T, Storey BC (1990) Modified Gulf of California model for South Georgia, north Scotia Ridge, and implications for the Rocas Verdes back-arc basin, Southern Andes. *Geology* 18:497–500
- Anguita N (2010) Petrogénesis de diques lamprofídicos posttectónicos y su relación con el magmatismo shoshonítico cretácico de la Formación Barros Arana y el Complejo La Pera, Magallanes, XII Región, Chile. Graduate Thesis, Univ. Chile, p 237
- Barazangi M, Isacks B (1976) Spatial distribution of earthquakes and subduction of the Nazca plate beneath South America. *Geology* 4:686–692
- Barbeau DL, Gombosi DJ, Zahid KM, Bizimis M, Swanson-Hysell N, Valencia V, Gehrels GE (2009) U-Pb zircon constraints on the age and provenance of the Rocas Verdes basin-fill, Tierra del Fuego, Argentina. *Geochem Geophys Geosys* 10:Q12001
- Barker PF (2001) Scotia Sea regional tectonic evolution: implications for mantle flow and palaeocirculation. *Earth Sci Rev* 55:1–39
- Breitsprecher K, Thorkelson DJ (2009) Neogene kinematic history of Nazca-Antarctic-Phoenix slab windows beneath Patagonia and the Antarctic Peninsula. *Tectonophysics* 464:10–20
- Bruce RM, Nelson EP, Weaver SG, Lux DR (1991) Temporal and spatial variations in the Southern Patagonian Batholith; constraints on magmatic arc development. In: Harmon RS, Rapela CW (eds) *Andean Magmatism and its tectonic setting*. *Geol S Am S* 265:1–12
- Bruhn RL (1979) Rock structures formed during back-arc basin deformation in the Andes of Tierra del Fuego. *Geol Soc Am Bull* 90:998–1012
- Bruhn RL, Stern CR, de Wit MJ (1978) Field and geochemical data bearing on the development of a Mesozoic volcano-tectonic rift zone and back-arc basin in southernmost South America. *Earth Planet Sc Lett* 41(1):32–46
- Calderón M, Fildani A, Hervé F, Fanning CM, Weislogel A, Cordani U (2007) Late Jurassic bimodal magmatism in the northern sea-floor remnant of the Rocas Verdes basin, Southern Patagonian Andes. *J Geol Soc Lond* 164:1011–1022
- Calderón M, Fosdick JC, Warren C, Massonne HJ, Fanning CM, Fadel Cury L, Schwanethal J, Fonseca PE, Galaz G, Gaytán D, Hervé F (2012) The low-grade Canal de las Montañas Shear Zone and its role in the tectonic emplacement of the Sarmiento Ophiolitic complex and Late Cretaceous Patagonian Andes orogeny, Chile. *Tectonophysics* 525:165–185

- Calderón M, Hervé F, Fuentes F, Fosdick JC, Sepúlveda F, Galaz G (2016) Tectonic evolution of Paleozoic and Mesozoic andean metamorphic complexes and the Rocas Verdes ophiolites in southern Patagonia. In: Ghiglione MC (ed) *Geodynamic Evolution of the Southernmost Andes*. Springer Earth System Sciences, pp 7–36
- Carey SW (1955) The orocline concept in geotectonics. *P Roy Soc of Tasmania* 89:255–288
- Castelli J, Robertson R, Harambour S (1992) Evaluación Geológica y Petrolera, bloques Última Esperanza Sur e Isla Riesco. Unpubl. report. Empresa Nacional del Petróleo, Chile, p 160
- Cerredo ME, Tassone A, Rapalini A, Hervé F, Fanning M (2011a) Campanian magmatism in the Fuegian Andes: new SHRIMP age of JeuJepen pluton. Argentina. XVIII Argentinian Geological Congress, Neuquén, pp 714–715
- Cerredo ME, Tassone A, Peroni J, Menichetti M (2011b) Late Cretaceous magmatism in central Tierra del Fuego: Kranck Pluton, Fuegian Andes, Argentina. I Symposium on Igneous Petrology and Associated Metallogenesis, San Miguel de Tucumán, p 1
- Cunningham WD (1993) Strike-slip faults in the Southernmost Andes and the development of the Patagonian Orocline. *Tectonics* 12:169–186
- Cunningham WD (1995) Orogenesis at the southern tip of the Americas: the structural evolution of the Cordillera Darwin metamorphic complex, Southernmost Chile. *Tectonophysics* 244:197–229
- Cunningham WD, Klepeis KA, Gose WA, Dalziel IW (1991) The Patagonian Orocline: new paleomagnetic data from the Andean magmatic arc in Tierra del Fuego, Chile. *J Geophys Res* 96:16061–16069
- Dalziel IWD (1981) Backarc extension in the Southern Andes: a review and critical reappraisal. *Philos Trans R Soc Lond* 300:319–335
- Dalziel IWD (1986) Collision and Cordilleran orogenesis: an Andean perspective. In: Coward MP, Riers AC (eds) *Collision Tectonics*, Geol Soc Spec Publ 19:389–404
- Dalziel IWD, de Wit MF, Palmer KF (1974) Fossil marginal basin in the Southern Andes. *Nature* 250:291–294
- Davidson J, Mpodozis C, Godoy E, Hervé F, Muñoz N (1989) Jurassic accretion of a high buoyancy guyot in the southernmost South America: the Diego Ramirez Islands. *Rev Geol Chile* 16:247–251
- de Wit MJ (1977) The evolution of the Scotia Arc as a key to the reconstruction of Southwestern Gondwanaland. *Tectonophysics* 37:53–81
- Diraison M, Cobbold PR, Gapais D, Rossello EA, Le Corre C (2000) Cenozoic crustal thickening, wrenching and rifting in the foothills of the Southernmost Andes. *Tectonophysics* 316:91–119
- Dott R, Winn R, de Wit M, Bruhn L (1977) Tectonic and sedimentary significance of Cretaceous Tekonika Beds of Tierra del Fuego. *Nature* 266:620–622
- Eagles G, Gohl K, Larter RD (2009) Animated tectonic reconstruction of the Southern Pacific and alkaline volcanism at its convergent margins since Eocene times. *Tectonophysics* 464:21–29
- Eagles G, Scott B (2014) Plate convergence west of Patagonia and the Antarctic Peninsula since 61 Ma. In: Maldonado A, Dalziel IWD, Leat PT (eds) *Scotia arc evolution: global implications*. *Glob Planet Change* 123:189–198
- Eagles G (2016) Tectonic reconstructions of the Southernmost Andes and the Scotia Sea during the opening of the Drake Passage. In: Ghiglione MC (ed) *Geodynamic Evolution of the Southernmost Andes*. Springer Earth System Sciences, pp 75–108
- Elsztein C (2004) Geología y evolución del Complejo Intrusivo de la Península Ushuaia, Tierra del Fuego. Graduate Thesis (unpubl.), Univ. Buenos Aires, p 103
- Elliott T, Plank T, Zindler A, White W, Bourdon B (1997) Element transport from slab to volcanic front at the Mariana Arc. *J Geophys Res* 102:14991–15019
- Espinoza F, Morata D, Lagabrielle Y (2007) Chemical similarities between Miocene Patagonia Calc-alkaline magmatism and some “flat-slab” volcanics: a first approach. *International Congress on Geology and Geophysics of the Southern Hemisphere (GeoSur)*, Santiago de Chile, p 55
- Fildani A, Hessler AM (2005) Stratigraphic record across a retroarc basin inversion: Rocas Verdes Magallanes Basin, Patagonian Andes. *Geol Soc Am Bull* 117:1596–1614

- Folguera A, Ramos V (2011) Repeated eastward shifts of arc magmatism in the Southern Andes: a revision to the long-term pattern of Andean uplift and Magmatism. *J S Am Earth Sci* 32(4):531–546
- Fuenzalida R, Covacevich V (1988) Volcanismo y bioestratigrafía del Jurásico Superior y Cretácico Inferior en la Cordillera Patagónica, Región de Magallanes, Chile. V Chilean Geological Congress, Santiago, Actas 3(H):159–183
- Galaz G, Hervé F, Calderón M (2005) Metamorfismo y deformación de la Formación Tobífera en la Cordillera Riesco, Región de Magallanes, Chile. *Rev Asoc Geol Argent* 60:762–774
- Gealey WK (1980) Ophiolite obduction mechanisms. In: Panatiouyou A (ed) *Ophiolites, Proceedings International Ophiolite Symposium, Cyprus*. Cyprus Geological Survey, Nicosia, pp 228–243
- Ghiglione MC, Ramos VA (2005) Chronology of deformation in the Southernmost Andes of Tierra del Fuego. *Tectonophysics* 405:25–46
- Ghiglione MC, Cristallini E (2007) Have the Southernmost Andes been curved since Late Cretaceous time? An analog test for the Patagonian Orocline. *Geology* 35:13–16
- Gill JB (1981) *Orogenic andesite and plate tectonics*. Springer, New York
- Gombosi DJ, Barbeau DL, Garver J (2009) New thermochronometric constraints on the rapid Paleogene exhumation of the Cordillera Darwin complex and related thrust sheets in the Fuegian Andes. *Terra Nova* 21:507–515
- González Guillot M (2009) Estudio petrogenético de plutones de la Cordillera Fueguina entre el lago Fagnano y el canal Beagle y algunas consideraciones sobre las mineralizaciones asociadas. Ph.D. thesis (unpubl.), Univ. Nac. La Plata, p 327
- González Guillot M, Acevedo D (2009) Facies con biotita y granate en plutones de los Andes Fueguinos de Argentina. XII Chil Geol Congr, Santiago de Chile S8–014:4
- González Guillot M, Schalamuk I (2009) Mineralizaciones metalíferas en rocas ultramáficas de Tierra del Fuego. Argentina. IX Argentinian Congress of Economic Geology, Catamarca, pp 19–24
- González Guillot M, Escayola M, Acevedo R, Pimentel M, Seraphim G, Proenza J, Schalamuk I (2009) The Plutón Diorítico Moat: Mildly alkaline monzonitic magmatism in the Fuegian Andes of Argentina. *J S Am Earth Sci* 28:345–359
- González Guillot M, Escayola M, Acevedo R (2011) Calc-alkaline rear-arc magmatism in the Fuegian Andes: implications for the mid-Cretaceous tectonomagmatic evolution of southernmost South America. *J S Am Earth Sci* 31:1–16
- González Guillot M, Prezzi C, Acevedo RD, Escayola M (2012) A comparative study of two rear-arc plutons and implications for the Fuegian Andes tectonic evolution: mount Kranck Pluton and Jeu-Jepén Monzonite, Argentina. *J S Am Earth Sci* 38:71–88
- González Guillot M, Urraza I, Acevedo RD, Escayola M (2016) Magmatismo básico Jurásico-Cretácico en los Andes Fueguinos y su relación con la cuenca marginal Rocas Verdes. *Rev Asoc Geol Argentina* (in press)
- Grunow AM (1993) Creation and destruction of Weddell Sea floor in the Jurassic. *Geology* 21:647–650
- Gust DA, Biddle KT, Phelps DW, Uliana MA (1985) Associated middle to late Jurassic volcanism and extension in southern South America. *Tectonophysics* 116:223–253
- Halpern M (1973) Regional geochronology of Chile South of 50° Latitude. *Geol Soc Am Bull* 84(7):2407–2422
- Halpern M, Rex DC (1972) Time of folding of the Yahgan Formation and age of the Tekenika beds, Southern Chile, South America. *Geol Soc Am Bull* 83:1881–1886
- Hanson R, Wilson T (1991) Submarine rhyolitic volcanism in a Jurassic proto-marginal basin; Southern Andes, Chile and Argentina. In: Harmon R, Rapela C (eds) *Andean Magmatism and its tectonic setting*. *Geol S Am S* 265:13–27
- Hanyu T, Gill J, Tatsumi Y, Kimura JI, Sato K, Chang Q, Senda R, Miyazaki T, Hirahara Y, Takahashi T, Zulkarnain I (2012) Across- and along-arc geochemical variations of lava chemistry in the Sangihe arc: various fluid and melt slab fluxes in response to slab temperature. *Geochem Geophys Geosys* 13(10):Q10021

- Hawkesworth C, Turner S, Peate D, McDermott F, van Calsteren P (1997) Elemental U and Th variations in island arc rocks: implications for U-series isotopes. *Chem Geol* 139:207–221
- Hervé F, Nelson E, Kawashita K, Suárez M (1981) New isotopic ages and the timing of orogenic events in the Cordillera Darwin, Southernmost Chilean Andes. *Earth Planet Sc Lett* 55(2): 257–265
- Hervé F, Pankhurst R, Fanning C, Calderón M, Yaxley G (2007a) The South Patagonian Batholith: 150 my of granite magmatism on a plate margin. *Lithos* 97:373–394
- Hervé F, Massonne HJ, Calderón M, Theye T (2007b) Metamorphic P-T conditions of Late Jurassic rhyolites in the Magallanes fold and thrust belt, Patagonian Andes, Chile. *J Iberian Geol* 33(1):5–16
- Hervé M, Suárez M, Puig A (1984) The Patagonian Batholith south of Tierra del Fuego, Chile. Timing and tectonic implications. *J Geol Soc Lond* 141(5):909–917
- Johnson M, Plank, T (1999) Dehydration and melting experiments constrain the fate of subducted sediments. *Geochem Geophys Geosys* 1 GC000014
- Katz HR, Waters WA (1966) Geological investigations of the Yahgán Formation (Upper Mesozoic) and associated igneous of Navarino island, southern Chile. *N Z J Geol Geophys* 9(3):323–359
- Kay SM, Mpodozis C (2002) Magmatism as a probe to the Neogene shallowing of the Nazca plate beneath the modern Chilean flat-slab. *J S Am Earth Sci* 15:39–57
- Kay SM, Ramos VA, Mpodozis C, Sruoga P (1989) Late Paleozoic to Jurassic silicic magmatism at the Gondwana margin: analogy to the middle Proterozoic in North America. *Geology* 17:324–328
- Kimura J-I, Kent A, Rowe M, Katakuse M, Nakano F, Hacker B, van Keken P, Kawabata H, Stern R (2010) Origin of cross-chain geochemical variation in Quaternary lavas from the northern Izu arc: Using a quantitative mass balance approach to identify mantle sources and mantle wedge processes. *Geochem Geophys Geosys* 11(10):Q10011
- Klepeis KA (1994a) Relationship between uplift of the metamorphic core of the Southernmost Andes and shortening in the Magallanes foreland fold and thrust belt, Tierra del Fuego, Chile. *Tectonics* 13:882–904
- Klepeis KA (1994b) The Magallanes and Deseado fault zones: major segments of the South American-Scotia transform plate boundary in Southernmost South America, Tierra del Fuego. *J Geophys Res* 99(B11):22,001–22,014
- Klepeis KA, Austin JA (1997) Contrasting styles of superposed deformation in the Southernmost Andes. *Tectonics* 16(5):755–776
- Klepeis K, Betka P, Clarke G, Fanning M, Hervé F, Rojas L, Mpodozis C, Thomson S (2010) Continental underthrusting and obduction during the Cretaceous closure of the Rocas Verdes rift basin, Cordillera Darwin, Patagonian Andes. *Tectonics* 29 TC3014
- Kohn MJ, Spear FS, Harrison TM, Dalziel IWD (1995) $^{40}\text{Ar}/^{39}\text{Ar}$ geochronology and P-T-t paths from the Cordillera Darwin metamorphic complex, Tierra del Fuego, Chile. *J Met Geol* 13:251–270
- Kraemer PE (2003) Orogenic shortening and the origin of the Patagonian orocline (56 S Lat). *J S Am Earth Sci* 15:731–748
- Kranck EH (1932) Geological investigations in the Cordillera of Tierra del Fuego. *Acta Geogr Helsinki* 4(2):1–231
- Lameyre J (1987) Granites and evolution of the crust. *Rev Bras Geociências* 17(4):349–359
- Lameyre J, Bowden P (1982) Plutonic rock type series: discrimination of various granitoids series and related rocks. *J Volcanol Geoth Res* 14:169–186
- Lameyre J, Bonin B (1991) Granites in the main plutonic series. In: Didier J, Barbarin B (eds) *Enclaves and granite petrology*. *Dev Petrol* 13:3–17. Elsevier
- Likerman L, Burlando JF, Cristallini EO, Ghiglione MC (2013) Along-strike structural variations in the Southern Patagonian Andes: insights from physical modeling. *Tectonophysics* 590:106–120
- Lodolo E, Menichetti M, Bartole R, Ben-Avraham Z, Tassone A, Lippai H (2003) Magallanes-Fagnano continental transform fault (Tierra del Fuego, southernmost South America). *Tectonics* 22:1076

- Maffione M (2016) Kinematic evolution of the Southern Andean orogenic arc. In: Ghiglione MC (ed) *Geodynamic Evolution of the Southernmost Andes*. Springer Earth System Sciences, pp 173–200
- Maffione M, Speranza F, Faccenna C, Rossello E (2010) Paleomagnetic evidence for a pre-early Eocene (~50 Ma) bending of the Patagonian orocline (Tierra del Fuego, Argentina): Paleogeographic and tectonic implications. *Earth Plan-Net Sc Lett* 289:273–286
- Maffione M, Fernandez-Moreno C, Ghiglione M, Speranza F, van Hinsbergen DJJ, Lodolo E (2015) Constraints on deformation of the Southern Andes since the Cretaceous from anisotropy of magnetic susceptibility. *Tectonophysics* 665:236–250
- Maloney KT, Clarke GL, Klepeis KA, Fanning CM, Wang W (2011) Crustal growth during back-arc closure: Cretaceous exhumation history of Cordillera Darwin, Southern Patagonia. *J Metamorph Geol* 29(6):649–672
- Marsh BD (1979) Island arc development: some observations, experiments, and speculations. *J Geol* 87:687–713
- Martin M, Pankhurst R, Fanning C, Thompson S, Calderón M, Hervé F (2001) Age and distribution of plutons across the Southern Patagonian Batholith: new U-Pb data on zircons. South American symposium on Isotope Geology. Sociedad Geológica de Chile, Santiago. Extended Abstracts (CD): 585–588
- Martinioni DR, Linares E, Acevedo RD (1999) Significado de la edad isotópica de diques básicos intruidos en la Formación Beauvoir (Cretácico temprano) Tierra del Fuego. Argentina. *Rev Asoc Geol Argentina* 54(1):88–91
- McAtamney J, Klepeis K, Mehrtens C, Thomson S, Betka P, Rojas L, Snyder S (2011) Along-strike variability of back-arc basin collapse and the initiation of sedimentation in the Magallanes foreland basin, Southernmost Andes (53–54.5°S). *Tectonics* 30 TC5001
- Menichetti M, Lodolo E, Tassone A (2008) Structural geology of the Fuegian Andes and Magallanes fold and thrust belt-Tierra del Fuego island. *Geologica Acta* 6:19–42
- Michael PJ (1991) Intrusion of basaltic magmas into a crystallizing granitic magma chamber; the Cordillera del Paine Pluton in southern Chile. *Contrib Miner Petr* 108:396–418
- Michel J, Baumgartner L, Putlitz B, Schaltegger U, Ovtcharova M (2008) Incremental growth of the Patagonian Torres del Paine laccolith over 90 ky. *Geology* 36:459–462
- Middlemost EAK (1991) Towards a comprehensive classification of igneous rocks and magmas. *Earth Sc Rev* 31:73–87
- Miller CA, Barton M, Hanson RE, Fleming TH (1994) An Early Cretaceous volcanic arc/marginal basin transition zone, Peninsula Hardy, southernmost Chile. *J Volcanol Geoth Res* 63(1–2): 33–58
- Miyashiro A (1978) Nature of alkalic volcanic rock series. *Contrib Miner Petr* 66:91–104
- Morris JD, Ryan JG (2003) Subduction zone processes and implications for changing composition of the upper and lower mantle. In: Carlson RW (ed) *The mantle and core, vol 2*. Treatise on Geochemistry, Elsevier-Pergamon-Oxford, pp 451–470
- Morrison GW (1980) Characteristics and tectonics of the shoshonite rock association. *Lithos* 13:97–108
- Mpodozis C (2006) Revisión de la estratigrafía y facies de la cuenca de antepaís cretácica entre Lago Argentino y Península Brunswick. Unpubl. report. Empresa Nacional del Petróleo, Chile, p 161
- Mpodozis C, Rojas L (2006) Orogénesis en los Andes Patagónicos Australes de Tierra del Fuego: cierre de una “cuenca marginal” o colisión intracontinental? XI Chil Geol Congr, Antofagasta, Chile 2:283–286
- Mpodozis C, Alvarez P, Elgueta S, Mella P, Hervé F, Fanning M (2007) Revised Cretaceous stratigraphy of the Magallanes Foreland Basin at Seno skyring: regional implications of new SHRIMP age data on detrital zircon populations. *International Congress on the Geology and Geophysics of the Southern Hemisphere (GeoSur)*, Santiago de Chile, p 106
- Mukasa SB, Dalziel IWD (1996) Southernmost Andes and South Georgia island, north Scotia Ridge: zircon U-Pb and muscovite Ar/Ar age constraints on tectonic evolution of southwestern Gondwanaland. *J S Am Earth Sci* 9:349–365

- Mukasa SB, Brueckner HK, Dalziel IWD (1988) Zircon U-Pb constraints on the kinematic evolution of the Northern Scotia Arc. *Geol Soc Am Abstr Programs* 20:A12
- Nelson EP (1982) Posttectonic uplift of the Cordillera Darwin orogenic core complex: evidence for fission track geochronology and closing temperature time relationships. *J Geol Soc Lond* 139:755–761
- Nelson EP, Dalziel IWD, Milnes AG (1980) Structural geology of the Cordillera Darwin-collision style orogenesis in the Southernmost Andes. *Eclogae Geol Helv* 73:727–751
- Nelson E, Bruce B, Elthon D, Kammer D, Weaver S (1988) Regional lithologic variations in the Patagonian Batholith. *J S Am Earth Sci* 1(3):239–247
- Olivero E, Martinioni D (2001) A review of the geology of the Argentinian Fuegian Andes. *J S Am Earth Sci* 14:175–188
- Olivero E, Malumian N (2007) Mesozoic-Cenozoic stratigraphy of the Fuegian Andes Argentina. *Geologica Acta* 6(1):5–18
- Pagel M, Leterrier J (1980) The subalkaline potassic magmatism of the Ballons massif (Southern Vosges, France): shoshonitic affinity. *Lithos* 13:1–10
- Pankhurst RJ, Leat PT, Sruoga P, Rapela CW, Márquez M, Storey BC, Riley TR (1998) The Chon Aike province of Patagonia and related rocks in West Antarctica: a silicic large igneous province. *J Volcanol Geoth Res* 81:113–136
- Pearce J, Stern R, Bloomer S, Fryer P (2005) Geochemical mapping of the Mariana Arc-Basin System: implications for the nature and distribution of subduction components. *Geochem Geophys Geosys* 6 2004GC000895
- Pelayo A, Wiens D (1989) Seismotectonics and relative plate motions in the Scotia Sea region. *J Geophys Res* 94:7293–7320
- Peroni J, Tassone A, Menichetti M, Cerredo M (2009) Geophysical modeling and structure of Ushuaia Pluton, Fuegian Andes, Argentina. *Tectonophysics* 476:436–449
- Poblete F, Roperch P, Hervé F, Diraison M, Espinoza M, Arriagada C (2014) The curved Magallanes fold and thrust belt: tectonic insights from a paleomagnetic and anisotropy of magnetic susceptibility study. *Tectonics* 33(12):2526–2551
- Prades CF (2008) Petrología y metamorfismo de las rocas basálticas en Isla Capitán Aracena, Isla Carlos III y Estero La Pera, Región de Magallanes, Chile. Graduate Thesis, Univ. Chile, p 145
- Puig A, Hervé M, Suárez M, Saunders A (1984) Calc-alkaline and alkaline Miocene and calc-alkaline recent volcanism in the Southernmost Patagonia Cordillera, Chile. *J Volcanol Geoth Res* 20:149–163
- Ramírez de Arellano C, Putlitz B, Müntener O, Ovtcharova M (2012) High precision U/Pb zircon dating of the Chaltén Plutonic Complex (Cerro Fitz Roy, Patagonia) and its relationship to arc migration in the Southernmost Andes. *Tectonics* 31 TC4009
- Ramos VA, Haller MJ, Butrón F (1986) Geología y Evolución tectónica de las Islas Barnevelt. *Rev Asoc Geol Argentina* 15:137–154
- Ramos VA, Kay SM, Singer B (2004) Las adakitas de la Cordillera Patagónica: Nuevas evidencias geoquímicas y geocronológicas. *Rev Asoc Geol Argentina* 59(4):693–706
- Rapalini A, Peroni J, Luppo T, Tassone A, Cerredo ME, Esteban F, Lippai H, Vilas F (2015) Palaeomagnetism of Mesozoic magmatic bodies of the Fuegian Cordillera: implications for the formation of the Patagonian Orocline. In: Pueyo EL, Cifelli F, Sussman AJ, Oliva-Urcia B (eds) *Palaeomagnetism in Fold and Thrust Belts: New Perspectives*. *Geol Soc Spec Publ* 425 <http://doi.org/10.1144/SP425.3>
- Rickwood PC (1989) Boundary lines between petrologic diagrams which use oxides of major and minor elements. *Lithos* 22:247–263
- Rollinson HR (1993) Using geochemical data: evaluation presentation, interpretation. Longman Scientific & Technical, England, p 352
- Rossello EA (2005) Kinematics of the Andean sinistral wrenching along the Fagnano-Magallanes fault zone (Argentina-Chile Fuegian foothills). 6th International Symposium on Andean Geodynamics (ISAG), Barcelona. Extended Abstracts, pp 623–626
- Rubio E, Torné M, Vera E, Díaz A (2000) Crustal structure of the Southernmost Chilean margin from seismic and gravity data. *Tectonophysics* 323:39–60

- Sakuyama N, Nesbitt RW (1986) Geochemistry of the Quaternary volcanic rocks of the Northeast Japan arc. *J Volcanol Geoth Res* 29:413–450
- Sánchez A, Saint-Blanquat M, Hervé F, Pankhurst RJ, Fanning CM (2006) A Shrimp U-Pb zircon late Miocene crystallization age for the Torres Del Paine Pluton, Chile. In: *Proceedings of V South American Symposium on Isotope Geology*, Punta del Este, Uruguay, 24–27 April, 2006
- Saunders AD, Tarney J, Stern CR, Dalziel IWD (1979) Geochemistry of Mesozoic marginal basin floor igneous rocks from southern Chile. *Geol Soc Am Bull* 90:237–258
- Sernageomin (2003) Mapa Geológico de Chile: versión digital, escala 1:1,000,000. Servicio Nacional de Geología y Minería, Santiago, Chile
- Soffia JM (1988) Evaluación geológica y petrolera del sector sur de la provincia de Última Esperanza. Unpubl. report. Empresa Nac del Petróleo, Chile, p 89
- Stern CR (1979) Open and closed system igneous fractionation within two Chilean ophiolites and their tectonic implications. *Contrib Miner Petr* 68:243–258
- Stern CR (1980) Geochemistry of Chilean ophiolites, evidence for the compositional evolution of the mantle source of back-arc basin basalts. *J Geophys Res* 85(B2):955–966
- Stern CR (1991) Role of subduction erosion in the generation of Andean magmas. *Geology* 19: 78–81
- Stern CR, De Wit MJ (2003) Rocas Verdes ophiolites, Southernmost South America: remnants of progressive stages of development on oceanic-type crust in a continental margin back-arc basin. In Dilek Y, Robinson PT (eds) *Ophiolites in earth history*. *Geol Soc Spec Publ* 218:1–19
- Stern CR, Kilian R (1996) Role of the subducted slab, mantle wedge and continental crust in the generation of adakites from the Andean Austral Volcanic Zone. *Contrib Miner Petr* 123: 263–281
- Stern CR, Mohseni PP, Fuenzalida R (1991) Petrochemistry and tectonic significance of Lower Cretaceous Barros Arana Formation basalts, Southernmost Chilean Andes. *J S Am Earth Sci* 4:331–342
- Storey BC, Alabaster T (1991) Tectonomagmatic controls on Gondwana break-up models: Evidence from the proto-Pacific margin of Antarctica. *Tectonics* 10:1274–1288
- Suárez M (1977a) Notas geoquímicas preliminares del Batolito Patagónico al sur de Tierra del Fuego, Chile. *Rev Geol Chile* 4:15–33
- Suárez M (1977b) Aspectos geoquímicos del Complejo Ofolítico Tortuga en la Cordillera Patagónica del sur de Chile. *Rev Geol Chile* 4:3–14
- Suárez M, Pettigrew TH (1976) An upper Mesozoic island-arc back-arc system in the Southern Andes and South Georgia. *Geol Mag* 113:305–400
- Suárez M, Hervé M, Puig A (1985) Hoja Isla Hoste e islas adyacentes, XII Región. *Carta Geológica de Chile* 1:250.000, no. 65. Servicio Nacional de Geología y Minería, Chile, p 113
- Suárez M, Puig A, Hervé M (1986) K-Ar dates on granitoids from Archipiélago Cabo de Hornos, Southernmost Chile. *Geol Mag* 123(5):581–584
- Suárez M, Naranjo JA, Puig A (1990) Mesozoic “S-like” granites of the central and Southern Andes: a review. In: Kay SM, Rapela CW (eds) *Plutonism from Antarctica to Alaska*. *Geol S Am S* 241:27–32
- Sun SS, McDonough WF (1989) Chemical and isotopic systematics of oceanic basalts: implications for mantle composition and processes. In: Saunders AD, Norry MJ (eds) *Magmatism in Ocean Basins*. *Geol Soc Spec Publ* 42:313–345
- Tatsumi Y (2003) Some constraints on arc magma genesis. In: Eiler J (ed) *Inside the subduction factory*. *AGU, Geophys Monogr* 138:277–292
- Tatsumi Y, Eggins S (1995) *Subduction zone magmatism*. Blackwell, Boston
- Tatsumi Y, Kogiso T (1997) Trace element transport during dehydration processes in the subducted oceanic crust: 2. Origin of chemical characteristics in arc magmas. *Earth Planet Sc Lett* 148:207–222
- Tatsumi Y, Sakuyama M, Fukuyama H, Kushiro I (1983) Generation of arc basalt magmas and thermal structure of the mantle wedge in subduction zones. *J Geophys Res* 88:5815–5825
- Taylor SR, McLennan SM (1985) *The Continental crust: its composition and evolution*. Blackwell, Boston, MA

- Torres Carbonell P, Dimieri L (2013) Cenozoic contractional tectonics in the Fuegian Andes, Southernmost South America: a model for the transference of orogenic shortening to the foreland. *Geol Acta* 11:331–357
- Torres Carbonell P, Dimieri L, Olivero E, Bohoyo F, Galindo-Zaldívar J (2014) Structure and tectonic evolution of the Fuegian Andes (Southernmost South America) in the framework of the Scotia Arc development. *Glob Planet Change* 123:174–188
- Yogodzinski G, Volynets O, Koloskiv A, Seliverstov N, Matvenkov V (1994) Magnesian andesites and the subduction component in a strongly calc-alkaline series at Piip volcano, Far Western Aleutians. *J Petrol* 35:163–204
- Yogodzinski G, Kay R, Volynets O, Koloskov A, Kay S (1995) Magnesian andesite in the western Aleutian Komandorsky region: implications for slab melting and processes in the mantle wedge. *Geol Soc Am Bull* 107:505–519

Tectonic Reconstructions of the Southernmost Andes and the Scotia Sea During the Opening of the Drake Passage

Graeme Eagles

Abstract Study of the tectonic development of the Scotia Sea region started with basic lithological and structural studies of outcrop geology in Tierra del Fuego and the Antarctic Peninsula. To nineteenth- and early twentieth-century geologists, the results of these studies suggested the presence of a submerged orocline running around the margins of the Scotia Sea. Subsequent increases in detailed knowledge about the fragmentary outcrop geology from islands distributed around the margins of the Scotia Sea, and later their interpretation in the light of the plate tectonic paradigm led to large modifications in the hypothesis such that by the present day the concept of oroclinal bending in the region persists only in vestigial form. Of the early comparative lithostratigraphic work in the region, only the likenesses between Jurassic–Cretaceous basin floor and fill sequences in South Georgia and Tierra del Fuego are regarded as strong enough to be useful in plate kinematic reconstruction by permitting the interpretation of those regions' contiguity in mid-Mesozoic times. Marine and satellite geophysical data sets reveal features of the remaining, submerged, 98 % of the Scotia Sea region between the outcrops. These data enable a more detailed and quantitative approach to the region's plate kinematics. In contrast to long-used interpretations of the outcrop geology, these data do not prescribe the proximity of South Georgia to Tierra del Fuego in any past period. It is, however, possible to reinterpret the geology of those two regions in terms of the plate kinematic history that the seafloor has preserved.

Keywords Southernmost Andes · Scotia Sea · Scotia Ridge · Antarctica · Antarctic Peninsula · Drake Passage

G. Eagles (✉)

Helmholtz Centre for Marine and Polar Research, Alfred Wegener Institute,
Bremerhaven, Germany
e-mail: geagles@awi.de

1 Introduction

The Scotia Sea is the name given to the area of the Southern Ocean lying to the east of Drake Passage, the strait that separates Tierra del Fuego from the Antarctic Peninsula (Fig. 1). It is named after the ship *S.Y. Scotia* that brought W.S. Bruce's Scottish National Antarctic Expedition to the region in 1902–1904, but has been known to Western scientists, including the young Charles Darwin, since the early nineteenth century. Since that time, Drake Passage and the Scotia Sea have been suggested to play important roles for processes as diverse as migration, colonisation and evolution of the land fauna of South America and Australia (e.g. Reguero and Marensi 2010), evolution and migration of volcanic vent-specific fauna between the Pacific and Atlantic oceans (Roterman et al. 2013), whale and penguin evolution (Fordyce 2003; Hospitaleche et al. 2013) and the flow of asthenospheric rocks from beneath the Pacific plates to beneath those of the Atlantic (Helfrich et al. 2002; Müller 2001; Nerlich et al. 2013). Most famously, however, an open Drake Passage is frequently referred to as a necessary prerequisite for, or even a driver of, the onset of the Antarctic Circumpolar Current and the attendant permanent glaciation of Antarctica in Neogene times (Kennett 1977; Toggweiler and Björnsson 2000).

All these processes are active and changeable on geological timescales, making the question of the first completion of Drake Passage pertinent to understanding them better. The passage exists as a result of oblique separation of the South American and Antarctic plates, which in turn caused the local development and relative motion of a number of smaller, shorter-lived plates, whose remnants constitute the floor of the Scotia Sea and its margins. The main archives of the motions of these plates are the exposed rocks dotted around the Scotia Sea margins, and the patterns of fracture zones and magnetic reversal isochrons in the floor of the Scotia Sea itself. This chapter reviews what can be interpreted of the plate tectonic history of the region by using these resources.

2 Comparative Tectonostratigraphy

Similarities between the Southernmost Andes and the mountain ranges of the Antarctic Peninsula have been sought and presented since the early nineteenth century. Arctowski (1895) first proposed that the similarities are the result of oroclinal folding on a grand scale and that the rocks of the Andes continue into the peninsula via Shag Rocks and South Georgia on the North Scotia Ridge, the South Sandwich Islands, the South Orkney Islands on the South Scotia Ridge and the South Shetland Islands. These rocks and islands are all remote and their emergent parts encompass less than 2 % of the Scotia Sea (Fig. 1). Less still is accessible outcrop.

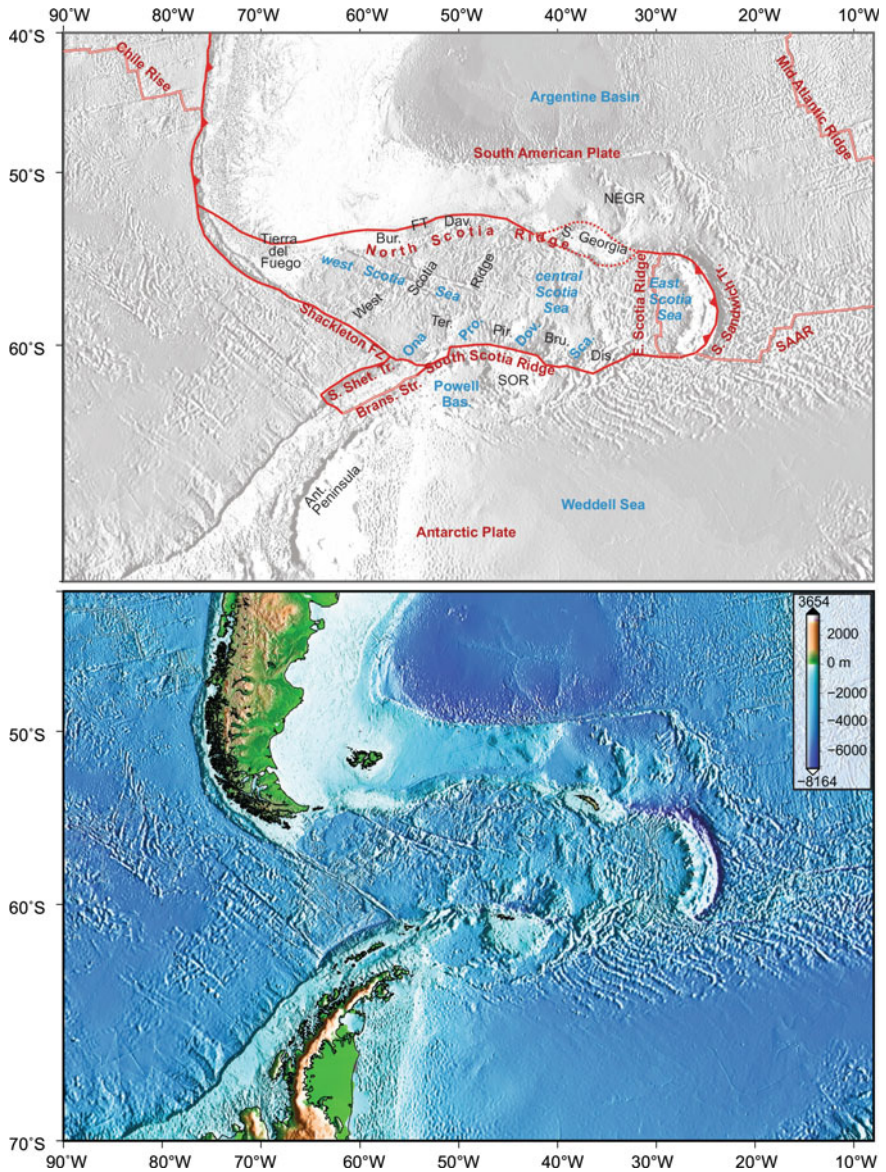


Fig. 1 Overview of the Scotia Sea region in bathymetric data (SRTM 15 PLUS; Becker et al. 2009). *Top Red lines*—present-day plate boundaries (modified from Bird 2003). *Red labels*: presently active tectonic features. *Blue labels*: basins and basin regions. *Black labels*: extinct tectonic features and bathymetric highs. *Brans. Str.*: Bransfield Strait; *Bru*: Bruce Bank; *Bur*: Burdwood Bank; *Dav*: Davis Bank; *Dis*: Discovery Bank; *Dov*: Dove Basin; *FT*: Falkland Trough; *NEGR*: North-east Georgia Rise; *Pir*: Pirie Bank; *Pro*: Protector Basin; *Sca*: Scan Basin; *SOR*: South Orkney Microcontinent; *S. Sandw. Tr.*: South Sandwich Trench; *S. Shet. Tr.*: South Shetland Trench; *Ter*: Terror Rise. *Bottom colour* background image without references

The idea of a tremendous Scotian Orocline remained popular through the first part of the twentieth century as visits to these outcrops confirmed the presence of Mesozoic rock assemblages like those of the Southernmost Andes and Antarctic Peninsula (Pirie 1905; Suess 1909; Tilley 1935; Trendall 1953, 1959). The topic of oroclinal bending in the region has remained the subject of intense debate amongst structural geologists and palaeomagnetists to this day (e.g. Cunningham 1995; Maffione et al. 2010, 2015; Maffione 2016).

By the second half of the twentieth century, the explanatory power of plate tectonics, along with improved sampling and dating techniques, brought the opportunity to assess details of the similarities of exposed rocks around the Scotia Sea's margins. The tectonostratigraphy of the Antarctic Peninsula and Tierra del Fuego came to be differentiated on the basis of differences in lithology, rock age and metamorphism. By then, close comparisons between the rocks of the South Orkney Islands and those of South Georgia or the South Shetland Islands were no longer supported by observations. Where correlations for the South Orkney Islands are still suggested, these are with upper Palaeozoic and lower Mesozoic rocks of the Antarctic Peninsula and the Southern Patagonian Andes north of Tierra del Fuego. These correlations are interpreted in terms of a shared history of subduction during that period, prompting suggestions of geographical proximity (Barron et al. 1978; Calderón et al. 2007, 2016; Hervé et al. 2003, 2005).

The most celebrated set of affinities in the region, however, are those between the Upper Jurassic and Lower Cretaceous rocks of Tierra del Fuego and South Georgia, which today occupy locations 1600 km apart at opposing ends of the boundary between the Scotia and South American plates (Fig. 1). These affinities are seen in the age and source of deposition of turbidites and interpreted for the timing and setting of their deformation. The inset in Fig. 2 summarises the often-reported 'grain for grain' comparability of the Aptian–Albian, Sandebugten and Cumberland Bay formations of South Georgia to the Yahgán Formation of central Tierra del Fuego (Dalziel et al. 1975; Winn 1978). Both sequences consist of turbidites of andesitic debris overlain by more quartz-rich turbidites sourced by erosion of rhyolitic rocks to the north. Carter et al. (2014) presented U–Pb dating work on zircon grains that confirm how the three formations share similar Mesozoic sources. Furthermore, both turbiditic sequences are bounded to the south by ophiolitic complexes of Early Cretaceous age. The rocks are folded on similar wavelengths and the axes have similar orientations, which have been interpreted to indicate a common deformational setting at some period. This period has usually been put in mid-Cretaceous times, because various lines of evidence from the Yahgán rocks and elsewhere in Tierra del Fuego suggest that a protracted period of basin closure started in the period before 86 Ma (Klepeis et al. 2010). Less prescriptively, Rb–Sr analyses on minerals from a biotite schist (84 Ma; Curtis et al. 2010) and K–Ar whole-rock dating (135–51 Ma with best fits for 92–81 Ma; Thomson et al. 1982) record the timing of greenschist facies metamorphism around the same time near the Cooper Bay Shear Zone in south-eastern South Georgia. At other locations on the island, widespread prehnite occurrence and zircon- and apatite-based thermal histories show that granites were intruded at ~100 Ma, that

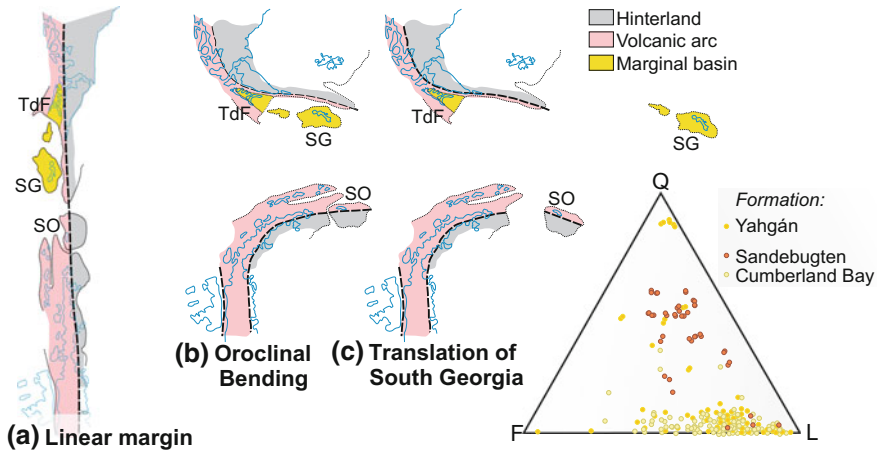


Fig. 2 Survival of the late-nineteenth-century orocline concept into the plate tectonic age and its modification by **a** segregation of the limbs into three elements related to subduction (volcanic arc, back-arc marginal basin and hinterland) and **b** bending and **c** post-bending translation of continental fragments (South Georgia; SG) and the South Orkney microcontinent (SO) away from Tierra del Fuego (TdF) (redrawn from Dalziel and Elliot 1971). *Bottom right*: Quartz–feldspar–lithics plots demonstrate the comparability of sedimentary rocks on South Georgia (Cumberland Bay and Sandebugten Formations) to those of similar age on Tierra del Fuego (Yahgán Formation). From Dalziel et al. (1975) and Winn (1978)

the neighbouring Cumberland Bay and Sandebugten formations were subsequently buried at shallow-to-moderate depths and that rapid uplift occurred starting in Eocene times (Clayton 1982; Carter et al. 2014).

These correlations are strong enough to support the notion of South Georgia having occupied a location immediately to the east of Isla Navarino and Tierra del Fuego in Early Cretaceous times (Dalziel and Elliot 1971). According to this idea, the Yahgán, Cumberland Bay and Sandebugten formations were deposited at that time side-by-side in a basin floored by oceanic crust, the so-called Rocas Verdes Marginal Basin (Fig. 3) (see Calderón et al. 2016; Guillot 2016). Later, both sets of rocks experienced orogenesis as the basin closed, which is usually attributed to an acceleration in the rate of seafloor spreading in the South Atlantic that increased the vigour of collision between the plates of the palaeo-Pacific ocean and South America (Dalziel 1986; Curtis et al. 2010). Since significant lateral translation is required for South Georgia to have subsequently reached its present-day position on the North Scotia Ridge, the orocline concept had to be modified to accommodate the idea of its limbs' fragmentation (Dalziel and Elliot 1971; Fig. 2a–c).

Figure 3 summarises the power of tectonostratigraphic correlations for regional reconstructions of the Scotia Sea. Available correlations can clearly support a wide range of such reconstructions. The similarities of South Georgia and Tierra del Fuego constitute essentially a single correlation point, permitting a wide angular range of possible locations for South America with respect to the Antarctic peninsula. Dalziel (1983) notes that, without additional information from plate kinematic

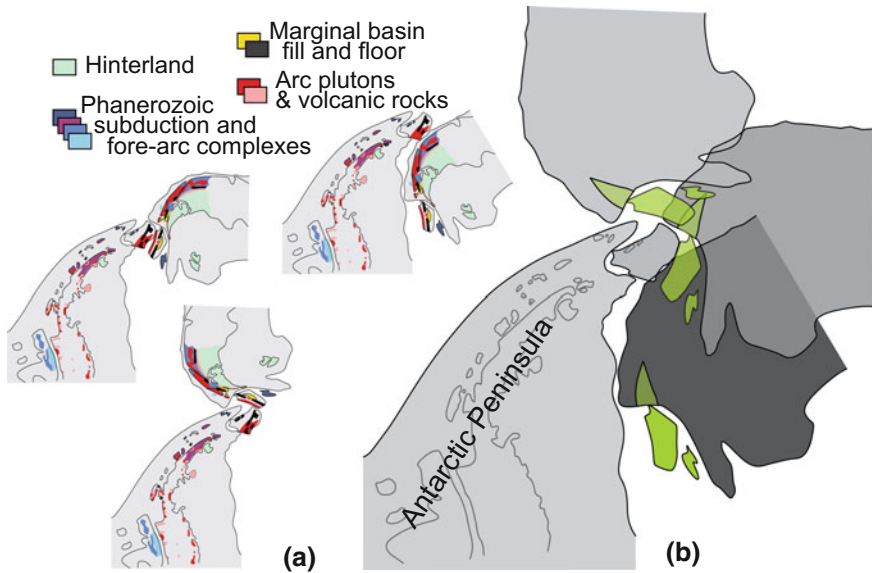


Fig. 3 **a** Three regional reconstructions that can be built on the basis of tectonostratigraphic correlations between outcrop geology in and around the Scotia Sea. Redrawn from Dalziel (1983). **b** Without other sources of constraint than the sedimentological similarities between the Cumberland Bay, Sandebugten and Yahgán formations of South Georgia and the Rocas Verdes basin (*green*), the three reconstructions must be seen as equally likely and thus of limited value for reconstructing the opening of the Scotia Sea

studies of the basins forming the Scotia Sea floor, there would be little reason to prefer any of these possibilities over the others. The next section reviews studies of this kind and their results, which have been developed since the late 1960s.

3 Basin Restoration

The recognition of magnetic anomaly isochrons over the seafloor in the Scotia Sea accompanied publication of the first magnetic reversal timescales in the late 1960s and early 1970s (Barker 1970, 1972). Using those timescales, a number of oceanic crustal provinces were identified on the basis of variable anomaly orientations and tentatively dated to periods over the last 40 Ma (Fig. 4). These provinces were identified as the products of episodes of plate divergence that had given rise to the creation of oceanic crust by volcanism. Taking advantage of the tenets of plate tectonics, that the interiors of plates are rigid and that deformation occurs only at the boundaries between pairs of plates, it is possible to reconstruct the development of the seafloor by reuniting the magnetic isochron pairs. The newly identified isochrons showed that the majority of the Scotia Sea floor had developed by east–west

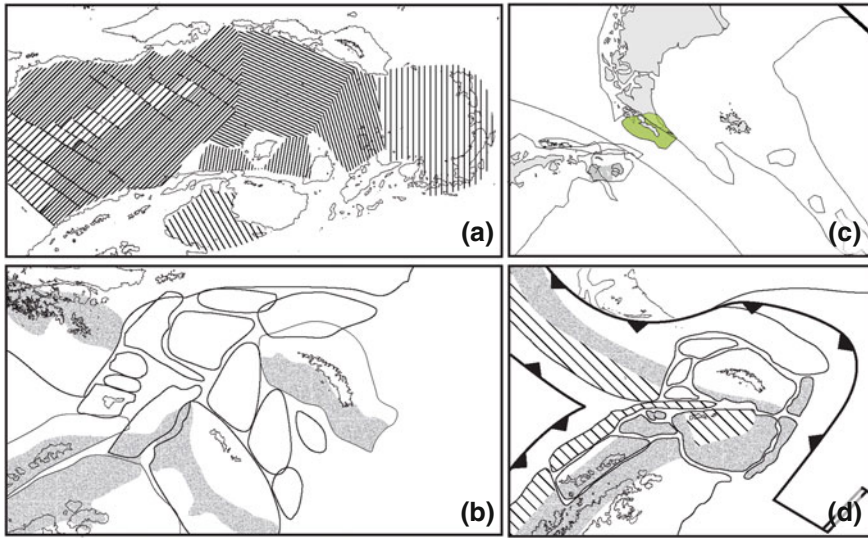


Fig. 4 **a** Magnetic anomaly provinces as interpreted from magnetic anomalies over the floor of the Scotia Sea by Barker (1970, 1972). The orientation of the hatching indicates the strike of the magnetic anomalies. Close hatching dated as 'post-Cretaceous' and wide hatching as <10 Myr old seafloor. **b** Plate kinematic reconstruction produced on a flat map by removing the oceanic crustal provinces between shallower, presumed continental, areas of crust. Stipple: areas of intense magnetic anomalies. Note that a close placement of South Georgia to Tierra del Fuego, as prescribed by sedimentological comparisons, is not a simple result of closing the oceanic basins of the Scotia Sea. **a** and **b** both redrawn from Barker and Griffiths (1972). **c** 50 Ma sphere-based plate reconstruction adapted from Lawver and Gahagan (2003), with emphasis on fidelity to tectonostratigraphic comparisons between South Georgia (green) and Tierra del Fuego. Note that this reconstruction, despite its numerical precision, ignores much of the detail addressed by Barker and Griffiths (1972). **d** Flat map reconstruction with all basins closed, generating a cuspsate connection and placing South Georgia and Tierra del Fuego in closer proximity than (**b**). Stipple: areas with strong magnetic anomalies. Hatching: areas with weak magnetic anomalies. Redrawn with modifications from King and Barker (1988)

or ESE–WNW-directed plate divergence episodes. Restoring the plate divergence that had led to their formation allowed for a compact cusp-like restoration of the basins' bounding blocks (Fig. 4b, c). The main exception to this pattern was an area in the central Scotia Sea that appeared to have opened by north–south-directed divergence. This province made it conceivable to restore South Georgia via two phases of plate motion, one oriented north–south and one ESE–WNW, to a position close, but not directly adjacent, to the continental margin SE of Tierra del Fuego (Barker and Griffiths 1972). A variety of smaller continental blocks were depicted, from the margins of the closed basins, tightly packed into the spaces around and between South Georgia and Tierra del Fuego (Fig. 4b).

Figure 4 gives a feeling for the sources of complexity in reconstructing the numerous continental and arc blocks of the Scotia Sea to one another by the removal of intervening oceanic basins. This complexity became clear after much effort was invested in characterising the floor of the Scotia Sea in detail both magnetically and bathymetrically (e.g. Barker and Burrell 1977; Hill and Barker 1980; Barker et al. 1982, 1984). Hence, whilst conclusions about the locations and opening directions of the individual basins in the Scotia Sea remained largely unchanged after the early 1970s, ideas about the number and the shapes of the continental blocks bounding the numerous individual basins evolved considerably. Knowledge about the basins thus enabled the relative locations of the blocks to be reconstructed with confidence, although the short lengths of palaeoplate boundaries that the basins represent, mean inevitably that the reconstructions could not be of particularly high resolution.

Seismic reflection profiles were also added to the regional data set during this second phase of marine geophysical discovery, allowing detailed interpretations of the Scotia Sea's active and fossil plate boundaries to be made (e.g. King and Barker 1988; Maldonado et al. 2003; Kavoun and Vinnikovskaya 1994; Coren et al. 1997). A lack of well-tie locations has consistently made these data difficult to use for correlating the basin's fills and therefore their stratigraphic age. Despite this, seismic data collection allowed for numerous refinements to Barker et al. (1982) reconstruction (Fig. 4b) and its placement in a plausible geodynamic context dominated by back-arc extension behind a migrating west-directed subduction zone that is today expressed by the South Sandwich Trench (Fig. 1).

Until this point, Scotia Sea reconstructions had all been built like jigsaw puzzles using paper and scissors, or simply sketched directly onto paper. Both of these methods fail to account for the distortions inherent in projecting features of a spherical surface onto a flat sheet of paper. Some of the first computer-based map-projected reconstructions of the region were presented by the PLATES group at the University of Texas (Lawver et al. 1992; Lawver and Gahagan 1998). Although the PLATES treatment at this time did not explicitly account for all of the basins and bounding blocks of the Scotia Sea floor, the South Georgia microcontinent was shown moving in ways consistent with ideas developed, using marine geophysical data, on the basis of Barker and Griffiths (1972) interpretation of plate motions in the west and central Scotia Sea.

By the mid-1990s, therefore, near-consensus had been reached that both the tectonostratigraphic and basin restoration approaches advocate pre-Scotia reconstructions featuring a compact Andean cusp at ~ 40 Ma built around a close placement of South Georgia to Tierra del Fuego (Fig. 4d). Around this time, processing of satellite altimeter data to give an idea of sea surface slope, and with it free-air gravity over the oceans, greatly increased detail in knowledge about the shapes of the basin floors (Livermore et al. 1994). This data set paved the way for plate kinematic reconstruction techniques whose aims were to minimise and quantify uncertainties in basin restorations and allow their full integration into map-projected plate kinematic reconstructions (Eagles 2000, 2004; Eagles et al. 2005). Using the results of these techniques to build reconstructions of gridded data

sets allowed for new constraints, implicit in the rules of plate tectonics, to play a role in reconstructing the Scotia Sea. The most important of these constraints are those that concern plate rigidity and plate boundary continuity. The most relevant consequence was the recognition that the central Scotia Sea was unlikely to house both halves of a Cenozoic-aged basin. Multiple lines of evidence instead suggested that the basin formed during Cretaceous north–south-directed plate divergence (Eagles 2000, 2010b; Dalziel et al. 2013a). This, in turn, removed the principal supporting interpretation of the mid-1990s consensus, as it implied South Georgia could not have reached its present location by a combination of ESE–WNW plate divergence in the southern Scotia Sea and north–south-directed divergence in the central Scotia Sea.

By today, therefore the largest remaining controversy in reconstruction of the Scotia Sea concerns whether or not the tectonostratigraphic correlations between South Georgia and Tierra del Fuego really should prescribe their geographical contiguity for any time in the past. The PLATES group continues to generate reconstructions that assume it should (e.g. Dalziel et al. 2013b), whilst acknowledging the lack of evidence for eastwards translation of South Georgia that is required of doing so. In contrast to this, the following pages present a plate tectonic history of the Scotia Sea in reverse stratigraphic order from 6 Ma until 50 Ma that has been derived with stricter adherence to the seafloor tectonic record. In detail, it is based on the plate kinematic model of Eagles and Jokat (2014) and illustrated by a set of reconstructions of Sandwell et al. (2014) gravity anomaly grid. A later section will reconsider the strength of testimony from South Georgia’s tectonostratigraphy in the context of some pre-50 Ma reconstructions of the region.

4 Development of the Scotia Sea

4.1 6 Ma

The Scotia Sea has probably existed in its current plate tectonic form since around 6 Ma, when the mid-ocean ridge in the western part of the Scotia Sea ceased to operate. The two plates that had been diverging on its north-western and south-eastern flanks amalgamated to form the modern Scotia Plate (Fig. 5). This instituted a long and complex transcurrent plate boundary between the Scotia and South American plates along the North Scotia Ridge, and a similarly long and complex transcurrent plate boundary along the South Scotia Ridge that separates the Scotia and Antarctic plates. The South Scotia Ridge is characterised by a handful of deep basins that seem to form at releasing bends on the plate boundary (Galindo-Zaldívar et al. 1996). At the eastern end of the Scotia Plate, a divergent plate boundary is working by seafloor spreading to generate the oceanic floor of a small back-arc basin called the East Scotia Sea (Fig. 1). The eastern half of the basin is floored by the small Sandwich plate, whose eastern margin is a convergent margin at which part of the South American plate is being subducted towards the

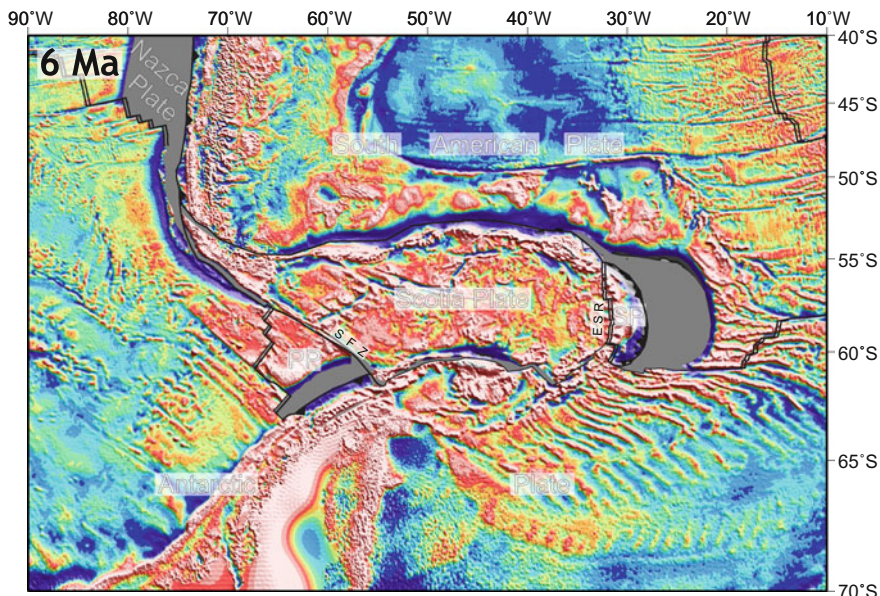


Fig. 5 Reconstruction of gridded free-air gravity anomalies (Sandwell et al. 2014) at 6 Ma, using rotations from Eagles and Jokat (2014). *ESR* East Scotia Ridge; *PP* Phoenix Plate; *SFZ* Shackleton Fracture Zone; *SP* Sandwich Plate

west beneath the Scotia Sea (Figs. 1 and 5). At the western end of the Scotia Sea, a SE-trending segment of the Scotia Plate's margin runs along the Shackleton Fracture Zone, separating it from the small oceanic Phoenix plate. At the Shackleton Fracture Zone, part of this plate has experienced flexural uplift owing to a very slight component of plate convergence at its margin with the plates in the West Scotia Sea (Livermore et al. 2004). Other parts of the Phoenix Plate at this time are undergoing subduction at a short segment of its margin, in the south-east, which sees it thrust beneath the Antarctic plate at the South Shetland Islands. The opposing segments of the Phoenix Plate's margin, also shared with the Antarctic plate, are divergent and experiencing seafloor spreading. This unusually simple plate kinematic setting has seen the Phoenix Plate used as a laboratory for studying plate driving forces. These studies have repeatedly shown that slab pull seems to have played an important role in its motion with respect to the Antarctic plate (Larter and Barker 1991; Eagles 2004; Eagles and Scott 2014).

4.2 10 Ma

The reconstruction in Fig. 6 illustrates the situation shortly before the extinction of the West Scotia Ridge, when the floor of the West Scotia Sea was subdivided into

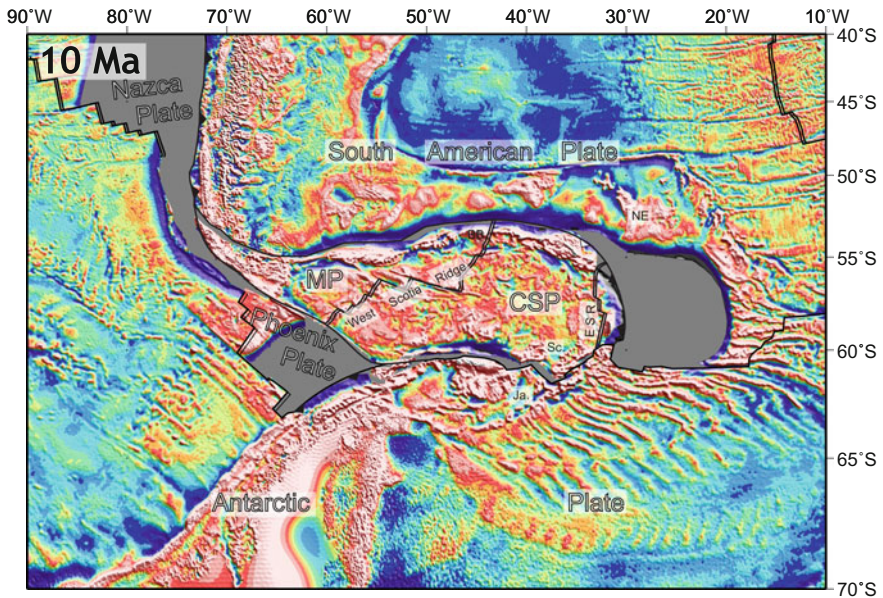


Fig. 6 Reconstruction of gridded free-air gravity anomalies (Sandwell et al. 2014) at 10 Ma, using rotations from Eagles and Jokat (2014). *BB* Aurora (Barker) Bank; *CSP* Central Scotia Plate; *MP* Magallanes Plate; *Sc*. Scan Basin, *Ja*. Jane Basin; *NE* NE Georgia Rise

sections carried on the Magallanes and Central Scotia Plates (Fig. 6) (Eagles et al. (2005)). A small 15-km underlap suggests that slow sinistral transpression has been accommodated along the North Scotia Ridge since the time of this reconstruction. The spreading rate on the West Scotia Ridge is quite slow (~ 10 km/Myr half rate) at this time (Eagles et al. 2005). This is reflected in the rough seafloor fabric close to the flanks of the present-day extinct ridge (Fig. 1). Dalziel et al. (2013a) and Pearce et al. (2014) relate intraplate volcanism in the Central Scotia Plate to low-angle subduction of part of the North-east Georgia Rise large igneous province beneath the Scotia Sea. This subduction occurs at the South Sandwich Trench, the eastern boundary of a young and small Sandwich plate (Fig. 6).

4.3 17 Ma

The 17 Ma period (Fig. 7) marks two important aspects of the evolution of the West Scotia Sea, which developed shortly before it reached almost its full volume. The first is the onset of a period of slow spreading rates in the west Scotia Sea. The second is that the West Scotia Ridge has propagated northwards to reach the Barker/Aurora Bank, reaching its full length. Eagles and Jokat (2014) estimated that this occurred close to 18.5 Ma, based on magnetic anomalies crossing the bank, which may

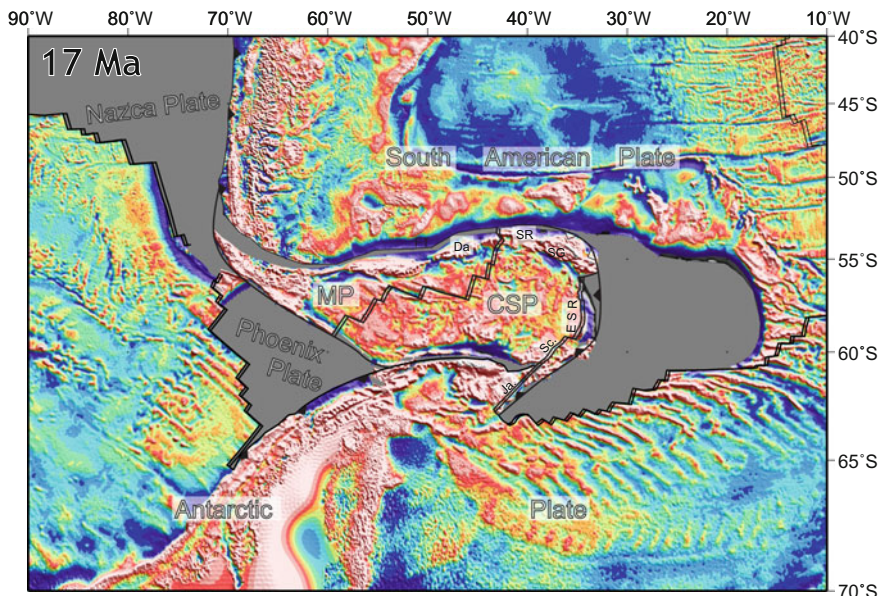


Fig. 7 Reconstruction of gridded free-air gravity anomalies (Sandwell et al. 2014) at 17 Ma, using rotations from Eagles and Jokat (2014). *Da* Davis Bank; *SG* South Georgia; *SR* Shag Rocks

therefore consist largely of sediments resting on oceanic crust. The subsequent plate divergence at this latitude led to development of a gap in the North Scotia Ridge that today allows deep water of the Antarctic Circumpolar Current to cross out of the Scotia Sea and into the South Atlantic. Tectonically, the rest of the North Scotia Ridge acts in much the same way as in the 10-Ma reconstruction. A narrow underlap depicted across the South Scotia Ridge is consistent with interpretations of light transpressional strain made from seismic reflection profiles across it (Galindo-Zaldívar et al. 1996; Kavoun and Vinnikovskaya 1994; Lodolo et al. 2010).

A very small Sandwich Plate is shown in the East Scotia Sea, based on Vanneste and Larter's (2002) interpretation of isochron 5C on the western flank of the East Scotia Ridge. Those authors suggested that the absence of a conjugate 5C on the Sandwich Plate is a consequence of subduction erosion, the process of mechanical removal of crustal material from the leading edge of the overriding plate and its delivery into the mantle by the subducting plate. This earliest Sandwich Plate is shown with a longer north–south extent than at later times, which Eagles and Jokat (2014) attributed to opening of the Scan and Jane basins behind a longer ancestral trench. Barker et al. (1982, 1984) show how parts of this trench may have deactivated, shortening the plate, as segments of the South American–Antarctic Ridge in the Weddell Sea collided with it in Miocene times. Eagles et al. (2005) noted that the initiation of this young Sandwich Plate meant that a lesser proportion of the eastwards migration of the trench would need to be accommodated at the West Scotia Ridge, consistent with its deceleration at this time.

The description of Scotia Sea tectonics at 17 Ma given above can be challenged based on alternative interpretations of basin ages given in the literature. These interpretations concern the Protector, Scan and Jane basins and the central Scotia Sea. Lawver et al. (1991) suggested, on the basis of heat flow determinations from sediment temperature gradients, that Jane Basin may have opened far earlier than shown here, in the period 32–25 Ma. This would allow for the basin to have played an important role in early deep water circulation through Drake Passage. Although the interpretation requires the basin fill to be dominated by clay, which could be considered unusual for a back-arc basin, its adoption in Fig. 7 would not strongly alter the overall plate kinematic scenario depicted.

This is not the case for Protector Basin and the central Scotia Sea, both of which in Fig. 7 are shown as open and passive at 17 Ma. Hill and Barker (1980) suggested in contrast that both Protector Basin and the central Scotia Sea were opening by seafloor spreading at 17 Ma. Maldonado et al. (2003) and Galindo-Zaldívar et al. (2006) have reproduced the magnetic anomaly models that these young interpretations are based on and depicted them in kinematic sketches. Figure 8 portrays what these interpretations would mean for plate boundaries within the Scotia Sea at 17 Ma. The thick black lines depict those parts of the plate boundaries that have been identified and suggested as active at 17 Ma. The dashed red lines depict additional tectonic features that would be required to maintain a closed circuit of plate boundaries around rigid plates within the Scotia Sea. Dashed black lines depict the magnetic bights that would be expected at the junction of the spreading centres in the central and east Scotia Seas. Evidence for these extinct plate boundaries and magnetic bight has not yet been found.

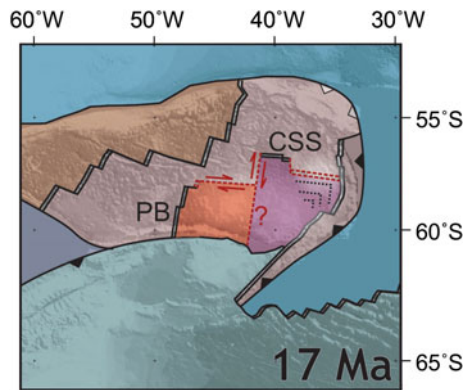


Fig. 8 Unsubstantiated plate tectonic complexity of a Scotia Sea with active mid-ocean ridges in the central Scotia Sea (CSS) and Protector Basin (PB) at 17 Ma. *Red shading*: plates within the Scotia Sea. *Blue shading*: plates in the surrounding circuits. *Red and black dashed lines*: implied plate boundary segments and magnetic bights for which no evidence is known. Background shows the 17 Ma bathymetric reconstruction of Eagles and Jokat (2014)

4.4 20 Ma

Figure 9 illustrates the tectonics of the Scotia Sea at 20 Ma. In contrast to the situation at 17 Ma, the back-arc basin in the eastern part of the Scotia Sea has yet to form and, concomitantly, the West Scotia Ridge is spreading more rapidly. The West Scotia Ridge is also shorter; its northern end lies somewhere east of Davis Bank. Just north of this, the reconstruction underlap on continental crust at the North Scotia Ridge is broader than that shown for 17 Ma. This implies ~ 75 km of shortening on the Scotia–South America plate boundary in the intervening period. Eagles and Jokat (2014) showed that the magnitude of this shortening is smaller than the uncertainties involved in constructing the plate circuit that depicts it. The occurrence of this convergence, however, is more confidently implied by the presence of a seemingly young accretionary prism at the southern edges of Burdwood and Davis banks, and of Miocene transpression in Tierra del Fuego and along northern Burdwood Bank (Bry et al. 2004; Cunningham et al. 1995; Klepeis and Austin 1997; Kraemer 2003). The South Scotia Ridge, in contrast, is depicted much as in the later reconstructions, implying its history since Miocene times has been one of very slow sinistral transpression. As such, this reconstruction shows a period very early in the evolution of the Scotia Sea with northern and southern boundaries similar to today's.

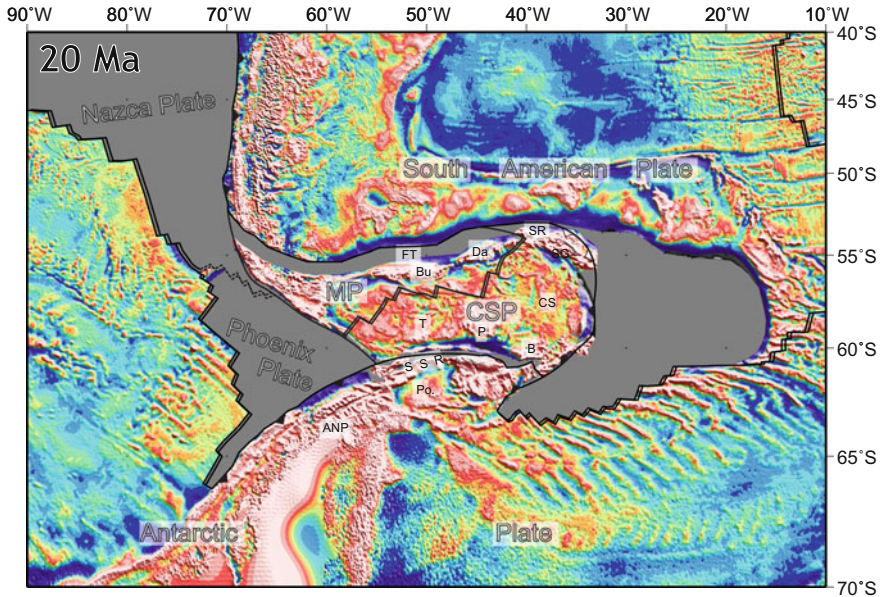


Fig. 9 Reconstruction of gridded free-air gravity anomalies (Sandwell et al. 2014) at 20 Ma, using rotations from Eagles and Jokat (2014). ANP Antarctic Peninsula; B Bruce Bank; Bu. Burdwood Bank; CS Central Scotia Sea; FT Falkland Trough; P Pirie Bank; Po. Powell Basin; SSR South Scotia Ridge; T Terror Rise

Further in the west, Fig. 7 shows the possibility that a segment of the Phoenix–Nazca plate boundary was subducted beneath Cape Horn. Ongoing divergence of the surface portions of the two plates would have seen a space open within the mantle between their subducted parts. Breitsprecher and Thorkelsen (2009) and Eagles et al. (2009) have suggested that decompression melting of mantle rocks rising through this so-called slab window produced melts that are represented by minor occurrences of alkali basalts in Tierra del Fuego (Puig et al. 1984). Eagles and Jokat (2014) suggested that the loss of this ridge in subduction may have presented a new barrier to the dispersal of vent-specific Kiwaid crabs, whose Pacific and Atlantic lineages are reckoned to have diverged in the period 25.9–13.4 Ma (Roterman et al. 2013).

As in the 17 Ma reconstruction, there are alternative interpretations of some of the smaller basins in the Scotia Sea that could alter the picture of plate tectonics in the Scotia Sea at 20 Ma. As well as the central Scotia Sea, whose interpretation as a Miocene back-arc basin (Hill and Barker 1980) would affect the 20 Ma reconstruction in much the same way as the 17 Ma reconstruction, there is also the suggestion that the Scan and Dove basins may have been active at 20 Ma (Galindo-Zaldívar et al. 2014). Figure 10 shows the implication of these ages for the plate tectonic setting in the Scotia Sea at 20 Ma. The red dashed lines show plate boundaries for which good evidence is missing. Most conspicuous amongst these is a mid-ocean ridge in Scan Basin. The sketch also shows one of the best-known puzzles concerning Hill and Barker’s (1980) back-arc interpretation for the central Scotia Sea: why should a back-arc basin behind an east-migrating trench have opened by north–south extension?

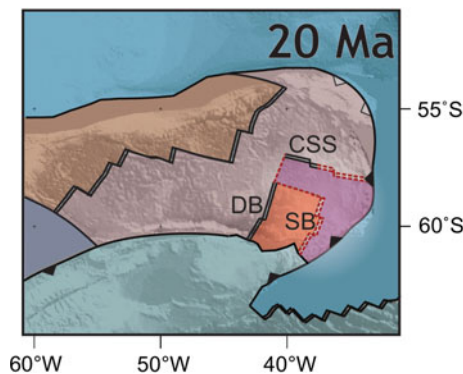


Fig. 10 Unsubstantiated plate tectonic complexity of a Scotia Sea with active mid-ocean ridges in the central Scotia Sea (CSS), Dove Basin (DB) and Scan Basin (SB) at 20 Ma. *Red shading*: plates within the Scotia Sea. *Blue shading*: plates in the surrounding circuits. *Red black dashed lines*: implied plate boundary segments for which no evidence is known. Background shows the 17 Ma bathymetric reconstruction of Eagles and Jokat (2014)

4.5 26 Ma

26 Ma was part of a transitional period in the development of the Scotia Sea (Fig. 11). Although seafloor spreading was underway on the young West Scotia Ridge, its flanking magnetic isochrons suggested it had yet to propagate any further north than the eastern margin of Burdwood Bank. Dredging work has returned evidence for volcanism near what was the northern end of the ridge at 29 Ma (Dalziel et al. 2013a; Pearce et al. 2014). Dalziel et al. (2013a) suggest that this volcanism was related to subduction of South American lithosphere beneath the Scotia Sea, on the basis of the geochemical signature of the dredged rocks. Eagles and Jokat (2014) noted that this would require a very shallow angle ($10\text{--}20^\circ$) slab, based on the distance to the trench in the reconstruction. They suggested alternatively that the source of the dredged rocks may be immature lower crust remelted by the addition of mantle melts during extension related to the northward propagation of the West Scotia Ridge, noting the analogy to the region's older Chon Aike large igneous province (Pankhurst and Rapela 1995).

Regardless of its role in this melting, it seems that the divergent Magallanes–Central Scotia plate boundary reached far enough north that parts of the North Scotia Ridge could have adopted a role as the northern margin of the Scotia Sea, acting as it did later as two separate plate boundaries between the South American

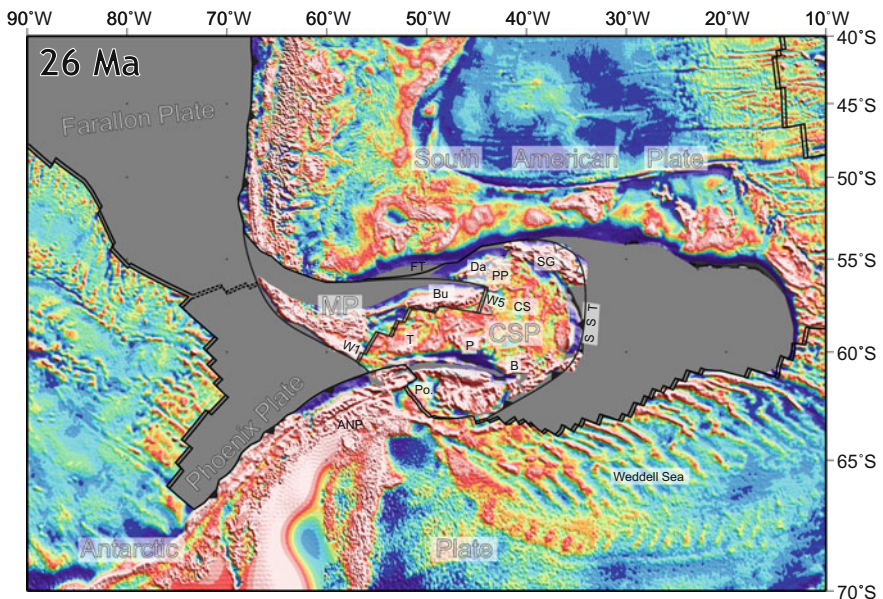


Fig. 11 Reconstruction of gridded free-air gravity anomalies (Sandwell et al. 2014) at 26 Ma, using rotations from Eagles and Jokat (2014). *PP* magmatic Pirie Province of Dalziel et al. (2013a, b); *SST*: South Sandwiche Trench; *W1*, *W5*: numbered spreading corridors of the west Scotia Sea (Eagles et al. 2005)

plate and the Magallanes and Central Scotia plates. The reconstruction underlap on the Magallanes–South America segment implies continuous slow convergence in the period 26–20 Ma, albeit below the statistical resolution of the plate circuit Eagles and Jokat (2014) built. Further south, in contrast to later times, the southern margin of the Scotia Sea did not run along the South Scotia Ridge but instead through a small oceanic basin off the northern end of the Antarctic Peninsula, Powell Basin. There is consensus that seafloor spreading in Powell Basin was an Oligocene and earliest Miocene process (King and Barker 1988; Lawver et al. 1994; Coren et al. 1997; Eagles and Livermore 2002). The southern boundary's location may have switched in response to early Miocene collision of segments of the South American–Antarctic Ridge with the eastern convergent plate boundary of the South Orkney Microcontinent, beyond Powell Basin's eastern flank (Barker 1995; Barker et al. 1982, 1984; Hamilton 1989). The approach and eventual collision of the ridge may have reduced subduction-related driving forces that contributed to the basin's opening.

4.6 30 Ma

30 Ma (Fig. 12) marks what has been presented as an important epoch in the development of the Scotia Sea. This period has returned the oldest direct evidence for active subduction of South American lithosphere beneath the central Scotia Sea, in the form of calc-alkaline volcanic rocks dredged from a rotated fault block in the modern fore-arc (Barker 1995; Livermore et al. 1994). Eagles and Jokat (2014) suggested this could be interpreted to mean that the South Sandwich Trench had, for the first time, reached as far north as South Georgia, where it bent into an east–west orientation to take up the very earliest transcurrent plate motions on the eastern North Scotia Ridge. The reconstruction shows no back-arc basin immediately behind the trench at this time, although suggestions that Scan Basin may date from around this time, based on heat flow values modelled from sediment temperature gradient data (Barker et al. 2013), could be interpreted in terms of such a feature. Further west, the reconstruction shows the young West Scotia Ridge reaching only as far north as Isla de los Estados, where its motion is taken up on an oblique transform fault running NW into Tierra del Fuego. Here, this transform meets the east-trending transform fault that runs through or near South Georgia to the trench. Together with the young divergent plate boundary in Powell Basin, these plate boundaries enabled Eagles and Jokat (2014) to interpret this period as the one in which the central Scotia Sea first came to be encircled by plate boundaries, setting in place the core of the modern Scotia Plate.

The shape of the reconstruction misfit occupied by this plate boundary in Tierra del Fuego is largely unchanged in the 26 Ma reconstruction, suggesting at least the possibility that there were periods of no relative movement between the Magallanes and South American plates during the early development of the Scotia Sea.

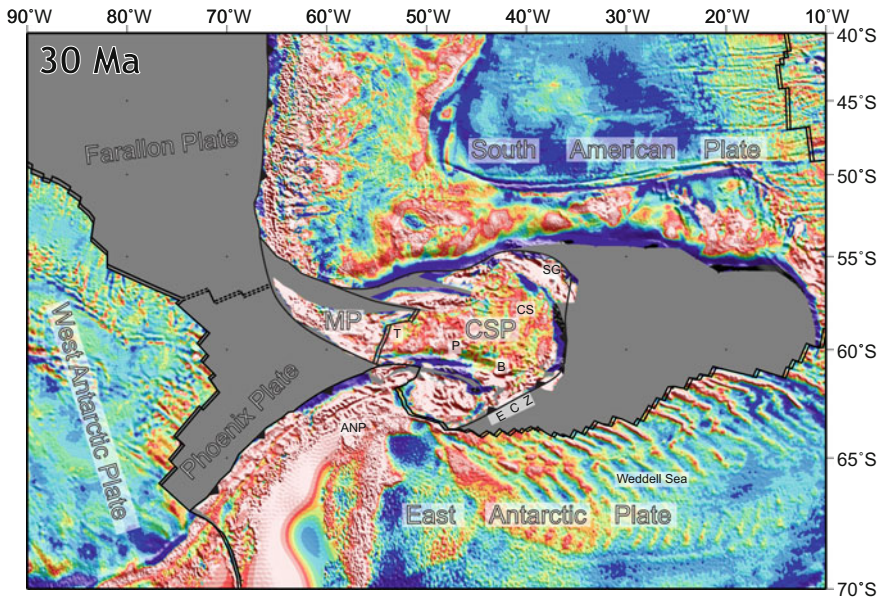


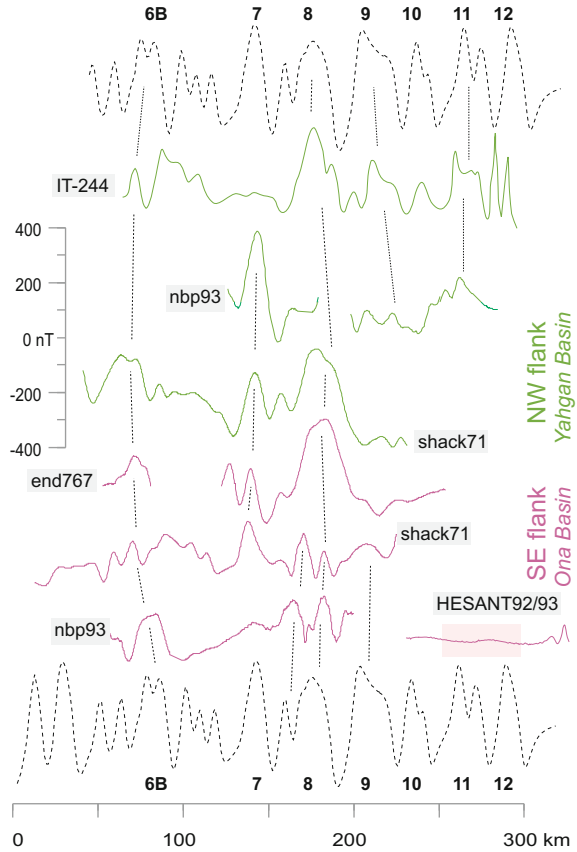
Fig. 12 Reconstruction of gridded free-air gravity anomalies (Sandwell et al. 2014) at 30 Ma, using rotations from Eagles and Jokat (2014). *ECZ* Endurance Collision Zone (Ghidella et al. 2002)

The West Scotia Ridge in this reconstruction is the very oldest that Eagles and Jokat (2014) show. Following Livermore et al. (2005), they noted that a tight fit between the eastern and western margins of the West Scotia Sea (at Terror Rise and Tierra del Fuego) dated to this time when using a spreading rate before chron 8 that was the same as immediately afterwards. They further noted that this is the same time that Eagles et al. (2006) determined for the end of seafloor spreading in Protector Basin on the opposing side of Terror Rise, suggesting simple abandonment of one mid-ocean ridge had occurred in favour of another.

Direct evidence for this earliest phase of spreading on the West Scotia Ridge is difficult to interpret, however, and is the subject of moderate controversy because the time frame lies very close to the end-Eocene build up of ice on Antarctica, which has been linked to the onset of the Antarctic Circumpolar Current that in turn has been suggested as a simple consequence the opening of the Drake Passage (Kennett 1977; De Conto and Pollard 2003). Figure 13 summarises this evidence, which comes from magnetic anomaly profiles crossing the southernmost corridors of seafloor spreading in the West Scotia Sea, directly adjacent to the Shackleton Fracture Zone.

The profiles, three for each flank in these corridors, show that anomaly isochrons younger than and including 8 are interpretable in many locations, although by no

Fig. 13 Magnetic anomaly wiggles in the south-westernmost spreading corridors of the West Scotia Sea. Old end of profiles towards the right. Green lines show profiles from the NW flank, pink lines the SE flank. Dashed profiles are synthetic magnetic anomalies generated for a source layer 1 km thick lying at 4.5 km depth, labelled with chron number. Pink box shows the portion of the HESANT92/93 profiles in which reversal isochrons 11 and 12 were modelled at very small amplitudes by Maldonado et al. (2014)



means are they ubiquitously so. Three of the profiles supply hints that isochron 9 may be present in these corridors. Beyond this, two profiles confined to the north-western half of the corridors have been interpreted to reveal isochrons 10 and 11 (Lodolo et al. 2006), although it should be noted that the waveforms are far from coherent between them. Chron 12 has recently been interpreted from the south-eastern flank in magnetic profiles crossing the Ona Basin, close to the continental shelf north of Elephant Island (Maldonado et al. 2014). Plotted at the same scale as the profiles in which the younger magnetic isochrons were identified, it is clear, however, that this interpretation requires oceanic crust with an order of magnitude smaller magnetic susceptibility than anywhere else in the West Scotia Sea. It seems then that the oldest likely oceanic crust preserved in the West Scotia Sea dates from chron 11 (~30 Ma; Gradstein et al. 2012), as in the reconstruction. Whether this crust was developed on an organised linear mid-ocean ridge, as depicted, or in a more transitional setting like that described as ‘chaotic seafloor spreading’ by Barker and Burrell (1977), remains unclear with current data.

4.7 33 Ma

All of the Oligocene or younger reconstructions shown so far have featured one or more plate boundary segments along the North Scotia Ridge. The 33 Ma reconstruction in Fig. 14 represents a step further back towards an embryonic Scotia Sea by being the youngest to lack such a plate boundary. At this time, the reconstruction shows the young South Sandwich Trench reaching only as far north as Discovery Bank, although dating of available samples only confirm the bank as a site of subduction-related volcanism as far back as 20–12 Ma (Barker et al. 1982).

At the northern edge of Discovery Bank, the reconstruction shows the palaeo-subduction zone bending abruptly into an east–west orientation much like its present-day manifestation does to run along the North Scotia Ridge near South Georgia. Both of these features are examples of so-called tear faults (Fig. 15). Eagles and Jokat (2014) termed the 33 Ma tear fault the Burdwood transform fault. Other than the gravity anomalies along the northern edges of Bruce and Pirie banks, and the southern edge of Burdwood Bank, there is little direct evidence for the remnants of this fault, although it should be noted that the area is buried by thick sediments (Perez et al. 2014) and the plate circuit, as constructed, suggests the cross-axial component of the movements it accommodated may have been slight. The 30.2 Ma basement heat flow estimate at the northern edge of Scan Basin (Barker et al., 2013) might be interpreted, instead of in terms of basin age, as the time

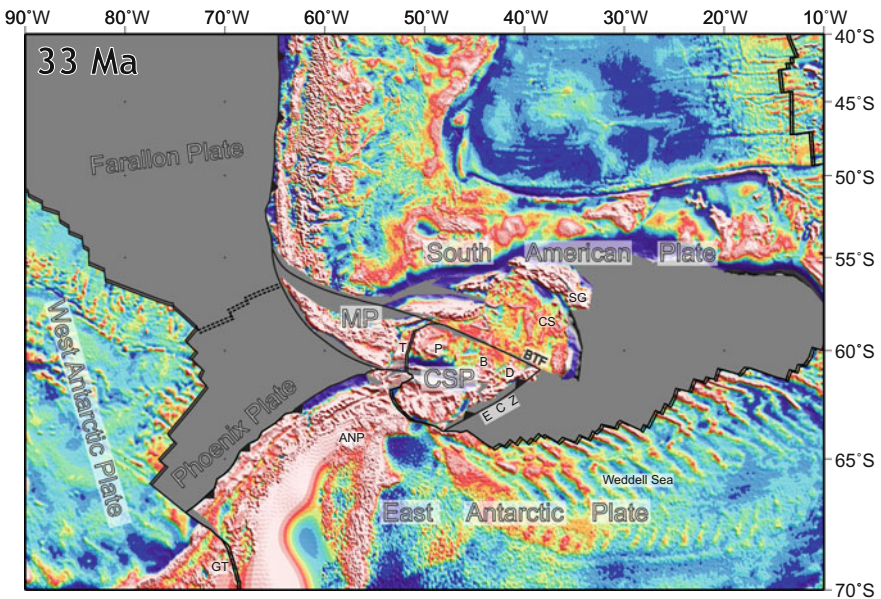
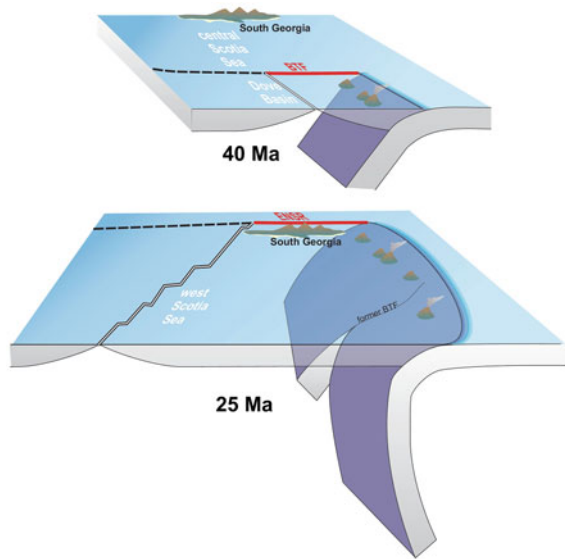


Fig. 14 Reconstruction of gridded free-air gravity anomalies (Sandwell et al. 2014) at 33 Ma, using rotations from Eagles and Jokat (2014). *D* Discovery Bank

Fig. 15 Successive locations of tear faults in the Scotia Sea following northwards propagation of the ancestral South Sandwich Trench. *BTF* Burdwood tear fault; *ENSR* eastern North Scotia Ridge



of cessation of the fault's movement. This aside, there is stronger evidence for other plate boundaries further south in the form of the continental extensional basins bordering Powell Basin (King and Barker 1988) and the short mid-ocean ridge in Protector Basin (Eagles et al. 2006). The reconstruction shows these boundaries, along with the Burdwood transform fault, as defining the body of an independently moving small overriding arc plate at the ancestral South Sandwich Trench.

With the Burdwood transform fault running along part of its southern edge, the central Scotia Sea and South Georgia are shown as features embedded within the body of the South American Plate. To the west, the length of plate boundary running through continental South America is much shorter than in all the younger reconstructions; it is confined to Tierra del Fuego where a smaller underlap than in the next-younger (30 Ma) reconstruction can be interpreted in terms of a phase of plate divergence. As for Eagles and Jokat's (2014) reconstructions at all other times, the amount of divergence shown on this particular boundary is unlikely to be greater than the uncertainties in the various elements of the plate circuit might combine to show, whereas the evidence for continental extension in the Sloggett Basin of south-eastern Tierra del Fuego (Ghiglione et al. 2008) is not.

4.8 41 Ma

The general configuration at 41 Ma (Fig. 16) is in most aspects a shortened version of that at 33 Ma, suggesting a simple evolution from one to the other by ongoing action of the plate boundaries. The only large difference is in the location of the

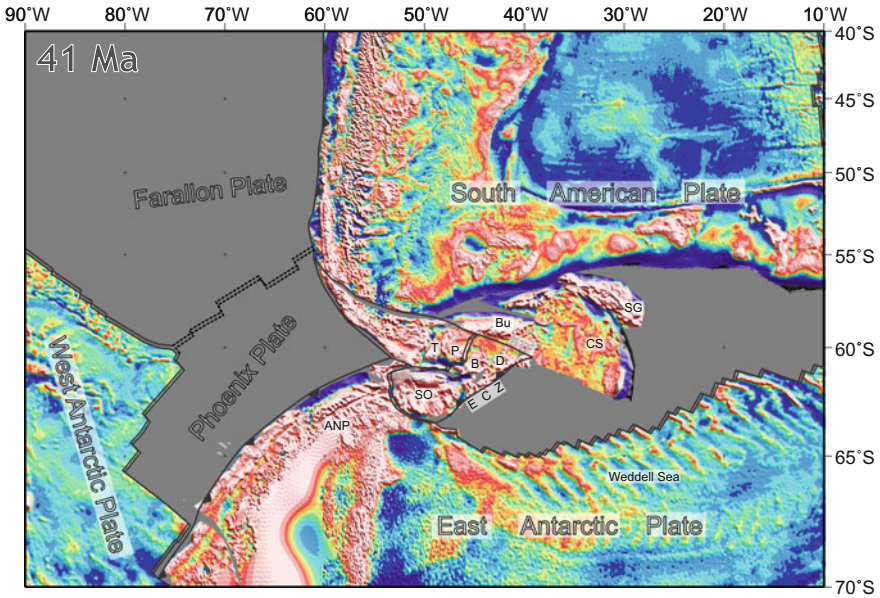


Fig. 16 Reconstruction of gridded free-air gravity anomalies (Sandwell et al. 2014) at 41 Ma, using rotations from Eagles and Jokat (2014). SO South Orkney microcontinent

western, divergent boundary of the arc plate, whose northern reaches pass along a mid-ocean ridge in Dove Basin, rather than Protector Basin. The Burdwood transform fault is somewhat shorter because the Protector Basin was yet to open. These configurations for Protector and Dove Basin allow the Scotia Sea to be depicted as a relatively simple system of two plates behind the ancestral South Sandwich Trench at any time between 42 and 30 Ma. One of these plates is the overriding plate at the trench and probably featured a volcanic arc at its eastern edge. The plate behind the arc plate bears Tierra del Fuego and moves only slowly in a collisional sense, if at all, with respect to the South American plate. As before, the resolution of the plate circuit is too coarse to be able to define this motion, or the lack of it, as statistically relevant, but interpretations of active shortening in Tierra del Fuego in middle Eocene times seem to confirm that convergence did occur (Ghiglione and Ramos 2005; Gombosi et al. 2009; see Ghiglione 2016 for a review).

Eagles and Jokat (2014) calculated that the arc plate was moving rather more slowly with respect to Antarctica than with respect to South America in this period and noted that this slow motion did not give rise to oceanic growth, but rather to continental extension, as expressed in the eruption of alkali basalts and the formation of grabens around and across the South Orkney Microcontinent (Barber et al. 1991; King and Barker 1988).

4.9 50 Ma

The onset of independent motions of small plates in the Scotia Sea began with continental crustal extension over the South Orkney Microcontinent and of Pirie and Bruce banks, which gave way eventually to seafloor spreading in the Powell and Dove basins. Figure 17 shows the region before any of these motions had started, at around 50 Ma but neither it, nor that in Eagles and Jokat (2014), attempts to reconstruct any of the continental extension. Eagles and Livermore’s (2002) reconstruction of Powell Basin gives an idea of how such a reconstruction might appear around the South Scotia Ridge. Beyond this, the reconstruction can be directly compared to the tectonostratigraphic and flat map reconstructions of Figs. 3 and 4. The clearest difference between them is in the area south of Burdwood Bank, where Pirie and Bruce banks and Terror Rise lie as a result of reconstructing the growth of the West Scotia Sea, Protector and Dove basins. The dredged stratigraphy and magnetic anomalies of these blocks match comfortably those of Tierra del Fuego (Eagles et al. 2006; Schenke and Udintsev 2009; Udintsev et al. 2012). South Georgia, on the other hand, lies south of Maurice Ewing Bank at the eastern end of the Falkland Plateau, a few hundred kilometres west of its current location. As the previous reconstructions have shown, there is no preserved evidence anywhere in the seafloor of the Scotia Sea for its translation from a location further west, in spite of the widely reported tectonostratigraphic arguments for such.

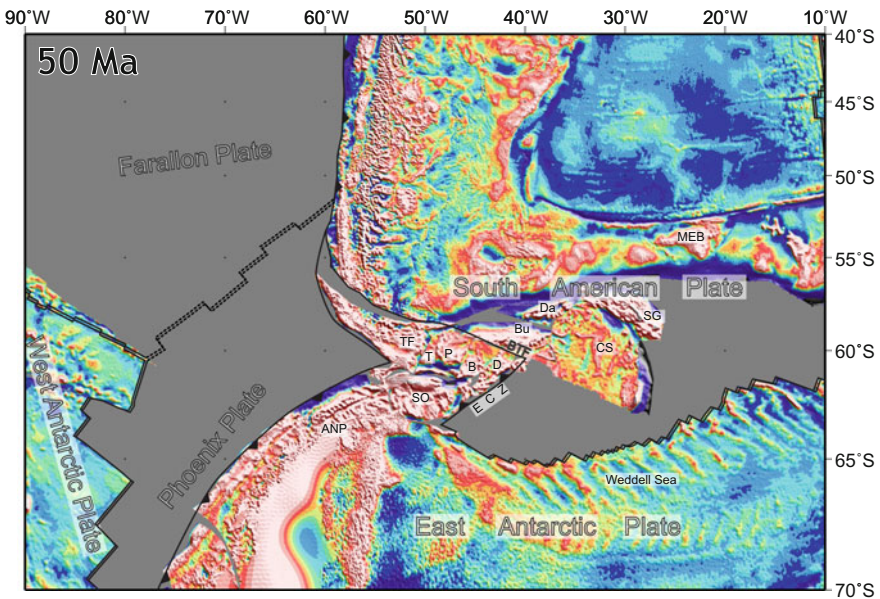


Fig. 17 Reconstruction of gridded free-air gravity anomalies (Sandwell et al. 2014) at 6 Ma, using rotations from Eagles and Jokat (2014). *MEB* Maurice Ewing Bank; *TF* Tierra del Fuego

Ghiglione et al. (2008) detail observations in geophysical and outcrop data for South American–Antarctic early Eocene plate divergence in Tierra del Fuego further north, which Livermore et al. (2005) had modelled as being slow, north–south-directed, and coming to an end soon after 50 Ma. Prior to this, the eastern margin of Omond Land, the continental mass formed of contiguous South Orkney Microcontinent, Terror Rise, Pirie, Bruce and Discovery banks had evolved from a transform fault into a continent–ocean collision zone as the azimuth of South American–Antarctic plate motions rotated from NE–SW to NW–SE in Maastrichtian through Palaeogene times (Barker et al. 1991; Eagles 2010b). It was this so-called Endurance Collision Zone (Ghidella et al. 2002) that evolved to become the ancestral South Sandwich subduction zone, which slowly propagated northwards and migrated eastwards, as seen from Antarctica, throughout Cenozoic times. The 50 Ma reconstruction shows the tear fault, the Burdwood transform fault, at the northern end of this collision zone. At this time, the fault’s shortness and orientation allow it to act as a simple transcurrent fault between the South American and Antarctic plates. In this way, relative motions of the Endurance Collision Zone/South Sandwich Trench, and the South American and Antarctic plates at 50 Ma are accommodated by plate boundary-scale processes on a single fault. As previous sections have shown, the subsequent plate tectonic history of the Scotia Sea can be seen as the history of this fault’s lengthening and elaboration to accommodate changes in those relative motions by plate-scale processes instead.

5 Pre-scotia Sea Times

Unlike the reconstructions shown so far, Sandwell et al.’s (2014) gravity data for the 125 Ma reconstruction in Fig. 18 have been filtered to remove long wavelengths, probably related to very large-scale convection-related structures in the mantle, so that the remaining anomaly field matches across the mid-ocean ridge in the South Atlantic. This eases visualisation of the tectonic fabric, which tends to occur on shorter wavelengths. The reconstruction is developed by rotating the 50 Ma configuration of the Scotia Sea as if it had been embedded within the South American plate in the period 125–50 Ma. Doing this requires the assumption that the Burdwood transform fault had been newly inaugurated at 50 Ma and that at earlier times the South American–Antarctic plate boundary lay further south, in the Weddell Sea, as suggested by magnetic seafloor spreading anomalies there (Livermore and Woollett 1993; Livermore and Hunter 1996; Livermore et al. 2005). The reconstruction shows a pair of extended continental margins that formed in the divergence of west and east Gondwana, and areas of Mesozoic oceanic crust that accreted to them in the central Scotia Sea (Eagles 2010a) and Weddell Sea (Livermore and Hunter 1996).

Further west, the reconstruction shows Graham Land and other parts of the Antarctic Peninsula as if they had been embedded within the South American plate for a period ending at 103 Ma, the time of the Palmer Land Event, a Cretaceous

collisional episode interpreted from sparse outcrop data in southern parts of the peninsula (Vaughan et al. 2012). The placement should be viewed as speculative; not only does it rely on disputed tectonostratigraphic correlations between the South Orkney Islands and rocks further north in the Patagonian Andes, but also the very occurrence of a Palmer Land Event has recently been called into question (Burton-Johnson and Riley 2015).

Figure 18 also shows where, at 125 Ma, the Yahgán, Cumberland Bay and Sandebugten formations would have been deposited at widely separated sites in the Rocas Verdes Basin of Tierra del Fuego and in South Georgia. By this, it is evident that the plate kinematic history given so far fails to reconcile with the long-suspected geographical proximity of South Georgia and Tierra del Fuego in Aptian–Albian times. Faced with this, Eagles (2010b) attempted to reinterpret the similarities between South Georgia and Tierra del Fuego in terms of an Early Cretaceous plate boundary configuration from which the 125 Ma setting shown

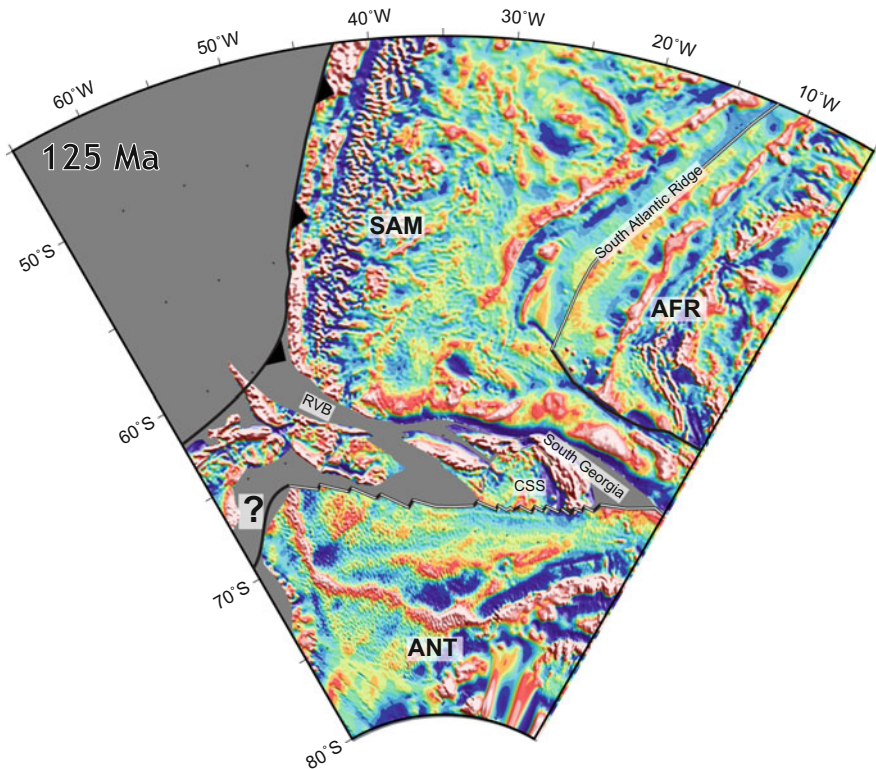


Fig. 18 125 Ma reconstruction. *AFR* African plate; *ANT* Antarctic plate; *SAM* South American plate ‘?’: Precursor plate boundary to Palmer Land Shear Zone of Vaughan et al. (2012); *CSS* central Scotia Sea; *RVB* inactive Rocas Verdes Basin

above might have evolved. His scheme presented South Georgia as part of the South American conjugate to the extended continental margin in the southern Weddell Sea. He suggested that breakup-related volcanism at this margin was distinguished geochemically because of its occurrence in lithosphere that had previously experienced an unusual combination of processes including metasomatism during flat-slab subduction and the arrival of a mantle plume (Pankhurst and Rapela 1995; Pankhurst et al. 2000). The Chon Aike large igneous province represents this volcanism in outcrop and subcrop at sites spread throughout Patagonia and the Antarctic Peninsula (Pankhurst et al. 2000). This volcanic province probably extends from the Deseado Massif in Patagonia offshore towards the Rio Chico high, and from there to the North Scotia Ridge and Falkland Plateau (Baristead et al. 2013). It occurs in association with sites of crustal extension and is characterised by bimodal andesitic–rhyolitic volcanism, as reflected in the petrographic detrital composition of Yahgán, Cumberland Bay and Sandebugten formations. Detrital zircon U–Pb ages from Sandebugten Formation of South Georgia Island includes a strong 171 Ma peak (Carter et al. 2014) corresponding to the V2 Jurassic volcanic stage of the Chon Aike province where it crops out in the Deseado Massif (Pankhurst et al. 2000).

Figure 19 summarises this new tectonostratigraphic interpretation and compares it to that of Dalziel and Elliot (1971). Both have been annotated with proposed locations for the sources of the South Georgia's sequences. Neither scenario requires any of the Cumberland Bay or Sandebugten formations' sediments to have been sourced from the Falkland Islands, despite Carter et al.'s (2014) attempt to distinguish between them on the basis of the absence of Proterozoic 'Gondwanan interior' zircons from South Georgia. If anything, it is the active margin location that is more difficult to reconcile with this absence, given the palaeocurrent directions shown. Seen in this context, the sedimentological similarities between the Yahgán, Cumberland Bay and Sandebugten formations need not be prescriptive of geographical proximity.

The other claimed strong correlation between South Georgia and Tierra del Fuego is in the timing of tectonism that occurred to close the Rocas Verdes and 'Cumberland Bay' basins. In both locations, this event is dated to 86–84 Ma, or beforehand. This requires a plate boundary location for both basins at that time. Figure 20 shows a reconstruction for 84 Ma that enables interpretation of the locations of plate boundaries in the region. This reconstruction is well constrained because of the ease of identifying magnetic reversal isochron 34y; statistical reconstructions for this isochron using three pairs of plates or three plates simultaneously have repeatedly demonstrated that a fourth plate did not exist in the Weddell Sea at this time (Livermore and Hunter 1996; Nankivell 1997; Eagles and Vaughan 2009). There are no indications from structural geology or palaeomagnetic work that the Antarctic Peninsula at this time was anything other than fixed with respect to the interior of Antarctica, just as it is today (Vaughan et al. 2012; Grunow 1993). The plate boundaries shown are thus necessary and sufficient to explain all known plate kinematic and palaeomagnetic constraints. Within the constraints of these boundaries, the N–S trending path sketched through the Rocas Verdes Basin

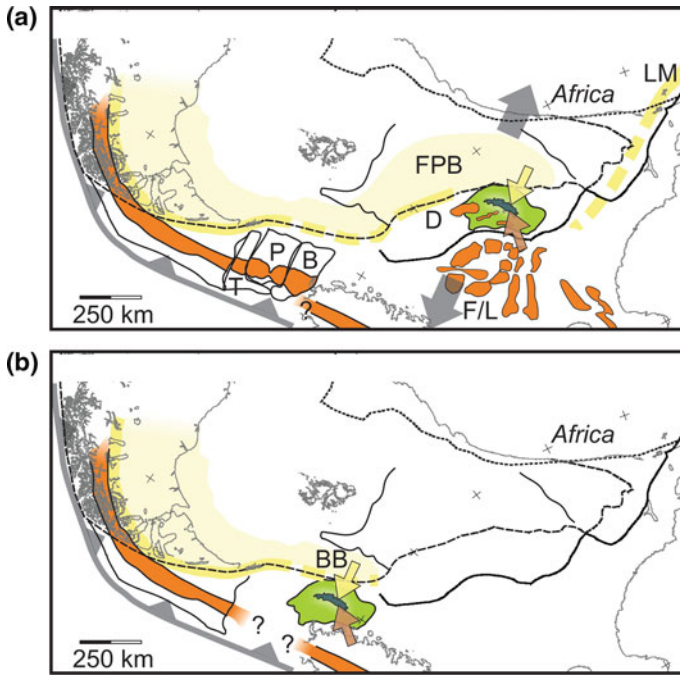


Fig. 19 Alternative contexts for deposition of the Yahgán, Cumberland Bay and Sandebugten formations. The basemaps, redrawn from Dalziel et al. (1975), depict a time early in the Cretaceous. **a** Gondwana breakup over metasomatised mantle, **b** subduction and back arc extension *Bright yellow lines*: outcrop or suspected outcrop (*dashed*) of silicic volcanic rocks of the Chon Aike large igneous province. *Orange*: interpreted locations of andesitic volcanic rocks. *BB* Burdwood Bank; *TPB* 'batholith' magnetic anomalies of Terror Rise, Pirie Bank and Bruce Bank. *D* Davis Bank dredge sample (Pandey et al. 2010); *LM* Lebombo monocline rhyolites; *F/L* Filchner and 'Lozengé' magnetic anomalies of Ferris et al. (2000); *FPB* Falkland Plateau Basin. *Yellow* and *orange* arrows: palaeocurrent directions determined for later deposition of Sandebugten and Cumberland Bay formations rocks. *Grey* arrows: orientation of Gondwana breakup-related plate divergence

can explain the basin's shortening along a segment of the Antarctic–South American plate boundary. The main faults and folds of South Georgia, in contrast, suggest a plate boundary segment oriented ESE. This orientation could not have acted in a convergent sense in either of the locations suggested for South Georgia. The evidence for Rb–Sr system closure in South Georgia's schists and the K–Ar dating of its biotites' growth are therefore very difficult to relate to Andean orogenesis at ~84 Ma without invoking extra plates whose motion would be otherwise unattested. An alternative setting, consistent with the thermal history presented by Carter et al. (2014) and with the location of the highest metamorphic grades in the closest proximity to the exposed basement and oceanic complexes in the SE of the island, may simply be deep burial of sediments in a basin situated on a young, warm, continental margin.

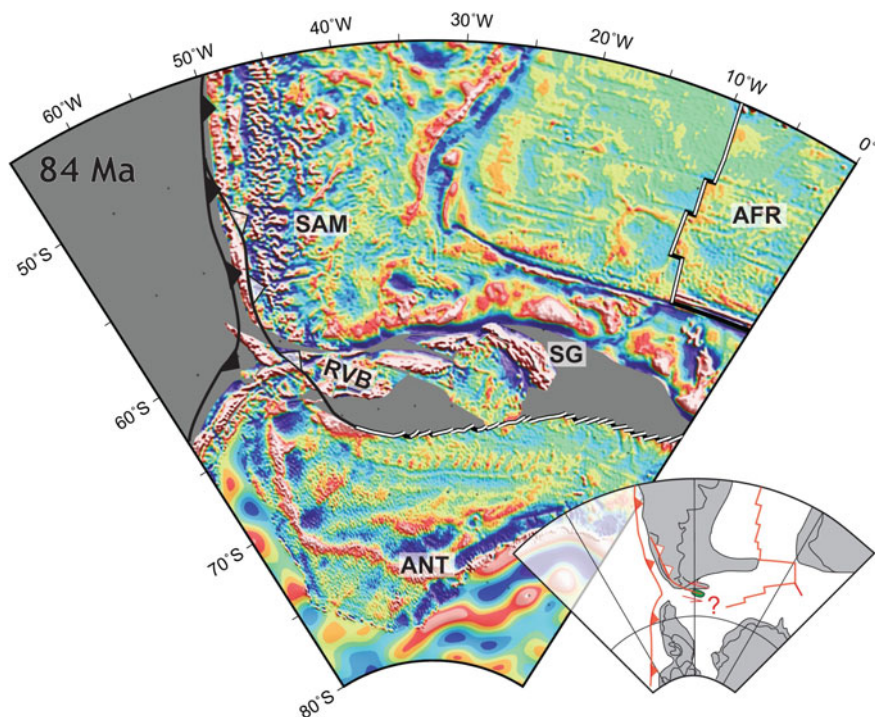


Fig. 20 The South Atlantic at 84 Ma, around the time of inversion of the Rocas Verdes Basin (RVB) and of the ‘Cumberland Bay’ basin in South Georgia (SG). At this time, the region was evolving by divergence of three large plates, South America (SAM), Africa (AFR) and Antarctica (ANT) beneath which plates of the palaeo-Pacific margin were subducting from the west. The Antarctic Peninsula was not moving with respect to the interior of Antarctica. Neither of the locations implied by reconstruction of the seafloor in the Scotia Sea (shown) or by comparative tectonostratigraphy (in the *inset*) places South Georgia near the Pacific margin, or indeed any plate margin, that might be invoked to explain the deformation proposed from dating of Rb–Sr closure in biotite and titanite minerals at this time. *Inset* non-closure (?) of plate boundaries with ‘Rocas Verdes’ location of South Georgia, redrawn and adapted from Curtis et al. (2010)

6 Summary

This chapter has revisited and summarised nearly 200 years of thinking on the tectonic history of the Scotia Sea region, which started from basic and fragmentary information on outcrop geology in Tierra del Fuego and the Antarctic Peninsula. The first century and a half of this work was dominated by increasing knowledge and understanding of the intervening outcrops, dotted amongst islands around the periphery of the Scotia Sea. By the time of the plate tectonic revolution, much was known in detail about contrasts and correlations between these outcrops, and little of the early conviction that an orocline of uniform Andean composition snaked continuously around the Scotia Sea could be sustained. Only a set of strong

likenesses between the Jurassic oceanic basement rocks, and Aptian–Albian basin fills of South Georgia and Tierra del Fuego, and interpretations of their shared experience of orogenesis later in the Cretaceous remained. Since the second half of the twentieth century, new data sets offering new chances to consider the Scotia Sea's growth became available from marine and satellite geophysical techniques that revealed the bathymetric, gravimetric and magnetic structure of the 98 % of the Scotia Sea that had previously lain hidden beneath the sea surface between its islands. Until now, these data have proved impossible to interpret in any way that enables the likenesses between the late Jurassic and Cretaceous rocks of South Georgia and Tierra del Fuego to be explained in terms of their contiguity at any time in the past. An alternative tectonostratigraphy that is consistent with the plate kinematic history interpretable from the seafloor has been suggested and is beginning to be tested. This task is of importance in more than just its own right, because it stands in the foreground of a set of interdisciplinary studies that all stand to benefit from a more precise and confident understanding of the tectonic and bathymetric development of the Scotia Sea.

References

- Arctowski H (1895) Observations sur l'intérêt qui présente l'exploration des Terres Australes. *Bull Soc Geol Fr (ser 3)* 23:589–591
- Barber PL, Barker PF, Pankhurst RJ (1991) Dredged rocks from Powell Basin and the South Orkney microcontinent. In: Thomson MRA, Crame JA, Thomson JW (eds) *Geological evolution of Antarctica*. Cambridge University Press, Cambridge, pp 361–367
- Baristean N, Anka Z, di Primio R, Rodriguez JF, Marchal D, Dominguez F (2013) New insights into the tectono-stratigraphic evolution of the Malvinas Basin, offshore of the southernmost Argentinean continental margin. *Tectonophysics*. doi:[10.1016/j.tecto.2013.06.009](https://doi.org/10.1016/j.tecto.2013.06.009)
- Barker PF (1970) Plate tectonics of the Scotia Sea region. *Nature* 228:1293–1296
- Barker PF (1972) Magnetic lineations in the Scotia Sea. In: Adie RJ (ed) *Antarctic geology and geophysics*. Universitetsforlaget, Oslo, pp 3–11
- Barker PF (1995) Tectonic framework of the east Scotia Sea. In: Taylor B (ed) *Backarc Basins: tectonics and magmatism plenum*. New York, pp 281–314
- Barker PF, Burrell J (1977) The opening of Drake Passage. *Mar Geol* 25:15–34
- Barker PF, Griffiths DH (1972) The evolution of the Scotia Ridge and Scotia Sea. *Philos T Roy Soc A* 271:151–183
- Barker PF, Hill IA, Weaver SD, Pankhurst RJ (1982) The origin of the eastern South Scotia ridge as an intra-oceanic island arc. In: Craddock C (ed) *Antarctic Geosciences* Univ Wisc Press, Madison, pp 203–211
- Barker PF, Barber PL, King EC (1984) An early miocene ridge crest–trench collision on the South Scotia Ridge near 36°W. *Tectonophysics* 102:315–332
- Barker PF, Lawver LA, Larter RD (2013) Heat-flow determinations of basement age in small oceanic basins of the southern central Scotia Sea. *Geol Soc Spec Pub*, 381:139–150
- Barron EJ, Harrison CGA, Hay WW (1978) A revised reconstruction of the southern continents. *Eos T Am Geophys U* 59:436–449
- Becker JJ, Sandwell DT, Smith WHF, Braud J, Binder B, Depner J, Weatherall P (2009) Global bathymetry and elevation data at 30 arc seconds resolution: SRTM30_PLUS. *Mar Geod* 32 (4):355–371

- Bird P (2003) An updated digital model of plate boundaries. *Geochem Geophys Geosy* 4(3)
- Breitsprecher K, Thorkelson DJ (2009) Neogene kinematic history of Nazca-Antarctic-Phoenix slab windows beneath Patagonia and the Antarctic Peninsula. *Tectonophysics* 464:10–20
- Bry M, White N, Singh S, England R, Trowell C (2004) Anatomy and formation of oblique continental collision: South Falkland basin. *Tectonics* 23(4):TC401
- Burton-Johnson A, Riley TR (2015) Autochthonous vs accreted terrane development of continental margins: a revised in situ tectonic history of the Antarctic Peninsula. *J Geol Soc London* 172:822–835
- Calderón M, Fildani A, Hervé F, Fanning CM, Weislogel A, Cordani U (2007) Late Jurassic bimodal magmatism in the northern sea-floor remnant of the Rocas Verdes basin, Southern Patagonian Andes. *J Geol Soc London* 164:1011–1022
- Calderón M, Hervé F, Fuentes F, Fosdick JC, Sepúlveda F, Galaz G (2016) Tectonic evolution of Paleozoic and Mesozoic andean metamorphic complexes and the Rocas Verdes ophiolites in southern Patagonia. In: Ghiglione MC (ed) *Geodynamic Evolution of the Southernmost Andes*. Springer Earth System Sciences, pp 7–36
- Carter A, Curtis M, Schwannethal J (2014) Cenozoic tectonic history of the South Georgia microcontinent and potential as a barrier to Pacific-Atlantic through flow. *Geology* 42(4):299–302
- Clayton (1982) The Geology of North-Western South Georgia: III petrology of the Cumberland Bay formation. *Br Antarct Surv Bull* 51:79–88
- Coren F, Ceccone G, Lodolo E, Zanolla C, Zitellini N, Bonazzi C, Centonze J (1997) Morphology, seismic structure and tectonic development of the Powell Basin, Antarctica. *J Geol Soc London* 154:849–862
- Cunningham WD (1995) Orogenesis at the southern tip of the Americas: the structural evolution of the Cordillera Darwin metamorphic complex, southernmost Chile. *Tectonophysics* 244:197–229
- Cunningham WD, Dalziel IW, Lee TY, Lawver LA (1995) Southernmost South America-Antarctic Peninsula relative plate motions since 84 Ma: Implications for the tectonic evolution of the Scotia Arc region. *J Geophys Res-Sol EA* 100(B5):8257–8266
- Curtis ML, Flowerdew MJ, Riley TR, Whitehouse MJ, Daly JS (2010) Andean sinistral transpression and kinematic partitioning in South Georgia. *J Struct Geol* 32:464–477
- Dalziel IWD (1983) The evolution of the Scotia Arc: a review. In: Oliver RL, James PR, Jago JB (eds) *Antarctic earth science*. Cambridge University Press, Cambridge, pp 283–288
- Dalziel IWD (1986) Collision and cordilleran orogenesis: an Andean perspective. *Geol Soc Spec Pub*, 19:389–404
- Dalziel IWD, Elliot DH (1971) Evolution of the Scotia Arc. *Nature* 233:246–251
- Dalziel IWD, Dott Jr RH, Winn Jr RD, Bruhn RL (1975) Tectonic relations of South Georgia Island to the Southernmost Andes. *Geol Soc Am Bull* 86:1034–1040
- Dalziel IWD, Lawver LA, Pearce JA, Barker PF, Hastie AR, Barfod DN, Schenke H-W, Davis MB (2013a) A potential barrier to deep Antarctic circumpolar flow until the late Miocene?. *Geology* 41(9):947–950
- Dalziel IWD, Lawver LA, Norton IO, Gahagan LM (2013b) The Scotia Arc: genesis, evolution, global significance *Annu Rev Earth Pl Sci* 41, 767–793
- De Conto RM, Pollard D (2003) Rapid Cenozoic glaciations of Antarctica induced by declining atmospheric CO₂. *Nature* 421:245–249
- Eagles G (2000) Modelling plate kinematics in the Scotia Sea. Unpubl. Ph.D. Thesis, University of Leeds, UK
- Eagles G (2004) Tectonic evolution of the Antarctic-Phoenix plate system since 15 Ma. *Earth Planet Sci Lett* 217:97–109
- Eagles G (2010a) South Georgia and Gondwana's Pacific margin: lost in translation? *J S Am Earth Sci* 30:65–70
- Eagles G (2010b) Age and origin of the central Scotia Sea. *Geophys J Int* 183:587–600
- Eagles G, Jokat W (2014) Tectonic reconstructions for paleobathymetry in Drake Passage. *Tectonophysics* 611:28–50

- Eagles G, Livermore RA (2002) Opening history of Powell Basin, Antarctic Peninsula. *Mar Geol* 185:195–205
- Eagles G, Scott B (2014) Plate convergence west of Patagonia and the Antarctic Peninsula since 61 Ma. *Global Planet Change* 123:189–198
- Eagles G, Vaughan APM (2009) Gondwana breakup and plate kinematics: business as usual. *Geophys Res Lett* 36:L10302
- Eagles, G, Livermore, RA, Fairhead, JD, Morris, P, (2005) Tectonic evolution of the west Scotia Sea *J Geophys Res* 110:B02401
- Eagles G, Livermore RA, Morris P (2006) Small basins in the Scotia Sea: the Eocene drake passage gateway. *Earth Planet Sci Lett* 242:343–353
- Eagles G, Gohl K, Larter RD (2009) Animated tectonic reconstruction of the Southern Pacific and alkaline volcanism at its convergent margins since Eocene times. *Tectonophysics* 464:21–29
- Ferris JK, Vaughan APM, Storey BC (2000) Relics of a complex triple junction in the Weddell Sea embayment, Antarctica. *Earth Planet Sci Lett* 178(3):215–230
- Fordyce RE (2003) Cetacea evolution and Eocene-Oligocene oceans revisited. In: Prothero DR, Ivany LC, Nesbitt E (eds) *From greenhouse to icehouse: the marine eocene-oligocene transition*. Columbia University Press, New York, pp 154–170
- Galindo-Zaldívar J, Jabaloy A, Maldonado A, Sanz de Galdeano C (1996) Continental fragmentation along the South Scotia Ridge transcurrent plate boundary (NE Antarctic Peninsula). *Tectonophysics* 258:275–301
- Galindo-Zaldívar J, Bohoyo F, Maldonado A, Schreider A, Suriñach E, Vázquez JT (2006) Propagating rift during the opening of a small oceanic basin: the Protector Basin (Scotia Arc, Antarctica). *Earth Planet Sc Lett* 241:398–412
- Galindo-Zaldívar J, Puga E, Bohoyo F, González FJ, Maldonado A, Martos YM, de Federico Antonio D (2014) Magmatism, structure and age of Dove Basin (Antarctica): A key to understanding South Scotia Arc development. *Glob Planet Change* 122:50–69
- Ghidella ME, Yáñez G, LaBrecque JL (2002) Revised tectonic implications for the magnetic anomalies of the western Weddell Sea. *Tectonophysics* 347:65–86
- Ghiglione MC (2016) Orogenic growth of the Fuegian Andes (52–56°) and its relation with tectonics of the Scotia Arc. In: Folguera A, Naipauer M, Sagripanty L, Ghiglione MC, Orts D, Giambiagi LB (eds) *Growth of the Southern Andes*. Springer Earth System Sciences, pp 241–267
- Ghiglione MC, Ramos VA (2005) Chronology of deformation in the Southernmost Andes of Tierra del Fuego. *Tectonophysics* 405:25–46
- Ghiglione MC, Yagupsky D, Ghidella M, Ramos VA (2008) Continental stretching preceding the opening of the drake passage: evidence from Tierra del Fuego. *Geology* 36:643–646
- Gombosi DJ, Barbeau DL, Garver J (2009) New thermochronometric constraints on the rapid Paleogene exhumation of the Cordillera Darwin complex and related thrust sheets in the Fuegian Andes. *Terra Nova* 21:507–515
- Guillot MG (2016) Magmatic evolution of the Southernmost Andes and its relation with subduction processes. In: Ghiglione MC (ed) *Geodynamic Evolution of the Southernmost Andes*. Springer Earth System Sciences, pp 37–74
- Gradstein FM, Ogg JG, Schmitz M, Ogg G (2012) *The geologic time scale 2012*, 2-volume set, Elsevier
- Grunow AM (1993) New paleomagnetic data from the Antarctic Peninsula and their tectonic implications. *J Geophys Res* 98:13815–13833
- Hamilton IW (1989) *Geophysical investigations of subduction related processes in the Scotia Sea*. Unpubl. Ph.D. thesis, University of Birmingham, Birmingham, UK
- Helfrich G, Wiens DA, Vera E, Barrientos S, Shore P, Robertson S, Adaros R (2002) A teleseismic shear-wave splitting study to investigate mantle flow around South America and implications for plate-driving forces. *Geophys J Int* 149(1):F1–F7
- Hervé F, Fanning CM, Pankhurst RJ (2003) Detrital zircon age patterns and provenance of the metamorphic complexes of southern Chile. *J South Am Earth Sci* 16:107–123

- Hervé F, Miller H, Pimpirev C (2005) Patagonia-Antarctica connections before Gondwana Break-Up. In: Fütterer DK, Damaske D, Kleinschmidt G, Miller H, Tessensohn F (eds) *Antarctica: contributions to global earth sciences*. Springer, Berlin, Heidelberg & New York, pp 215–226
- Hill IA, Barker PF (1980) Evidence for Miocene back-arc spreading in the central Scotia Sea. *Geophys J Roy Astr S* 63:427–440
- Hospitaleche CA, Reguero M, Scarano A (2013) Main pathways in the evolution of the Paleogene Antarctic Sphenisciformes. *J S Am Earth Sci* 43:101–111
- Kavoun M, Vinnikovskaya O (1994) Seismic stratigraphy and tectonics of the north-western Weddell Sea (Antarctica) inferred from marine geophysical surveys. *Tectonophysics* 240:299–323
- Kennett JP (1977) Cenozoic evolution of Antarctic glaciation, the circum-Antarctic Ocean, and their impact on global paleoceanography. *J Geophys Res* 82:3843–3860
- King EC, Barker PF (1988) The margins of the South Orkney microcontinent. *J Geol Soc London* 145:317–331
- Klepeis KA, Austin JA Jr (1997) Contrasting styles of superposed deformation in the Southernmost Andes. *Tectonics* 16:755–776
- Klepeis K, Betka P, Clarke G, Fanning M, Hervé F, Rojas L, Mpodozis C, Thomson S (2010) Continental underthrusting and obduction during the Cretaceous closure of the Rocas Verdes rift basin, Cordillera Darwin, Patagonian Andes. *Tectonics* 29(3):TC3014
- Kraemer PE (2003) Orogenic shortening and the origin of the Patagonian orocline (56 S Lat). *J S Am Earth Sci* 15:731–748
- Larter RD, Barker PF (1991) Effects of ridge crest–trench interaction on Antarctic-Phoenix spreading: forces on a young subducting plate. *J Geophys Res* 96:19583–19607
- Lawver LA, Gahagan LM (1998) Opening of drake passage and its impact on Cenozoic ocean circulation. *Oxf Monogr Biogeogr* 39:212–226
- Lawver LA, Gahagan LM (2003) Evolution of Cenozoic seaways in the circum-Antarctic region. *Palaeogeogr Palaeoclimatol Palaeoecol* 198(1):11–37
- Lawver LA, Della Vedova B, Von Herzen RP (1991) Heat flow in Jane Basin, northwest Weddell Sea. *J Geophys Res Sol EA* 96(B2):2019–2038
- Lawver LA, Gahagan LM, Coffin MF (1992) The development of paleoseaways around Antarctica. In: Kennett JP, Warkne DA (eds) *The Antarctic Paleoenvironment: a perspective on global change: part one*. *Antarct Res Ser*, vol 56 AGU, Washington DC, pp 7–30
- Lawver LA, Williams T, Sloan B (1994) Seismic stratigraphy and heat flow of Powell Basin. *Terra Ant Reports* 1(2):309–310
- Livermore RA, Hunter R (1996) Mesozoic seafloor spreading in the southern Weddell Sea. *Geol Soc Spec Publ* 108:227–241
- Livermore RA, Woollett RW (1993) Seafloor spreading in the Weddell Sea and southwest Atlantic since the Late Cretaceous. *Earth Planet Sci Lett* 117:475–495
- Livermore RA, McAdoo D, Marks K (1994) Scotia Sea tectonics from high-resolution satellite gravity. *Earth. Planet Sci Lett* 123:255–268
- Livermore RA, Eagles G, Morris P, Maldonado A (2004) Shackleton Fracture Zone: no barrier to early circumpolar ocean circulation. *Geology* 32:797–800
- Livermore RA, Nankivell AP, Eagles G, Morris P (2005) Paleogene opening of Drake Passage. *Earth Planet Sci Lett* 236:459–470
- Lodolo E, Donda F, Tassone A (2006) Western Scotia Sea margins: improved constraints on the opening of the Drake Passage. *J Geophys Res* 111:B06101
- Lodolo E, Civile D, Vuan A, Tassone A, Geletti R (2010) The Scotia-Antarctica plate boundary from 35°W to 45°W. *Earth Planet Sci Lett* 293:200–215
- Maffione M (2016) Kinematic evolution of the Southern Andean orogenic arc. In: Ghiglione MC (ed) *Geodynamic Evolution of the Southernmost Andes*. Springer Earth System Sciences, pp 173–200

- Maffione M, Speranza F, Faccenna C, Rossello E (2010) Paleomagnetic evidence for a pre-early Eocene (~50 Ma) bending of the Patagonian orocline (Tierra del Fuego, Argentina): Paleogeographic and tectonic implications. *Earth Planet Sci Lett* 289:273–286
- Maffione M, Fernandez-Moreno C, Ghiglione M, Speranza F, van Hinsbergen DJJ, Lodolo E (2015) Constraints on deformation of the Southern Andes since the Cretaceous from anisotropy of magnetic susceptibility. *Tectonophysics* 665:236–250
- Maldonado A, Barnolas A, Bohoyo F, Galindo-Zaldívar J, Hernández-Molina J, Lobo F, Rodríguez-Fernández J, Somoza L, Vázquez JT (2003) Contourite deposits in the central Scotia Sea: the importance of the Antarctic Circumpolar Current and the Weddell Gyre flows. *Palaeogeogr Palaeoclimatol Palaeoecol*, 198:187–221
- Maldonado A, Bohoyo F, Galindo-Zaldívar J, Hernández-Molina FJ, Lobo FJ, Lodolo E, Somoza L (2014) A model of oceanic development by ridge jumping: opening of the Scotia Sea. *Global Planet Change* 123:152–173
- Müller C (2001) Upper mantle seismic anisotropy beneath Antarctica and the Scotia Sea region. *Geophys J Int* 147:105–122
- Nankivell AP (1997) Tectonic evolution of the Southern Ocean between Antarctica, South America and Africa over the last 84 Ma. Ph.D. thesis Univ of Oxford, Oxford, UK
- Nerlich R, Clark SR, Bunge HP (2013) The Scotia Sea gateway: no outlet for Pacific mantle. *Tectonophysics* 604:41–50
- Pandey A, Parson L, Milton A (2010) Geochemistry of the Davis and Aurora Banks: possible implications on evolution of the North Scotia Ridge. *Mar Geol* 268:106–114
- Pankhurst RJ, Rapela CW (1995) Production of Jurassic rhyolite by anatexis of the lower crust of Patagonia. *Earth Planet Sci Lett* 134:23–36
- Pankhurst RJ, Riley TR, Fanning CM, Kelley SP (2000) Episodic silicic volcanism in Patagonia and the Antarctic Peninsula: chronology of magmatism associated with the break-up of Gondwana. *J Petrol* 41:605–625
- Pearce JA, Hastie AR, Leat PT, Dalziel IWD, Lawver LA, Barker PF, Bevins RE (2014) Composition and evolution of the Ancestral South Sandwich Arc: implications for the flow of deep ocean water and mantle through the Drake Passage gateway. *Glob Planet Change* 123:298–322
- Pérez LF, Lodolo E, Maldonado A, Hernández-Molina FJ, Bohoyo F, Galindo-Zaldívar J, Lobo FJ, Burca M (2014) Tectonic development, sedimentation and paleoceanography of the Scan Basin (southern Scotia Sea, Antarctica). *Global Planet Change*, 123:344–358
- Pirie JHH (1905) On the graptolite-bearing rocks of the South Orkneys. *Proc R Soc Edinb* 25:463–470
- Puig A, Herve M, Suarez M, Saunders AD (1984) Calc-alkaline and alkaline Miocene and calc-alkaline recent volcanism in the southernmost Patagonian cordillera, Chile. *J Volcanol Geotherm Res* 21:149–163
- Reguero MA, Marensi SA (2010) Paleogene climatic and biotic events in the terrestrial record of the Antarctic Peninsula: an overview. In: Madden RH, Carlini AA, Vucetich MG, Kay RF (eds) *The paleontology of Gran Barranca—evolution and environmental change through the Middle Cenozoic of Patagonia*. Cambridge University Press, Cambridge, UK, pp 383–397
- Roterman CN, Copley JT, Linse KT, Tyler PA, Rogers AD (2013) The biogeography of the yeti crabs (Kiwaidae) with notes on the phylogeny of the Chirostyloidea (Decapoda: Anomura). *Proc R Soc Biol Sci Ser B* 280:20130718
- Sandwell DT, Müller RD, Smith WH, Garcia E, Francis R (2014) New global marine gravity model from CryoSat-2 and Jason-1 reveals buried tectonic structure. *Science* 346:65–67
- Schenke HW, Udintsev GB (2009) The Central Scotia Sea floor—is it an paleo-oceanic plate, a young rifted plate or an paleo-land Scotia? *Ukrainian Antarct J* 8:36–45
- Suess E (1909) *Das Antlitz der Erde* Freytag. Leipzig 3 volumes
- Thomson MRA, Tanner PWG, Rex DC (1982) Fossil and radiometric evidence for ages of deposition and metamorphism of the sedimentary sequences on South Georgia. In: Craddock C (ed) *Antarctic Geoscience*. University of Wisconsin Press, Madison, pp 177–184
- Tilley CE (1935) Report on rocks from the South Orkney Islands. *Discov Rep* 10:383–390

- Toggweiler JR, Bjornsson H (2000) Drake Passage and paleoclimate. *J Quat Sci* 15:319–328
- Trendall AF (1953) The geology of South Georgia: I Falkland Islands. Dependencies survey scientific reports 7, 26 p
- Trendall AF (1959) The geology of South Georgia: II Falkland Islands. Dependencies survey scientific reports 19, 48 p
- Udintsev GB, Kurentsova NA, Beresnev AF, Koltsova AV, Domoratskaya LG, Schenke GV, Bakhmutov VG, Solovev VD (2012) Tectonics of the Drake Passage-Scotia Sea zone in the southern ocean. *Dokl Earth Sci* 445:1029–1035
- Vanneste LE, Larter RD (2002) Sediment subduction, subduction erosion and strain regime in the northern South Sandwich forearc. *J Geophys Res Sol EA* 107:EPM 5
- Vaughan APM, Eagles G, Flowerdew MJ (2012) Evidence for a two-phase Palmer Land event from crosscutting structural relationships and emplacement timing of the Lassiter Coast Intrusive Suite, Antarctic Peninsula: implications for mid-Cretaceous Southern Ocean plate configuration. *Tectonics* 31:TC1010
- Winn RD (1978) Upper Mesozoic flysch of Tierra del Fuego and South Georgia Island: a sedimentologic approach to lithosphere plate restoration. *Geol Soc Am Bull* 89(4):533–547

The Relation Between Neogene Denudation of the Southernmost Andes and Sedimentation in the Offshore Argentine and Malvinas Basins During the Opening of the Drake Passage

Matías C. Ghiglione, Christian Sue, Miguel E. Ramos,
Jonathan E. Tobal and Rocío E. Gallardo

Abstract The Neogene orogenic growth of the Southern Patagonian Andes has been related to the approximation and collision of a series of segments of the Chile seismic ridge, which separates the Antarctic and Nazca plates, against South America. The compiled thermochronological data consistently indicates an eastward moving trend of exhumation, where uplift of the western basement domain occurred from ~ 34 to 15 Ma, and was followed by denudation of the basement front and the fold and thrust belt between ~ 20 and 5 Ma. There has been an assumption that tectonic growth in southern Patagonia ended in late Miocene times, largely based on the top age of the molasse deposits of the Santa Cruz Formation, spanning from ~ 22 –19 to 14 Ma. There is, however, multiple thermochronological evidence that exhumation in the hinterland continued profusely, with large volumes of rock denudated rapidly between ~ 15 and 5 Ma, and steadily since ~ 7 Ma. However, continental sedimentation rate was very low in the Magallanes–Austral Basin of the Southernmost Andes after 14 Ma, an effect produced by the dynamic uplift of Patagonia. Contrastingly, the upper Miocene–lower Pliocene constitutes an aggradational period very well developed in the offshore Argentine continental margin. We propose that the great volumes of sediments produced by Miocene–Pliocene denudation of the Southernmost Andes bypassed Patagonia and reached the Argentine and Malvinas basins, where they were accommodated in thick sequences with high sedimentation rates. Those sediments were distributed along the Southern Atlantic margin by sub-Antarctic currents, which propagated into the Argentine continental margin during the deepening of the Drake Passage. The sediments were

M.C. Ghiglione (✉) · M.E. Ramos · J.E. Tobal · R.E. Gallardo
Departamento de Ciencias Geológicas, Instituto de Estudios Andinos “Don Pablo Groeber”
CONICET, FCEN—Universidad de Buenos Aires, Buenos Aires, Argentina
e-mail: matias@gl.fcen.uba.ar

C. Sue
Bourgogne Franche-Comté University, Laboratoire Chrono-environnement, Besançon,
France

probably funneled through gargantuan fluvial and glacifluvial W–E systems, similar to those preserved in Patagonia from the last glaciation, and axially through the Fuegian Andes foothills toward the offshore basins.

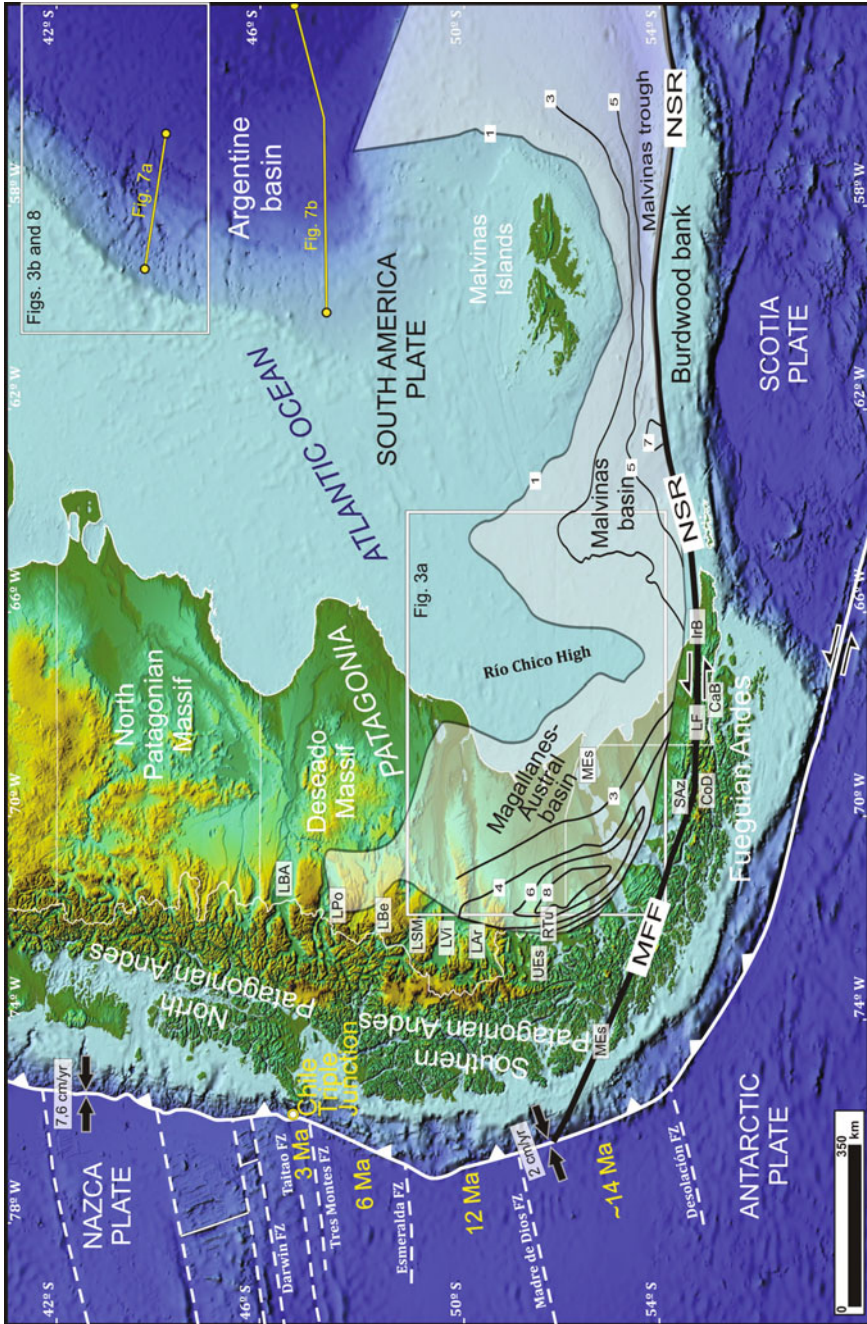
Keywords Atlantic offshore basins • Argentine Basin • Malvinas Basin • Magallanes–Austral Basin • Patagonian Andes • Fuegian Andes • Drake Passage • Malvinas Current • Sub-Antarctic Current

1 Introduction

The beginning of the Oligocene–Neogene orogenic cycle of the Southernmost Andes is marked by the exhumation of its western crystalline domain (Fig. 1) (Nelson 1982; Thomson et al. 2001; Gombosi et al. 2009) and the onset of a widespread clastic wedge with conglomerates resting on a lower Oligocene regional unconformity (Malumián et al. 2000; Marensi et al. 2005; Barreda et al. 2009; Malumián and Jannou 2010). The kinematics involved in each Andean segment during the Oligocene–Neogene deformation was markedly different, from compression linked to ridge collision in the Southern Patagonian Andes (Ramos 1989; see Ghiglione et al. 2016 for a review), to wrench kinematics associated to the opening of the Scotia Sea in Tierra del Fuego (Fig. 1) (Ghiglione 2002, 2016; Lodolo et al. 2003; Eagles et al. 2005; Eagles 2016; Lagabrielle et al. 2009; Ghiglione et al. 2010; Sue and Ghiglione 2016). These geodynamic processes sustained deformation and continuous orogenic denudation during the Neogene in the Southernmost Andes (Nelson 1982; Ghiglione and Ramos 2005; Thomson et al. 2010; Gombosi et al. 2009; Maffione et al. 2010, 2015).

The late Eocene–Oligocene was characterized by a generalized marine transgression that covered all of Patagonia and Tierra del Fuego. These conditions contrast with coeval global high $\delta^{18}\text{O}$ values and a late Eocene–early Oligocene regression in the Patagonian platform, suggesting that the water deepening recorded in the Fuegian (and Southern Patagonian) Andes was due mainly to tectonic loading that facilitated the incursion of Antarctic waters into the Magallanes–Austral basin (Malumián and Jannou 2010). The onset of this transgression appeared first in Tierra del Fuego, during the middle Eocene (Mella 2001; Malumián 2002; Gallardo 2014). In the Southern Patagonian Andes, the flooding of the shallow marine

Fig. 1 Location of main morphostructural units and tectonic features discussed in the text and location of figures in the following of this chapter, after Ghiglione et al. (2010) and references therein. *Yellow* Myr ages in the Pacific trench indicate the time of collision of each ridge segment between oceanic fault zones (refer to Fig. 6). *CaB* Canal Beagle; *CoD* Cordillera Darwin; *FZ* fault zone; *IrB* Irigoyen Basin; *LAr* Lago Argentino; *LBA* Lago Buenos Aires; *LBe* Lago Belgrano; *LF* Lago Fagnano; *LPo* Lago Posadas; *LSM* Lago San Martín; *LVi* Lago Viedma; *MEs* Magallanes Strait; *NSR* North Scotia Ridge; *RTu* Río Turbio; *SAz* Seno Almirantazgo; *UEs* Última Esperanza. Contours indicate sediment thickness in kilometers



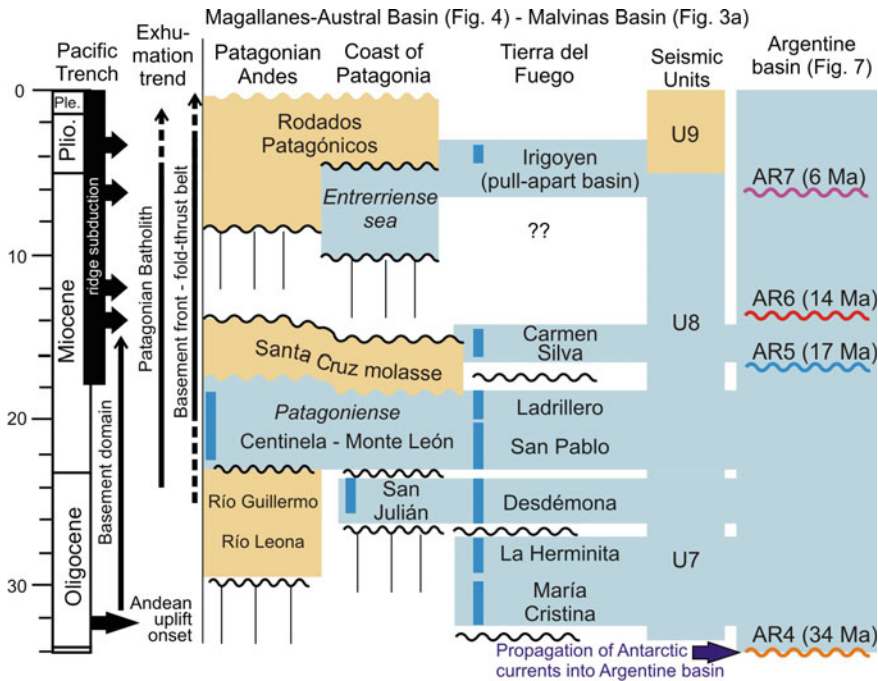


Fig. 2 Correlation of most relevant formations and transgressions in the Magallanes–Austral, Malvinas and Argentine basins. After Hinz et al. (1999), Ghiglione and Ramos (2005), Parras et al. (2008), Guillaume et al. (2009), Malumián and Jannou (2010), del Rio et al. (2013), Gruetzner et al. (2012), and Sachse et al. (2015). *Light blue bands* correspond to marine sequences and transgression periods; *brown background* to continental units. Tectonic events and exhumation trends: see discussion in Sect. 3.2 and references therein

“Patagoniense” transgression occurred later, during the latest Oligocene—early Miocene (Fig. 2) (Malumián 2002; Cuitiño and Scasso 2010; Parras et al. 2012; Cuitiño et al. 2012, 2013).

The transgressive marine phase was followed by a middle Miocene regressive event that marks the onset of continental conditions in Patagonia (Malumián and Jannou 2010), represented by a coarsening upward succession of fluvial deposits from the Santa Cruz Formation (Argentina) (Fig. 2) or the equivalent Zeballos Group (Chile), thinning eastward from a maximum 600 m in the foothills to 250 m on the Atlantic coast (Flynn et al. 2002; Malumián 2002). These continental deposits are considered the synorogenic molasse (Ramos 1989; Lagabriele et al. 2009) and the first-order indicator for the building up of the necessary topography to produce an effective rain shadow on the leeward side of the mountains (Blisniuk et al. 2005, 2006).

In Tierra del Fuego, an Oligocene prograding wedge visualized in seismic sections (Foreland III from Gallardo 2014), represented by outcrops of the shallow marine to deltaic Carmen Silva Formation (Fig. 2) (Malumián and Olivero 2006)

progressively advanced toward the east until the depositional shelf break reached the Atlantic platform during the Miocene (Galeazzi 1998).

Continental sedimentation rate was very low in the Magallanes–Austral Basin after the middle Miocene. The Santa Cruz Formation is overlain by a thin carpet of upper Cenozoic piedmont and glacial-fluvial gravel deposits (Panza 2002; Martínez et al. 2009) known as Rodados Patagónicos (Feruglio 1949) covering most of extra-Andean Patagonia (Fig. 2). Close to the foothills, widespread upper Miocene basaltic Mesetas and some thin sequences cover the Santa Cruz Formation.

Contrastingly, the upper Miocene–lower Pliocene constitutes a transgressive cycle very well developed in the offshore Argentine (Hinz et al. 1999; Hernández-Molina et al. 2009, 2010; Gruetzner et al. 2012, 2014) and Malvinas basins (Galeazzi 1998; Baristead et al. 2013) that partially filled the Malvinas Trough during the Pliocene (Fig. 1) (Fish 2005). The Miocene transgression reached only the present coast of Patagonia and is represented by thin marine sequences from the Entrerriense sea with abundant pectinid fossils of late Miocene age (Fig. 2) (Scasso et al. 2001; del Rio et al. 2013).

There has been an assumption that tectonic growth of the Southern Patagonian Andes ended in late Miocene times, largely based on the top age of the Santa Cruz Formation (Ramos 1989; Blisniuk et al. 2005; Lagabrielle et al. 2009) and the paucity of late Miocene–Pliocene or younger structures in the fold and thrust belt (Fosdick et al. 2013). There is, however, multiple thermochronological evidence that exhumation in the hinterland continued profusely, with large volumes of rock denudated rapidly between ~15 and 5 Ma, and steadily since ~7 Ma (Thomson et al. 2010; Guillaume et al. 2013; Fosdick et al. 2013).

The tectonic scenario was quite different in Tierra del Fuego and in the offshore Malvinas basin, where sub-horizontal sequences covering the fold and thrust belt indicate that orogenic growth stalled after the Oligocene (Ghiglione 2002; Malumián and Olivero 2006; Ghiglione et al. 2010; Baristead et al. 2012, 2013). Strike-slip dominated south of 53°, although slow, post-tectonic uplift and denudation of the Fuegian Andes basement domain was continuous and significant during the late Oligocene and Neogene (Nelson 1982; Gombosi et al. 2009), contemporary with the transpressional uplift of the fold and thrust belt (Ghiglione 2002; Punta Gruesa thrusting from Ghiglione and Ramos 2005).

Late Miocene to Pliocene uplift during denudation has been assigned to isostatic rebound (Fosdick et al. 2013; Nelson 1982) and dynamic topography due to an asthenospheric window (Guillaume et al. 2013). The Patagonian glaciations that started sometime between ~7 and 5 Ma as indicated by basalt intercalated between the oldest till deposits (Mercer and Sutter 1982; Ton-That et al. 1999; Lagabrielle et al. 2007), unquestionably played also an important role during the last phase of Andean denudation.

That leaves the open questions of which factors controlled the present distribution of main faults and structural domains delineating the orogen? And, at which time this configuration was consolidated? Thomson et al. (2010) argue that the timing of deformation and orogen dynamics was largely influenced by late

Cenozoic glaciations. On the other hand, Fosdick et al. (2013) propose a 22–18 Ma main phase of tectonic uplift and exhumation and attribute post-10 Ma denudation solely to fluvio-glacial processes without significant shortening being involved. Concomitant with orogen exhumation, in extra-Andean Patagonia a dynamic response to active spreading ridge subduction produced a late Miocene transition from subsidence to generalized uplift (Guillaume et al. 2009).

Regardless of the discussion about the mechanisms producing Neogene orogenic exhumation, that is the subject of another work in progress, we here question what happened to those large volumes of denudated rocks from the Andes. They were not deposited in Patagonia as shown by the stratigraphical record (Fig. 2), and although surely some volumes went westward to fill the forearc basins in the Pacific trench (cf. Melnick and Echtler 2006), we propose that a larger portion bypassed the continent toward the offshore Argentine and Malvinas basins where thick Neogene sequences were distributed by Antarctic waters and deposited along the Southern Atlantic margin (Fig. 1).

2 Geological and Tectonic Setting

The Southern Patagonian and Fuegian Andes are characterized by well-defined and continuous tectonomorphic zones. These zones are differentiated by their structural style and stratigraphy (Fig. 1) (following Kraemer 1998, 2003; Ghiglione et al. 2009, 2010) in a (i) basement domain encompassing the biggest volume of the Cordillera to the west, and an eastern, (ii) fold and thrust belt domain divided in an internal and external belt.

The basement domain presents internal ductile deformation and is characterized by a regional thick-skinned style, producing the uplift of the metamorphic and magmatic basement of the region. The core and backbone of this domain are the Patagonian and Fuegian batholiths encompassing Jurassic to Neogene calc-alkaline magmatic arc rocks (González Guillot et al. 2011, 2012; Guillot 2016). The Western Andes Metamorphic Complex outcropping along the Pacific archipelago west of the Patagonian Batholith represents the upper Paleozoic–Upper Triassic accretionary prism including exotic amalgamated blocks, such as the Madre de Dios platform (Hervé et al. 2008; cf. Calderón et al. 2016). The late Paleozoic geological history during Gondwana times is represented by widespread low-grade metamorphic rocks (Riccardi and Rolleri 1980; Giacosa and Márquez 2002) cropping out along the eastern flank of the Patagonian Batholith. These polydeformed turbiditic successions reaching up to greenschist facies interspersed with minor limestone and metabasites are grouped in the Eastern Andes Metamorphic Complex (Hervé et al. 2008; Calderón et al. 2016). In Tierra del Fuego, basement rocks are concentrated in Cordillera Darwin (Fig. 1), a high-grade metamorphic complex exposing kyanite–staurolite schist (Dalziel et al. 1974; Nelson 1982; Kohn et al. 1995). It is not known at present if these metamorphic rocks of Cordillera Darwin were originally part of the Eastern Andes Metamorphic Complex, or if they were

part of the Coastal Accretionary Complexes of the Southern Patagonian Andes (cf. Calderón et al. 2016). From a mechanical point of view, the eastern basement domain in the Patagonian Andes can be correlated with Cordillera Darwin in Tierra del Fuego, since they both transferred shortening to the fold and thrust belt during the Late Cretaceous and Cenozoic (Ghiglione and Cristallini 2007, Ghiglione et al. 2014; Maffione et al. 2015; Maffione 2016). The units outcropping along the concave edge of the basement domain in the Patagonian–Fuegian Andes are fault-controlled Jurassic synrift deposits.

The Early to Middle Jurassic was characterized by regional extension and the synrift deposition of basal conglomerates cover by thick volcanics of El Quemado Complex or Tobífera/Lemaire Formation (Pankhurst et al. 2000). The Jurassic fault array consists of N–NW-oriented extensional faults bounding grabens, and E–W-oriented transfer faults separating depocenters with different degrees of extension (Uliana et al. 1989; cf. Ghiglione et al. 2013). The Jurassic extensional faults and grabens were inverted during the Andean cycle, influencing style and distribution of compressional structural domain in the Southern Patagonian Andes (Kraemer 1998; Likerman et al. 2013; Ghiglione et al. 2014). The Lower Cretaceous Springhill and Río Mayer formations are interspersed in inversion structures along the basement front (Kraemer 1998; Ghiglione et al. 2009, 2014; Giacosa et al. 2012).

The Andean compressive cycle started during the Late Cretaceous in the Southernmost Andes of Patagonia and Tierra del Fuego, producing the onset of the foreland stage in the Magallanes–Austral Basin and offshore basins of southernmost South America (Ghiglione et al. 2010). Late Cretaceous metamorphism, uplift, and exhumation of the basement domain (Cunningham 1995), were followed by the onset of clastic foredeep sequences (Wilson 1991; Arbe and Hechem 1984; Kraemer and Riccardi 1997). The Upper Cretaceous sequences are well developed south of 49°S, reaching a thickness of ~3800 m between Lagos Viedma and Argentino and of ~4300 m in Última Esperanza (Fig. 1) (cf. Ghiglione et al. 2014, 2016).

The following cycle of synorogenic deposition and propagation of thrusts occurred during the latest Cretaceous–Paleogene (Biddle et al. 1986; Marensi et al. 2002) and was accompanied by strong sedimentary rates, as indicated by growth strata in Río Turbio (51°30'S, Fig. 1) (Malumián et al. 2000).

Tierra del Fuego was affected by middle Eocene–Oligocene coeval strike-slip and compressional deformation due, respectively, to the fast (2.4 cm/year) left-lateral motion between South America and Antarctica (Livermore et al. 2005), and the synergetic combination of fast spreading rates in the Drake Passage (Ghiglione et al. 2008; Barbeau et al. 2009) with rapid convergence and northward-directed subduction of the Farallón plate against South America (Ghiglione and Cristallini 2007). The progression of exhumation and sedimentation of the Oligocene–Neogene tectonic cycle is the topic of the current review and would be explained in detail below.

3 Oligocene–Neogene Tectonic Cycle

3.1 *Geodynamic Setting and Tectonic Style*

3.1.1 Southern Patagonian Andes

The last Andean tectonic cycle is very well developed in the Southern Patagonian Andes and has been related to the approximation and collision of a series of segments of the Chile seismic ridge, which separates the Antarctic and Nazca plates, below South America (Fig. 1) (Ramos 1989; Folguera and Ramos 2002; Lagabrielle et al. 2004; Scalabrino et al. 2009). The first segment of the Chile ridge collided nearly parallel to the Pacific trench around 18 Ma at $\sim 54^\circ\text{S}$ as calculated by kinematic reconstructions (Breitsprecher and Thorkelson 2008). The resulting Antarctica–Nazca–South America triple junction migrated progressively northward with each segment collision, to its present position at $\sim 46^\circ\text{S}$ (Fig. 1) (Forsythe and Nelson 1985; Cande and Leslie 1986). A speed difference between the Nazca (~ 10 cm/year) and Antarctica (~ 2 cm/year) plates produced an increasingly open asthenospheric slab window, giving way to widespread alkali Patagonian plateau lavas (Gorring et al. 1997; Bourgois and Michaud 2002).

Although there is a time lag between the ~ 18 Ma first ridge collision, and the 30 Ma onset of exhumation in the basement domain (Fig. 2) (Thomson 2002), a cause to effect relationship has been proposed (Ramos 1989). Compression preceding ridge subduction could have been the result of increased coupling and shallow subduction due to the approach of progressively younger and more buoyant oceanic crust to the trench (Thomson et al. 2001; Folguera and Ramos 2002). Another timing discrepancy exists between an important 10 to <5 Ma denudation of the cordillera (Thomson et al. 2001), and the ~ 22 –19 to 14 Ma deposition of the Santa Cruz Formation synorogenic deposits (Fig. 2) (Marensi et al. 2005; Blisniuk et al. 2005; Cuitiño et al. 2012, 2015) that would be discussed below (Sect. 4).

3.1.2 Fuegian Andes, Antarctica, and the Scotia Sea

After the middle Eocene–Oligocene compressional event in Tierra del Fuego (Ghiglione and Ramos 2005), the tectonic plate scenario changed drastically for the Southernmost Andes–Antarctica region (see Ghiglione 2016 for a review). Relative movement between South America and Antarctica was accommodated by spreading in the West Scotia Sea from about 28 Ma (Lodolo et al. 2006) until ~ 16 Ma when the future Scotia Plate started to move independently of the South American plate (cf. Eagles 2016; Eagles et al. 2005; Lagabrielle et al. 2009). A sinistral strike-slip fault zone on the offshore North Scotia Ridge and continental Magallanes–Fagnano fault system (Fig. 1) was developed to accommodate the movement between the two plates (Thomas et al. 2003). A left-lateral strike-slip regime produced widespread deformation in Tierra del Fuego Island ever since

(Diraison et al. 2000; Lodolo et al. 2003; Sue and Ghiglione 2016). A still active rift system perpendicular to the orogen produced the opening of the eastern Magallanes Strait (Diraison et al. 1997, 2000) and the transverse segmentation of the external fold and thrust belt (Ghiglione et al. 2013). Since spreading rates in Drake Passage were higher than required by South America–Antarctica motion, this resulted in deformation within southern South America (Livermore et al. 2005). Transpressional structures have been reported in Miocene sequences outcropping in the Atlantic coast of Tierra del Fuego (Ghiglione et al. 2002). Transpression along the proto-North Scotia Ridge–Magallanes–Fagnano fault system during the 26–14 Ma period produced a change from deep marine to very shallow conditions along the newly formed plate boundary (Lagabrielle et al. 2009). Baristean et al. (2012, 2013) defined a transpressional foreland phase for the Malvinas Basin, during which the sediments were derived from the uplifted Burdwood bank (Fig. 1) (cf. Galeazzi 1998). Recently, deformation along the North Scotia Ridge is transpressive due to a restraining bend geometry, while along the Magallanes–Fagnano fault system a releasing bend develops (Lodolo et al. 2003).

3.2 *Exhumation Age from Thermochronological Data*

The samples with the oldest exhumation ages in the Southern Patagonian Andes are also the westernmost, located in outcrops along the Pacific archipelago in metamorphic and magmatic rocks of the Basement domain, around 100 km from the trench. These samples show similar apatite fission-track (AFT) central ages between ~34 and 25 Ma, indicative of rapid cooling through the apatite partial annealing zone (APAZ) from above ~110 to ~60 °C (Thomson et al. 2001, 2010). The AFT data indicate at least ~4 km of denudation in the western basement domain since 30 Ma (Thomson et al. 2001), while apatite (U–Th)/He (AHe) cooling ages within the same sector indicate similar denudation rates between 24 and 15 Ma (Thomson et al. 2010).

Along the central and eastern Patagonian Batholith, AFT ages between ~24–18 and 15 Ma are in many cases concordant with zircon fission-track ages (ZFT) (Thomson et al. 2010). The coincidence can be explained by in situ cooling, following intrusion into cool shallow crust (Thomson et al. 2001). The total amount of cooling in these rocks since 24 Ma is restricted between the APAZ (110 °C) and the closure temperature of fission tracks in zircon (~280 °C), representing between 9 and 4 km of denudation (Thomson et al. 2001). When AHe from the Patagonian Batholith is considered, ages between 20 and 11 Ma seem to be consistently distributed, although also some ages between 10 and 5 Ma are found north of 49°S.

Between the 50 and 52°S parallels, AFT and ZFT show active denudation of the basement front and the fold and thrust belt between 24 and 5 Ma (Fosdick et al. 2013), while to the north of 48°30'S ages between 14 and 5 Ma prevail (Thomson et al. 2010). Along the eastern margin of the basement domain (Eastern Andes Metamorphics), young AFT ages between 14 and 5 Ma (Fosdick et al. 2013) or

12–8 Ma (Thomson et al. 2001) indicate between 9 and 4 km of denudation. Zircon (U–Th)/He (ZHe) results from the basement front and the fold and thrust belt in Última Esperanza indicate an approximate ~6 km exhumation depth since ~22 Ma (Fosdick et al. 2013). AHe results from that region record young ages centered between 6 and 4 Ma, indicating significant late Miocene and Pliocene denudation, consistent with efficient fluvio-glacial erosion (Fosdick et al. 2013).

Haschke et al. (2006) analyzed an AFT vertical profile from the basement front at Cerro Barrancos granite, southwest of Lago Posadas at 47°30'S (Fig. 1). These authors estimated accelerated cooling between 17 and 10 Ma with a minimum of 3–4 km of exhumation. A reheating between 10 and 6 Ma followed, and final cooling commenced at ~4 Ma until the samples were exhumed to the surface (Haschke et al. 2006). Guillaume et al. (2013) reappraised the thermal history of Cerro Barrancos granite by adding AHe data and calculated slow (~70 m/Myr) denudation rates for the 25–15 Ma and 10–5 Ma periods, followed by a phase of rapid cooling, with denudation values as high as 650 m/Myr between 5 and 3 Ma.

The compiled thermochronological data consistently indicates the following, eastward moving trend of exhumation in the Southern Patagonian Andes (left column in Fig. 2): (i) western basement domain from ~34 to 15 Ma, (ii) Patagonian Batholith since 24 Ma, (iii) basement front and the fold and thrust belt between ~25 or 15 Ma and 5–3 Ma, and several kilometers of denudation since ~7–5 Ma.

Toward the south, multiple AHe data indicate sustained exhumation in the 25–3 Ma period along the southern Patagonian Batholith between 52° and 54°S (Thomson et al. 2010). Along the Canal Beagle (Fig. 1), three AFT ages reached post-Eocene exhumation ages ranging between 29 and 1 Ma (Thomson et al. 2010). Nelson (1982) using fission tracks and geochronology argued that a significant uplift and exhumation of Rocas Verdes and Cordillera Darwin occurred post-tectonically since 30 Ma. This late Oligocene–Holocene uplift of up to ~2 km, representing around two-thirds of the actual relief, occurred at constant low rates (0.05–0.20 mm/year) (Nelson 1982). Modeling of new thermochronometry data from the basement domain in the Fuegian Andes also reveals a slow but sustained post-Eocene cooling (Gombosi et al. 2009).

3.3 *Synorogenic Sequences*

The Oligocene–Neogene cycle of sedimentation forms a clastic wedge that thickens to the west and to the south of the Magallanes–Austral Basin (Malumián 2002). This synorogenic sequence presents very continuous exposures in the Patagonian Andes's foothills and overlaps the offshore basement Río Chico high (Fig. 3a) (Baristead et al. 2013; Sachse et al. 2015).

The upper Cenozoic foredeep sequence starts with the Oligocene–lower Miocene fluvial systems of the Río Guillermo and Río Leona formations (Kraemer 1998; Marensi et al. 2005) resting unconformably on a discontinuity formed

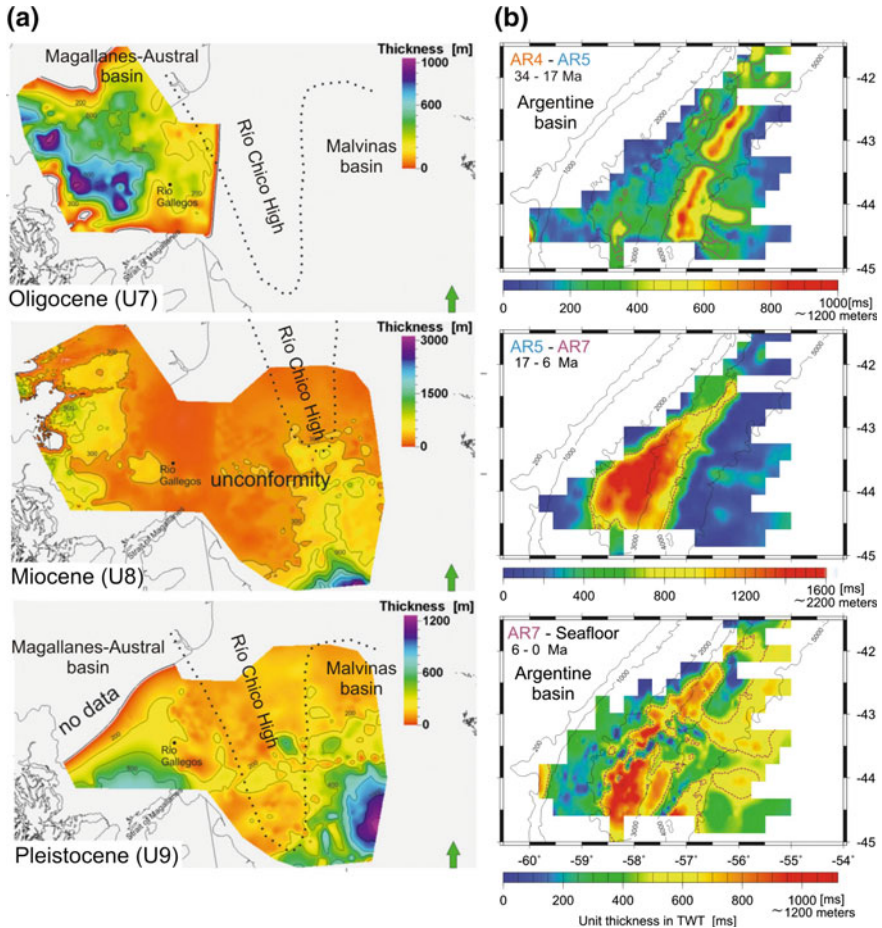


Fig. 3 Comparison between Oligocene–Neogene thickness patterns of sedimentation from seismic information, between Magallanes–Austral Basin (*to the left* in meters) and Argentine Basin (*to the right* in ms two-way traveltime, twt). See Fig. 1 for location and Fig. 2 for correlation of seismic and outcrop units: **a** thickness maps (meters) of the Austral and western Malvinas basins from Sachse et al. (2015). **b** Maps of unit thicknesses in twt for identified seismic units (approximate equivalence in meters is indicated). Purple hatched lines mark depocenter outlines (rms of unit thickness). Bathymetric contours are indicated as thin black lines. From Gruetzner et al. (2012)

during late Eocene and early Oligocene times (Fig. 2) (Malumián et al. 2000). A fining upward trend for Rio Leona Formation indicates a tectonically derived upward increase in accommodation space (Marensi et al. 2005). This deepening trend resulted in the flooding of the shallow marine Patagoniense transgression (Fig. 4a) (Malumián 2002), represented by lower Miocene deposits of the Centinela Formation (Fig. 2) (equivalent to Estancia 25 de Mayo and El Chacay formations) outcropping along the Patagonian foothills (Cuitiño and Scasso 2010; Cuitiño et al. 2012). To the east, the Monte León, Chenque, and Gaiman Formations (Malumián 2002; Parras et al. 2008, 2012), and in Tierra del Fuego the San Pablo and

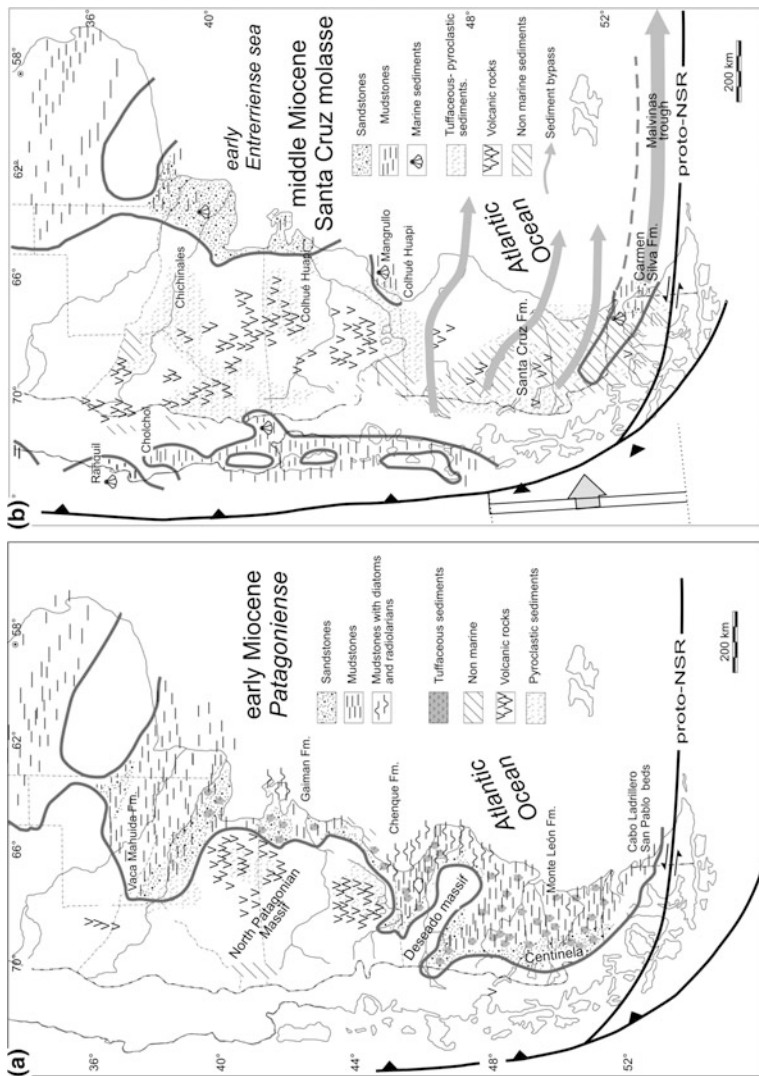


Fig. 4 Paleogeographic reconstructions from the **a** early and **b** middle Miocene. See text for discussion. NSR North Scotia Ridge. Modified from Malumian and Nañez (2011) and references therein

Ladrillero beds represent distal equivalents for the early Miocene transgression (Fig. 4a) (Malumián and Jannou 2010). The age of the Patagoniense has been constrained by high resolution isotopic ages between 20 and 18 Ma for the western wedge (lower Miocene; Cuitiño et al. 2012, 2015). These ages overlap with a low eustatic sea level interval, and an erosional sequence boundary, suggesting an origin caused by a strong basin floor subsidence event related to tectonic loading (Cuitiño and Scasso 2010).

The onset of the late Cenozoic transgression occurred during the middle Eocene in Tierra del Fuego, i.e. earlier than in Patagonia (Mella 2001; Malumián 2002) reaching deep water facies in the early Oligocene (María Cristina beds, Fig. 2) (Malumián and Jannou 2010). The south to north diachronism can be related to an earlier phase of deformation in Tierra del Fuego (middle to late Eocene Río Bueno thrusting; Ghiglione and Ramos 2005) that can be related to the accelerated opening of the Scotia Sea (Ghiglione et al. 2008; Barbeau et al. 2009; Gombosi et al. 2009; Eagles 2016).

The continued advance of topographic uplift produced an ensuing regression in the Southern Patagonian Andes, represented by the fluvial and lacustrine Santa Cruz Formation (Fig. 4b). There is a transitional contact with the various underlying marine units (Fig. 2), evidenced by intermediate estuarine deposits (Feruglio 1938; Cuitiño and Scasso 2010; Cuitiño et al. 2013). The age of the conglomeratic to mammal-bearing lacustrine sediments of the Santa Cruz Formation is bracketed by intercalated tuffs between ~ 22 –19 and 14 Ma (Marshall et al. 1997; Blisniuk et al. 2005; Perkins et al. 2012). Calculated average sediment accumulation rates are high, in the range of 200–100 m/Myr (Blisniuk et al. 2005; Perkins et al. 2012).

Patagonian sedimentation practically stalled after the middle Miocene. Southwest of Lago Posadas a $\sim 14 \pm 1$ Ma tuff from the Santa Cruz Formation is just 3 m below the base of a 12 Ma old basalt which is topped by a scarce succession of basalts and sediments (Blisniuk et al. 2005; Goring et al. 1997). In extra-Andean Patagonia widespread gravel mantels known as *Rodados Patagónicos* cover the Santa Cruz Formation (Fig. 2). As expressed in a recent review by Martínez and Kutschker (2011), these conglomerates are one of the most distinctive features of the regional landscape in extra-Andean Patagonia (see also Panza 2002). Their significant roundness, along with additional sedimentary and geomorphological evidence, indicates that their origin is linked to surface drainage networks of relatively high energy (Martínez and Kutschker 2011). Such high energy was induced by powerful flow rates and/or strong water gradients, attributable to tectonism, epirogenesis, and/or lowering of sea level (Martínez and Kutschker 2011).

A mapping and morphological study of these post-middle Miocene fluvial terraces carry out by Guillaume et al. (2009) in the southern part of the North Patagonian Massif (Fig. 1) evidenced regional-scale tilting of terraces overlaid by coarse fluvial series. These authors suggest a generalized dynamic uplift of the continental plate from the Andes to the Atlantic Ocean that started in the middle–late Miocene, during the opening of the asthenospheric window (Fig. 5). This uplift probably migrated toward the northeast, following the procession of ridge segment collisions (Fig. 6).

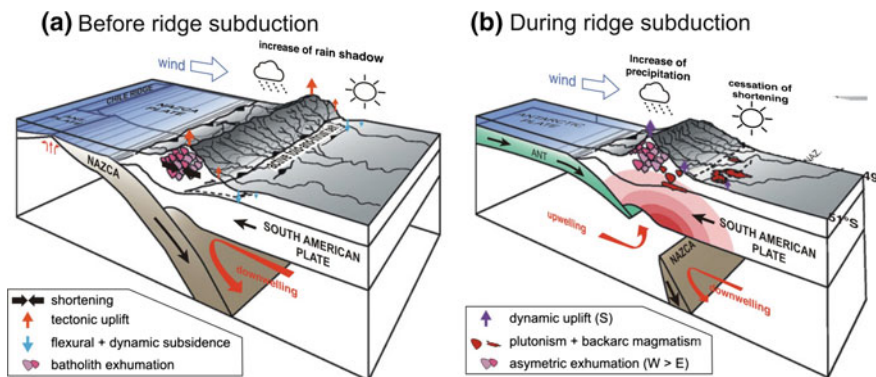
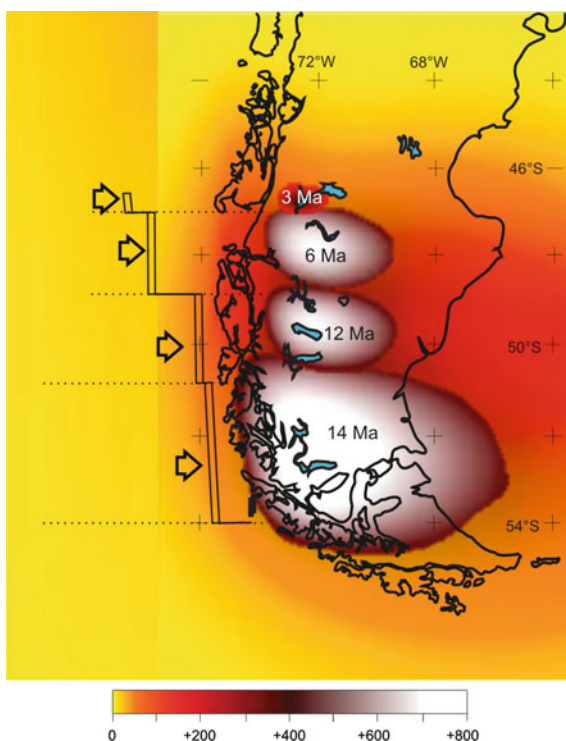


Fig. 5 Synthetic 3D sketch showing the response of the South America plate to the formation of the slab window between 51° and 47°S (modified from Guillaume et al. 2009): **a** segments of the Chile Ridge did not yet reach the trench, and convergence is accommodated by shortening in the fold and thrust belt. **b** Subduction of the ridge segments produces the opening of a slab window inducing magmatism that advect heat through the lithosphere, and a dynamic uplift associated with upwelling of sub-slab mantle

Fig. 6 Sketch showing the uplift of Patagonia resulting from the episodic subduction of ridge segments accompanying the northward migration of the triple junction. Model of ~800 m dynamic uplift in response to subduction of four Chile Ridge's segments with lengths of 400 (14 Ma), 200 (12 Ma), 200 (6 Ma), and 50 km (3 Ma). Redrawn from Guillaume et al. (2009)



Contrasting with the situation in continental Patagonia, the middle Miocene is an aggradational phase in the Argentine continental margin (Figs. 3b and 7) (Hinz et al. 1999; Gruetzner et al. 2012) associated with major subsidence during the deepening of the Drake Passage (Hernández-Molina et al. 2010). Post-middle Miocene seismic sequences are very thick and well developed in the Argentine Basin (Figs. 3b and 7) (Hinz et al. 1999; Hernández-Molina et al. 2009, 2010; Gruetzner et al. 2014); registering an up to tenfold increase in sedimentation rate after the AR5 (17 Ma) unconformity (Fig. 8; Gruetzner et al. 2012). The middle Miocene–Pleistocene conform seismic units up to ~ 2000 ms (two-way traveltime) in vertical extension (Fig. 7) (around 2400 m thick, Gruetzner et al. 2012). On the other hand, the upper Miocene–lower Pliocene sequences of the Entrerriense Sea (Fig. 2) cropping out along the coast of Patagonia are less than 50 m thick. Based on $^{87}\text{Sr}/^{86}\text{Sr}$ dating of calcite shells belonging to pectinids, this sea flooding event that barely reached the Atlantic coast in the Magallanes–Austral Basin (Fig. 4b) was dated between ~ 10 and 5 Ma (Scasso et al. 2001; del Rio et al. 2013). At that time, a carpet of the mainly fluvial Rodados Patagónicos was covering Patagonia (Fig. 2).

In Tierra del Fuego, sedimentation was active during the middle–late Miocene transgression that completed the remaining accommodation space with shallow marine, deltaic system, and fluvial deposits of the Carmen Silva Formation (Fig. 4b) (Malumián and Jannou 2010; Gallardo 2014). However, sedimentation was funneled toward the offshore afterward, filling the Malvinas trough during the Pliocene (Fish 2005). Post-Miocene sequences show highest sediment accumulations in the Malvinas Basin (Pliocene U9, Fig. 3a). The Magallanes–Austral Basin could not accumulate significant sediments anymore; thus, it is highly likely that the sediments were further transported into the offshore basins (Sachse et al. 2015).

4 Discussion and Concluding Remarks: The Relation Between Andean Deformation, Dynamic Topography, and Sediment Bypass Toward the Offshore

Approximation and collision of the Chile ridge produced renewed tectonic uplift of the Southern Patagonia Andes since ~ 30 Ma, with denudation focused in the eastern sector of the Basement domain (Thomson et al. 2010), and the fold and thrust belt after ~ 20 Ma (Fig. 2) (Fosdick et al. 2013). The ensuing opening of an asthenospheric window produced the dynamic uplift of the retroarc, migrating from the foothills (Scalabrino et al. 2009) toward extra-Andean Patagonia (Fig. 5) (Guillaume et al. 2009). The wave of dynamic topography and a late Miocene transition from subsidence to generalized uplift could have migrated also from south to north, as different spreading segments entered the trench (Fig. 6) (Guillaume et al. 2009, 2013), and toward the east, ultimately producing the uplift of shorelines along the Atlantic coast (Pedoja et al. 2011; Isla and Angulo 2015).

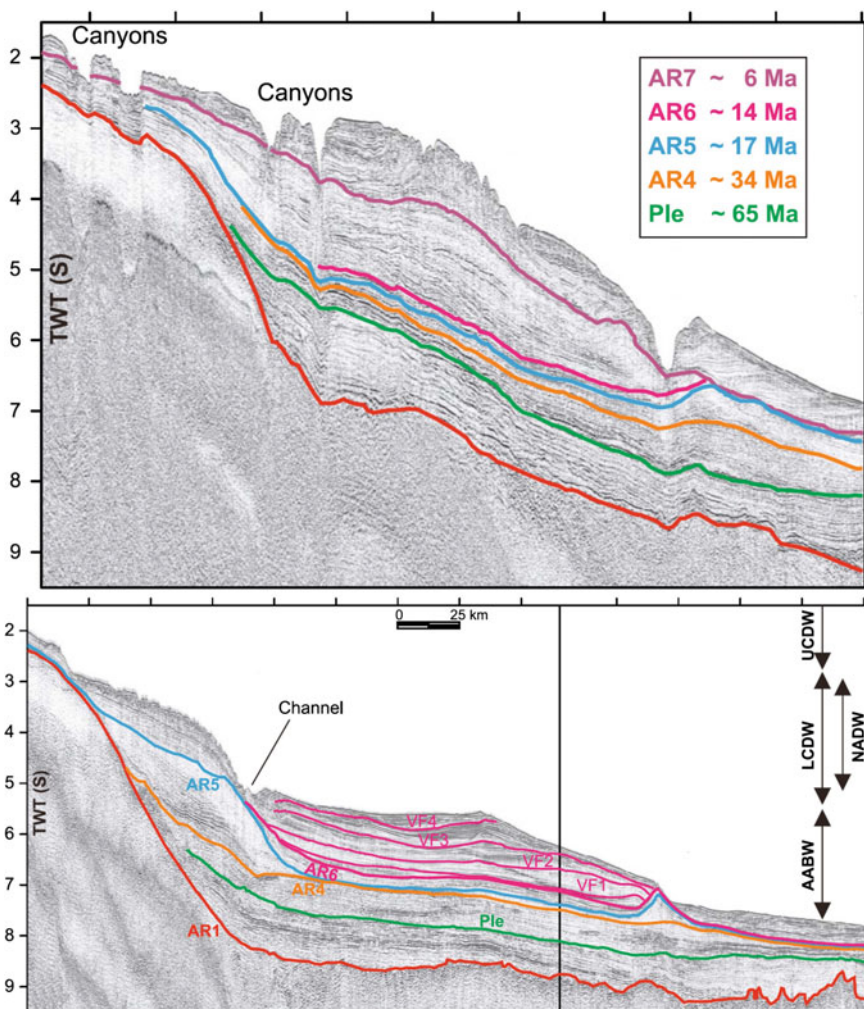
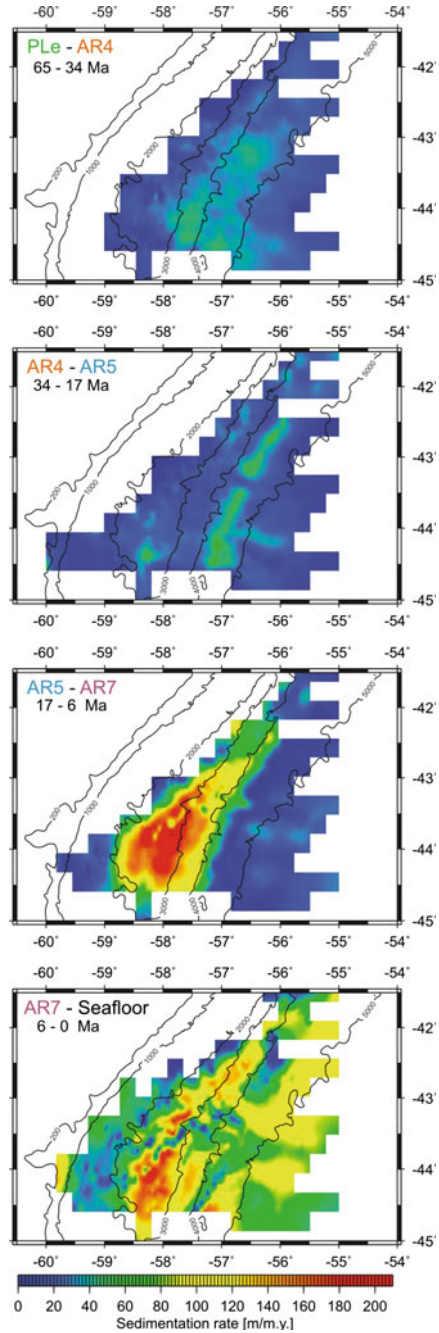


Fig. 7 Seismic profiles across the Argentine Basin. See Fig. 1 for location and Fig. 2 for correlation of seismic and outcrop units. *Arrows* indicate the extent of present-day water masses AABW (Antarctic Bottom Water), LCDW (Lower Circumpolar Deep Water), UCDW (Upper Circumpolar Deep Water), and NADW (North Atlantic Deep Water). Reflectors VF1 to VF4 indicate a refined seismostratigraphic model, where reflector VF3 is an elongated mounded drift interpreted to indicate strengthening of bottom flow during the late Miocene/early Pliocene. Modified from Gruetzner et al. (2012)

Fig. 8 Maps of sedimentation rates in the Argentine Basin from seismic data. Notice the tremendous increase in sedimentation after AR5. See Fig. 1 for location and Fig. 2 for correlation of seismic and outcrop units. Sedimentation rates were derived from reflector depths based on a velocity–depth model and age information. Bathymetric contours are indicated as *thin black lines*. From Gruetzner et al. (2012)



4.1 Miocene–Pleistocene Distribution of Sedimentation in the Basins of Southernmost South America

While exhumation in the Southernmost Andes was continuous during the Oligocene–Neogene, an important change in the Magallanes–Austral Basin dynamics occurred during that period, related to uplift of the retroarc. While Late Cretaceous to Eocene foreland depocenters were concentrated in the 200-km-wide strip bounding the basement thrust front (cf. Ghiglione et al. 2010, 2016), the locus of sedimentation migrated rapidly toward the offshore basins after the Oligocene (Fig. 3) (Gruetzner et al. 2012; Sachse et al. 2015). Along the foothills of the Patagonian and Fuegian Andes, sedimentation almost ceased at 14 Ma (Blisniuk et al. 2005; Malumián and Olivero 2006). In contrast with the situation in continental Patagonia, major subsidence and sedimentation is registered in the Argentine continental margin and Malvinas basin since the middle Miocene (Figs. 3 and 8) (Hinz et al. 1999; Baristead et al. 2012, 2013; Gruetzner et al. 2012; Sachse et al. 2015). It seems that since that time, Andean sediments bypassed Patagonia to reach the offshore Argentine and Malvinas basin.

Continental uplift produced a marked regression in Tierra del Fuego, where the shelf break migrated toward the east, reaching the actual Atlantic coast ($\sim 68^\circ\text{W}$) by middle Miocene times (east of Carmen Silva delta, Fig. 4b). Since the Miocene, overall sediment accumulation in the Malvinas Basin exceeded those of the Magallanes–Austral Basin (Fig. 3a) (Sachse et al. 2015). After 5.5 Ma, during the Pliocene–Pleistocene, marine sedimentation was focused east of $\sim 65^\circ\text{S}$ (Galeazzi 1998), while the Río Chico high was under erosion, and an important depocenter was developed along its eastern flank (Fig. 3a) (Baristead et al. 2013; Sachse et al. 2015).

Sediment bypass produced a strong change and long-lasting trend in sedimentation along the Argentine continental margin, marked by the A5–17 Ma unconformity (Figs. 7 and 8). Below A5, the 65–17 Ma seismic sequence has low sedimentation rates (10–46 m/Myr), similar to hemipelagic settings in the oceans (Fig. 8) (Gruetzner et al. 2012). On the other hand, the 17–0 Ma sequences exhibit 120–140 m/Myr sedimentation rates, that is, >200 m/Myr in some depocenters (Fig. 8) (Gruetzner et al. 2012), i.e. similar or higher than the calculated average 200–100 m/Myr sediment accumulation rates for the Santa Cruz Formation (Blisniuk et al. 2005; Perkins et al. 2012). At the same time, an elongated mounded drift is interpreted to indicate strengthening of bottom flow during the late Miocene/early Pliocene (Fig. 7) (Gruetzner et al. 2012).

4.2 Dynamic Uplift in Patagonia, Wrench Deformation in Tierra del Fuego and Sedimentation Bypass

Late Miocene interruption of the long-lasting Magallanes–Austral foreland depocenter (Fig. 2) seems to be the product of dynamic uplift produced by an

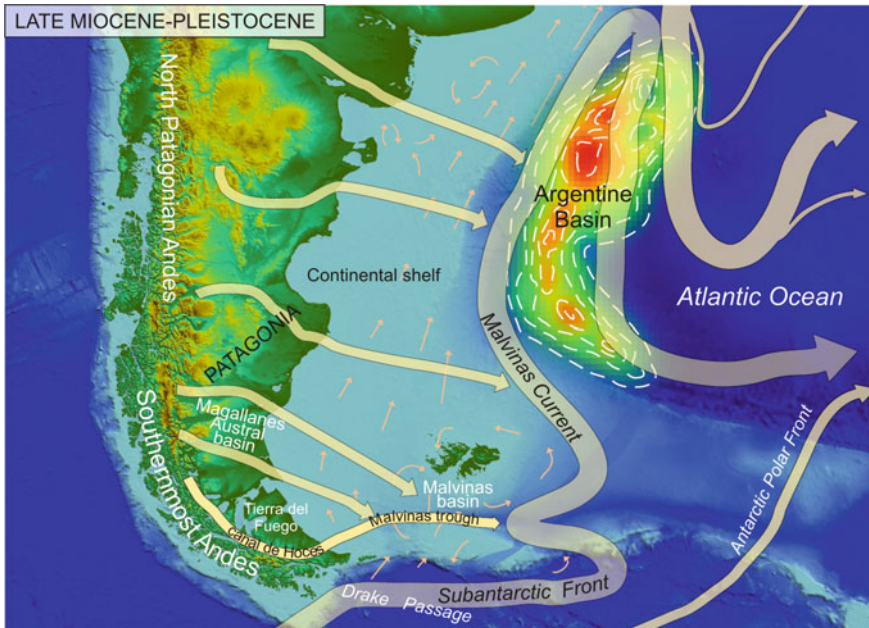


Fig. 9 Post-Miocene paleogeography, after the deepening of the Drake Passage and the onset of the sub-Antarctic Front and Malvinas Current, during the exhumation of the Patagonian–Fuegian Andes. The sedimentary systems bypassing the continent toward the depicted offshore depocenters are shown. Main ocean currents are from Piola and Matano (2001). Post-A5 (17 Ma) sediment thickness in the Argentine Basin was compiled and drawn from Hinz et al. (1999), Hernández-Molina et al. (2009, 2010) and Gruetzner et al. (2012, 2014)

asthenospheric window (Fig. 6), as proposed by Guillaume et al. (2009). To the north of 52°S, it is unclear to us by which mechanism the great volumes of rocks from the late Miocene to Pliocene exhumation and denudation of the Cordillera reached the Argentine continental shelf. Clearly some significant amount of sediment flux was diverted toward the Pacific trench (cf. Melnick and Echtler 2006). It seems probable, however, that fluvial and fluvio-glacial systems similar to those actual present in Patagonia could have acted as effective means of sediment transport toward the offshore (Fig. 9). The increase in sediment transport from the river and shelf toward the deeper part of the basin has been previously assigned to a relative sea level fall and/or tectonic uplift by Gruetzner et al. (2012).

To the south of 52°S, in the Tierra del Fuego sector affected by Neogene wrench kinematics (cf. Sue and Ghiglione 2016), the Foreland III prograding wedge (Gallardo 2014), represented by the shallow marine to deltaic Carmen Silva Formation (Fig. 2) (Malumián and Olivero 2006), formed a sedimentary system axial to the Fuegian Andes, that prograded toward the offshore Malvinas and South Malvinas basins (Fig. 4b).

There are two different deformation mechanisms to explain the existence of a Fuegian axial trough in its context of wrench kinematics, a first one acting from ~ 26 to 16 Ma, and a second one active after that period onwards.

26–16 Ma transpression along the proto-North Scotia Ridge fault system was proposed by Lagabrielle et al. (2009) based on tectonic models by Eagles et al. (2005) showing shortening on the Scotia–South America plate boundary in the intervening period (cf. Eagles 2016). The depicted late Oligocene–early Miocene context is also in agreement with the 24–16 Ma Punta Gruesa stage of transpressional faulting recognized along the Atlantic coast of Tierra del Fuego (Ghiglione and Ramos 2005) and in the Malvinas basin (Baristead et al. 2012, 2013). The sediments could have been funneled along a transpressional depression in the Fuegian Andes, and toward the offshore Malvinas trough (Fig. 4b). The southern trough was probably accentuated by tectonic load due to transpressional uplift of the Basement domain and the Burdwood bank along the North Scotia Ridge that also acted as source of sediments (Galeazzi 1998; Baristead et al. 2013).

Plate divergence since ~ 18 Ma (Eagles 2016) produced generalized transtensional deformation in Tierra del Fuego (Ghiglione et al. 2013), and in particular a series of pull-apart depocenters along the South America–Scotia continental plate boundary, such as the eastern Magallanes Strait, the Seno Almirantazgo, Lago Fagnano (Lodolo et al. 2003), and Irigoyen river basins (Fig. 1) (Ghiglione 2003; Ghiglione and Ramos 2005; Malumián and Jannou 2010). This concatenation of pull-apart depocenters could have acted as an effective way of funneling detritus from the continent toward the offshore (Fig. 9). The possibility that those pull-apart depocenters allowed the interchange of Pacific and Atlantic waters was already proposed by Malumián and Scarpa (2005), based on the presence of assemblages of benthic foraminifers with Pacific affinity in the Irigoyen Basin in the Atlantic coast (Fig. 1). These authors suggested a direct shallow connection between the Atlantic and Pacific Oceans by means of the Canal de Hoces along the Magallanes–Fagnano fault system (Fig. 9).

4.3 Onset of sub-Antarctic Front–Malvinas Current During the Opening of the Drake Passage and Distribution of Sediments

Plate divergence since 18 Ma led to development of a gap in the North Scotia Ridge that today allows deep water of the Antarctic Circumpolar Current to cross out of the Scotia Sea and into the South Atlantic (Fig. 9) (Eagles 2016). Modern hydrographic observations suggest that most of the water flowing eastward along the sub-Antarctic Front, in the northern Drake Passage, loops northward to form the Malvinas Current heading toward the Argentine Basin (Piola and Matano 2001). Accordingly, an elongated mounded drift (VF3 in Fig. 7) is interpreted to indicate strengthening of bottom flow during the late Miocene/early Pliocene (Gruetzner

et al. 2012). Before the onset of these conditions, the 65–17 Ma seismic sequence in the Argentine Basin shows low bottom current activity, similar to an hemipelagic setting (Fig. 8) (Gruetznier et al. 2012).

It seems that the moment at which orogenic denudation, together with uplift in the retroarc, produced sediment bypass toward the offshore, coincided with the onset of the Southpolar Front–Malvinas Current circuit during the opening of a deep Drake Passage that helped distribute the sediments in the Argentinean continental shelf (Fig. 9).

Acknowledgements This work has been carried out with the financial support of grants projects Agencia PICT-2013-1291 and CONICET PIP 2014-2016 GI directed by M.C. Ghiglione, and the ECOS-SUD project A15U02 (Sue and Ghiglione). The authors are grateful to Parques Nacionales de Argentina for granting access to the study zone. Valuable discussions during fieldwork with José Cuitiño are greatly acknowledged.

References

- Arbe HA, Hechem JJ (1984) Estratigrafía y facies de depósitos marinos profundos del Cretácico Superior, Lago argentino, Provincia de Santa Cruz. IX Congreso Geológico Argentino (Bariloche). Actas 5:7–41
- Barbeau DL, Olivero E, Swanson-Hysell N, Zahid K, Murray K, Gehrels G (2009) Detrital-zircon geochronology of the eastern Magallanes foreland basin: Implications for Eocene kinematics of the northern Scotia Arc and Drake Passage. *Earth Planet Sci Lett* 20:23–45
- Baristean N, Ankyr Z, di Primio R, Rodríguez JF, Marchal D, Dominguez F (2012) Distribution of hydrocarbon leaky indicators in the Malvinas Basin, offshore Argentine continental margin. *Mar Geol* 332:56–74
- Baristean N, Ankyr Z, di Primio R, Rodríguez JF, Marchal D, Dominguez F (2013) New insights into the tectono-stratigraphic evolution of the Malvinas Basin, offshore of the southernmost Argentinean continental margin. *Tectonophysics* 604:280–295
- Barreda VD, Palazzesi L, Marenssi S (2009) Palynological record of the Paleogene Río Leona Formation (southernmost South America): stratigraphical and paleoenvironmental implications. *Rev Palaeobot Palynol* 151:22–33
- Biddle KT, Uliana MA, Mitchum RM, Fitzgerald MG, Wright RC (1986) The stratigraphy and structural evolution of the central and eastern Magallanes Basin, southern South America. In: Allen A, Homewood P (eds) *Foreland basins*. Blackwell Scientific Publications, London. *Int Assoc Sediment, Spec Publ* 8: 41–61
- Blisniuk PM, Stern LA, Chamberlain CP, Idleman B, Zeitler PK (2005) Climatic and ecologic changes during Miocene surface uplift in the Southern Patagonian Andes. *Earth Planet Sci Lett* 230:169–186
- Blisniuk PM, Stern LA, Chamberlain CP, Zeitler PK, Ramos VA, Sobel ER, Haschke M, Streckler MR, Warkus F (2006) Links between mountain uplift, climate, and surface processes in the Southern Patagonian Andes. *The Andes*. Springer, Berlin, pp 429–440
- Bourgeois J, Michaud F (2002) Comparison between the Chile and Mexico triple junction areas substantiates slab window development beneath northwestern Mexico during the past 12–10 Myr. *Earth Planet Sci Lett* 201:35–44
- Breitsprecher K, Thorkelson DJ (2008) Neogene kinematic history of Nazca–Antarctic–Phoenix slab windows beneath Patagonia and the Antarctic Peninsula. *Tectonophysics* 464:10–20
- Calderón M, Hervé F, Fuentes F, Fosdick JC, Sepúlveda F, Galaz G (2016) Tectonic evolution of Paleozoic and Mesozoic andean metamorphic complexes and the Rocas Verdes ophiolites in

- southern Patagonia. In: Ghiglione MC (ed) *Geodynamic Evolution of the Southernmost Andes*. Springer Earth System Sciences, pp 7–36
- Cande SC, Leslie RB (1986) Late Cenozoic tectonics of the southern Chile Trench. *J Geophys Res-Sol EA* 91(B1):471–496
- Cuitiño JI, Scasso RA (2010) Sedimentología y paleoambientes del Patagoniano y su transición a la Formación Santa Cruz al sur del Lago Argentino Patagonia Austral. *Rev Asoc Geol Argentina* 66:406–417
- Cuitiño JI, Pimentel MM, Ventura Santos R, Scasso RA (2012) High resolution isotopic ages for the early Miocene “Patagoniense” transgression in Southwest Patagonia: stratigraphic implications. *J S Am Earth Sci* 38:110–122
- Cuitiño JI, Ventura Santos R, Scasso RA (2013) Insights into the distribution of shallow marine/estuarine early Miocene oysters from Southwestern Patagonia: sedimentologic and stable isotope constraints. *Palaios* 28:583–598
- Cuitiño JI, Santos RV, Muruaga PJ, Scasso RA (2015) Estratigrafía de Sr y evolución sedimentaria de los depósitos marinos del Mioceno temprano en el antepaís del norte de la Cuenca Austral (o Magallanes), Argentina. *Andean Geol* 42(3):364–385
- Cunningham WD (1995) Orogenesis at the southern tip of the Americas: the structural evolution of the Cordillera Darwin metamorphic complex, southern Chile. *Tectonophysics* 244(4):197–229
- Dalziel IWD, De Wit MF, Palmer KF (1974) Fossil marginal basin in the southern Andes. *Nature* 250:291–294
- del Rio CJ, Griffin M, McArthur JM, Martinez S, Thirlwall MF (2013) Evidence for early Pliocene and late Miocene transgressions in southern Patagonia (Argentina): Sr-87/Sr-86 ages of the pectinid “Chlamys” actinodes (Sowerby). *J S Am Earth Sci* 47:220–229
- Diraision M, Cobbold PR, Gapais D, Rossello EA (1997) Magellan strait: part of a neogene rift system. *Geology* 25:703–706
- Diraision M, Cobbold PR, Gapais D, Rossello EA, Le Corre C (2000) Cenozoic crustal thickening, wrenching and rifting in the foothills of the Southernmost Andes. *Tectonophysics* 316:91–119
- Eagles G (2016) Tectonic reconstructions of the Southernmost Andes and the Scotia Sea during the opening of the Drake Passage. In: Ghiglione MC (ed) *Geodynamic Evolution of the Southernmost Andes*. Springer Earth System Sciences, pp 75–108
- Eagles G, Livermore RA, Fairhead JD, Morris P (2005) Tectonic evolution of the west Scotia Sea. *J Geophys Res-Sol EA* 110:1–19
- Feruglio E (1938) Relaciones estratigráficas entre el Patagoniano y el Santacruciano en la Patagonia Austral. *Rev Museo de La Plata, Geología* 4:129–159
- Feruglio E (1949) Descripción Geológica de la Patagonia. Dirección General de Yacimientos Petrolíferos Fiscales, Buenos Aires, p 334
- Fish P (2005) Frontier South, East Falkland basins reveal important exploration potential. *Oil Gas J* 103:34–40
- Flynn JJ, Novacek MJ, Dodson HE, Frassinetti D, McKenna M, Norell M, Sears K, Swisher C, Wyss A (2002) A new fossil mammal assemblage from the southern Chilean Andes: implications for geology, geochronology, and tectonics. *J S Am Earth Sci* 15:285–302
- Folguera A, Ramos VA (2002) Partición de la deformación durante el Neógeno en los Andes Patagónicos Septentrionales (37°–46°S). *Rev Soc Geol España* 15:81–93
- Forsythe R, Nelson E (1985) Geological manifestations of ridge collision: evidence from the Golfo de Penas-Taitao basin, southern Chile. *Tectonics* 4:477–495
- Fosdick JC, Grove M, Hourigan JK, Calderón M (2013) Retroarc deformation and exhumation near the end of the Andes, southern Patagonia. *Earth Planet Sci Lett* 361:504–517
- Galeazzi JS (1998) Structural and stratigraphic evolution of the Western Malvinas Basin, Argentina. *Am Assoc Petrol Geol Bull* 82:596–636
- Gallardo RE (2014) Seismic sequence stratigraphy of a foreland unit in the Magallanes-Austral Basin, Dorado Riquelme Block, Chile: implications for deep-marine reservoirs. *Lat Am J Sed Basin Anal* 21(1):49–64
- Ghiglione MC (2002) Diques clásticos asociados a deformación transcurrente en depósitos sinorogénicos del Mioceno inferior de la Cuenca Austral. *Rev Asoc Geol Argentina* 57:103–118

- Ghiglione MC (2003) Estructura y evolución tectónica del Cretácico-Terciario de la costa Atlántica de Tierra del Fuego. Unpublished PhD thesis, Facultad de Ciencias Exactas y Naturales, Universidad de Buenos Aires, p 150
- Ghiglione MC (2016) Orogenic growth of the Fuegian Andes (52–56°) and its relation with tectonics of the Scotia Arc. In: Folguera A, Naipauer M, Sagripanty L, Ghiglione MC, Orts D, Giambiagi LB (eds) Growth of the Southern Andes. Springer Earth System Sciences, pp 241–267
- Ghiglione MC, Cristallini E (2007) Have the Southernmost Andes been curved since Late Cretaceous time? An analog test for the Patagonian Orocline. *Geology* 35:13–16
- Ghiglione MC, Ramos VA (2005) Chronology of deformation in the Southernmost Andes of Tierra del Fuego. *Tectonophysics* 405:25–46
- Ghiglione MC, Ramos VA, Cristallini EO (2002) Estructura y estratos de crecimiento en la faja plegada y corrida de los Andes fueguinos. *Rev Geol Chile* 29:17–41
- Ghiglione MC, Yagupsky D, Ghidella M, Ramos VA (2008) Continental stretching preceding the opening of the drake passage: evidence from Tierra del Fuego. *Geology* 36:643–646
- Ghiglione MC, Suarez F, Ambrosio A, Da Poian G, Cristallini EO, Pizzio MF, Reinoso RM (2009) Structure and evolution of the Austral basin fold–thrust belt, Southern Patagonian Andes. *Rev Asoc Geol Argentina* 65:215–226
- Ghiglione MC, Quinteros J, Yagupsky D, Bonillo-Martínez P, Hlebszevtich J, Ramos VA, Vergani G, Figueroa D, Quesada S, Zapata T (2010) Structure and tectonic history of the foreland basins of southernmost South America. *J S Am Earth Sci* 29:262–277
- Ghiglione MC, Navarrete-Rodríguez AT, González Guillot M, Bujaleski G (2013) The opening of the Magellan Strait and its geodynamic implications. *Terra Nova* 25(1):13–20
- Ghiglione MC, Likerman J, Barberón V, Giambiagi L, Aguirre-Urreta MB, Suarez F (2014) Geodynamic context for the deposition of coarse-grained deep-water axial channel systems in the Patagonian Andes. *Basin Res* 26(6):726–745
- Ghiglione MC, Naipauer M, Sue C, Barberón V, Valencia V, Aguirre-Urreta MB, Ramos VA (2015) U-Pb zircon ages from the northern Austral basin and their correlation with the Early Cretaceous exhumation and volcanism of Patagonia. *Cretac Res* 55:116–128
- Ghiglione MC, Ramos V, Cuitiño J, Barberón V (2016) Growth of the Southern Patagonian Andes (46–53°S) and its relation with subduction processes. In: Folguera A, Naipauer M, Sagripanty L, Ghiglione MC, Orts D, Giambiagi LB (eds) Growth of the Southern Andes. Springer Earth System Sciences, pp 201–240
- Giacosa RE, Márquez MM (2002) El basamento paleozoico de la cordillera Patagónica. In Haller MJ (ed) *Geología y Recursos Naturales de Santa Cruz*, Relatorio XV Congreso Geológico Argentino, pp 45–55
- Giacosa R, Fracchia D, Heredia N (2012) Structure of the Southern Patagonian Andes at 49°S. *Geológica Acta* 10:265–282
- Gombosi DJ, Barbeau DL, Garver J (2009) New thermochronometric constraints on the rapid Paleogene exhumation of the Cordillera Darwin complex and related thrust sheets in the Fuegian Andes. *Terra Nova* 21:507–515
- Guillot MG (2016) Magmatic evolution of the Southernmost Andes and its relation with subduction processes. In: Ghiglione MC (ed) *Geodynamic Evolution of the Southernmost Andes*. Springer Earth System Sciences, pp 37–74
- González Guillot M, Escayola M, Acevedo R (2011) Calc-alkyline rear-arc magmatism in the Fuegian Andes: implications for the mid-Cretaceous tectonomagmatic evolution of southernmost South America. *J S Am Earth Sci* 31:1–16
- González Guillot M, Prezzi C, Acevedo RD, Escayola M (2012) A comparative study of two rear-arc plutons and implications for the Fuegian Andes tectonic evolution: mount Kranck Pluton and Jeu-Jepén Monzonite, Argentina. *J S Am Earth Sci* 38:71–88
- Gorring ML, Kyry SM, Zeitler PK, Ramos VA, Rubiolo D, Fernandez MI, Panza JL (1997) Neogene Patagonian plateau lavas: continental magmas associated with ridge collision at the Chile Triple Junction. *Tectonics* 16:1–17

- Gruetznier J, Uenzelmann-Neben G, Franke D (2012) Variations in sediment transport at the central Argentine continental margin during the Cenozoic. *Geoch Geophys Geosyst* 13(10): Q10003
- Gruetznier J, Uenzelmann-Neben G, Franke D, Arndt JE (2014) Slowdown of Circumpolar Deepwater flow during the Late Neogene: evidence from a mudwave field at the Argentine continental slope. *J Geophys Res Lett* 41:2070–2076
- Guillaume B, Martinod J, Husson L, Roddaz M, Riquelme R (2009) Neogene uplift of central eastern Patagonia: Dynamic response to active spreading ridge subduction? *Tectonics* 28(2)
- Guillaume B, Gautheron C, Simon-Labric T, Martinod J, Roddaz M, Douville E (2013) Dynamic topography control on Patagonian relief evolution as inferred from low temperature thermochronology. *Earth Planet Sci Lett* 364:157–167
- Haschke M, Sobel ER, Blisniuk P, Strecker MR, Warkus F (2006) Continental response to active ridge subduction. *Geophys Res Lett* 33:L15315
- Hernández-Molina FJ, Paterlini M, Violante R, Marshall P, de Isasi M, Somoza L, Rebesco M (2009) Contourite depositional system on the Argentine Slope: an exceptional record of the influence of Antarctic water masses. *Geology* 37:507–510
- Hernández-Molina FJ, Paterlini M, Somoza L, Violante R, Arecco MA, De Isasi M, Rebesco M, Uenzelmann-Neben G, Nebeng S, Marshall P (2010) Giant mounded drifts in the Argentine Continental Margin: origins, and global implications for the history of thermohaline circulation. *Mar Petrol Geol* 27:1508–1530
- Hervé F, Calderón M, Faúndez V (2008) The metamorphic complexes of the Patagonian and Fuegian Andes. *Geologica Acta* 6:43–53
- Hinz K, Neben S, Schreckenberger B, Roeser HA, Block M, de Souza KG, Meyer H (1999) The Argentine continental margin north of 48 S: sedimentary successions, volcanic activity during breakup. *Mar Petrol Geol* 16:1–25
- Isla FI, Angulo RJ (2015) Tectonic Processes along the South America Coastline Derived from Quaternary Marine Terraces. *J Coastal Res*
- Kohn MJ, Spear FS, Harrison TM, Dalziel IWD (1995) 40Ar/39Ar geochronology and P–T–t paths from the Cordillera Darwin metamorphic complex, Tierra del Fuego, Chile. *J Met Geol* 13:251–270
- Kraemer PE (1998) Structure of the Patagonian Andes: regional balanced cross section at 50°S. *Argentina Int Geol Rev* 40:896–915
- Kraemer PE (2003) Orogenic shortening and the origin of the Patagonian orocline (56 S Lat). *J S Am Earth Sci* 15:731–748
- Kraemer PE, Riccardi AC (1997) Estratigrafía de la región comprendida entre los lagos Argentino y Viedma (49°40–50°10 lat. S), Provincia de Santa Cruz. *Rev Asoc Geol Argentina* 52:333–360
- Lagabrielle Y, Suarez M, Rossello EA, Hérail G, Martinod J, Régnier M, De la Cruz R (2004) Neogene to Quaternary tectonic evolution of the Patagonian Andes at the latitude of the Chile Triple Junction. *Tectonophysics* 385:211–241
- Lagabrielle Y, Suárez M, Malavieille J, Morata D, Espinoza F, Maury RC, Bellon H (2007) Pliocene extensional tectonics in the Eastern Central Patagonian Cordillera: geochronological constraints and new field evidence. *Terra Nova* 19:413–424
- Lagabrielle Y, Goddérís Y, Donnadiou Y, Malavieille J, Suarez M (2009) The tectonic history of Drake Passage and its possible impacts on global climate. *Earth Planet Sci Lett* 279:197–211
- Likerman L, Burlando JF, Cristallini EO, Ghiglione MC (2013) Along-strike structural variations in the Southern Patagonian Andes: insights from physical modeling. *Tectonophysics* 590:106–120
- Livermore RA, Nankivell AP, Eagles G, Morris P (2005) Paleogene opening of Drake Passage. *Earth Planet Sci Lett* 236:459–470
- Lodolo E, Menichetti M, Bartole R, Ben-Avraham Z, Tassone A, Lippai H (2003) Magallanes-Fagnano continental transform fault (Tierra del Fuego, southern-most South America). *Tectonics* 22:1076

- Lodolo E, Donda F, Tassone A (2006) Western Scotia Sea margins: improved constraints on the opening of the Drake Passage. *J Geophys Res-Sol EA* 111(B6)
- Maffione M (2016) Kinematic evolution of the Southern Andean orogenic arc. In: Ghiglione MC (ed) *Geodynamic Evolution of the Southernmost Andes*. Springer Earth System Sciences, pp 173–200
- Maffione M, Speranza F, Faccenna C, Rossello E (2010) Paleomagnetic evidence for a pre-early Eocene (~50 Ma) bending of the Patagonian orocline (Tierra del Fuego, Argentina): paleogeographic and tectonic implications. *Earth Planet Sci Lett* 289:273–286
- Maffione M, Fernandez-Moreno C, Ghiglione M, Speranza F, van Hinsbergen DJJ, Lodolo E (2015) Constraints on deformation of the Southern Andes since the Cretaceous from anisotropy of magnetic susceptibility. *Tectonophysics* 665:236–250
- Malumián N (2002) El Terciario marino. Sus relaciones con el eustatismo. In: Haller MJ (ed) *Geología y Recursos naturales de Santa Cruz*. Asociación Geológica Argentina, Relatorio XV Congreso Geológico Argentino, pp 237–244
- Malumián N, Jannou G (2010) Los Andes Fueguinos: el registro micropaleontológico de los mayores acontecimientos paleoceanográficos australes del Campaniano al Mioceno. *Andean Geol* 37:345–374
- Malumián N, Nañez C (2011) The Late Cretaceous-Cenozoic transgressions in Patagonia and the Fuegian Andes: foraminifera, palaeoecology, and palaeogeography. *Biol J Linnean Soc* 103:269–288
- Malumián N, Olivero EB (2006) The Cabo Domingo Group, Tierra del Fuego: Biostratigraphy, paleoenvironments, and events of the marine Eocene-Miocene. *Rev Asoc Geol Argentina* 61:139–160
- Malumián N, Scarpa R (2005) Foraminíferos de la Formación Irigoyen, Neogeno, Tierra del Fuego, Argentina: su significado paleobiogeográfico. *Ameghiniana* 42:363–376
- Malumián N, Panza JL, Parisi C, Nañez C, Caramés A, Torre E (2000) Hoja Geológica 5172-III-Yacimiento Río Turbio, provincia Santa Cruz, 1:250.000. Servicio Geológico Minero Argentino, Boletín 247, p 108
- Marensi SA, Casadio S, Santillana S (2002) La Formación Man Aike al sur de El Calafate (Provincia de Santa Cruz) y su relación con la discordancia del Eoceno medio en la cuenca Austral. *Rev Asoc Geol Argentina* 57:341–344
- Marensi SA, Limarino CA, Tripaldi A, Net L (2005) Fluvial systems variations in the Rio Leona Formation: tectonic and eustatic controls on the Oligocene evolution of the Austral (Magallanes) Basin, southernmost Argentina. *J S Am Earth Sci* 19:359–372
- Marshall LG, Sempere T, Butler RF (1997) Chronostratigraphy of the mammal-bearing Paleocene of South America. *J S Am Earth Sci* 10:49–70
- Martínez OA, Kutschker A (2011) The ‘Rodados Patagónicos’ (Patagonian shingle formation) of Eastern Patagonia: environmental conditions of gravel sedimentation. *Biol J Linnean Soc* 103:336–345
- Martínez OA, Rabassa J, Coronato A (2009) Charles Darwin and the first scientific observations on the Patagonian shingle formation (Rodados Patagónicos). *Rev Asoc Geol Argentina* 64:90–100
- Mella PE (2001) Control Tectónico en la Evolución de la Cuenca de Antepais de Magallanes, XII Región, Chile. Unpubl. Memoria para optar al título de Geólogo, Facultad de Ciencias Químicas, Departamento Ciencias de la Tierra, Universidad de Concepción, Concepción, p 149
- Melnick D, Echtler HP (2006) Inversion of forearc basins in south-central Chile caused by rapid glacial age trench fill. *Geology* 34:709–712
- Mercer JH, Sutter JF (1982) Late Miocene—earliest Pliocene glaciation in southern Argentina: implications for global ice-sheet history. *Palaeogeog Palaeoclim Palaeoeco* 38:185–206
- Nelson EP (1982) Posttectonic uplift of the Cordillera Darwin orogenic core complex: evidence for fission track geochronology and closing temperature time relationships. *J Geol Soc London* 139:755–761

- Pankhurst RJ, Riley TR, Fanning CM, Kelley SP (2000) Episodic silicic volcanism in Patagonia and the Antarctic Peninsula: chronology of magmatism associated with the break-up of Gondwana. *J Petrology* 41:605–625
- Panza JL (2002) La cubierta detrítica del Cenozoico superior. In Haller MJ (ed) *Geología y Recursos Naturales de Santa Cruz, Relatorio XV Congreso Geológico Argentino*, pp 259–284
- Parras A, Griffin M, Feldmann R, Casadio S, Schweitzer C, Marensi S (2008) Correlation of marine beds based on Sr-and Ar-date determinations and faunal affinities across the Paleogene/Neogene boundary in southern Patagonia, Argentina. *J South Am Earth Sc* 26:204–216
- Parras A, Dix GR, Griffin M (2012) Sr-isotope chronostratigraphy of Paleogene-Neogene marine deposits: Austral Basin, southern Patagonia (Argentina). *J South Am Earth Sc* 37:122–135
- Pedoja K, Regard V, Husson L, Martinod J, Guillaume B, Fucks E, Iglesias M, Weill P (2011) Uplift of Quaternary shorelines in Eastern Patagonia: Darwin revisited. *Geomorphology* 127:121–142
- Perkins ME, Fleagle JG, Heizler MT, Nash B, Bown TM, Tauber A, Dozo MT (2012) Tephrochronology of the Miocene Santa Cruz and Pinturas Formations, Argentina. *Early Miocene Paleobiology in Patagonia: High-Latitude Paleocommunities of the Santa Cruz Formation, Vizcaíno, SF*, pp 23–40
- Piola AR, Matano RP (2001) Brazil and Falklands (Malvinas) currents. In: Steele JH, Thorpe SA, Turekian KK (eds) *Ocean currents: a derivative of the encyclopedia of ocean sciences*. Academic Press, New York, pp 35–43
- Ramos VA (1989) Andean foothills structures in Northern Magallanes Basin, Argentina. *Am Assoc Pet Geol Bull* 73:887–903
- Riccardi AC, Roller E (1980) Cordillera Patagónica Austral. In Turner JCM (ed) *Simposio de Geología Regional Argentina*, vol 2, pp 1173–1306
- Sachse VF, Stozkyk F, Ankyr Z, Rodriguez JF, Primio R (2015) The tectono-stratigraphic evolution of the Austral Basin and adjacent areas against the background of Andean tectonics, southern Argentina, South America. *Basin Res.* [10.1111/bre.12118](https://doi.org/10.1111/bre.12118)
- Scalabrino B, Lagabrielle Y, de la Rupelle A, Malavieille J, Polvé M, Espinoza F, Morata D, Suarez M (2009) Subduction of an active spreading ridge beneath southern South America: a review of the Cenozoic geological records from the Andean foreland, central Patagonia (46–47 S). *Subduction Zone Geodynamics*. Springer, Berlin, pp 227–246
- Scasso RA, McArthur JM, Del Rio CJ, Martínez S, Thirlwall MF (2001) 87 Sr/86 Sr Late Miocene age of fossil molluscs in the 'Entrerriense' of the Valdés Peninsula (Chubut, Argentina). *J South Am Earth Sci* 14:319–329
- Sue C, Ghiglione MC (2016) Wrenching tectonism in the Southernmost Andes and the Scotia Sea Constrained from Fault Kinematic and Seismotectonic Overviews. In: Ghiglione MC (ed) *Geodynamic Evolution of the Southernmost Andes*. Springer Earth System Sciences, pp 137–171
- Thomas T, Livermore RA, Pollitz F (2003) Motion of the Scotia Sea plates. *Geophys J Int* 155:789–804
- Thomson SN (2002) Late Cenozoic geomorphic and tectonic evolution of the Patagonian Andes between latitudes 42° and 46°S: an appraisal based on fission-track results from the transpressional intra-arc Liquine-Ofqui fault zone. *Geol Soc Am Bull* 114:1159–1173
- Thomson SN, Herve F, Stockhert B (2001) The Mesozoic-Cenozoic denudation history of the Patagonian Andes (southern Chile) and its correlation to different subduction processes. *Tectonics* 20:693–711
- Thomson SN, Brandon MT, Reiners PW, Tomkin JH, Vásquez C, Wilson NJ (2010) Glaciation as a destructive and constructive control on mountain building. *Nature* 467:313–317
- Ton-That T, Singer B, Mörner NA, Rabassa J (1999) Datación de lavas basálticas por 40 Ar/39 Ar y geología glacial de la región del lago Buenos Aires, Provincia de Santa Cruz, Argentina. *Rev Asoc Geol Argentina* 54:333–352

- Uliana VMA, Biddle KT, Cerdan J (1989) Mesozoic extension and the formation of Argentine sedimentary basins. In: Tankyrrd AJ, Balkwill HR (eds) Extensional tectonics and stratigraphy of the North Atlantic Margins. Am Assoc Pet Geol Bull, Memoirs 46:599–613
- Wilson TJ (1991) Transition from back-arc to foreland basin development in the Southernmost Andes: stratigraphic record from the Ultima Esperanza District, Chile. Geol Soc Am Bull 103:98–111

Wrenching Tectonism in the Southernmost Andes and the Scotia Sea Constrained from Fault Kinematic and Seismotectonic Overviews

Christian Sue and Matías C. Ghiglione

Abstract The geodynamics of the study area includes subduction, orogen dynamics, and major transcurrent tectonics at a complex transform margin in the southern ocean. We present a synthesis of the fault system associated to major fault zones in the Fuegian Andes and the Scotia Sea and review the available kinematic databases from microtectonic measurements. Our synthesis of six independent fault kinematic studies is coherent with a very consistent shortening direction-oriented NE–SW in the Southernmost Andes. The stability of the stress pattern and orientation of the shortening axes on a more regional scale involving the Scotia Sea indicate a steady E–W to NNE–SSW σ_1 /shortening direction since middle Eocene times. This observations reflect that the global left-lateral motion between Antarctica–Scotia–South America plates circuit is the main driving force for the entire area and in particular for the Southernmost Andes, over the last ~ 45 Ma. Both the observed short-term geodetic and the long-term geological slip rates of the Magallanes–Fagnano fault system from Tierra del Fuego are moderate (~ 5 mm/year), and the expected time span between major M8 earthquakes would be around 10 kyr. Yet the time between the two most recent large earthquakes was about 70 years. Such a great discrepancy suggests a complex mechanics on the Magallanes–Fagnano fault system, leading to complex recurrence time history for the characteristic earthquake ($M \geq 7$).

Keywords Fuegian andes · Scotia plate · Fault kinematic · Seismotectonics · Wrenching · Magallanes–Fagnano fault system · North scotia ridge

C. Sue (✉)

Bourgogne Franche-Comté University, Laboratoire Chrono-environnement, Besançon, France

e-mail: christian.sue@univ-fcomte.fr

M.C. Ghiglione

Departamento de Ciencias Geológicas, Instituto de Estudios Andinos “Don Pablo Groeber” CONICET, FCEN—Universidad de Buenos Aires, Buenos Aires, Argentina

1 Introduction

Since the very first expedition in Tierra del Fuego and southern Patagonia, a mythic end-of-the-world in our collective unconscious (Fig. 1a) (Darwin 1845, 1846), a growing number of scientific and more specifically geoscientific researches have been led in this fascinating region from the twentieth century onward. Given the local geography, a lot of these studies approached their topic by sea, despite the rough weather conditions in this part of the world leading to navigation comparable to the drunken boat of Rimbaud (1871). Beyond its formal beauty (Fig. 2), the geodynamic complexity of the connection between the Southernmost Andes and the Scotia plate, through the Magallanes–Fagnano fault system (MFF) and the North Scotia Ridge (NSR), demands for proper geodynamic models. They concern the evolution of the overall system from 200 Ma onward (e.g., V erard et al. 2012; Eagles et al. 2005), the development of the Southernmost Andes’ orogenic arc (e.g., Ghiglione and Cristallini 2007; Maffione et al. 2010, 2015; see Maffione 2016 for a review) and related crustal rotations, the matters of triple junction between the major plates and plate boundaries, the dislocation in continental blocks of the southern tip of the South American plate along the NSR (Eagles 2016), and the concomitant opening of the Drake passage and Magallanes Strait (e.g., Ghiglione et al. 2013), which had serious implications in terms of global climatology (e.g., Livermore et al. 2004; Lagabrielle et al. 2009). Indeed, these questions are addressed as a whole in the present book. In this chapter, we focus on the most recent and current deformation of the region, including a synthesis on the fault

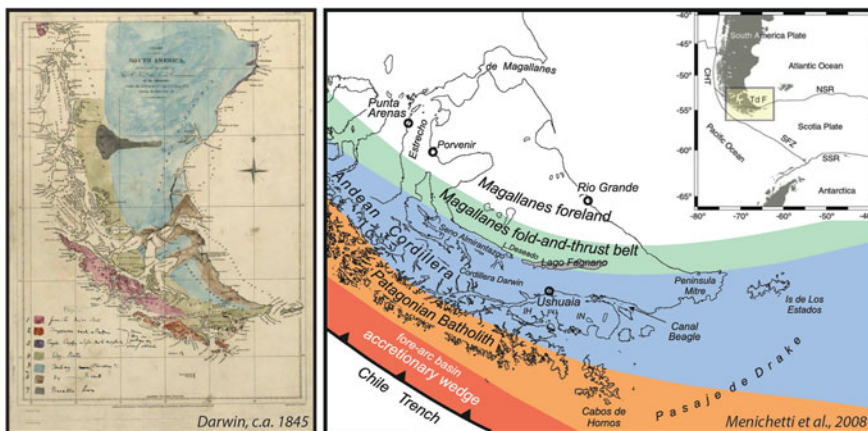


Fig. 1 *Left* Very first geological map of Patagonia and Tierra del Fuego drafted by Darwin (1845, 1846). *Right* Tectonostratigraphic provinces in the Southernmost Andes (modified from Menichetti et al. 2008)

system carving the area, together with a critical review of the available kinematic and microtectonic data, an overview of the seismicity and paleoseismicity leading to current fault mechanism and actual seismic deformation, which then could be compared to geodetically related deformation observed by GPS.

The geodynamics of the study area between 50°S–57°S and 55°W–75°W (Fig. 2) includes subduction, orogen and orogenic arc dynamics, and major transcurrent tectonism at a complex transform margin. The complexity of this system rises up from the variety of geodynamic processes still ongoing. Indeed, the main one is related to the left-lateral movement between the South America and Scotia plates (e.g., Pelayo and Wiens 1989).

The Andes is one of the longest orogenic belts on earth. They run N–S linearly from 18°S to 50°S over almost 4000 km and abruptly turn to E–W direction in the so-called Patagonian orocline between 50°S and 56°S. The transform plate limit south of the system acted and still acts as first-order tectonic feature in the area and is probably at least partly linked to the bending of the Southernmost Andes (e.g., Cunningham 1993; Ghigliione et al. 2010; Maffione 2016).

In this chapter, we will firstly present a synthesis of the fault system associated with the MFF, both from geometric and kinematic viewpoints. Then, we will review the available kinematic databases from microtectonic measurements and present a comprehensive model. Neotectonic observations on this fault system will then allow opening on the current tectonics.

Indeed, along the MFF and satellite faults, evidence of active left-lateral movement is described in response to the ongoing westward motion of Scotia plate relative to South America (Perucca et al. 2015). The overall area undergoes a diffuse and moderate seismicity (Febrer et al. 2000). Nevertheless, paleoseismological observation established the occurrence of large earthquakes along this fault system (e.g., Pedrera et al. 2014; Perucca et al. 2015), and major earthquakes stroke the area during the last century. The strongest sequence happened in the seventeenth of December 1949 (Forsyth 1975; Jaschek et al. 1982; Pelayo and Wiens 1989).

The overall MFF–NSR left-lateral strike-slip fault is actually quite active and also produced the recent M7.0 strike-slip earthquake, southeast of the Malvinas Island on November 25, 2013 (Fig. 3). It is clear that this fault system remains a source of actual seismic risk, as it may produce major events close to quite large cities such as Ushuaia, Rio Grande, or Punta Arenas. In terms of a geodetic approach, some recent works quantificate the current deformation (Smalley et al. 2003, 2007; Mendoza et al. 2011). They led to an estimation of the relative left-lateral velocity of about 4–6 mm/year between Scotia and South America plates, coherently with the focal mechanisms of the earthquakes in the region, and with structural studies. In this framework, we present hereafter a new synthesis of brittle deformation, fault kinematics and related seismicity, and deformation pattern in the Southernmost Andes and surrounding southern oceans.

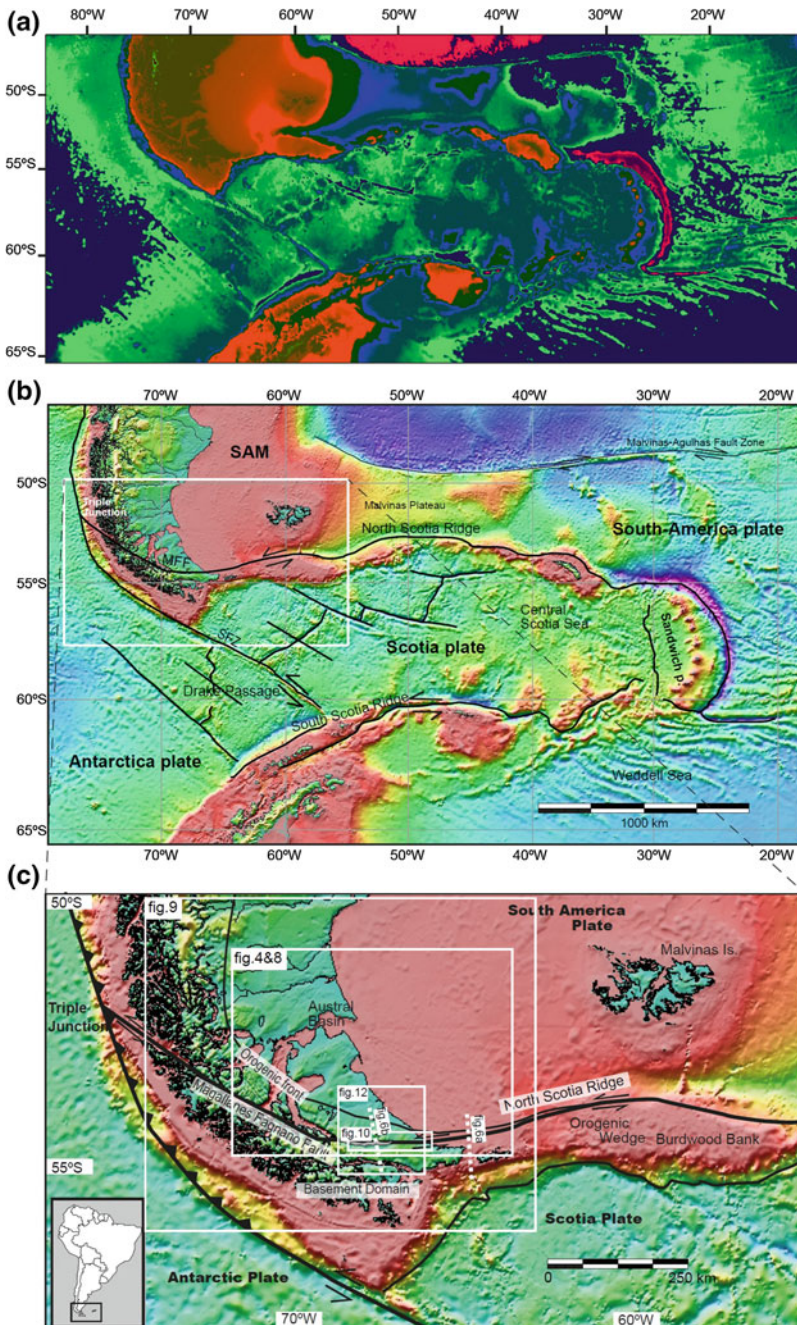


Fig. 2 a Morphological settings of the overall Scotia area (data from ETOPO1). b Major tectonic features enclosing the Scotia Sea region, c Location of main morphostructural units and location of figures in the following of this chapter. *MFF* Magallanes–Fagnano fault system; *SFZ* Shakleton fault zone

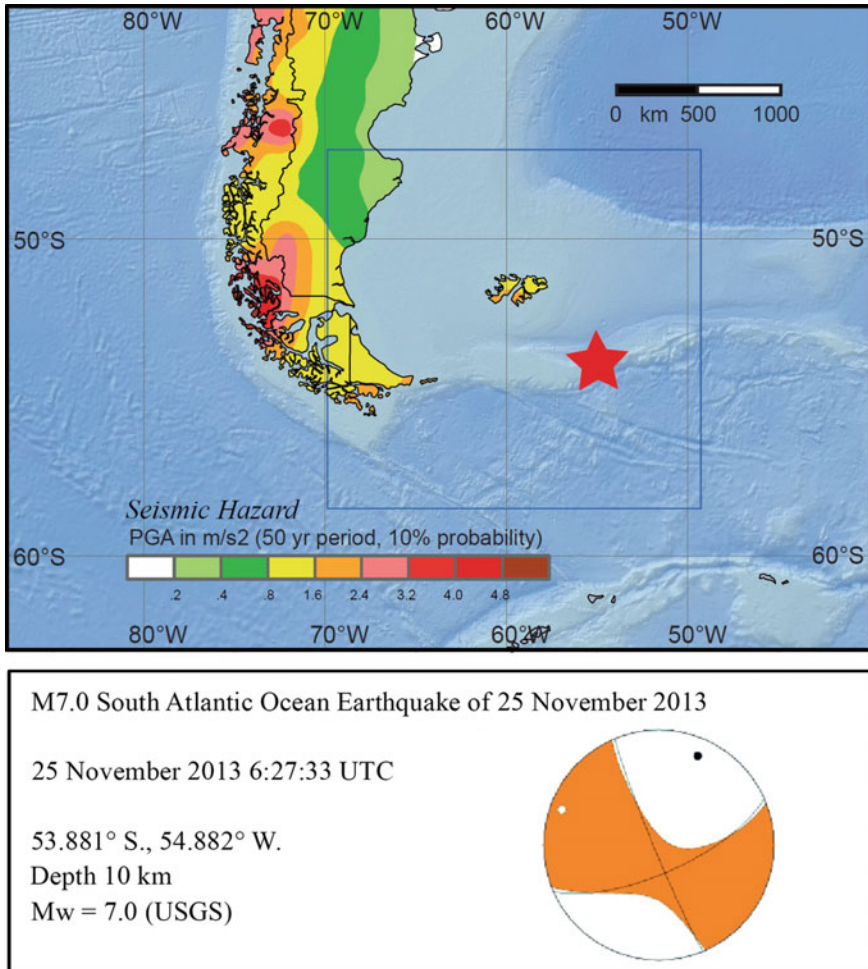


Fig. 3 Location of the November 25, 2013, M7.0 South Atlantic Earthquake (*red star*) together with the focal solution and the onshore seismic hazard map (from USGS Web site <http://earthquake.usgs.gov/>)

2 Brittle Deformation in the Southernmost Andes

2.1 Geodynamic Setting and Fault Systems

At continental scale, three main fault systems shape the study area (Fig. 2a, b) (see Eagles 2016 for a review on the geometry and evolution of this plate tectonic configuration): (i) the Chile trench to the west, which evolves southeastward into the Shackleton fracture zone, and the boundary between the South America and Scotia plates composed of (ii) the North Scotia Ridge (NSR) offshore to the east,

which evolves into (iii) the continental Magallanes–Fagnano fault system (MFF), cutting through the Tierra del Fuego Island and its surroundings (Fig. 4).

In the studied region South of 50°S, the Pacific trench corresponds to the subduction of the Antarctica plate underneath South America (Fig. 2c), with a relative velocity of about 20 mm/year (Barker 2001). Therefore, intersection of the MFF with the Chile trench conforms a triple junction (Fig. 2c), defining one of the major boundaries of the overall study area. Southeastward of the active subduction, the geometry and kinematics of the plate boundary lead to a transcurrent motion: the Shackleton fracture zone, which forms the boundary between the Antarctica and Scotia plates in the Drake Passage (Fig. 2b) (Livermore et al. 2004). The SFZ is a left-lateral transform boundary with relative velocities of about 8 mm/year (Thomas et al. 2003), active since the formation of the Scotia plate at approximately 50 Ma (Eagles 2016).

The NSR bounding the Scotia and the South American plates is moving at a rate of about 7 mm/year (Thomas et al. 2003). It is a major left-lateral fault, which produced the recent Mw 7.0 Malvinas Island earthquake (November 25, 2013, Fig. 3). It is marked by an offshore system of shallow banks and ridges, which corresponds to continental dislocated blocks. It extends about 2000 km from the Tierra del Fuego's tip (Isla de los Estados) to South Georgia Island, in a slightly arcuated overall W–E linear shape (Fig. 2b) (Ludwig and Rabinowitz 1982). Northward, the Malvinas Trough, a Cenozoic foreland basin (Ghiglione et al. 2010), separates the North Scotia Ridge from the Malvinas Plateau on the South America plate. The NSR worked as a transpressional system with accretionary complex (Ludwig and Rabinowitz 1982) and a strong left-lateral component; although in its western segment toward the onshore, it has an overall transtensional component (Lodolo et al. 2003). The general evolution of the NSR is coeval with the development of the west Scotia Sea domain (Barker 2001; Thomas et al. 2003; Eagles et al. 2005). The lithologies observed along the NSR are those of Mesozoic South America rocks (Macfadyen 1933; Tyrrell 1945; Dalziel et al. 1975), which allow connecting these blocks with the Fuegian Andes. Actually, the transpressional deformation is well described up to the South Georgia Island, both in ductile and in brittle domains, and related to the mid-Cretaceous Andean tectonic phase (Curtis et al. 2010). Thus, the left-lateral component of the deformation appears as a very steady tectonic feature all along the development of the NSR domain in space and time. The cumulative deformation may reach 1500 km of transcurrent movement along the NSR (Cunningham 1993).

The western tip of the NSR connects with the MFF (e.g., Kranck 1932; Winslow 1982; Dalziel and Brown 1989), a unique onshore transform plate boundary in the world (Fuenzalida 1972, 1976; Lodolo et al. 2003). This left-lateral fault crosscuts the Tierra del Fuego Island, from the eastern tip of the continent to the Chile subduction trench, along a ~600-km-long lineament well visible on every remote sensing images (Fig. 4). Nevertheless, the exact path followed by the MFF from the Chile trench to the west toward the NSR to the east remains unclear (Lodolo et al. 2003). It follows part of the western Magallanes Strait and runs through the south of the Dawson Island, and through the Lago Fagnano to the Irigoyen river valley

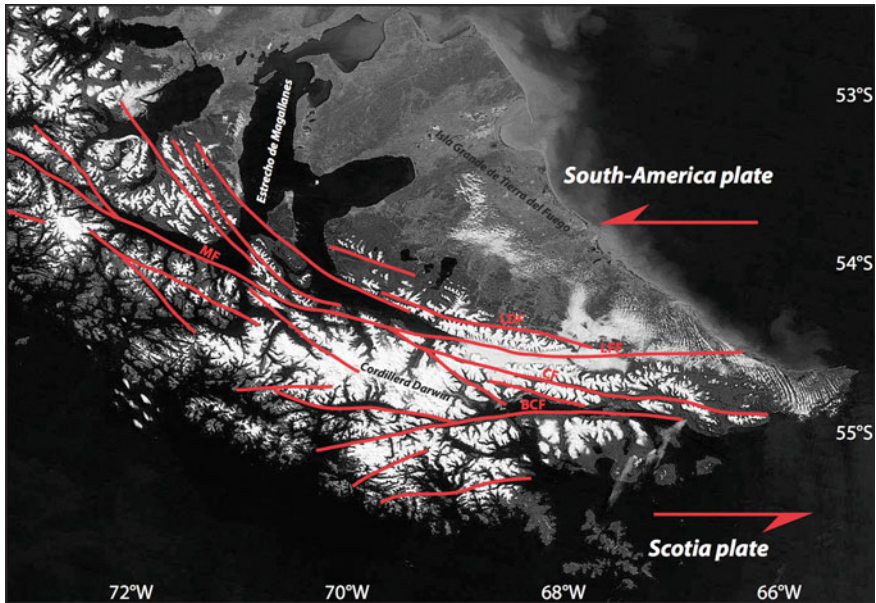


Fig. 4 Overall fault system corresponding to the Magallanes–Fagnano continental strike-slip plate boundary and related individual strike-slip faults. *BCF* Canal Beagle fault; *CF* Carbajal valley fault zone; *LFF* Fagnano fault (Eastern part of the MFF system); *LDF* Lago Deseado fault; *MF* Magallanes fault (Western part of the MFF system)

toward the Atlantic coast (Ghiglione 2002). Actually, most authors agree that left-lateral strike-slip deformations along the MFF system are active since the Oligocene (e.g., Ghiglione 2002; Lodolo et al. 2003; Menichetti et al. 2008).

The strong morphological expression, the size of the linear structure, and the connection with the NSR, together with signs of recent activity (Fuenzalida 1972; Winslow 1982; Lodolo et al. 2002, 2003; Ghiglione et al. 2013), support the interpretation of the MFF as the actual plate boundary between the continental crust of the Scotia and South America plates (Fuenzalida 1972; Cunningham et al. 1995; Eagles et al. 2005; Galindo-Zaldívar et al. 2006). Indeed, it accommodates the current left-lateral relative movement between the two plates (Pelayo and Wiens 1989), with some transtensive component affecting the Fuegian Andes (Ghiglione 2002; Lodolo et al. 2003). The left-lateral movement on the MFF is ongoing for at least 30 Myr (Cunningham et al. 1995; Ghiglione 2002) and developed in close relation to the Scotia plate oceanic floor opening (Barker and Burrell 1977; Eagles et al. 2005) and to the Shackleton fracture zone (Fig. 2b). Sinistral deformation along the MFF could have increase after the end of western Scotia's seafloor opening (~9 Myr, Eagles et al. 2005). Prior to the Scotia's history, strike-slip deformation has been suggested along the Canal Beagle fault zone since Late Cretaceous time, implying reactivation of inherited basement structures (Klepeis and Austin 1997; Grunow et al. 1992; Cunningham et al. 1995).

The quantification of the transcurrent deformation along the whole MFF system still remains a matter of debate. The displacement along the main MFF fault could reach up to a 55 km (Rossello 2005) or 80 km offset (Cunningham 1993; Lodolo et al. 2003), and satellite faults connected on the same system also exhibit large left-lateral displacements (e.g., 25 km for the north segment in the Deseado fault zone, Klepeis 1994). The overall displacement along the MMF system may reach ~ 100 km, but still remains much lower than the 1500 km proposed for the NSR (Cunningham 1993 and references herein). For a fault system active since ~ 30 Ma (Ghiglione 2002; Eagles 2016), that means low slip rates of around ~ 2.5 mm/year.

The present-day GPS-measured deformation also shows a slow slip rate of ~ 5 mm/year (Del Cogliano et al. 2000; Mendoza et al. 2011), while the movement across the MFF system as a whole reaches rates as high as 6.6–9.6 mm/year (Smalley et al. 2003; DeMets et al. 2010).

Beyond the major morphological expression of the 600-km-long lineament of its main branch, the MFF is made of several tectonic structures segmented in a wide system of subvertical faults. Kinematic indicators show left-lateral movement along major faults running from the front of the Magallanes fold and thrust belt to the north, to the Canal Beagle and the Navarino Island to the south (Fig. 4). In the Isla Grande de Tierra del Fuego, it comprises in particular the MFF itself running along the Magallanes Strait–Seno Almirantazgo–Lago Fagnano–Irigoyen river (Ghiglione 2002, 2003; Lodolo et al. 2003), the Deseado fault to the north (Winslow 1982), the Canal Beagle fault to the south (Cunningham 1993), and the Carbajal fault in between (Figs. 4 and 5) (Caminos et al. 1981).

The Lago Deseado fault is a linear structure about 100 km long, marked by a wide zone of fault breccias, which follows a steep valley across the external Magallanes fold and thrust belt (Klepeis 1994). Kinematic analysis of mesoscale faults measured in this area indicates a major left-lateral movement, with some extensional component, within the same overall tectonic scheme as the MFF. Sag ponds along the fault with clear neotectonic lineaments suggest that it could have been active during Quaternary times (Winslow 1982).

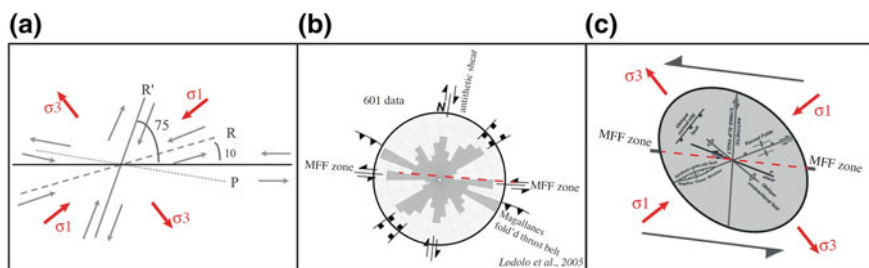


Fig. 5 **a** Theoretical Riedel fault system and its corresponding principal stress direction orientation, **b** Rose diagram summarizing the azimuth and length distribution of 601 lineaments identified in satellite images from Tierra del Fuego, and their tectonic interpretation. **c** Geometric relation of faults and folds to left-lateral wrench fault combined schematically with a strain ellipse and their equivalent principal stress directions. Modified from Lodolo et al. (2003)

The Carbajal fault is a ~100-km-long linear structure, which seems to connect the MFF with the Canal Beagle fault (Fig. 4). It strikes very slightly oblique on the MFF direction and is marked by a wide valley carved in the Central Cordillera. Left-lateral movement is also documented along strike-slip faults that cut through the fold and thrust belt (Caminos et al. 1981).

The Canal Beagle fault is a former extensional detachment, which constitutes an important tectonic and metamorphic discontinuity in the Fuegian Andes linked to the Andean orogenesis (e.g., Darwin 1846; Dalziel and Brown 1989). Strike-slip faulting plays an important role in the tectonic history of this fault, both in ductile and brittle conditions, probably from the Cretaceous onward (Cunningham 1993). It has evolved toward a left-lateral brittle strike-slip branched into MFF system as a whole. The most recent movements of this fault linked to the development of the MFF probably occurred in brittle conditions and were favored by inherited structures. Kinematic indicators in this area are numerous mesoscale left-lateral faults and en-échelon Riedel structures at mesoscale and regional scale (Cunningham 1993).

These main faults in Tierra del Fuego (MFF, Canal Beagle, Carbajal, and Deseado) have been carefully analyzed from a structural viewpoint, and fault kinematic data are available in their vicinities (Cunningham 1993; Klepeis 1994; Diraison et al. 2000; Lodolo et al. 2003; Menichetti et al. 2008; see below for an overview of microtectonic data). Associated to these main faults, the whole Tierra del Fuego presents a set of lineaments that could be related to the overall faulting. Indeed, Lodolo et al. (2002) proposed a map of 601 lineaments analyzed using remote sensing images (SPOT and SAR satellites). The 2-D statistics of these lineaments (Fig. 5) (Lodolo et al. 2002, 2003) provides a straight interpretation of the whole system as a large-scale Riedel system perfectly coherent with the main transcurrent kinematics rising up from direct fault analysis, i.e., with NE–SW-oriented shortening axis, and NW–SE-oriented extensional axis. The left-lateral crustal wrenching is thus responsible for both the main morphotectonic features, directly related to major faults, and for most of the incipient morphologic markers of the area, which suggest its very recent activity.

Along the main branch of the overall fault system, and specially in the Lago Fagnano's vicinity, several geological and geophysical campaigns (bathymetry, seismic profiles, gravimetry) have been achieved to constrain the morphology, geometry, kinematics, and timing of the brittle deformation by Lodolo and collaborators (e.g., Lodolo et al. 2002, 2003; Tassone et al. 2008; Menichetti et al. 2008 and references therein). They pointed out in particular the asymmetric pull-apart geometry of the Lago Fagnano, which is also observed along most of the MFF system in seismic profiles (Fig. 6). The lake itself is interpreted as a large pull-apart basin (Lodolo et al. 2003). The Fig. 6 shows an overview of crustal cross sections across the MFF system (from Tassone et al. 2008; Menichetti et al. 2008) and underlines the transtensional behavior of the whole system, with several negative flower-like structures, which suggest coeval strike-slip and extensional components of the deformation. Actually, the deformation history of the area is quite complex, with first shortening phases (Late Cretaceous), predating the

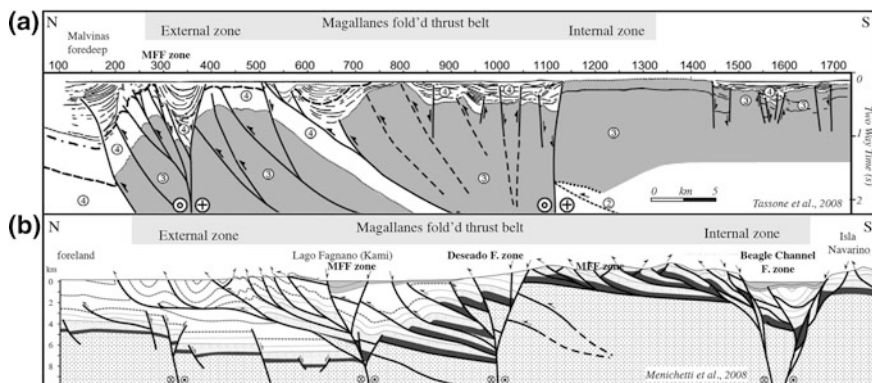


Fig. 6 Overview of crustal cross sections across the MFF system from **a** Tassone et al. (2008) and **b** Menichetti et al. (2008). See section's traces on Fig. 2

evolution of the MFF system toward a crustal wrenching, with an extensional component, potentially during Miocene times (Ghiglione 2002).

This scenario would imply potential reactivation of compressional structures in transpressive ones. Note that the extensional component is also locally observed on the field by kinematic indicators (see below, Sect. 2.2). In terms of geodynamic interpretation, the extensional part of the overall transcurrent deformation could be associated with rotational movement of Scotia plate with respect to South America.

2.2 Kinematic Indicators and Paleostrain/Stress Determination

Complementary to morphotectonic analyses and field mapping of fault systems, the systematic and statistical analysis of brittle deformation measured on the field at meso-/microscale allows quantifying the corresponding kinematic axes, namely either strain or stress axes, depending on the methodological and theoretical backgrounds. In terms of methodology, fault slickenside analysis is based on the Wallace and Bott principle (Wallace 1951; Bott 1959), which has long been discussed and still remains a matter of debate concerning stress/strain relations (e.g., Angelier and Mechler 1977; Angelier and Goguel 1979; Angelier 1990; Gephart 1990; Twiss and Unruh 1998; Yamaji 2000, 2003, 2006; Lacombe 2012 and references herein). Regardless of whether the stress or kinematic hypothesis is assumed, this principle states that fault slip parallels the direction of maximum resolved shear stress (on the considered plane) of the local spatially homogeneous stress tensor. Basic assumptions for its application are the following: (i) The rock volume should be isotropic and homogeneous; (ii) displacements on faults should be incremental and faults should slip independently; (iii) the stress/strain field

should be uniform and steady during a given tectonic phase; (iv) the deformation is non-rotational; and (v) no post-faulting reorientation of the fault-slip data has occurred. In practice, the direction of movement is given by slickensides, striae, and grooves on the fault plane. The sense of movement is generally given by calcareous fibers, drag folds, steps impressed in the plane by striator objects, and Riedel criteria (Riedel 1929), among other less common indicators. Although the related methods have proved their robustness in many areas and various tectonic contexts (e.g., Sue and Tricart 2002, 2003; Champagnac et al. 2003; Sue et al. 2014), fault-slip data may depart from these basic assumptions, mainly because of strong local deformation and stress variations due to preexisting anisotropies and inherent rock heterogeneities (see for instance Homberg 2000).

The long-lasting discussions brought by these methods concerning strain versus stress are beyond the scope of this paper. A critical discussion on this point has been recently published by Lacombe (2012). We refer to this paper and references herein for further precisions. Several methods are available for fault kinematic quantification. We can quote for instance a non-exhaustive list: the geometrical right dihedral method (RD, Angelier and Mechler 1977; Pfiffner and Burkhard 1987), the pressure–tension method (PBT), the numerical dynamic analysis (NDA), the direct inversion Angelier’s method (INVD, Angelier 1990) (all implemented in the TectonicsFP software from Sperner et al. 1993), the XYZ method (Marrett and Allmendinger 1990), the Etchecopar’s method (Etchecopar et al. 1981), and the Yamaji’s method (Yamaji et al. 2006), among others.

In the study area, several fault kinematic analyses have been achieved with various methods during the last 20 years. We synthesize hereafter the data provided by Cunningham (1993) in the Canal Beagle area, Klepeis (1994) along the Deseado fault, Klepeis and Austin (1997) in the Seno Almirantazgo fiord, Diraison et al. (2000) in the Magallanes fold and thrust belt, and Menichetti et al. (2008) and Branellec (2010) in the Lago Fagnano–Carbajal valley–Beagle channel area. Although these papers do not use all the same theoretical background, all of them present mesoscale to microscale fault-striae measurements.

We made a global synthesis of these data, in terms of kinematic axes, that is to say main strain/stress axes. Figure 7 shows an overview of the data published by these authors. We refer to each specific paper for a more precise discussion on fault measurement.

Cunningham (1993) studied the ductile and brittle kinematic of the Canal Beagle faults (corresponding to the SW and NW arms of the channel) (Fig. 4). This author measured about 400 single faults and reported them following their kinematics and orientation (Fig. 7a). The offsets range from millimeters to kilometers. The measured faults can be divided into two families: left-lateral faults oriented N45E to N135E and right-lateral faults oriented N30W to N35E. These two families correspond to conjugated fault system kinematically compatible. Although a proper inversion or geometrical reconstruction of the kinematic axes was not performed, an overall shortening axis-oriented N40E (red arrows in Fig. 7a), and a corresponding N130E-oriented extensional axis, is coherent with Cunningham (1993)’s data.

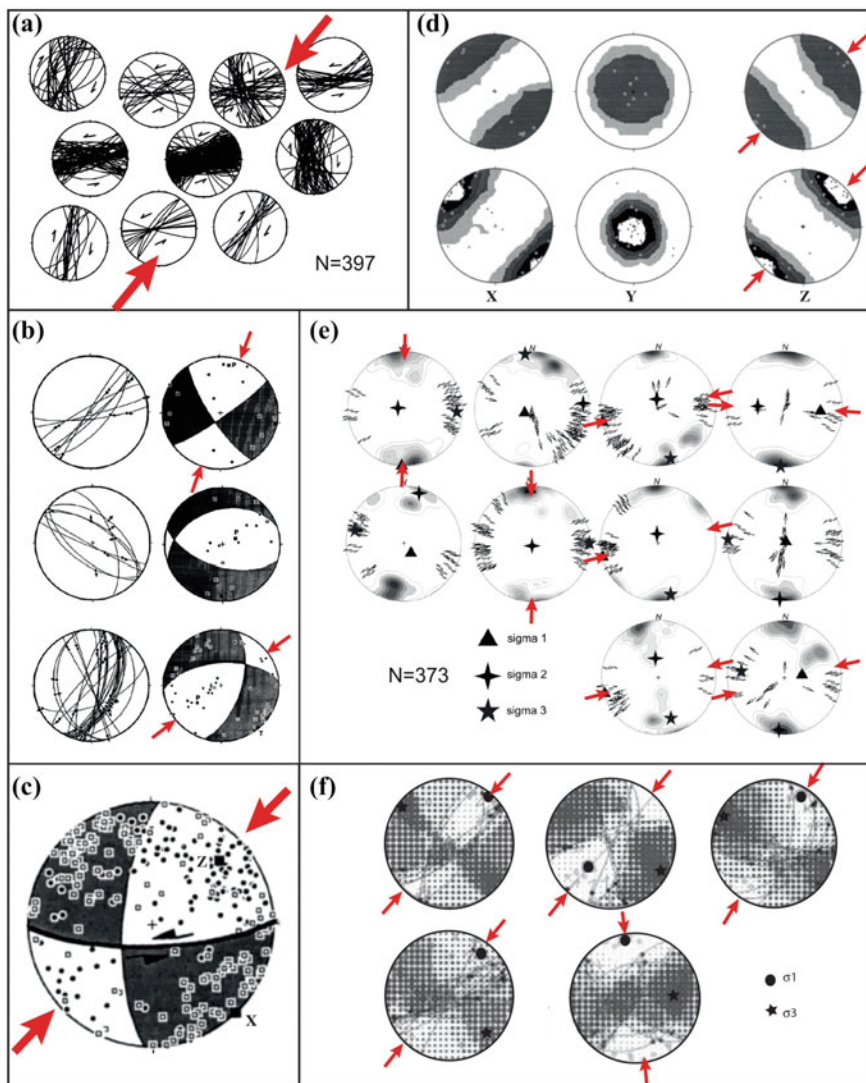


Fig. 7 Fault kinematic analyses achieved with various methods in the study area. *Red arrows* show the orientations of compressional stress axis σ_1 . Data are from: **a** Cunningham (1993) in the Canal Beagle area. **b** Klepeis (1994) along the Deseado fault. **c** Klepeis and Austin (1997) in the Seno Almirantazgo fiord. **d** Diraison et al. (2000) in the Magallanes fold and thrust belt and foreland and in the Lago Fagnano's vicinity. **e** Menichetti et al. (2008) in the Fagnano–Carbajal–Beagle area. **f** Branellec (2010) along the Lago Fagnano and Yehuín lakes shores

Klepeis (1994) investigated the Deseado fault zone, describing a major left-lateral system, with typical Riedel shear geometry, made of a set of late faults, cutting compressional structures. The fault measurements were subdivided into

three families: (i) left-lateral faults oriented $\sim N75E$ and interpreted as R shear planes, (ii) a left-lateral fault family oriented $N125E$, corresponding to P shear planes, and (iii) a right-lateral fault family oriented $N20E$ and interpreted as R' shear planes. The respective kinematics of these three families is represented in Fig. 7b, using the Marrett and Allmendinger's method (1990) method. As in Cunningham (1993), the fault was divided by sense of movement and orientation. The R family exhibits almost pure strike-slip movement, whereas the R' and P families show an oblique normal transcurrent component (Fig. 7b). In consequence, the Deseado fault zone seems to accommodate a transtensional overall deformation in brittle conditions. Indeed, the three kinematics (fault plane solutions) are compatible with a main shortening axis oriented in the $\sim N40^{\circ}E$ direction, and an extensional axis in the $\sim N130$ direction, and are largely comparable in direction with the results obtained by Cunningham (1993) to the south.

Klepeis and Austin (1997) applied the same approach and the method of Marrett and Allmendinger (1990), to the region of Seno Almirantazgo as Klepeis (1994) did on the Deseado fault. The Seno Almirantazgo area belongs to the central part of the MFF system, just east of the Deseado fault (Fig. 4). Indeed, a similar relation between three fault families in terms of a Riedel shear scheme was suggested. Beyond surface mapping showing that the transtensional deformation overprints the former compressional deformation along the MFF (Winslow 1982; Klepeis 1994), they constrained the corresponding strain axes. For the last transtensional phase, they computed an average kinematic solution using 136 measurements for the whole area (Fig. 7c), which exhibits an outstanding strike-slip solution, with a minor extensional component. A main left-lateral plane E–W-oriented symbolizes the orientation of the MMF in the area. It is related to a $N45^{\circ}E$ z-axis (shortening) associated with a $N135^{\circ}E$ -oriented x-axis (extension). Indeed, this kinematic solution provides a proper view to sum up the regional tectonics controlled by the transtensional deformation along the entire MFF system.

Diraison et al. (2000) led a widespread tectonic analysis in the Patagonian and Fuegian Andes on minor faults of Cenozoic age, mainly in the foothills of the belt. These authors reported that shortening directions vary in trend, from ENE in the Patagonian foothills with dominant thrusting (following the results of Coutand et al. 1999), to NE in the Fuegian cordillera, where wrenching is dominant. In the following, we will restrict our synthesis to the southern part of their work (named regions 3 and 4 in Diraison et al. 2000). They used the geometrical method of the right dihedral to determine the strain axes (Angelier and Mechler 1977; Pfiffner and Burkhard 1987) computed with the code published by Marrett and Allmendinger (1990). The corresponding datasets are represented in Fig. 7d. In the Fuegian Andes, strike-slip faults dominate, either left lateral or right lateral in the same proportion. The two families trend about N–S for the dextral family and E–W for the sinistral one, with strain ellipsoids generally of plane-strain type. In the axial zone of the Magallanes–Austral Basin and in the foreland of eastern Tierra del Fuego, some localities display a transtensional stress regime. The average directions of shortening strike from $N52^{\circ}E$ for the axial zone in the west Magallanes Strait (zone 3 in Diraison et al. 2000), to $N43^{\circ}E$ for the Fuegian foothills (zone 4).

The synthetic paper on Fuegian Andes' structural geology from Menichetti et al. (2008) also includes a specific brittle deformation section, with new data in the Lago Fagnano–Canal Beagle area (Fig. 6b). They worked in terms of paleostress axes, using the Angelier's methods (Angelier 1990). Their data plotted in Fig. 7e show a combination of strike-slip (σ_1 and σ_3 horizontal, σ_2 vertical) and extensional stress regime (σ_2 and σ_3 horizontal, σ_1 vertical). Looking carefully at their dataset (Fig. 7e), one can see that some extensional tensors are computed with a majority of strike-slip faults. Indeed, such inversion may somehow lead to stress inversion between σ_2 and σ_3 (Sue et al. 2014). Even if such a discussion is not the scope of our paper, anyhow, the overall system exhibits a global transtensional regime, with six strike-slip tensors (over ten tensors) showing σ_1 oriented in the NE–SW direction, and four extensional tensors showing N–S-oriented σ_2 (namely sh_{max} in this case). This study confirms the overall orientation of the main stress/strain axis (σ_1 /shortening) in the NE–SW direction, as described above. Moreover, it quantifies the extensional part of the deformation, with noticeable sites showing E–W extension, in close relation to the pull-apart-like geometry described along the MFF (see above, and Lodolo et al. 2003).

Finally, we report the data from Branellec (2010) corresponding to a fieldwork during spring 2010, mainly along the north shore of Lago Fagnano (C. Sue Unpubl. data). Using the stress inversion method of Angelier (1990), we also found a combination of strike-slip tensors, with globally NE–SW-oriented σ_1 , and extensional tensors, with roughly NW–SE-oriented σ_2 (sh_{max}) axes. Our data are reported in Fig. 7f. Using this more local work, we can confirm the quantification of the overall stress/strain scheme obtained by the previous authors, that is to say the overall transtensional system along the MFF, with left-lateral movements along the globally E–W planes. It is quite important using such kinematic analyses of small or “minor” fault planes to cross-correlate and compare the results of different research teams, as the methodology itself remains quite controversial (see Lacombe 2012 for a review).

In an attempt of synthesis, we combined the results presented above in a single map (Fig. 8). The overall synthesized database includes 63 axes, with 40 axes from Diraison et al. (2000), 10 from Menichetti et al. (2008), and 8 from Branellec (2010). We also added the main axis that can be inferred from Cunningham (1993), the main transcurrent structures from Klepeis and Austin (1997), and the 3 from Klepeis (1994). We mapped the main shortening axes: Z/σ_1 for strike-slip kinematics and Y/σ_2 for extensional kinematics.

The density of data is much more important in the Lago Fagnano–Canal Beagle area and in the foreland than in the rest of the Fuegian Andes. Nevertheless, we obtain a very homogeneous map, with a quite regular field for the main shortening axes (Fig. 8). Wrenching appears largely dominant, not only in the MFF's realm, but also in the whole Tierra del Fuego. Indeed, strike-slip is the main signal obtained all along the Southernmost Andes cordillera (inner zones), the Magallanes fold and thrust belt, as well as the northeastern sector, in the foreland of the belt (Magallanes-Austral basin).

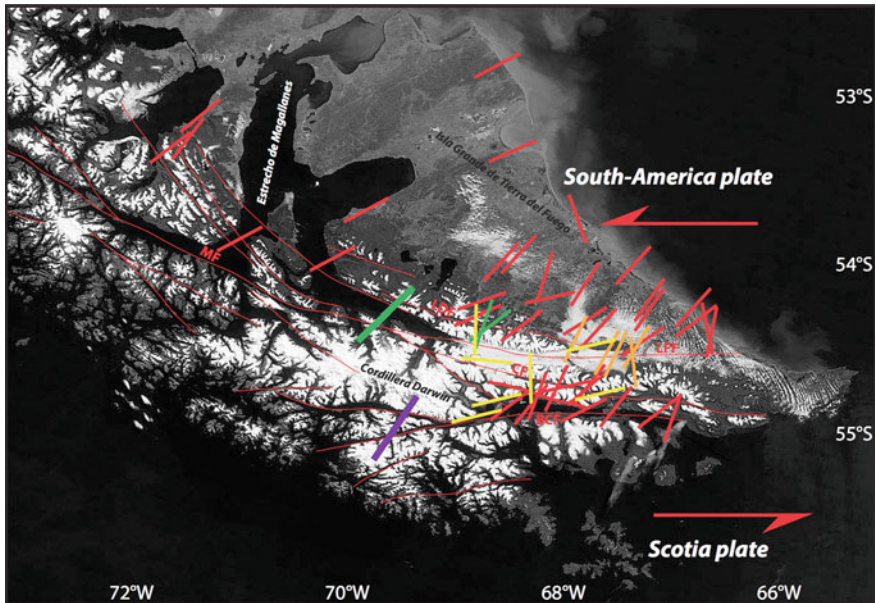


Fig. 8 Synthesized map of 63 principal stress axes (shmax) from fault kinematic analysis presented in Fig. 7. Z/σ_1 for strike-slip kinematics and Y/σ_2 for extensional kinematics are plotted. Data from Cunningham (1993) in purple (average axis); Klepeis (1994) in green (small symbols); Klepeis and Austin (1997) in green (large symbol; average axis); Diraison et al. (2000) in red; Menichetti et al. (2008) in yellow; and Branellec (2010) in orange. See text for discussion

The six independent studies are coherent with a main shortening axis-oriented NE–SW, associated with a main extensional axis-oriented NW–SE. Actually, we do not observe any significant rotation of the main stress axes along the MFF system. Although kinematic data are still missing in the westernmost part of the system, it seems that the overall strain/stress scheme is very stable in the whole domain. It could correspond to far field, directly linked to the boundary condition of the system, that is to say the wrenching kinematic between Scotia and South America plates. In this interpretation, the stress/strain field would stay very steady, whatever was the orientation of the main fault system (MFF) from E–W to ENE–WSW.

However, such a steadiness could also be interpreted in term of chronology and related to a late faulting or coeval deformation with respect to the bending of the Southernmost Andes (e.g., Maffione et al. 2010, 2015; Ghiglione et al. 2013; Maffione 2016). The precise timing of the overall brittle deformation remains a matter of debate (e.g., Cunningham 1993; Diraison et al. 2000; Menichetti et al. 2008) and could have last from the Late Cretaceous onward. Our synthetic map arises from faulting that more probably acted during the last 40 Myr, in close relation to the opening of the Drake Passage and Scotia plate’s development (Eagles 2016). The problem of the beginning of this overall wrenching could hardly be addressed due to the lack of absolute fault dating in the area. However, this

tectonics has controlled the deformation of the whole Fuegian Andes and surrounding area during at least Oligo–Miocene times. Beyond the matter of timing of the incipient wrenching tectonics, the question of its present-day activity is of first importance as it bears implications in terms of seismic risk assessment.

3 Seismotectonics at the Boundary Between South America and Scotia Plates

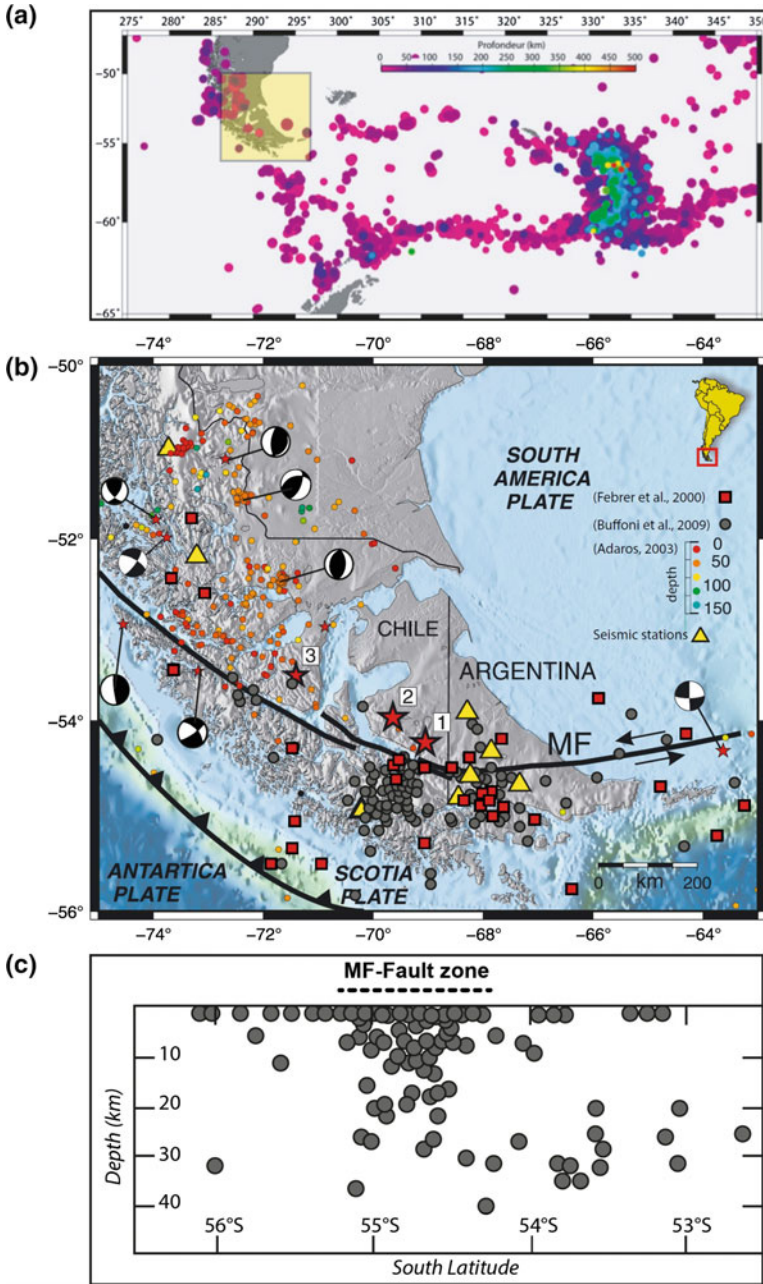
3.1 Seismicity in the Vicinity of the Magallanes–Fagnano Fault System

Among a large cluster of shallow earthquakes that originate on the plate boundary (Fig. 9a), the largest earthquake ever recorded in Tierra del Fuego stroked on December 17, 1949, between the Magallanes Strait and the western tip of the Lago Fagnano. Two successive events occurred at 6h53' and 15h06' (GMT time), with magnitudes estimated at 7.5 and 7.8, respectively (Lomnitz 1970; Goodstein et al. 1980; Febrer et al. 2000). According to Perucca et al. (2015), the second shock was stronger in magnitude than the first one, based on wave amplitudes recorded in Weston (USA). Indeed, the first event could be described as a foreshock for the largest one. Among the classical aftershock sequence (Scholz 1990), the largest event stroked on January 30, 1950. These 3 events are represented by red stars in Fig. 9b (modified from Perucca et al. 2015). The locations of the foreshock, mainshock, and aftershock have been reassessed by Bonorino et al. (2012), following Jaschek et al. (1982). A discussion on the precision of the location of these events has also been proposed by Adaros Cárcamo (2003). Bonorino et al. (2012) proposed the following locations: (53.89°S, 69.67°W) for the mainshock, (54.24°S, 69.03°W) for the foreshock, and (53.50°S, 71.50°W) for the aftershock. Indeed, these three major quakes seem organized in a direction subparallel to the MFF, with a rupture length of about 300 km, which is consistent with a M7.5 earthquake (Wells and Coppersmith 1994).

Prior to this major earthquake, another large one has been reported on February 2, 1879, which strokes the region of Ushuaia and Tierra del Fuego as a whole, with a MSK intensity estimated at VIII in Tierra del Fuego, and an estimated magnitude

Fig. 9 a Worldwide seismicity around the Scotia Sea realm, from IRIS database, www.iris.edu. ►

b Epicentral location of the largest instrumentally recorded earthquakes on December 17, 1949, numbered as (1) and (2) (Jaschek et al. 1982), and the January 1950 (3) aftershock. *Red squares* represent the seismicity recorded in 1998–1999 by Febrer et al. (2000). *Colored circles* represent the seismicity recorded from local deployments in 1997–1998 studied by Adaros Cárcamo (2003). *Dark gray dots* represent the seismicity recorded by the 2007 campaign of Buffoni et al. (2009). Focal mechanisms are from Forsyth (1975), Pelayo and Wiens (1989), Adaros Cárcamo (2003), and USGS database. Map has been modified from Perucca et al. (2015). **c** seismic cross section across the MFF modified from Buffoni et al. (2009). See text for details



M7, i.e., on the same order as the 1949's events (Lomnitz 1970; Febrer et al. 2000; Pedrera et al. 2014). Perucca and Moreiras (2009) also reported an ancient earthquake that occurred before the European colonization according to a Yahgán (indigenous Fuegian) legend. The area of the Fuegian Andes, often described as a region of "moderate seismicity" (e.g., Lodolo et al. 2002), is actually a zone of potential $M \sim 7-8$ earthquakes.

Although the seismic hazard is consequently important, given the high level of historical seismicity, the overall area is poorly instrumented, from the Atlantic shore to the western part of Tierra del Fuego and the labyrinthic fiords of the Southernmost Andes, due to the remoteness of the region and the difficulties of access. Indeed, a quick look at the worldwide database (Fig. 9a; worldwide seismicity from IRIS database, www.iris.edu) and from the USGS site for the Ushuaia's region (<http://earthquaketrack.com/ar-23-ushuaia/biggest>) gives only 3 $M > 4$ recent events, well localized along the MFF system. A network of 5 permanent stations (Fig. 9b) is installed in the Ushuaia's vicinity (Argentina) and 3 in the western side of Southernmost Andes (Chile).

Beyond the historical events (1879, 1929, 1930, 1944, 1949, 1950, 1970; see Febrer et al. 2000; Buffoni et al. 2009), instrumental seismicity has been investigated in 3 recent studies. They correspond to temporary seismic recording, over a one year each at the end of the 1990s. We synthesized these data in Fig. 9b (after Febrer et al. 2000; Adaros Cárcamo 2003; Buffoni et al. 2009).

Febrer et al. (2000) analyzed the regional seismicity in Tierra del Fuego and surrounding areas using single station localization (SSL) technique with the data recorded at the broadband seismic station of Ushuaia (USHU) from June 1998 to June 1999. They detected and analyzed 39 events in this time window with magnitudes ranging from 2.0 to 5.4 (Table 3 in Febrer et al. 2000; red squares in Fig. 9b). This moderate seismicity recorded over one year of observation is largely consistent in terms of localization with the major historical earthquakes described above. Given the scarcity of seismic stations, and the location method used (SSL, see description in Febrer et al. 2000), the error in estimating the azimuth of the earthquakes is $\sim 3^\circ$. The errors in the epicentral distance are mainly caused by inaccuracy on the velocity model. The final location errors are estimated $\sim 5\%$ for the transverse position and 10% for the radial position, in respect of the azimuth of the station-epicenter path. On the map from Fig. 9b (red squares), 2 groups of events cluster close the MFF system. One east of the Lago Fagnano and a second one in the vicinity of the Canal Beagle and near the Navarino Island show the actual activity on the MFF as a whole (Winslow 1982; Klepeis 1994). The positions of the 3 main earthquakes of the 1949s sequence are also located on the same fault system, taking into account the large uncertainty of their precise epicenters (Adaros Cárcamo 2003). Epicenters located eastward in the Atlantic Ocean could be linked to the continuation of the MFF toward the NSR. The southernmost event in the Pacific-Atlantic boundary could be associated with the Chilean trench and with its southward continuation in the Shackleton fracture zone. The relatively moderate size seismicity recorded during one year suggests a continuous release of seismic energy, in relation to the driving mechanism of plates wrenching at larger scale.

Anyhow, a specific study on the regional value, as investigated in various tectonic contexts (e.g., Sue et al. 2002), and taking into account the Febrer's database, together with the historical one, and the more recent ones by Adaros Cárcamo (2003) and Buffoni et al. (2009) could bring new constrain on the mechanism of faulting in this area. Indeed, a state-of-the-art work dedicated to the seismotectonics of the MFF system as whole is still missing.

A precise work on the recent seismicity of Southernmost Andes has been achieved in the PhD. of Adaros Cárcamo (2003), analyzing the data of the SEPA experiment. He worked on the seismicity of southernmost Chile and includes the connection with the MFF system to the south. His data have been reanalyzed by Cisternas and Vera (2008) and Perucca et al. (2015). Figure 9b shows the earthquakes recorded during the experiment used in this PhD. (colored dots, depending on the event's depth) and conducted from February 1997 to November 1998 using a local network of 5 seismometers installed in Southernmost Andes and in the foreland (see location in Adaros Cárcamo 2003). The recorded seismicity corresponds to 320 crustal earthquakes, which are registered within a depth lower than 40 km, with magnitudes below $M_{4.5}$. On quality consideration, Adaros Cárcamo (2003) reduced the published catalogue to 250 events. Seismicity north of the MFF corresponds to the convergence between the South America and Antarctic plates, and mechanisms of the observed earthquakes show roughly E–W-oriented compression axes (Adaros Cárcamo 2003). The seismicity viewed by this network is less frequent south of Magallanes Strait and MFF. Indeed, some events seem to locate on the MFF system, with WNW–ESE elongated clusters. As a whole, the seismic activity is clearly greater in the frontal part of the Southernmost Andes (the fold and thrust belt), and north of the Evangelista lighthouse, which corresponds to the western end of the MFF. Cisternas and Vera (2008) also pointed out the potential active volcanic activity linked to the seismicity. In terms of plate motions, this greater activity to the north than in the southern part of the area (namely the MFF system) would rise up from the velocity of convergence between South America plate and Antarctic plate (20 mm/year), compared to the velocity in strike-slip between the Scotia and Antarctica plates (~ 7 mm/year). The low seismicity observed by this experiment along the MFF system has been interpreted by Adaros Cárcamo (2003) in terms of seismic gap: Such failure would be activated only by large earthquakes (e.g., the 1949's sequence), energy accumulated through being partly released by small events on lateral faults, organized as Riedel shear. This would imply an overall locked MFF system, in-between major earthquakes. This interpretation is at least partly invalidated by the data of Febrer et al. (2000), who observed a quite steady seismic activity along the MFF system. Much longer recording of local seismicity would be necessary to better constrain the fault mechanism along the MFF. The particular case of the diffuse seismicity located east of the frontal fold and thrust belt, in Santa Cruz Province of Argentina, would be associated with seismicity induced by oil and gas exploration and exploitation in southern Argentina (e.g., Grasso 1992), although it is likely that such activity is associated with the reactivation of preexisting Jurassic upper crustal faults (Ghiglione et al. 2013).

A third analysis of the regional (micro)-seismicity in the Magallanes Strait and overall Tierra del Fuego area has been recently published by Buffoni et al. (2009). They used the recording provided by 5 seismic stations located in eastern Isla Grande (yellow triangles in Fig. 9b), from January to December 2007, and provided a careful assessment of the event's location. Due to the scheme of the seismic network with respect to the main active zones, the overall precision of this database remains quite rough, with uncertainties most of the time over 5 km in horizontal and depth location (see discussion in Buffoni et al. 2009). However, there were 185 recorded events, with local magnitudes between 2 and 5 (dark gray dots in Fig. 9b, c). As for the previous studies, the small time window, together with the geometry of the network, prevents to obtain a long-term and regional analysis. Nevertheless, this work provides a good idea of the current activity in the MFF. The distribution of epicenters shows that earthquakes concentrate in several clusters: The main one seems located in the vicinity of the Cordillera Darwin, another one around the Lago Fagnano, and probably a third one close to the Canal Beagle. Indeed, this database clearly shows that the MFF system, and more generally speaking the actual limit between Scotia and South America plates, is currently seismically active, with earthquakes of low to medium magnitude, but steadily occurring. Consequently, the MFF system would not be seismically locked as suggested by Adaros Cárcamo (2003). The cross section (Fig. 9c) shows that the seismicity along the MFF system locates mainly in the first 30 km of the crust. On this N–S section, the activity on the MFF is clearly visible, with an elongated subvertical cluster at $\sim 55^\circ\text{S}$.

3.2 Paleoseismicity and Neotectonics Along the Magallanes–Fagnano Fault System

Complementary to actual seismic monitoring, several studies reported neotectonic and paleoseismologic features on the MFF system, which allow investigating its Quaternary tectonics. Evidences are found in the best outcrops of the MFF, along the Turbio and Irigoyen rivers (Fig. 10) (Costa et al. 2006). Several morphotectonic evidences are reported by Perucca et al. (2015), such as linear valleys, deflected river streams, shutter ridges, sag ponds, and pressure ridges. This kind of drainage anomalies can be followed downstream from Tolhuin to the Atlantic shore and could be quantitatively analyzed using river profile analyses (e.g. Rabin et al. 2015). According to Coronato et al. (2002), drainage diversion must have occurred during the late glacial period sometime after 12 kyr. For instance, the Turbio River flowed into the Atlantic Ocean before being diverted into Lago Fagnano by the Fagnano fault scarp. River drainages exhibit subtle topographic modifications concerning for instance the incision depth along the river. Another feature corresponds to the change in the river pattern (from anastomosing to meandering) or in the alluvial plain width, which would indicate uplift or sagging (Audemard 1999). Sag ponds are also recognized along the subsiding bedrock and glacial plains, with a W–

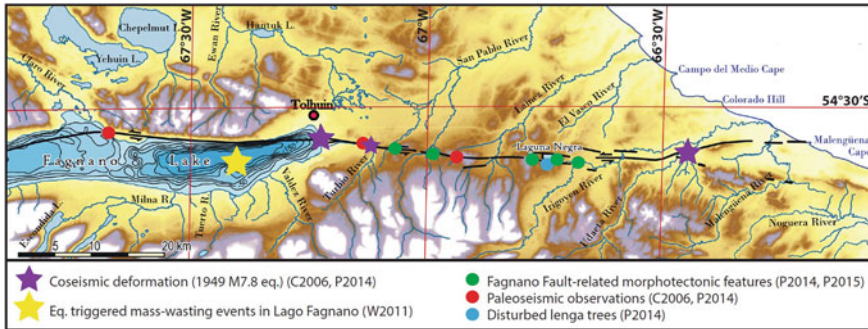


Fig. 10 Paleoseismological map of Lago Fagnano–Irigoyen river area including observations from C2006, Costa et al. (2006); W2011, Waldmann et al. (2011); P2014, Pedrera et al. (2014); and P2015, Perucca et al. (2015). Map modified after Pedrera et al. 2014 and Perucca et al. 2015

E-trending orientation. In particular, the area of Laguna Negra constitutes a pull-apart basin developed between two overlapping segments of the MFF (Fig. 10). Perucca et al. (2015) reviewed the tectonic-related anomalies (green dots in Fig. 10) and propose the left-lateral, and actually transtensive, movement of the MFF during quaternary times (probably post-LGM).

In terms of quantitative paleoseismology (see McCalpin 2009 for methodologies), several methods complementary to morphotectonics have been applied to the MFF system: trenching of fault scarp in Quaternary rocks (Costa et al. 2006), high-resolution seismic imaging of the sediments in the Lago Fagnano (Waldmann et al. 2011), geophysics (ground-probing radar, vertical electric sounding, seismic refraction; Bonorino et al. 2012), and disturbed tree analyses (Pedrera et al. 2014).

Costa et al. (2006) analyzed paleoseismic record associated with the ruptures of the twin 1949s earthquakes (M7.8 and 7.5) and recognized 3 or 4 events within the last 9 kyr, in which ruptures reached the surface (indeed M6 or more, Scholz 1990). They observed the fault scarp at several localities east of Lago Fagnano, and they dug a trench across a secondary fault of the MFF at Río San Pablo. The cumulative scarp reaches heights up to 11 m in late Pleistocene–Holocene deposits. The components of the 1949 events reach maximum 1 m vertically and 4 m horizontally. A maximum average recurrence interval of 2 kyr is thus estimated for major earthquake ruptures. Other palaeoseismic studies have proposed comparable recurrence intervals: 750 years for M7.8 earthquakes (Smalley et al. 2003) and 2–2.7 kyr for surface rupture earthquakes over the last 8 kyr (Schwartz et al. 2001).

Using high-resolution seismic imaging, coring, and dating methods (AMS-14C), Waldmann et al. (2011) provided a very accurate analysis of the sediment infill in the Lago Fagnano and thus quantified and dated a sequence of 19 Holocene mass-wasting events (subwater landslides) over the last 2 kyr. They interpreted slope failures and mega-turbidites as driven by large earthquakes occurring along

MFF since the early Holocene. They suggested that the majority of repeated intervals lie within two clusters of events with recurrence time of 350 and 850 years.

Another recurrence-time estimation proposed by Bonorino et al. (2012) using subsurface geophysics (radar, electric sounding, seismic refraction) indicates that strand plain deposits have been affected by rupture along the MFF at least six times between 0.9 and 6.4 ky, giving an average recurrence rate of about 1 kyr.

More recently, a study of seismically disturbed lenga trees across the MFF system was presented by Pedrera et al. (2014), together with a new neotectonic map (blue dots in Fig. 10). This analysis shows that the lenga trees recorded the 1879 and 1949 earthquakes close to the fault trace (asymmetric growth rings) and thus established the possible location of the earthquake on this fault.

To sum up the paleoseismological results, it appears that the MFF would produce major earthquakes comparable to the 1879 and 1949 events (i.e., with magnitude ~ 7 or more) with a recurrence time in the order of 1 kyr. Anyhow, the recent seismic activity, with major earthquakes in 1879 and 1949, plus on reported by the Yahgán people “before the colonization”, that is to say probably in the eighteenth century, exhibits a noticeable lower recurrence time, in the order of one century or less. This apparent discrepancy rises up the matter of the tectonic coupling between the actual driving geodynamics and the regional fault mechanism (see discussion in Sect. 4).

3.3 Focal Mechanisms and Stress Inversion at the Scotia and South America Plate Boundaries

Few focal mechanisms are actually available in the literature in the vicinity of the MFF system (Fig. 9b). Forsyth (1975) published 3 focal mechanisms in the study area, together with a first complete analysis of Scotia’s tectonics. Pelayo and Wiens (1989) reassessed one of the Forsyth’s solutions. Adaros Cárcamo (2003) computed 2 focal mechanisms using the SEPA database (see above) and also reported 3 mechanisms from the USGS Harvard-CMT database (<http://www.globalcmt.org>). The parameters of these 8 solutions are given in Table 1. The scarcity of focal mechanisms in the overall Southernmost Andes rises up from the configuration of the seismological permanent networks, which have a quite low density of stations. Indeed, the available mechanisms have been generally computed with earthquakes strong enough to be detected by worldwide networks. The typical magnitudes of these events are about M5.5 (Forsyth 1975; Pelayo and Wiens 1989). The solutions computed by Adaros Cárcamo with the SEPA database correspond to M4.5 and M4.3 events detected during the SEPA experiment’s data acquisition.

The synthesized seismotectonic map shown in Fig. 9b allows investigating the overall geodynamics of the Southernmost Andes’ realm. To the west, one solution in reverse faulting with a flat focal plane is probably linked to the subduction in the

Table 1 Parameters of the focal mechanisms drawn in Fig. 9

Date	Lat (S)	Ion (W)	Depth	Mag.	Strike	Dip	Rake	Ref
14/06/1970	52.0	73.8	33	6.0	315	12	14	F
15/06/1970	54.3	63.6	10	5.6	179	87	192	F-P&W
09/02/1972	51.8	74.0	33	5.5	305	27	27	F
06/06/1979	52.9	74.6	15	5.6	7	8	104	USGS-A
30/07/1992	51.1	72.6	15	5.4	31	25	114	USGS-A
31/08/1996	53.4	73.1	30	4.9	54	77	-148	USGS-A
27/05/1998	51.5	72.4	22	4.5	5	55	90	A
26/04/1997	52.2	71.6	19	4.3	2	50	90	A

Data after Forsyth (1975) (F), Pelayo and Wiens (1989) (P&W), Adaros Cárcamo (2003) (A) including three solutions he took from the USGS database (USGS-A)

Chile trench. In the northeastern part of the study area, 3 reverse faulting mechanisms oriented more or less N–S are related to active thrusting in the frontal fold and thrust belt. Concerning the MFF system, 3 focal mechanisms establish clearly its left-lateral transcurrent behavior. Eastward of the MFF, the left-lateral movement is transferred to the North Scotia Ridge, which behavior in terms of focal mechanisms has been well investigated by Thomas et al. (2003). This regional-scale analysis is integrated in the large-scale processes acting between Antarctica, South America, and Scotia plates (Eagles et al. 2005, Galindo-Zaldívar et al. 2006).

Focal mechanisms are classically used to determine the actual stress of a geodynamic system (see for instance Zoback et al. 1989 at worldwide scale). At the scale of the South America plate, the stress field has been investigated by Stefanick and Jurdy (1992) and Coblentz and Richardson (1996). A recent study including focal mechanism inversion, and numerical modeling at the scale of the Scotia plate (Sue et al. 2012; Sue et al. in prep.), allows to better characterize the stress field in the realm of the Scotia plate in general and in the Southernmost Andes in particular (Fig. 11 and Table 2). This study provides a new regionalization and quantification of the stress variations in the larger South America–Scotia–Antarctic plate system. It rises up the matter of regional evolution from compressional (Patagonian Andes–Southernmost Andes, Sandwich subduction front), to strike-slip (North and South Scotia ridges, Shackleton fracture zone), and extensional areas (Bransfield basin, Sandwich subduction zone).

By zooming on the northwestern part of the work of Sue et al. (2012) (Fig. 11a, b), we can propose a new map of the actual stress in the Fuegian Andes and surrounding areas (Fig. 11b). We applied stress inversion methods to the subsets of focal mechanisms extracted from the USGS Harvard-CMT database (<http://www.globalcmt.org>) from 1976 to 2009 (Fig. 11c, see Sue et al. 2012; Sue et al. in prep for details). We used the software ZMAP (Wiemer 2001) to perform the stress inversions from focal mechanisms. Stress inversion methods assume a uniform state of stress within the study area as well as newly formed faults. Furthermore, in contrast to the inversion of fault-striae data (see above), standard inversion of earthquake data (e.g., Michael 1987; Gephart 1990; Delvaux 1993) does not a priori

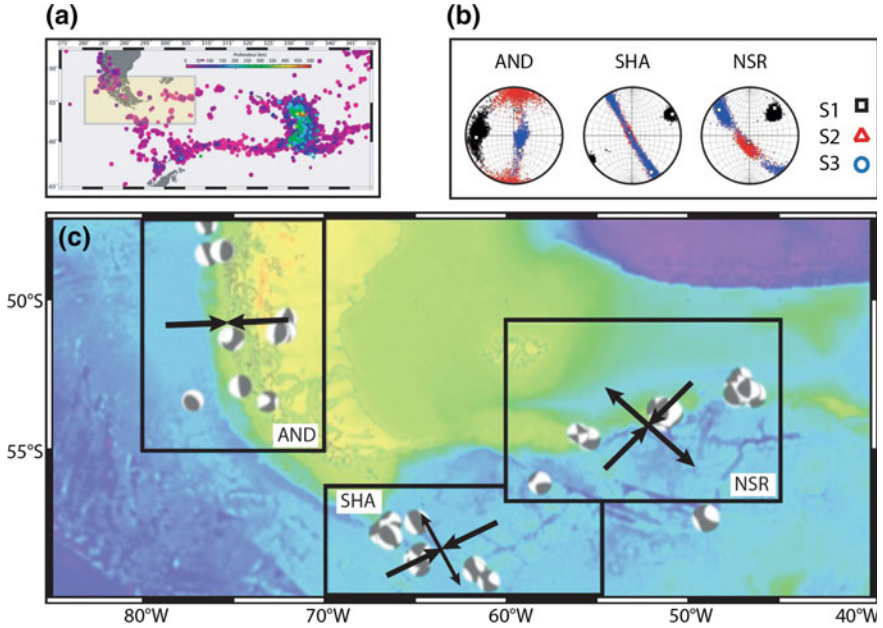


Fig. 11 **a** Location of the study area on the IRIS database (from Fig. 9a). **b** Stress tensors of the 3 inversions (AND, SHA, NSR). **c** Stress map obtained with the 3 inversions, with horizontal s_1 and/or s_3 (see parameters in Table 2)

Table 2 Parameters of the stress inversion performed in the Southernmost Andes (AND), Shackleton fracture zone (SHA), and North Scotia Ridge area (NSR)

Zone	N	s_1 az	s_1 pl	s_2 az	s_2 pl	s_3 az	s_3 pl	Var	phi ratio
AND	12	93.3	13.9	6.2	33.8	157.7	52.7	0.07	0.20
SHA	26	62.1	3.1	-47.3	80.6	152.5	8.8	0.07	0.26
NSR	17	42.3	14.5	173.9	72.1	-50.3	10.1	0.04	0.41

Data from sue et al. (2012, 2016 in prep.). N number of focal mechanisms used in the inversion; S_x -az and S_x -pl azimuth and plunge of the x stress axis. Var variance of the inversion; phi phi ratio of the stress tensor

discriminate between the active and the virtual nodal plane. Despite such restrictions, stress inversion has been shown to provide a powerful tool to analyze focal plane mechanism datasets (e.g., Sue et al. 1999; Kastrup et al. 2004; Delacou et al. 2004).

The aim of the inversion of focal plane data is the determination of a regional stress tensor that satisfies most, if not all, observed individual earthquakes in a given area. In contrast to the simple interpolation of isolated, projected p - and t -axis directions, inversion methods take the entire 3-D orientation of focal planes into account and search for a common stress tensor.

Our inversion is based on an objective, visual selection of large homogeneous zones, which are characterized by an apparently uniform type of deformation. Indeed, a synthetic analysis combining the various information coming from seismicity (active zones), focal mechanisms (type of deformation), DEM (topography plus bathymetry), structural setting, and geophysical data allows to differentiate regionally three tectonically active homogeneous sectors (Fig. 11b): (i) the southern Patagonian Andes and west of Tierra del Fuego, namely the Southernmost Andes (AND), (ii) the North Scotia Ridge (NSR), and (iii) the Shackleton fracture zone (SHA). These three sectors related to specific plate tectonic boundaries (Fig. 2b, c) have been used to decipher the current stress pattern and its variation in the overall area, using state-of-the-art inversion method of focal mechanism subdatasets (Table 2, see Wiemer 2001, Gephart 1990). The overall current stress pattern is surprisingly coherent at the scale of the selected sectors (Fig. 11c) and is comparable to the kinematic results from Giner-Robles et al. (2003). Indeed, the tectonic complexities of the Scotia plate's surroundings induce stress variation from pure compression (AND), to transpression (SHA), and pure strike-slip (NSR). Nevertheless, the principal stress directions show a good stability with σ_1 oriented E–W to NNE–SSW and σ_3 oriented NW–SE to NNW–SSE.

The stability of the stress pattern reflects the global steady left-lateral motion between the Antarctic, Scotia, and South America plates (Fig. 11c) and the consequent westward movement of the Pacific trench (Fig. 2b), as the main driving force for the entire area.

4 Crustal Deformation at South America–Scotia Plate Boundaries Inferred from GPS

Current motion of South America with respect to Antarctica is left lateral along the E–W strike. In between, the intermediate Scotia plate also moves left laterally with respect to both the South America and Antarctic plates (Fig. 2b). Plate interaction is mainly distributed along the North and South Scotia Ridges, transcurrent faults, and the Shackleton fracture zone (Fig. 2b, c). The largest Scotia plate onshore exposure is the portion of Tierra del Fuego south of the left-lateral MFF, which is the landward continuation of the NSR and the current and active continental plate boundary (Fig. 4) (Smalley et al. 2007).

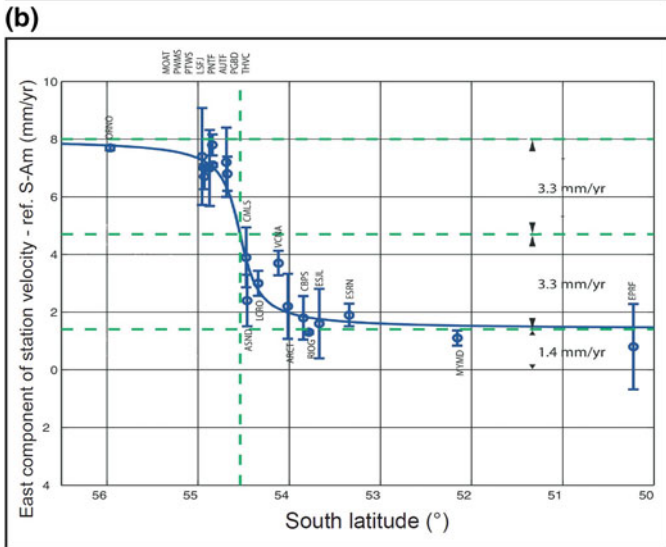
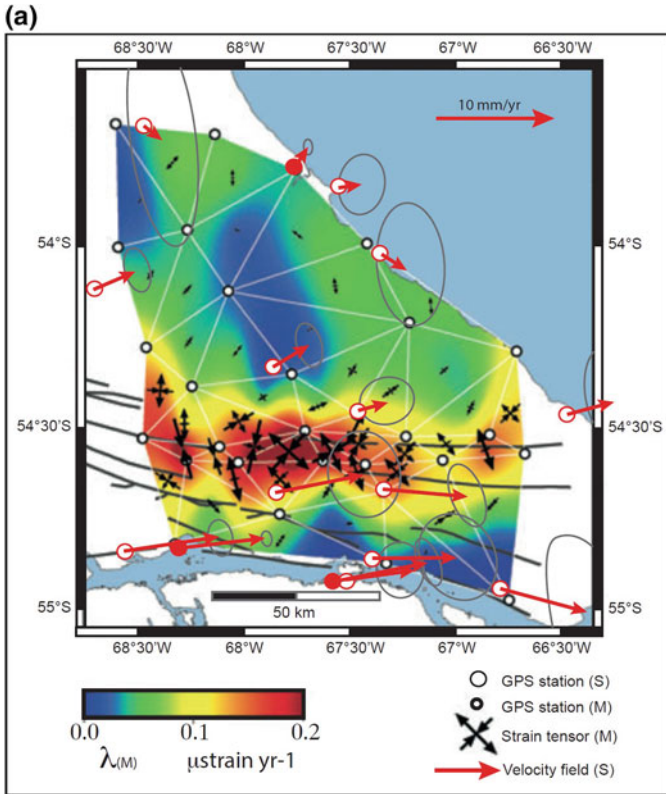
At the beginning of the 1990s, the Scotia plate was not tied into the global spreading circuit and could not be included in the NUVEL-1 plate model (DeMets et al. 1990). Using closure arguments and refined models, it subsequently integrated the NUVEL-1A model (DeMets et al. 1994). At plate scale, the current deformation is described by Smalley et al. (2007), who proposed a reassessment of the Scotia's Euler poles relatively to South America and Antarctica, using GPS measurements (King et al. 1997; Smalley et al. 2003) and earthquakes slip vectors (Pelayo and Wiens 1989; Thomas et al. 2003). They also integrated a modeling of the MFF

deformation and Antarctica subduction along the Chile trench. The Smalley et al. (2007)'s Euler vector for Scotia–South America relative movement is approximately parallel to that for Antarctic–South America movement, indicating that the overall motions of Scotia and Antarctica with respect to South America are sub-parallel and differ only in velocities. The poles or rotation previously proposed by Pelayo and Wiens (1989) and Thomas et al. (2003), together with the solution of Smalley et al. (2007), stays roughly on an N–S-oriented great circle perpendicular to the Scotia plate's along east–west axis.

Looking closer to the MFF system, two recent publications constrained the strain rates and crustal velocities in Tierra del Fuego, investigating the mechanical behavior of the eastern MFF (Smalley et al. 2003; Mendoza et al. 2011). Using repeated measurements of 20 GPS stations in Tierra del Fuego and southern Patagonia that spans the central portion of the MFF, Smalley et al. (2003) precisely constrained the velocity of the MFF at 6.6 ± 1.3 mm/year. This velocity is obtained by more regional databases, and somehow with less resolution, of 5 mm/year and 9.6 mm/year from Del Cogliano et al. (2000) and DeMets et al. (2010), respectively. Indeed, campaign measurement sites have been occupied between two and four times over total observation spans of two to six years between 1993 and 1998. The velocity field obtained by Smalley et al. (2003) (red arrows in Fig. 12a) shows an increase in velocity from north to south with respect to stable South America. The velocity gradient is concentrated in the region of the MFF and is associated with the plate boundary. Movements of the sites south of the fault are almost perfectly eastward, which is left lateral with respect to stable South America (Fig. 12a).

Beyond the GPS velocity quantification, this study also proposes a modeling of the MFF mechanism, on the basis of an E–W left-lateral strike-slip, assumed to be locked at 15 km. The formalism developed by Savage et al. (1975) for strike-slip modeling has been used (see discussion in Smalley et al. 2003), together with an inversion for the position, azimuth, and velocity of an E–W-striking fault. The position of the modeled fault is coincident with the surface trace of the MFF (54.54°S), defining a subvertical fault. The diagram in Fig. 12b, which fits the data with the modeling, clearly establishes the velocity of the deformation on the MFF. Assuming a 5 m offset for the M7.5 1949 event, the GPS rate of 6.6 mm/year results in a recurrence time in the order of 750 years. Although the uncertainty of this estimate is large, it is quite well coherent with the recurrence-time estimations proposed using paleoseismological observations. Actually, an additional 1–2 mm/year of relative plate motion may also be diffusely distributed across a

Fig. 12 **a** Positive strain rate principal components represented by strain tensors of each triangle cell are plotted (*black arrows*) and interpolated in the background (μ strain) from Mendoza et al. (2011). *Red arrows* are velocity field from Smalley et al. (2003). **b** Fit of GPS data to simple strike-slip model of Savage et al. (1975): cross section of eastward component of velocity (V_e). *Horizontal dashed green lines* show velocity asymptotes and relative velocity axis. *Vertical dashed green line* shows horizontal location of the down-dip end of the fault or location of the screw dislocation. Modified from Smalley et al. (2003)



larger region in northern Tierra del Fuego and southernmost Patagonia, as suggested by the velocities of some GPS stations south of the main fault (Smalley et al. 2003).

Beyond the search for velocity along the MFF, the overall strain pattern has recently been constrained by Mendoza et al. (2011). Using 29 GPS stations, repeatedly observed between 1993 and 2008, they determined both velocity field and strain field on the Argentinean side of Isla Grande de Tierra del Fuego, that is to say across the eastern branch of the MFF. Some sites investigated by Mendoza et al. (2011) correspond to that of Smalley et al. (2003), and both papers are largely complementary. Indeed, Fig. 12a combines both of them, with the velocity field from Smalley et al. (2003) (red arrows) and the strain field from Mendoza et al. (2011) (strain tensors drawn with black arrows). To quantify the present-day horizontal strain, with the assumption of stationary and homogeneous deformation rates in small finite areas, a strain analysis rising up from the regional velocity field has been performed within 44 triangular cells dividing the network as a whole (Fig. 12a). The parameters resulting from this analysis are invariants and constitute unbiased estimates for the regional strain rate (see Mendoza et al. 2011 for methodology and discussion on the database). The strain rate principal components (λ_1 , shortening, λ_2 extension) superimposed to the interpolated strain rate second invariant ($\lambda = (\lambda_1^2 + \lambda_2^2)^{1/2}$) are plotted Fig. 12a. This map locates and quantifies a strongest deformation zone concentrated along the main trace of the MFF, in a 30-km-wide E–W longitudinal strip between 54.5°S and 54.6°S. Within this belt, a maximum strain rate second invariant of 0.253 ± 0.004 $\mu\text{strain/year}$ is observed (within 2σ , 95 % confidence). For the areas, north and south of the zone of maximum deformation Mendoza et al. (2011) have shown that the deformation rates are one order of magnitude weaker, but still remain significant with values of about 0.03–0.05 $\mu\text{strain/year}$ (Fig. 12a). Then, the velocity comparison for stations located in both rather “stable” areas (north and south of the highly deforming strip) confirmed the relative rigidity of these blocks and gives a differential velocity of the south block with respect to the north one of 4.4 ± 1.1 mm/year eastward, and an almost null velocity southward (0.3 ± 0.8 mm/year) (Mendoza et al. 2011).

Although these results nicely confirm the pure left-lateral strike-slip along the MFF system, it provides a velocity value noticeably lower than the 6.6 mm/year provided by Smalley et al. (2003). The discrepancy may rise up from the longer time span for the GPS measurements in the more recent work, which would converge toward a more reliable quantification, as seen in very slow deforming areas (e.g., GPS studies in the European Alps by Sue et al. 2000; Delacou et al. 2005, 2008; Walpersdorf et al. 2015), but also from differences in the data processing strategy. Indeed, the higher value of ~ 6.6 mm/year from Smalley et al. (2003) could also integrate a significant part of the overall deformation diffusely distributed across a larger region.

5 Discussion and Concluding Remarks

It should be first highlighted that although the gathered information from previous works in the Southernmost Andes and the Scotia Sea is somehow scarce and scattered, such as fault kinematic data and focal mechanism, it was, however, very consistent. After data were filtered for minimum technical requisites, compiled in our regional databases, and reprocessed, they resulted in explanatory figures (e.g., Figs. 8 and 11b, c), illuminating some key discussion points in the geodynamic models of the Southernmost Andes.

Our synthesis of six independent fault kinematic studies is coherent with main shortening consistently oriented NE–SW, without significant rotation of the axes across the orogen (Fig. 8). The fault kinematic data present a very consistent shortening direction, i.e., on the lines of oblique convergence models presented by Ghiglione and Cristallini (2007). Instead of the two-stage orthogonal convergence model preferred by these authors, it seems that the oblique convergence of a basement indenter in one \sim NW steady direction, presented in the same paper, probably better explains the shortening direction of steady patterns around the Southernmost Andes, as proposed by Maffione et al. (2015) (cf. Maffione 2016). These observations, together with the stability of the stress pattern and orientation of the shortening axes on a bigger scale (Fig. 11b, c), reflect a steady E–W to NNE–SSW σ_1 /shortening direction since middle Eocene times (Ghiglione et al. 2013), reflecting that the global left-lateral motion between Antarctica–Scotia–South America plate circuit is the main driving force for the entire area and in particular for compression in the Southernmost Andes, over the last 50 or 40 Ma.

Elastic rebound theory predicts that the major earthquakes on a fault are time-dependent, as they are linked to a period of built-up energy (interseismic) with abrupt relaxation stages (coseismic). Both the short-term geodetic (Del Cogliano et al. 2000; Mendoza et al. 2011) and the long-term geological observation (i.e., Lodolo et al. 2003; Rossello 2005), slip rates of the MFF system are low (<5 mm/year). Therefore, the time span between major earthquakes should be larger than the one obtained over the last 2 or 3 centuries. Considering a simple tectonic setting of a pure left-lateral strike-slip fault with a constant 5 mm/year slip rate (geodetic slip rate, Mendoza et al. 2011) able to generate ~ 6 m of left-lateral maximum displacement at the surface during the largest earthquakes (effects of the 1949 Ms 7.8 earthquake; Costa et al. 2006), the expected time span between comparable earthquakes would be around 10 kyr. Yet the time between the two most recent large earthquakes on the eastern onshore fault section of the MFF was about 70 years. Such a great discrepancy could result (i) from the presence of locked sections along the MFF; (ii) variable slip rate history and tectonic loading; (iii) delayed and pulsed stress release due to steady tectonic loading and stored in the crust over millennium time scale; and (iv) the complexities of the extensional *en échelon* geometry of the MFF, which could rise up discrepancies from the simple strike-slip loading model.

Our results fill up the time gap between the 1949 event and the two, possibly three, paleoearthquakes detected by trenching over the last 9 kyr (Costa et al. 2006). The discrepancies between long-term and short-term velocities, that is to say between the evaluated tectonic loading and the actual recurrence time, suggest a complex mechanics on the MFF, leading to complex recurrence time history for the characteristic earthquake ($M \geq 7$).

Acknowledgements This work was supported by Buenos Aires and Besançon University (UBA and UBFC resp.), the Besançon Observatory (OSU-THETA), the French CNRS-INSU (project SCOPE), the Argentinean CONICET, and the ECOS-SUD comity (project A15U02). Many thanks to the people who came with us and helped us on the field and specifically to M. Branellec. Some maps were drawn using GMT code (Wessel and Smith 1991). Special thanks to Ombeline, Felix, and Simon.

References

- Adaros Cárcamo RE (2003) Sismicidad y Tectónica del extremo sur de Chile. Tesis Magíster, Universidad de Chile, 82 pp
- Angelier J (1990) Inversion of field data in fault tectonics to obtain the regional stress—III. A new rapid direct inversion method by analytical means. *Geophys J Int* 103:363–376
- Angelier J, Mechler P (1977) Sur une méthode graphique de recherche des contraintes principales également utilisable en tectonique et séismologie: la méthode des dièdres droits. *Bull Soc géol Fr* 19:1309–1318
- Angelier J, Goguel J (1979) Sur une méthode simple de détermination des axes principaux des contraintes pour une population de failles. *C R Acad Sci Paris* 282:307–310
- Audemard FA (1999) Morpho-structural expression of active thrust fault systems in the humid tropical foothills of Colombia and Venezuela. *Zeitschrift für Geomorphologie* 118:1–18
- Barker PF (2001) Scotia Sea regional tectonic evolution: implications for mantle flow and palaeocirculation. *Earth Sci Rev* 55:1–39
- Barker PF, Burrell J (1977) The opening of Drake Passage. *Mar Geol* 25:15–34
- Bonorino GG, Rinaldi V, del Valle Abascal L, Alvarado P, Bujalesky GG, Güell A (2012) Paleoseismicity and seismic hazard in southern Patagonia (Argentina-Chile; 50°–55°S) and the role of the Magallanes-Fagnano transform fault. *Nat Hazards* 61(2):337–349
- Bott MH (1959) The mechanism of oblique slip faulting. *Geol Mag* 96:109–117
- Branellec M (2010) Analyse morphotectonique de la terminaison des Andes Fuegonas (Terre de Feu, Argentine). Master thesis, Brest University, 90 pp
- Buffoni C, Sabbione NC, Connon G, Ormaechea JL (2009) Localización de hipocentros y determinación de su magnitud en Tierra del Fuego y zonas aledañas. *Geoacta* 34:75–86
- Caminos R, Haller M, Lapido J, Lizuain O, Page A, Ramos VA (1981) Reconocimiento geológico de los Andes Fueguinos, Territorio Nacional de Tierra del Fuego. VIII Congreso Geológico Argentino (San Luis) *Actas* 1:759–786
- Champagnac JD, Sue C, Delacou B, Burkhard M (2003) Brittle orogen-parallel extension in the internal zones of the Swiss Alps (south Valais). *Eclogae Geol Helvet* 96:325–338
- Cisternas A, Vera E (2008) Sismos históricos y recientes en Magallanes, Magallania (Punta Arenas) 36(1):43–51
- Coblentz DD, Richardson RM (1996) Analysis of the South American intraplate stress field. *J Geophys Res* 101:8643–8657

- Coronato A, Roig C, Mir X (2002) Geofformas glaciarias de la región oriental del Lago Fagnano, Tierra del Fuego, Argentina. In: Cabaleri N, Cingolani C, Linares E, López de Luchi M, Ostera H, Panarello H (eds) XV Congreso Geológico Argentino Actas, pp 457–462
- Costa CH, Smalley R, Schwartz D, Stenner H, Ellis M, Ahumada E, Velasco MS (2006) Paleoseismic observations of an onshore transform boundary: the Magallanes-Fagnano fault, Tierra del Fuego, Argentina. *Rev Asoc Geol Argentina* 61:647–657
- Coutand I, Diraison M, Cobbold PR, Gapais D, Rossello EA, Millar M (1999) Structure and kinematics of a foothills transect, Lago Viedma, southern Andes (49° 30'S). *J S Am Earth Sci* 12:1–15
- Cunningham WD (1993) Strike-slip faults in the Southernmost Andes and the development of the Patagonian Orocline. *Tectonics* 169–186
- Cunningham WD, Dalziel IW, Lee TY, Lawver LA (1995) Southernmost South America-Antarctic Peninsula relative plate motions since 84 Ma: implications for the tectonic evolution of the Scotia Arc region. *J Geophys Res-Sol EA* 100(B5):8257–8266
- Curtis ML, Flowerdew MJ, Riley TR, Whitehouse MJ, Daly JS (2010) Andean sinistral transpression and kinematic partitioning in South Georgia. *J Struct Geol* 32:464–477
- Dalziel IWD, Brown RL (1989) Tectonic denudation of the Cordillera Darwin metamorphic core complex, Tierra del Fuego: implications for cordilleran orogenesis. *Geology* 17:699–703
- Dalziel IWD, Dott RH Jr, Winn RD Jr, Bruhn RL (1975) Tectonic relations of South Georgia Island to the Southernmost Andes. *Geol Soc Am Bull* 86:1034–1040
- Darwin C (1845) In: Fitz Roy RN (ed) *Journal of researches into the natural history and geology of the countries visited during the voyage of H.M.S. Beagle round the world, under the Command of Capt, 2 edn.* John Murray, London, 519 p
- Darwin C (1846) *Geological observations on South America. Being the third part of the geology of the voyage of the Beagle, under the command of Capt. Fitzroy, R.N. during the years 1832 to 1836.* Smith Elder and Co, London 280 p
- Del Cogliano D, Perdomo R, Hormaechea J (2000) Desplazamiento entre placas tectónicas en Tierra del Fuego. XX Reunión Científica de la AAGG, Mendoza
- Delacou B, Sue C, Champagnac JD, Burkhard M (2004) Present-day geodynamics in the bend of the Western and Central Alps as constrained by earthquake analysis. *Geophys J Int* 158:753–774
- Delacou BC, Champagnac JD, Burkhard M (2005) Origin of the current stress field in the Western/Central Alps: role of gravitational reequilibration constrained by numerical modelling. *Geol Soc London Spec Publ* 243:295–310
- Delacou B, Sue C, Nocquet J-M, Champagnac J-D, Allanic C, Burkhard M (2008) Quantification of strain rate in the Western Alps using geodesy: comparisons with seismotectonics. *Swiss J Geosc* 101:377–385
- Delvaux D (1993) The TENSOR program for reconstruction: examples from the East African and the Baikyril rift systems. *TerraNova* 5:216
- DeMets C, Gordon RG, Argus DF, Stein S (1990) Current plate motions. *Geophys J Int* 10:425–478
- Demets C, Gordon RG, Argus DF, Stein S (1994) Effect of recent revisions to the geomagnetic reversal time scale on estimates of current plate motions. *Geophys Res Lett* 21:2191–2194
- DeMets C, Gordon RG, Argus DF (2010) Geologically current plate motions. *Geophys J Int* 181:1–80
- Diraison M, Cobbold PR, Gapais D, Rossello EA, Le Corre C (2000) Cenozoic crustal thickening, wrenching and rifting in the foothills of the Southernmost Andes. *Tectonophysics* 316:91–119
- Eagles G (2016) Tectonic reconstructions of the Southernmost Andes and the Scotia Sea during the opening of the Drake Passage. In: Ghiglione MC (ed) *Geodynamic Evolution of the Southernmost Andes.* Springer Earth System Sciences, pp 75–108
- Eagles G, Livermore RA, Fairhead JD, Morris P (2005) Tectonic evolution of the west Scotia Sea. *J Geophys Res* 110:B02401
- Etchecopar A, Vasseur G, Daignieres M (1981) An inverse problem in microtectonics for the determination of stress tensor from fault striation analysis. *J Struct Geol* 3:51–65

- Febrer JM, Plasencia MP, Sabbione NC (2000) Local and regional seismicity from Ushuaia broadband station observations (Tierra del Fuego). *Terra Antartica* 8:35–40
- Forsyth DW (1975) Fault plane solutions and tectonics of the South Atlantic and Scotia Sea. *J Geophys Res* 88:1429–1443
- Fuenzalida RH (1972) Geological correlation between the Patagonian Andes and the Antarctic Peninsula and some tectonic implications. Master Thesis, Stanford University
- Fuenzalida RH (1976) The Magellan fault zone. Symposium on Andean and Antarctic Volcanology Problems. Int Assoc Volcanol and Chem of the Earth Inter, Naples, Italy
- Galindo-Zaldívar J, Bohoyo F, Maldonado A, Schreider A, Suriñach E, Vázquez JT (2006) Propagating rift during the opening of a small oceanic basin: the Protector Basin (Scotia Arc, Antarctica). *Earth Planet Sci Lett* 241:398–412
- Gephart JW (1990) FMSI: A fortran program for inverting fault/ slickenside and earthquake focal mechanism data to obtain the regional stress tensor. *Comp Geosc* 16:953–989
- Ghiglione MC (2002) Diques clásticos asociados a deformación transcuente en depósitos sinorogénicos del Mioceno inferior de la Cuenca Austral. *Rev Asoc Geol Argentina* 57:103–118
- Ghiglione MC (2003) Estructura y evolución tectónica del Cretácico-Terciario de la costa Atlántica de Tierra del Fuego. Unpubl. PhD thesis, Facultad de Ciencias Exactas y Naturales, Universidad de Buenos Aires, 150 pp
- Ghiglione MC, Cristallini EO (2007) Have the Southernmost Andes been curved since Late Cretaceous times? An analog test for the Patagonian Orocline. *Geology* 35:13–16
- Ghiglione MC, Quinteros J, Yagupsky D, Bonillo-Martínez P, Hlebszevitch J, Ramos VA, Vergani G, Figueroa D, Quesada S, Zapata T (2010) Structure and tectonic history of the foreland basins of southernmost South America. *J S Am Earth Sci* 29:262–277
- Ghiglione MC, Navarrete-Rodríguez AT, González Guillot M, Bujaleski G (2013) The opening of the Magellan Strait and its geodynamic implications. *Terra Nova* 25(1):13–20
- Giner-Robles JL, González-Casado JM, Gumiel P, Martín-Velázquez S, García-Cuevas C (2003). A kinematic model of the Scotia plate (SW Atlantic Ocean). *J S Am Earth Sci* 16:179–191
- Goodstein J, Kymamori H, Lee W (1980) Seismological microfiche publications from the Caltech archives. *Bull Seism Soc Am* 70:657–665
- Grasso JR (1992) Mechanics of seismic instabilities induced by the recovery of hydrocarbons. *Pure appl Geophys* 139:507–534
- Grunow AM, Dalziel IWD, Harrison TM, Heizler MT (1992) Structural geology and geochronology of subduction complexes along the margin of Gondwanaland: new data from the Antarctic Peninsula and Southernmost Andes. *Geol Soc Am Bull* 104:1497–1514
- Homberg C (2000) Ruptures and stress deflections. In: III Conference on tectonic problems of the San Andreas fault system, Stanford, Proceedings, vol XXI. pp 324–332
- Jaschek E, Sabbione N, Sierra P (1982) Reubicación de sismos localizados en territorio argentino (1920–1963). Observatorio Astronómico de la Universidad Nacional de La Plata Serie Geofísica, Tomo XI, No 1
- King EC, Bevis MG, Larter RD, Reading AM, Dalziel IW, Taylor FW, Smalley R (1997) GPS measurements in the South Sandwich arc. *Eos Trans, AGU Fall Meet Suppl* F168:78(46)
- Klepeis KYR (1994) The Magallanes and Deseado fault zones: Major segments of the South American-Scotia transform plate boundary in southernmost South America. *Tierra del Fuego. J Geophys Res* 99(B11):22001–22014
- Klepeis KYR, Austin JA (1997) Contrasting styles of superposed deformation in the Southernmost Andes. *Tectonics* 16:755–776
- Kranck EH (1932) Geological investigations in the Cordillera of Tierra del Fuego. *Acta Geographica Helsinki* 4:1–231
- Kyrstrup U, Zoback ML, Deichmann N, Evans K, Giardini D (2004) Stress field variations in the Swiss Alps and the northern Alpine foreland derived from inversion of fault plane solutions. *J Geophys Res* 109:B01402
- Lacombe O (2012) Do fault slip data inversions actually yield ‘paleostresses’ that can be compared with contemporary stresses? A critical discussion. *Comptes Rendus Geosc* 344:159–173

- Lagabrielle Y, Godd ris Y, Donnadiou Y, Malavieille J, Suarez M (2009) The tectonic history of Drake Passage and its possible impacts on global cli-mate. *Earth Planet Sci Lett* 279:197–211
- Livermore RA, Eagles G, Morris P, Maldonado A (2004) Shackleton Fracture Zone: no barrier to early circumpolar ocean circulation. *Geology* 32:797–800
- Lodolo E, Menichetti M, Tassone A, Sterzai P (2002) Morphostructure of the central-eastern Tierra del Fuego Island from geological data and remote sensing images. *EGS Stephan Mueller Spec Publ Ser* 2:1–16
- Lodolo E, Menichetti M, Bartole R, Ben-Avraham Z, Tassone A, Lippai H (2003) Magallanes-Fagnano continental transform fault (Tierra del Fuego, southernmost South America). *Tectonics* 22:1076
- Lomnitz C (1970) Major earthquakes and tsunamis in Chile during the period 1535 to 1955. *Geol Rundsch* 59:938–960
- Ludwig WJ, Rabinowitz PD (1982) The collision complex of the North Scotia Ridge. *J Geophys Res* 87:3731–3740
- Macfadyen WA (1933) Fossil foraminifera from the Burdwood Bank and their geological significance. *Discovery Rep* 7:1–16
- Maffione M (2016) Kinematic evolution of the Southern Andean orogenic arc. In: Ghiglione MC (ed) *Geodynamic Evolution of the Southernmost Andes*. Springer Earth System Sciences, pp 173–200
- Maffione M, Speranza F, Faccenna C, Rossello E (2010) Paleomagnetic evidence for a pre-early Eocene (~50 Ma) bending of the Patagonian orocline (Tierra del Fuego, Argentina): Paleogeographic and tectonic implications. *Earth Planet Sc Lett* 289:273–286
- Maffione M, Fernandez-Moreno C, Ghiglione M, Speranza F, van Hinsbergen DJJ, Lodolo E (2015) Constraints on deformation of the Southern Andes since the Cretaceous from anisotropy of magnetic susceptibility. *Tectonophysics* 665:236–250
- Marrett RA, Allmendinger RW (1990) Kinematic analysis of fault-slip data. *J Struct Geol* 12:973–986
- McCalpin J (2009) *Paleoseismology*. Acad Press, 590 pp
- Mendoza L, Perdomo R, Hormaechea JL, Del Cogliano D, Fritsche M, Richter A, Dietrich R (2011) Present-day crustal deformation along the Magallanes-Fagnano Fault System in Tierra del Fuego from repeated GPS observations. *Geophys J Int* 184:1009–1022
- Menichetti M, Lodolo E, Tassone A (2008) Structural geology of the Fuegian Andes and Magallanes fold thrust belt—Tierra del Fuego Island. *Geologica Acta* 6:19–42
- Michael AJ (1987) Use of focal mechanisms to determine stress; a control study. *J Geophys Res* 92 (B1):357–368
- Pedrer a A, Galindo-Zald var J, Ruiz-Const n A, Bohoyo F, Torres-Carbonell P, Ruano P, Maestro A, Gonz lez-Castillo L (2014) The last major earthquakes along the Magallanes-Fagnano fault system recorded by disturbed trees (Tierra del Fuego, South America). *Terra Nova* 26:448–453
- Pelayo A, Wiens D (1989) Seismotectonics and relative plate motions in the Scotia Sea region. *J Geophys Res* 94:7293–7320
- Perucca LP, Moreiras SM (2009) Seismic and volcanic hazards in Argentina. *Dev Earth Surf Process* 13:267–300
- Perucca L, Alvarado P, Saez M (2015) Neotectonics and seismicity in southern Patagonia. *Geol J*. doi:10.1002/gj.2649
- Pfiffner OA, Burkhard M (1987) Determination of paleostress axes orientations from fault, twin and earthquake data. *Ann Tectonicae* 1:48–57
- Rabin M, Sue C, Valla P, Champagnac JD, Carry N, Bichet V, Eichenberger U, Mudry J (2015) Deciphering neotectonics from river profile analysis in the kyrst Jura Mountains (northern Alpine foreland). *Swiss J Geosc* 108:401–424
- Riedel W (1929) *Zur Mechanik geologischer Brucherscheinunge*. *Centralbl Mineral Geol Paleont* 1929B:354–368
- Rimbaud (1871) *Po sies compl tes*. Vanier, 1895

- Rossello EA (2005) Kinematics of the Andean sinistral wrenching along the Fagnano-Magallanes Fault Zone (Argentina-Chile Fuegian Foothills). VI International Symposium on Andean Geodynamics, Barcelona, Extended Abstracts, pp 623–626
- Savage JC, Burford RO, Kinoshita WT (1975) Earth movements from geodetic measurements. *Calif Div Mines Geol Bull* 196:175–186
- Scholz CH (1990) *The mechanics of earthquakes and faulting*. Cambridge University Press, 439 pp
- Schwartz DP, Stenner HD, Costa C, Smalley R, Ellis M, Velasco MS (2001) Paleoseismology at the End of the World: Initial observations of the Fagnano fault, Tierra del Fuego. Argentina. *Seismol Res Lett* 72:265
- Smalley R, Kendrick E, Bevis MG, Dalziel IWD, Taylor F, Lauría E, Piana E (2003) Geodetic determination of relative plate motion and crustal deformation across the Scotia-South America plate boundary in eastern Tierra del Fuego. *Geochem Geophys Geosyst* 4(9)
- Smalley R, Dalziel IWD, Bevis MG, Kendrick E, Stamps DS, King EC, Taylor FW, Lauría E, Zakrajsek A, Parra H (2007) Scotia arc kinematics from GPS geodesy. *Geophys Res Lett* 34: L21308
- Sperner B, Ott R, Ratschbacher L (1993) Fault-striae analysis: a turbo pascal program packyrge for graphical presentation and reduced stress-tensor calculation. *Comp Geosc* 19:1361–1388
- Stefanick M, Jurdy DM (1992) Stress observations and driving force models for the South American plate. *J Geophys Res* 97:11905–11913
- Sue C, Tricart P (2002) Widespread post-nappe normal faulting in the internal Western Alps: a new constrain on arc dynamic. *J Geol Soc London* 159:61–70
- Sue C, Tricart P (2003) Neogene to ongoing normal faulting in the inner Western Alps: a major evolution of the late alpine tectonics. *Tectonics* 22:1–25
- Sue C, Thouvenot F, Fréchet J, Tricart P (1999) Widespread extension in the core of the Western Alps revealed by earthquake analysis. *J Geophys Res* 104:25611–25622
- Sue C, Martinod J, Tricart P, Thouvenot F, Gamond JF, Fréchet J, Marinier D, Glot JP, Grasso JR (2000) Active deformation in the inner Western Alps inferred from comparison between 1972-classical and 1996-GPS geodetic surveys. *Tectonophysics* 320:17–29
- Sue C, Grasso JR, Lahaie F, Amitrano D (2002) Mechanical behavior of western alpine structures inferred from statistical analysis of seismicity. *Geophys Res Lett* 29:65–69
- Sue C, Branelllec M, Mazuel A, Ghiglione MC, Maia M (2012) Scotia Plate Dynamics: insights from seismotectonics and numerical modeling. EGU general assembly, Abstracts, vol 14, p 9277
- Sue C, Le Gall B, Daoud MA (2014) Stress field during early magmatism in the Ali Sabieh Dome, Djibouti, SE Afar rift. *J African Earth Sci* 97:56–66
- Sue C, Branelllec M, Mazuel A, Ghiglione MC (2016) Scotia Plate Dynamics: insights from seismotectonics and numerical modeling. In prep. for *J S Am Earth Sci*
- Tassone A, Lodolo E, Menichetti M, Yagupsky D, Caffau M, Vilas JF (2008) Seismostratigraphic and structural setting of the Malvinas Basin and its southern margin (Tierra del Fuego Atlantic offshore). *Geol Acta* 6:55–67
- Thomas T, Livermore RA, Pollitz F (2003) Motion of the Scotia Sea plates. *Geophys J Int* 155:789–804
- Twiss RJ, Unruh JR (1998) Analysis of fault slip inversion: Do they constrain stress or strain rate? *J Geophys Res* B103:12205–12222
- Tyrell GW (1945) Report on rocks from West Antarctica and the Scotia Arc. *Discovery Rep* 23:37–102
- Vérard C, Flores K, Stampfli G (2012) Geodynamic reconstructions of the South America-Antarctica plate system. *J Geodyn* 53:43–60
- Waldmann N, Anselmetti FS, Arizteguin D, Austin JA, Pirouzn M, Moyz CM, Dunbark R (2011) Holocene mass-wasting events in Lago Fagnano, Tierra del Fuego (54°S): implications for paleoseismicity of the Magallanes-Fagnano transform fault. *Basin Res* 23:171–190
- Wallace RE (1951) Geometry of shearing stress and relation to faulting. *J Geol* 59:118–130

- Walpersdorf A et al (2015) Coherence between geodetic and seismic deformation in a context of slow tectonic activity (SW Alps, France). *J Geodyn* 85:58–65.
- Wells DL, Coppersmith KJ (1994) New empirical relationships among magnitude, rupture length, rupture width, rupture area and surface displacement. *Bull Seismol Soc Am* 84:974–1002
- Wessel P, Smith WH (1991) Free software helps map and display data. *EOS Trans Am Geophys Union* 72:445–446
- Wiemer SA (2001) software package to analyse seismicity: ZMAP. *Seismol Res Lett* 72:373–382
- Winslow MA (1982) The structural evolution of the Magallanes basin and neotectonics in the Southernmost Andes. In: Craddock C (ed) *Antarctic geosciences, symposium on antarctic geology and geophysics*. University of Wisconsin Press, Madison, pp 143–154
- Yamaji A (2000) The multiple inverse method: a new technique to separate stresses from heterogeneous fault-slip data. *J Struct Geol* 22:441–452
- Yamaji A (2003) Are the solutions of stress inversion correct? Visualization of their reliability and the separation of stresses from heterogeneous fault-slip data. *J Struct Geol* 25:241–252
- Yamaji A, Otsubo M, Sato K (2006) Paleostress analysis using the Hough transform for separating stresses from heterogeneous fault-slip data. *J Struct Geol* 28:980–990
- Zoback ML, Zoback MD, Adams J, Assumpcao M, Bell S, Bergman EA (1989) Global patterns of tectonic stress. *Nature* 341:291–298

Kinematic Evolution of the Southern Andean Orogenic Arc

Marco Maffione

Abstract In the classic book ‘Origin of Continents and Oceans’ written 40 years before the plate tectonics theory was postulated, Alfred Wegener suggested that map-view curvatures in orogenic belts were the result of the motion of continents. In the mid-1950s, Carey coined the term ‘orocline’ to indicate a curved mountain belt formed by secondary bending of an originally straight orogen. Oroclines are genetically different from primary arcs, which are curved mountain belts whose curvature is primary and not due to secondary tectonic processes. A typical example of curved mountain belt is the southernmost segment of the Andean Cordillera, where the regional N–S trend of the Patagonian Andes sharply changes to ESE–WNW in the Fuegian Andes south of 53°S. Given the complex tectonic history of this region and the paucity of geological constraints, the nature, timing of deformation, and kinematics of formation of this orogenic bend have long been debated since its first definition by Carey as ‘Patagonian orocline.’ The dispute revolves around the question whether the southernmost Andes is an orocline or a primary arc. Implications for both options are significant and directly related to the understanding of fundamental tectonic processes operating at plate boundaries. More specifically, unraveling the tectonic evolution of the curved segment of the southernmost Andes is key to understand the geodynamic evolution of this region and the complex interaction between South America, Scotia, and Antarctica plates. Based on paleomagnetic, structural, and magnetic fabric data gathered in the last four decades, the orogenic curvature of the southernmost Andes does not specifically fit in any of the classic definitions of curved mountain belts, as it rather represents a ‘hybrid’ curved belt. While the outer side of the curvature (inner structural domains) seems to represent an orocline (or a progressive arc), the inner part of the curvature (external structural domains) developed as a primary arc throughout the Cenozoic. For this reason, the more generic term of ‘Patagonian Arc’ has recently been proposed as a more suitable name to describe the curved segment of the southernmost Andes. While oroclinal bending of the external part of the arc is generally associated with the closure of the Rocas Verdes marginal basin

M. Maffione (✉)

Department of Earth Sciences, Utrecht University, Utrecht, The Netherlands
e-mail: m.maffione@uu.nl

in Late Cretaceous–Early Paleocene times, the mechanisms of formation of the primary arc represented by the Magallanes fold and thrust belt are unclear. A recent model proposed that slip-partitioning mechanisms along preexisting fault controlled the formation of the Magallanes fold and thrust belt by enabling propagation of \sim N-ward and \sim ENE-ward contraction in the Fuegian and Southern Patagonian Andes, respectively. Future studies are, however, still needed to better constrain the timing and kinematics of formation of the Patagonian Arc.

Keywords Southernmost Andes · Magallanes fold and thrust belt · Orocline · Primary arc · Tectonics · Deformation · Paleomagnetism

1 Introduction

The area encompassing the South America, Scotia, and Antarctica plates underwent a complex tectonic history, characterized by alternation of extensional, compressive, and strike-slip tectonics over time and space (Klepeis and Austin 1997). Within this extremely variable tectonic regime, a regional-scale curvature developed in the southernmost segment of the Andean Cordillera at the tip of the South American plate, namely Patagonian orocline (Carey 1958). Ambiguities, however, reside on the use of the term ‘orocline’ for such curvature. While the term orocline (*sensu stricto*) denotes an orogenic curvatures developed after the bending of an originally straight mountain belt, the nature, style, and timing of the tectonic processes leading to the formation of the Patagonian orogenic curvature, as well as their timing and kinematics, have remained elusive for a long time and are still not entirely understood.

Curved mountain belts may be primary arcs, progressive arcs, or oroclines, depending on whether or not the curvature is acquired during secondary tectonic processes involving vertical-axis rotations of different portions of the arc. So far, all the three hypotheses have been considered to explain the present-day curvature of the southernmost Andes. Defining the true nature of this orogenic arc is key to constrain the fundamental tectonic processes operating at plate boundaries and, more in particular, the tectonic evolution of the region at the intersection between the South American, Scotia, and Antarctica plates.

For a long time, it has been thought that the specular curvature of the South American and Antarctic continents could be genetically connected with the formation of the Scotia plate and the opening of the Drake Passage between them. In the last four decades, structural geological, paleomagnetic, and magnetic fabric constraints have been instrumental to characterize the kinematics and timing of deformation at the southernmost Andes and frame these results into a broader regional context. Here, a comprehensive review of the up-to-date paleomagnetic, structural, and magnetic fabric data is presented, together with a discussion on current models and future challenges.

2 Geological and Tectonic Setting of the Southernmost Andes

The southernmost Andes is composed of five adjacent tectonic domains; from the hinterland toward the foreland, they are as follows: (1) a Late Jurassic–Neogene magmatic arc (Patagonian batholith, see Guillot 2016) formed during initial subduction below South America (Hervé et al. 1984, 2007; Pankhurst et al. 2000; González Guillot et al. 2011); (2) a marginal basin assemblage (Rocas Verdes basin) composed of oceanic floor relics (Stern and De Witt 2003; Cunningham 1994) and overlying sediments (Calderón et al. 2007; Olivero and Malumián 2008); (3) a metamorphic core zone (Cordillera Darwin) exposing uplifted blocks of the metamorphosed Paleozoic basement (Kohn et al. 1995; Klepeis 1994; Hervé et al. 2008; Klepeis et al. 2010; Maloney et al. 2011, 2013); (4) a fold and thrust belt (Magallanes fold and thrust belt) formed by deformation of a ~7-km-thick Upper Cretaceous–Miocene foreland marine sedimentary sequence (Biddle et al. 1986; Alvarez-Marrón et al. 1993; Klepeis 1994; Olivero and Malumián 1999; Olivero et al. 2003; Ghiglione et al. 2002; Ghiglione and Ramos 2005; Malumián and Olivero 2006; Olivero and Malumián 2008; Torres Carbonell et al. 2008); (5) an undeformed foreland basin (Magallanes-Austral basin). The E–W-trending Magallanes-Fagnano left-lateral strike-slip fault system cut preexisting structures of the Fuegian Andes from the Atlantic to the Pacific coast of South America and is considered the present-day South America–Scotia transform plate boundary (Cunningham 1993, 1995; Barker 2001; Lodolo et al. 2002, 2003; Eagles et al. 2005; Rossello 2005).

To the south, the deep-sea Drake Passage separates South America from Antarctica (Barker 2001; Eagles et al. 2005; Livermore et al. 2005; Lodolo et al. 1997, 2006; Eagles 2016). The opening of the Drake Passage is believed to have played an important role in global climate changes. The formation of this marine ‘gateway’ may have triggered the onset of the Antarctic Circumpolar Current (Lawver and Gahagan 2003; Barker et al. 2007a), which thermally isolated the Antarctic continent resulting in local development of permanent ice sheets (Barker et al. 2007b). Such event seems to have had global repercussion as suggested by its synchronicity with the onset of a global cooling event at the Eocene/Oligocene boundary (Zachos et al. 2001). The opening of the Drake Passage is commonly related to the spreading of the Scotia Sea, where oldest marine magnetic anomalies have been dated back to 34–28 Ma (Lawver and Gahagan 2003; Livermore et al. 2005; Lodolo et al. 2006).

Tectonic style changes considerably across the southernmost Andes. The internal structural domains exposing magmatic and metamorphic units are characterized by thick-skinned tectonics involving basement rocks; in the external domains, mainly non-metamorphic sedimentary rocks are involved in a thin-skinned deformation, which led to the formation of a fold and thrust belt (Ghiglione and Ramos 2005; Torres Carbonell et al. 2008, 2013). Overall, fold axes and thrust faults strike

sub-parallel to the regional trend of the orogenic curvature. Both domains are folded into a curved orogen showing an interlimb angle of $\sim 110^\circ$. In the northern segment of the curvature (Southern Patagonian Andes) the main structural directions (fold axes and faults) are NNW–SSE, while in the southern branch (Fuegian Andes), they progressively change from NW–SE in the bend hinge to E–W and ENE–WSW to the east along the Atlantic Coast.

3 Tectonic Evolution of the Southernmost Andes

To understand how a large-scale orogenic curvature developed at the southernmost Andes, it is essential to analyze the sequence of tectonic events that characterized the formation of the Andean Cordillera in this sector. During the first stages of emplacement of the magmatic arc, an extensional tectonic phase affected the western margin of the South American plate, resulting in lithospheric attenuation. The extensional faults cutting the continental margin of South America played a key role in controlling the subsequent sedimentation and deformation in the Magallanes-Austral foreland basin during the early orogenic phases (Winslow 1982; Fosdick et al. 2011, 2015; Likerman et al. 2013; Ghiglione et al. 2013). This extensional tectonic event culminated in the opening of the Rocas Verdes backarc marginal basin in the Late Jurassic (Kyrztz 1973; Dalziel et al. 1974; Bruhn and Dalziel 1977; Bruhn et al. 1978; Dalziel 1981; Calderón et al. 2007). Sedimentation in the marginal basin continued during the Early Cretaceous (Wilson 1991; Fildani and Hessler 2005; Olivero and Malumián 2008; Klepeis et al. 2010). Opening of the South Atlantic Ocean at ~ 100 Ma transmitted compression into the Rocas Verdes marginal basin, leading to widespread thrusting episodes (Hervé et al. 1981; Biddle et al. 1986). This regional tectonic event marked the onset of the main tectonic phase in the southernmost Andes during basin closure. Contraction propagating into the basin led to regional ductile deformation, isoclinal folding, and low-grade metamorphism of its sedimentary infill (Bruhn 1979). Deep burial of underthrust basement continental rocks of the South American plate currently exposed in Cordillera Darwin led to peak metamorphism at upper amphibolite facies conditions (7–11 kbar and 580–600 °C; Kohn et al. 1993) (Klepeis et al. 2010; Maloney et al. 2011).

In the Late Cretaceous between ~ 100 and 86 Ma, complete closure of the Rocas Verdes basin determined the collision of the Patagonian batholith against the South American continental margin (Halpern and Rex 1972; Bruhn and Dalziel 1977; Cunningham 1994, 1995; Klepeis et al. 2010; Calderón et al. 2012). This major event caused thick-skinned deformation in the South American continental margin and possibly initial continental basement blocks uplift. This early contractional episode has been constrained in time by $^{40}\text{Ar}/^{39}\text{Ar}$ and fission track thermochronology from Cordillera Darwin, which has shown cooling ages as old as

90–70 Ma (Nelson 1982; Kohn et al. 1995). Furthermore, growing of the orogenic wedge produced the first foreland deposits whose basal depositional age has been constrained at 101–88 Ma using U/Pb in tuffs and detrital zircons (Fildani et al. 2003; Fosdick et al. 2011; McAtamney et al. 2011).

Crustal thickening in the hinterland characterized by out-of-sequence thrusting, continued throughout the Late Cretaceous and Paleogene, yielding uplifting of the most internal structural domains, and continuous lithospheric loading, flexural subsidence, and sedimentation in the foreland basin (Winslow 1981; Biddle et al. 1986; Ramos 1989; Wilson 1991; Alvarez-Marrón et al. 1993; Klepeis 1994; Coutand et al. 1999; Fildani et al. 2003; Olivero et al. 2003; Ghiglione et al. 2010, 2016a, b). Since then, propagation of deformation in the foreland basin produced the Magallanes fold and thrust belt. In the Fuegian Andes, also thanks to the presence of well-developed syntectonic unconformities in the sedimentary record, most of the main compressive events have been identified and constrained in time. The first compressive event in the fold and thrust belt, marked by the San Vicente thrust, occurred at 61–55 Ma (Ghiglione and Ramos 2005) or slightly before (Torres Carbonell et al. 2013). Compression in the foreland basin continued through the Eocene with the Rio Bueno thrusting event (49–34 Ma; Ghiglione and Ramos 2005) and other minor events in the Early Eocene and Late Oligocene (Alvarez-Marrón et al. 1993; Olivero et al. 2003; Olivero and Malumián 2008; Torres Carbonell et al. 2008, 2013). The Punta Gruesa strike-slip event (~24–16 Ma) marked the beginning of the strike-slip tectonics associated with the development of the Magallanes-Fagnano fault system (Cunningham 1993, 1995; Ghiglione 2002; Lodolo et al. 2003; Eagles et al. 2005; Rossello 2005). Finally, sub-horizontal units above Lower Miocene beds marked the end of compressional tectonics in the southern Magallanes-Austral basin (Ghiglione et al. 2010).

Along-strike age constraints from the Southern Patagonian Andes are not sufficient to test whether the tectonic phases occurred synchronously throughout the southernmost Andes. Few events have been defined in the Patagonian Andes, suggesting that deformation may have been, at least occasionally, synchronous. Paleocene deformation in the Patagonian Andes was mainly localized in the Basement domain (Kraemer 1998). Collision of the Farallon–Phoenix ridge in the Middle Eocene (Cande and Leslie 1986; Somoza and Ghidella 2005, 2012) determined an eastward shifting of the orogenic front into the foreland. Angular unconformities and growth strata at Río Turbio (Malumián et al. 2000), and emplacement of an Eocene basaltic plateau (Mesetas) (Ramos 1989, 2005) were the direct evidence of this tectonic event. A major compressive phase and uplift in the Paleogene has also been identified in the eastern sectors of the Southern Patagonian Andes using zircon (U–Th)/He dating (Fosdick et al. 2013). To the south, fast ~NE-directed subduction of the Phoenix plate between 47 and 28 Ma resulted in more substantial tectonic deformations (Ramos and Aleman 2000; Kraemer 2003; Ghiglione and Ramos 2005; Somoza and Ghidella 2005, 2012; Ghiglione and Cristallini 2007). Compressive events in the western domains of the Patagonian

Andes during the Late Oligocene (30–23 Ma; Thomson et al. 2001) propagating to the east in the Early Miocene (22–18 Ma; Fosdick et al. 2013) and Middle to Late Miocene (12–8 Ma; Thomson et al. 2001) have also been identified using apatite fission track and apatite and zircon (U–Th)/He age constraints.

4 The Contribution of Paleomagnetism to the Study of Curved Mountain Belts

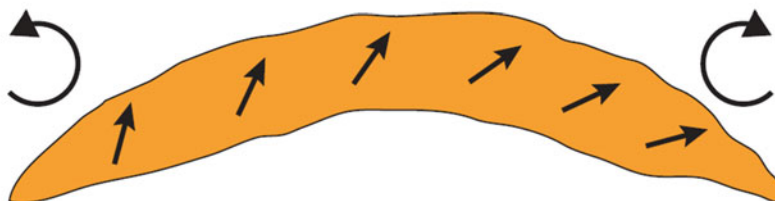
Carey (1955) first introduced the concept of ‘orocline’ to describe an originally straight mountain belt whose map-view curvature has been acquired during younger tectonic phases. Formation of oroclines, therefore, necessarily requires vertical-axis block rotation of different parts of the curvature. Oroclines are genetically distinguished from primary arcs where curvature is not acquired upon block rotation but represents a primary feature.

More recently, Weil and Sussman (2004) and Marshak (2004) proposed new classifications and terminology, respectively, for map-view curved orogens. Weil and Sussman (2004) distinguished three different types of orogenic arcs based on the time relationship between thrusting and vertical-axis rotations: non-rotational arcs, progressive arcs, and oroclines. Non-rotational (or primary) arcs are orogenic curves that formed originally curved, with no tectonic rotations occurring during their formation. Progressive arcs and oroclines are both secondary arcs, meaning that they acquired their curvature after secondary processes. Progressive arcs gradually increase their curvature during deformation, and tectonic rotations are synchronous to the main thrusting phase. In oroclines, the curvature develops after bending of an originally straight belt. Tectonic rotations in oroclines are therefore subsequent to the main tectonic phase, i.e., the one that produced the originally straight orogenic belt.

Being able to detect the amount and timing of tectonic rotations in curved mountain belts is therefore essential to constrain their nature and untangle the tectonic processes responsible for their formation. Since the 1980s, paleomagnetism has been widely used in the study of orogenic arcs (Van der Voo and Channell 1980; Eldredge et al. 1985; Lowrie and Hirt 1986; Van der Voo 1993, 2004; Van der Voo et al. 1997; Speranza et al. 1997; Muttoni et al. 1998; Marshak 2004; Cifelli et al. 2007; Maffione et al. 2008, 2009, 2010, 2013; Yonkee and Weil 2010; Weil et al. 2010; Weil and Sussman 2004). Paleomagnetism can in fact quantify absolute and relative magnitudes of block rotations by determining changes in paleomagnetic remanence vectors between individual localities (Fig. 1). Paleomagnetic data are key constraints to define horizontal- and vertical-axis rotation patterns in curved orogenic systems; yet, structural and strain data should also be considered and integrated to define the bulk translation (slip on major faults) and internal strain (accommodated by cleavage and minor folds and faults).



BEFORE: Straight mountain belt; the paleomagnetic directions (arrows) are parallel



AFTER: Orocline; the paleomagnetic directions (arrows) vary along the curvature

Fig. 1 Illustration of the consequences of oroclinal bending on the pattern of magnetic declination in a thrust belt. The *orange-shaded area* represents the mountain belt in map view, and the *arrows* represent paleomagnetic directions. (*Above*) Before bending, all *arrows* point in the same direction. (*Below*) Bending deflects the paleomagnetic directions along the strike of the bend

Reliable tectonic models should therefore be reconstructed using a combined approach where paleomagnetism and strain analysis represent the main tools.

5 Paleomagnetic Constraints from the Southernmost Andes

The observed geometrical relationships in the southernmost Andes initially induced Carey (1958) and then Dalziel and Elliot (1973) to propose a similar amount of bending that occurred to produce the present-day geometry, starting from a relatively straight orogen. In particular, Dalziel and Elliot (1973) put forward that a symmetrical bending of the southernmost Andes and northern tip of the Antarctic Peninsula occurred as a consequence of the opening of the Drake Passage. Since then, also because of the name (Patagonian orocline) given by Carey, this regional-scale curvature of the southernmost Andes has been considered an orocline until first controversial paleomagnetic data became available, questioning the real tectonic origin (rotational versus non-rotational arc, *sensu* Marshak 1988) of the curvature.

In this section, a comprehensive review of the available paleomagnetic data in the southernmost Andes is presented and discussed. The quality of these

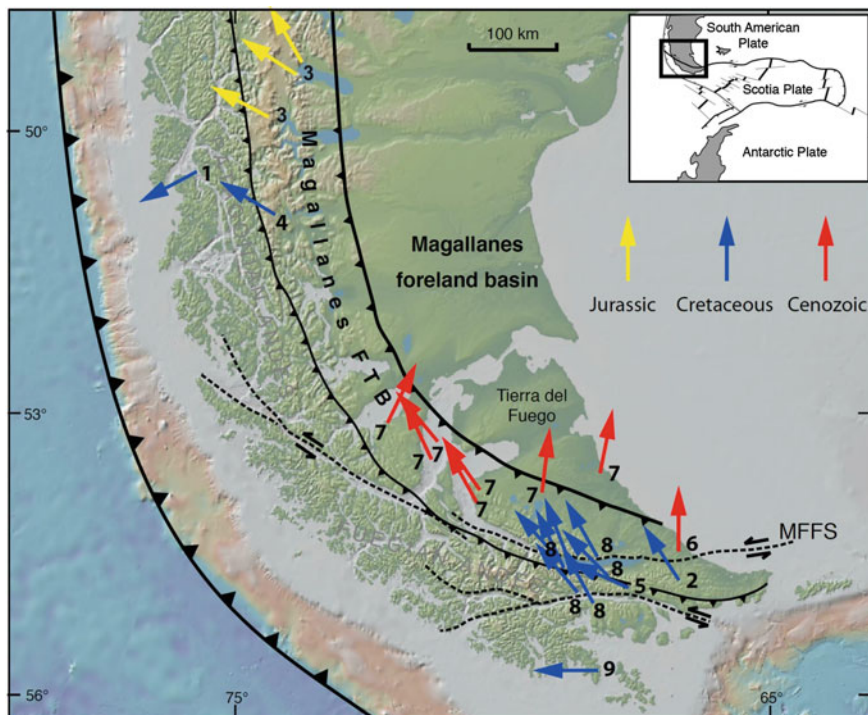


Fig. 2 Available paleomagnetic directions from the southernmost Andes (arrows). Numbers refer to the relative work: 1 Rapalini et al. (2001); 2 Baraldo et al. (2002); 3 Iglesia Llanos et al. (2003); 4 Rapalini et al. (2004); 5 Rapalini et al. (2005); 6 Maffione et al. (2010); 7 Poblete et al. (2014); 8 Rapalini et al. (2015); 9 Cunningham et al. (1991). *MFFS* Magallanes-Fagnano fault system. *FTB* fold and thrust belt

paleomagnetic data is critically evaluated, and the dataset filtered to consider only the most reliable data that are relevant for tectonic interpretations (Fig. 2 and Table 1). The adopted filtering criteria are as follows: (1) Paleomagnetic analyses followed modern standard techniques (e.g., stepwise demagnetization); (2) paleo-horizontal controls are available, or in their absence, a large dataset is considered; and (3) the age of magnetization can be identified.

5.1 Southern Patagonian Andes

A northern boundary located at $\sim 48^{\circ}\text{S}$ can be identified in the southernmost Andes for the area subjected to tectonic vertical-axis rotations. North of this boundary, the absence of tectonic rotations in Jurassic to Cretaceous rocks has been documented by several authors (Roperch et al. 1997; Beck et al. 2000; Iglesia Llanos et al. 2003).

Table 1 Available paleomagnetic results from the Southern Andes

Lithology	Age	Magnetization age (Ma)	N	Rotation	Flattening	Paleohorizontal control	Author
Sediments/volcanics	U. Jurassic-L. Cretaceous	Mid-Late Cretaceous?	7	-90.0 ± 12	-0.2	No	Cunningham et al. (1991)
Ignimbrite/tuff/lava	Upper Jurassic	Late Jurassic	5	-30 ± 14	-	Yes	Iglesia Llanos et al. (2003)
Ignimbrite/tuff/lava	Upper Jurassic	Late Jurassic	4	-57 ± 9	-	Yes	Iglesia Llanos et al. (2003)
Ignimbrite/tuff/lava	Upper Jurassic	Late Jurassic	4	-62 ± 15	-	Yes	Iglesia Llanos et al. (2003)
Basalts and limestones	U. Carboniferous-L. Permian	Post-Early Cretaceous	9	-117.7 ± 29.9	5.4 ± 9.7	No	Rapalini et al. (2001)
Lava/dykes/sills	Upper Jurassic	Late Cretaceous?	1	-59 ± 17	-	No	Rapalini et al. (2004)
Sills/volcanics	Upper Jurassic	Late Cretaceous?	3	-66 ± 10	-	No	Rapalini et al. (2005)
Monzodiorite	Upper Cretaceous (93 ± 4 Ma)	Late Cretaceous	1	-33 ± 7	-	No	Baraldo et al. (2002)
Sediments	lower Eocene	Lower Eocene	1	-5.6 ± 12.5	-33.8 ± 8.3	Yes	Maffione et al. (2010)
Sediments	lower Eocene	Lower Eocene	1	-3.7 ± 12.3	-50.4 ± 9.7	Yes	Maffione et al. (2010)
Sediments	middle-upper Eocene	middle-late Eocene	1	-16.7 ± 19.2	-36.0 ± 11.4	Yes	Maffione et al. (2010)
Sediments	middle-upper Eocene	middle-late Eocene	1	6.3 ± 15.9	-54.2 ± 9.9	Yes	Maffione et al. (2010)
Sediments	U. Eocene-L. Oligocene	L. Eocene-E. Oligocene	1	-19.2 ± 20.7	-37.9 ± 15.7	Yes	Maffione et al. (2010)
Sediments	Paleocene	Paleocene	1	-15.4 ± 8.5	-5.3 ± 3.5	Yes	Poblete et al. (2014)
Sediments	Paleocene	Paleocene	1	-26.3 ± 15.1	0.1 ± 5.3	Yes	Poblete et al. (2014)
Sediments	Paleocene	Paleocene	1	-1.6 ± 8.6	-6.9 ± 3.7	Yes	Poblete et al. (2014)
Sediments	Paleocene	Paleocene	1	-22.9 ± 11.6	6.5 ± 3.2	Yes	Poblete et al. (2014)
Sediments	Paleocene	Paleocene	1	-21.8 ± 8.9	0.3 ± 3.1	Yes	Poblete et al. (2014)
Sediments	Paleocene	Paleocene	1	26.1 ± 15.2	-0.5 ± 5.5	Yes	Poblete et al. (2014)
Sediments	Paleocene	Paleocene	1	16.7 ± 11.3	-9.1 ± 4.1	Yes	Poblete et al. (2014)
Pluton	Upper Cretaceous	Late Cretaceous	5	-29.2 ± 6.1	35.9 ± 3.9	No	Rapalini et al. (2015)
Pluton	Upper Cretaceous	Late Cretaceous	7	-20.8 ± 16.5	17.7 ± 13.3	No	Rapalini et al. (2015)
Dacite	Upper Cretaceous	Late Cretaceous	3	-40.2 ± 7.9	2.6 ± 5.7	No	Rapalini et al. (2015)
Pluton	Upper Cretaceous	Late Cretaceous	3	-28.5 ± 9.7	-3.3 ± 6.3	No	Rapalini et al. (2015)
Sills	Upper Jurassic	Late Cretaceous	1	-44.6 ± 12.0	9.7 ± 8.0	No	Rapalini et al. (2015)
Sills	Upper Jurassic	Late Cretaceous	1	-41.7 ± 17.7	-0.3 ± 13.4	No	Rapalini et al. (2015)
Sills	Upper Jurassic	Late Cretaceous	1	-25.4 ± 9.5	11.1 ± 5.1	No	Rapalini et al. (2015)

To the south, between 48°S and 50°S post-Late Jurassic counterclockwise (CCW) rotation of $30^\circ \pm 14^\circ$, $57^\circ \pm 9^\circ$, and $62^\circ \pm 15^\circ$ has been documented from the Upper Jurassic El Quemado Complex, a suite of sedimentary and volcanic rocks (Iglesia Llanos et al. 2003). The authors interpreted these rotations as the effect of local tectonics unrelated to the formation of the regional curvature of the orogen. Further south, remagnetized samples from upper Carboniferous to lower Permian basalts and lavas from the Madre de Dios Archipelago on the Pacific coast have shown $118^\circ \pm 30^\circ$ of CCW rotation of possible post-Early Cretaceous age (Rapalini et al. 2001), interpreted as the result of strike-slip tectonics characterizing the frontal part of the orogen, adjacent to the Pacific trench. At $\sim 52^\circ$ S, within more external domains of the belt, data from Upper Jurassic–Lower Cretaceous lava, dykes, and sills from the Sarmiento ophiolite have shown a $59^\circ \pm 17^\circ$ post-Late Cretaceous CCW rotation of possible local tectonics origin (Rapalini et al. 2004).

Excluding rotations associated with the local tectonics, it can be concluded that this sector of the southernmost Andes did not undergo significant rotation relative to stable South America.

5.2 *Fuegian Andes*

The first paleomagnetic data from the Fuegian Andes were obtained by Dalziel et al. (1973) from Mesozoic granodiorite plutons and Cenozoic dykes from 27 sites distributed across three main areas within the most internal structural domains of the belt: Navarino Island, the western Canal Beagle, and the southern Chile fiords region north of 52°S. These authors documented progressive variation of the paleomagnetic directions along the orogenic curvature, with CCW rotations increasing southward up to 150°. Conversely, paleomagnetic directions from the Cenozoic samples did not show significant geographical variation. The authors interpreted these results as clear evidence of a secondary origin of the curvature of the southernmost Andes, as previously speculated by Carey (1958). Shortly after, Burns et al. (1980) carried out a more extensive paleomagnetic sampling from Jurassic volcanics (Tobifera Formation) and Cretaceous to Cenozoic dykes and sills from more external structural domains of the belt. Maximum rotations up to 48° CCW, much lower than the whole curvature of the orogen ($\sim 90^\circ$) led these authors to propose that the paleomagnetic data recorded only part of the oroclinal bending. Burns et al. (1980) suggested that rotations started in the Late Jurassic and continued until Miocene times.

Although the early works of Dalziel et al. (1973) and Burns et al. (1980) have for long been the most significant to be consider for the oroclinal bending hypothesis, data processing and interpretation do not satisfy modern standard reliability criteria (Van der Voo 1990). The low reliability of these data is due to the fact that paleomagnetic directions were not obtained using (now broadly used) stepwise demagnetization technique and principal component analysis (Kirschvink 1980) to discriminate between different components of the magnetic remanence. These studies, in contrast, adopted old-fashioned blanket demagnetization techniques with

no application of vectorial analysis. For this reason, the paleomagnetic directions from these studies are not reliable and should not be used to test the orocline hypothesis in the southernmost Andes.

Paleomagnetic data satisfying standard reliability criteria were then gathered almost one decade later by Cunningham et al. (1991). These authors sampled seven sites within sedimentary rocks, mafic sills, volcanoclastic breccias, debris flow deposits, and a pyroclastic unit from the Lower Cretaceous Andean magmatic arc on Peninsula Hardy in the most internal structural domains of the orogen. Consistent normal polarity directions and a negative fold test indicated remagnetization of these rocks during the Cretaceous normal polarity super-chron (102–83.3 Ma). Based on the isolated paleomagnetic directions, a consistent $90^\circ \pm 12^\circ$ CCW rotation was calculated for the studied area. Cunningham et al. (1991) proposed that this rotation reflected a uniform $\sim 90^\circ$ rotation of the entire Fuegian Andes occurred between ~ 100 and 35 Ma, prior to the opening of the Drake Passage. A combined effect of the closure of the Rocas Verdes marginal basin and the regional transpressional regime was invoked as the main driving mechanisms for the oroclinal bending.

To the north, toward more external structural domains, Rapalini et al. (2005) reported $66^\circ \pm 10^\circ$ of CCW rotation from a Upper Jurassic basaltic sill of the Lemaire Formation, likely remagnetized during the Late Cretaceous and a Upper Cretaceous dacite near Ushuaia. CCW rotations of $33^\circ \pm 7^\circ$ were also documented from Upper Cretaceous (93 ± 4 Ma) monzodiorites from the hinterland in Tierra del Fuego (Baraldo et al. 2002). Within the same structural domain, Rapalini et al. (2015) sampled Upper Jurassic–Lower Cretaceous metabasalts and metagabbros. Reliable paleomagnetic directions were obtained from six different geological bodies at 26 sites. Ages of the plutons, previously established with different geochronological methods, range between 72 and 85 Ma. Since these intrusive bodies were emplaced after the main Andean tectonic phase in the hinterland of the Fuegian Andes, their remanences were interpreted to be primary (hence acquired during the cooling of the magmatic bodies). Less clear is the age of magnetization for the Upper Jurassic sills of the Lemaire Formation, which has been tentatively attributed by these authors to ~ 80 Ma. None of the units sampled by Rapalini et al. (2015) provided paleohorizontal controls, implying that in situ paleomagnetic direction was used for tectonic interpretations. Three out of ten mean directions showed unusual low inclinations, likely due to the effect of local tilt. The remaining seven reliable mean directions showed consistent CCW rotations varying between $21^\circ \pm 16^\circ$ and $45^\circ \pm 12^\circ$. Based on these data, Rapalini et al. (2015) proposed a uniform 30° of CCW rotation of the central structural domains of the Fuegian Andes occurred after Late Cretaceous times (72 Ma) following to (partial) oroclinal bending of the Fuegian Andes. However, these authors did not exclude the possibility for these rotations to be caused by local deformation.

Surprisingly, the Magallanes fold and thrust belt has only recently received the attention of paleomagnetists despite its high potential to preserve primary magnetizations, due to the absence of metamorphism, and provides paleohorizontal-controlled paleomagnetic directions. The most comprehensive paleomagnetic study

(85 sites), encompassing large part of the northern and southern branches of the Magallanes fold and thrust belt, is that of Poblete et al. (2014). Unfortunately, due to the low intensity and stability of magnetization, and the absence of paleohorizontal control for several sites, reliable paleomagnetic directions could be obtained from only seven sites from the Paleocene (~ 65 Ma) sedimentary units of the Magallanes fold and thrust belt in the Magallanes and Tierra del Fuego provinces. Excluding two sites that provided anomalous moderate clockwise (CW) rotations, and one site at the northern edge of the fold and thrust belt in Tierra del Fuego showing no significant rotation, the remaining four sites located in the Magallanes province and western Tierra del Fuego showed consistent CCW rotations ranging between $15^\circ \pm 9^\circ$ and $26^\circ \pm 15^\circ$. The authors interpreted these rotations as resulted from the accommodation of differential shortening, increasing eastward, rather than oroclinal bending of the Fuegian Andes.

The most external domains of the Magallanes fold and thrust belt were sampled by Maffione et al. (2010). Due to the low intensity and stability of the remanence, only five sites out of 22 provided reliable paleomagnetic directions. Although somewhat noisy, the remanence isolated at these five sites was interpreted to be pre-folding and likely primary, with opposite polarity directions that passed the fold test. The mean paleomagnetic directions at these five sites have an inclination that is substantially lower than expected, likely because of compaction of the clay-rich sediments during diagenesis. Despite the limitation due to the low number of sites and the not ideal quality of data, this study provided the first paleomagnetic constraints from the Cenozoic sedimentary sequences of the Magallanes-Austral basin. The results of this study have three major implications. First, the absence of rotations in the Fuegian Andes during the last ~ 50 Ma excluded that oroclinal bending occurred during the formation of the fold and thrust belt. Second, the curved Magallanes fold and thrust belt mainly developed during the Cenozoic; hence, the absence of tectonic rotations since 50 Ma classifies it as a non-rotational (primary) arc. Third, the present-day curvature of the southernmost Andes was already acquired prior to the opening of the Drake Passage in the Early Oligocene. This implies that the opening of the Drake Passage and growth of the Scotia plate did not play any role in the evolution of the curvature at the southernmost Andes.

5.3 *Antarctic Peninsula*

Data from the curved segment of the Antarctic Peninsula, mirroring the shape of the southernmost Andes, are scarce but sufficient to exclude any connection between the tectonic evolutions of the two continental margins. Early paleomagnetic data from the Antarctic Peninsula (Grunow 1993) documented in fact two distinct phases of earlier rotation: CW with respect to East Antarctica between 175 and 155 Ma due to the early opening in the Weddell Sea basin, and CCW with respect to West Antarctica in the 155–130 Ma time interval. Poblete et al. (2011) reported paleomagnetic results from Permo-Triassic and Jurassic rocks remagnetized during

the Middle Cretaceous and primarily magnetized Cretaceous and Cenozoic rocks. These data indicated no relative rotations between the different sectors of the Antarctic Peninsula since the Cretaceous. Therefore, well before the beginning of the Andean orogeny in the Late Cretaceous, the curved shape of the Antarctic Peninsula was already developed.

6 Structural and Strain Data from the Southernmost Andes

The most prominent structural feature of the southernmost Andes is the change in direction of its structural lineaments. The main strike of faults and fold axes varies from 345° in the Southern Patagonian Andes to 320° – 295° at the hinge of the bend and to 285° – 260° in the Fuegian Andes. This geometry is reflected in a similar variation of the shortening directions along the curvature. Diraison et al. (2000) carried out an extensive structural geological study measuring 1600 fault planes in Mesozoic–Cenozoic sedimentary units of the Magallanes fold and thrust belt. Shortening directions in the southernmost Andes are sub-perpendicular to major folds and thrusts and progressively rotate from 075° in the Southern Patagonian Andes to 052° in the western part of the Fuegian Andes and to 043° in the eastern Fuegian Andes (Fig. 3) (see Sue and Ghiglione 2016 for a review). At the easternmost tip of the Fuegian Andes \sim N–S, shortening directions have also been documented by Diraison et al. (2000) and Torres Carbonell et al. (2013).

These two studies also showed a progressive southeastward increase of the shortening in the Fuegian Andes from ~ 5 to ~ 22 %. Shortening estimates along the belt are quite variable. Regional balanced cross sections of the Fuegian Andes by Kraemer (2003) indicated a total shortening of 300–600 km. This author proposed that most of this shortening occurred in the Middle Cretaceous during the closure of the Rocas Verdes marginal basin, while minor shortening was accommodated during subsequent tectonic phases until the Neogene. Kraemer (2003) suggested that the amount of shortening in the southernmost Andes was consistent with a model of oroclinal bending.

Besides fault kinematic analyses, anisotropy of magnetic susceptibility (AMS) is a powerful tool to perform strain determination even when macroscopic kinematic constraints are either absent or difficult to identify (Tarling and Hrouda, 1993; Sagnotti et al. 1994; Parés et al. 1999). Clustering of the longest axis of the AMS ellipsoid defines a magnetic lineation, which tends to orient sub-parallel to the maximum axis of the strain ellipsoid during deformation. As a first-order approximation, magnetic lineation is parallel to the shortening direction in compressive settings, or to the stretching direction in extensional regimes. With AMS analyses, it is therefore possible to calculate the style of tectonics (compressive versus extensional) and the shortening or stretching directions.

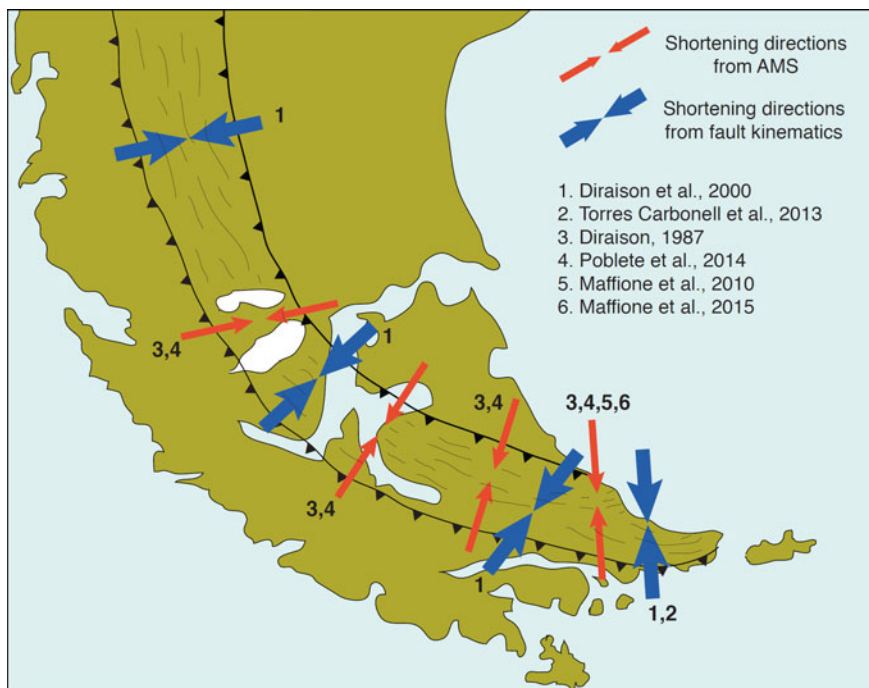


Fig. 3 Shortening directions in the southernmost Andes inferred from fault kinematics analyses (*blue arrows*) and anisotropy of magnetic susceptibility (AMS) analyses (*red arrows*)

Few AMS studies have been performed in the southernmost Andes (Diraison, 1998; Rapalini et al. 2005; Maffione et al. 2010, 2015; Esteban et al. 2011; Poblete et al. 2014). AMS analyses from the non-metamorphic sedimentary units of the Magallanes fold and thrust belt reveal the presence of well-developed magnetic lineations of clear compressive origin, which are sub-parallel to local faults and fold axes (see review by Maffione et al. 2015). These magnetic lineations change in direction following the curvature of the southernmost Andes and rotating from a \sim N-S direction in the Southern Patagonian Andes to a \sim NNE-SSW trend in the Fuegian Andes. Since the orientation of the AMS and strain ellipsoids are comparable, the lineations from the southernmost Andes identify a radial strain pattern where the shortening direction progressively rotate from \sim ENE-WSW in the Southern Patagonian Andes to \sim N-S in the eastern sectors of the Fuegian Andes (Fig. 3). Importantly, Maffione et al. (2015) show that this radial strain field was continuous in this region from the Early Cretaceous until at least the Oligocene (Fig. 4).

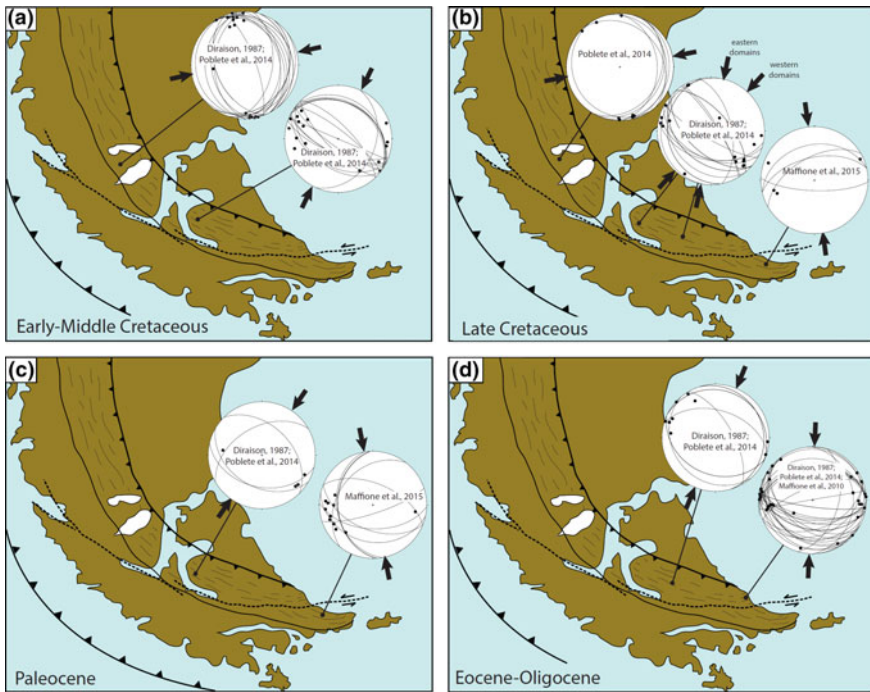


Fig. 4 Evolution of the paleostain field (*black arrows on the stereonets*) within the Magallanes fold and thrust belt during four progressive time intervals, inferred from the published AMS data. Stereonets in each figure show the site mean lineations (*black dots*) and local bedding planes (*great circles*). Redrawn from Maffione et al. (2015)

7 Nature and Tectonic Evolution of the Curved Segment of the Southernmost Andes as Inferred from Available Paleomagnetic and Strain Constraints

Several hypotheses on the origin of the curvature of the southernmost Andes have been put forward since the 1950s in the absence of paleomagnetic and structural constraints. Early models considered the formation of the orogenic curvature as due to the drag associated with the left-lateral shearing between the South America and Scotia–Antarctic plates (Carey 1958; Winslow 1982). Paleomagnetic data obtained since the first study of Dalziel et al. (1973) have been crucial to provide a first-order reconstruction of the main tectonic events responsible for the present-day geometry of the southernmost Andes. However, although the amount and quality of data have recently increased, more than forty years of paleomagnetic investigations in the southernmost Andes have not yet been sufficient to provide a straightforward answer to the key question: Is the curved segment of the southernmost Andes (so far ambiguously called Patagonian orocline) a primary arc or an orocline? In other

words, was the Fuegian Andes a southern extension of the \sim N–S-oriented Patagonian Andes that acquired its present-day ESE–WNW trend after $\sim 90^\circ$ of CCW rigid block rotation?

The causes for such uncertainty are multiple. First and most important cause is the relatively poor quality of the paleomagnetic data. Early works (Dalziel et al. 1973; Burns et al. 1980), which more strongly supported an oroclinal model for the southernmost Andes, cannot be considered, as they do not satisfy modern reliability criteria. Also, rocks exposed in the most internal domains of the belt are either magmatic or metamorphic. Typical magmatic rocks sampled in the previous studies are plutons, dykes, and sills (Cunningham et al. 1991; Rapalini et al. 2001, 2004, 2005; Baraldo et al. 2002). None of these units provide paleohorizontal controls that are necessary to remove the effect of local tilt on the isolated paleomagnetic directions (Morris et al. 1998). Only tilt-corrected directions should be used to calculate the correct magnitude of vertical-axis rotation. Several more recent studies have however proposed that the inevitable scatter of paleomagnetic directions due to local tilt is minimized in large datasets (Poblete et al. 2014; Rapalini et al. 2015). On the other hand, where metamorphic rocks are sampled for paleomagnetic studies, the main issue is related to the definition of the age of magnetization (Cunningham et al. 1991; Rapalini et al. 2004, 2005). During high-temperature metamorphism ($>500^\circ\text{C}$), the original remanence is likely to be reset as soon as the Curie temperatures of the main magnetic carrier are exceeded, with acquisition of a new remanence at the end of the metamorphism event. Large age uncertainties on the remagnetization event can therefore bias the estimates on the timing of the tectonic rotations. Most of the remagnetized samples from the hinterland of the Fuegian Andes have probably been magnetically overprinted during the Late Cretaceous tectonic phase (Menichetti et al. 2008); still, a precise definition of the timing of the rotations cannot be achieved using metamorphic rocks.

A second issue even when high-quality paleomagnetic data are available is the distinction between regional and local tectonic rotations. The southernmost sector of the Fuegian Andes was affected by widespread left-lateral strike-slip tectonics (Cunningham 1993; Diraison et al. 2000; Menichetti et al. 2008). CCW vertical-axis rotations can be associated with sinistral strike-slip faults. The tectonic rotations documented in the southern Patagonian Andes by Iglesia-Llanos et al. (2003) and Rapalini et al. (2001) are a typical example of rotation associated with local faulting, and similar data should therefore not be used to test the orocline hypothesis (Rapalini 2007). Large strike-slip fault-related rotations have also been identified in the most internal domains of the belt along the southern shore of the Canal Beagle (Rapalini et al. 2015). Local deformation was also invoked as a possible cause of the $\sim 20^\circ$ CCW rotations in the southern sectors of the Magallanes fold and thrust belt (Poblete et al. 2014).

Finally, a third potential cause for the ongoing debate on the nature of the curvature of the southernmost Andes is the scarce and unevenly distributed paleomagnetic sampling coverage that still inhibits precise tectonic reconstructions by shedding uncertainties on the local versus regional character of the tectonic rotations.

So far, all three possible models have been proposed for the nature of the curvature of the southernmost Andes: primary or non-rotational arc (Diraison et al. 2000; Ramos and Aleman 2000; Ghiglione and Cristallini 2007), rotational arc or orocline *sensu stricto* (Dalziel and Elliot 1973; Burns et al. 1980; Cunningham et al. 1991; Kraemer 2003), and a 'hybrid' structure composed of a rotational and a non-rotational arc (Poblete et al. 2014; Maffione et al. 2015; Rapalini et al. 2015). What seems to emerge from the most recent paleomagnetic and structural geological data is that the hybrid model seems the most plausible possibility.

Although, as discussed, paleomagnetic data from Burns et al. (1980) cannot be used for tectonic interpretation, these authors were the first to put forward the hypothesis of a systematic pattern in the Fuegian Andes in which the magnitude of rotations decreased northward from a maximum value of $\sim 90^\circ$ comparable with the interlimb angle between the Patagonian and Fuegian Andes. The available paleomagnetic data seem to confirm this scenario with $\sim 90^\circ$ of CCW rotation of the southernmost (most internal) domains of the Fuegian Andes (Cunningham et al. 1991), $\sim 30^\circ$ of CCW rotations in the central belt where metamorphic sedimentary and magmatic rocks are exposed (Baraldo et al. 2002; Rapalini et al. 2015), and little ($\sim 20^\circ$ CCW; Poblete et al. 2014) or no rotation (Maffione et al. 2010) affecting the non-metamorphic sedimentary sequences of the Magallanes fold and thrust belt in the most external domains of the belt. Furthermore, the timing of the rotations appears to decrease northward, from post-mid-Late Cretaceous (~ 90 Ma) in the south to post-Late Cretaceous (~ 72 Ma) in the central belt, and to post-Paleocene (~ 65 Ma) until ~ 50 Ma in the fold and thrust belt. Similar patterns of magnitude and timing of rotations are commonly found in fold and thrust belts like the Southern Apennines (Italy), where the magnitude of the rotations decrease from the firstly deformed nappes from the most internal paleogeographic domains to the youngest nappes from the frontal part of the belt (e.g., Maffione et al. 2013). This mechanism is typical of progressive arcs (*sensu* Weil and Sussman 2004) in which the tectonic rotations accompany the propagation of the orogenic front into the foreland. Based on the sparse data from the Fuegian Andes, it can only be speculated that a similar mechanism occurred here. According to this scenario, the largest rotations in Peninsula Hardy from the innermost domains of the belt (Cunningham et al. 1991) would be the effect of initial compressive deformation of the most internal paleogeographic domains.

Most of the tectonic models explaining the evolution of the curvature of the southernmost Andes invoked the closure of the Rocas Verdes marginal basin as a possible cause (Burns et al. 1980; Cunningham et al. 1991; Kraemer 2003; Maffione et al. 2010, 2015; Poblete et al. 2014; Rapalini et al. 2015). According to these reconstructions, at the beginning of the southern Andean orogeny (~ 100 Ma), the Jurassic magmatic arc (Patagonian Batholith) formed a relatively straight structure along the Pacific coast, bounding a triangle-shaped marginal basin to the west. Closure of the marginal basin occurred by continuous CCW rotation of the southern segment of the magmatic arc, leading to progressive nappe stacking in the basin's sedimentary cover until the magmatic arc collided with the South American continental margin in the Late Cretaceous. It is therefore plausible that

during this event, tectonic slices originally rooted in different paleogeographic domains of the basin recorded different amounts of rotation. After continental collision, rigid rotation of what is today the Fuegian Andes might have continued for few million years progressively involving more external paleogeographic domains. Evidence against this reconstruction is the magnitude of shortening along the Fuegian Andes. Although shortening increases from west to east (Diraison et al. 2000), the magnitude of the gradient is not enough to explain a $\sim 90^\circ$ bending, as inferred from paleomagnetic data (Cunningham et al. 1991) and the overall geometry of the southernmost Andes. The total amount of oroclinal bending remains therefore unclear.

The beginning of a possible rigid block rotation of the Fuegian Andes is constrained to a general Late Cretaceous time due to remagnetization of the rocks exposed in this region (Cunningham et al. 1991). Conversely, the end of the rotations is more precisely constrained at ~ 50 Ma by paleomagnetic data from the Cenozoic Magallanes fold and thrust belt (Maffione et al. 2010). These data for the first time proved that no rotations were produced during the deformation of the Magallanes-Austral foreland basin since ~ 50 Ma. Minor ($\sim 20^\circ$) post-65 Ma CCW rotations documented by Poblete et al. (2014), of possible local origin, seem to confirm this trend. Assuming that the formation of the Magallanes fold and thrust belt started at ~ 61 Ma (Ghiglione and Ramos 2005) or slightly earlier (Torres Carbonell et al. 2013) and ended in the Early Miocene, the absence of tectonic rotations since 50 Ma (and possibly 65 Ma) classifies this curved belt as a primary (non-rotational) arc.

Combining all the available paleomagnetic data, a complex tectonic evolution of the curved segment of the southernmost Andes emerges. What has been so far implicitly defined as an orocline due to its more popular name of Patagonian orocline is more likely a hybrid orogenic arc composed of two parts: an older orocline or progressive arc in the outer side of the curvature, mainly formed in Cretaceous times upon closure of the Rocas Verdes marginal basin, and a younger primary arc in the inner side of the orogenic arc, developed in the Cenozoic (Poblete et al. 2014; Maffione et al. 2015). For this reason, Maffione et al. (2015) have recently proposed to use the more generic name of 'Patagonian Arc' to describe the curved segment of the southernmost Andes.

Precise discrimination between temporal and geographical patterns of oroclinal bending is still necessary to validate this model.

8 Mechanisms of Bending of the Southernmost Andes

Considering the hypothesis that the southernmost Andes form a hybrid orogenic arc, it is likely that different tectonic processes contributed to their formation. As previously mentioned, oroclinal bending of the outer part of the arc has been commonly associated with the closure of the Rocas Verdes marginal basin in the mid-Late Cretaceous. Reconstructing the evolution of the primary arc in the inner

side of the orogenic curvature is much more complicated once strain data from fault kinematics, AMS, and analogue experiments are taken into account. The first high-resolution structural model for the Patagonian bending taking into account faults kinematics and Cenozoic brittle faulting was proposed by Cunningham (1993). This author proposed the Patagonian orocline to be the product of broad interplate shearing accommodated by strike-slip faulting, block rotation, and contraction, i.e., the strike-slip orocline model. However, this model implies a succession of E–W-oriented, left-lateral faults cutting the trend of folds and thrusts transversally to the orogen; the strike-slip faults recognized so far in the southernmost Andes are orogen-parallel; and faults and folds are continuous along strike (Figs. 2 and 3) (Ghiglione and Cristallini 2007).

Analogue sandbox experiments were performed by Ghiglione and Cristallini (2007) using both indentation of a curved rigid buttress and rotation of one arm of the indenter. Models using indentation of a rigid indenter provided the most consistent results with the geological evidence. In particular, these authors concluded that a two-phase indentation, NE-ward and then ESE-ward, was able to reproduce with a higher detail the deformation pattern observed in the fold and thrust belt. The deformation paths produced by this model are, however, not entirely consistent with the shortening directions from fault kinematic analysis reported by Diraison et al. (2000). While shortening directions show a progressive variation along the orogenic arc (Fig. 3), the models of Ghiglione and Cristallini (2007) indicate the formation of two distinct, overlapping families of shortening directions parallel to the motion of the indenter.

When shortening directions from both fault kinematic and AMS analysis are considered, a clear pattern emerges, defined by Maffione et al. (2015) as a radial strain field (Figs. 3 and 4). Different processes, other than oroclinal bending, need to be found to explain the presence of a radial strain field in a primary (non-rotational) arc such as the Magallanes fold and thrust belt. Although radial strain patterns have been documented in primary arcs, caused by, e.g., gravitational forces within the growing wedge (Ramsay 1981; Marshak 2004; Weil et al. 2010), extreme $\sim 90^\circ$ variation of the shortening directions as observed in the southernmost Andes is likely caused by more complex tectonic processes. Paleomagnetic data from Rapalini et al. (2015) indicate a post-72 Ma CCW rotation of $\sim 30^\circ$ in the central belt just south of the Magallanes fold and thrust belt. This result suggests that minor rotations could have occurred before the beginning of deformation in the foreland basin at ~ 60 Ma (Ghiglione and Ramos 2005). A rigid indenter model like that proposed by Ghiglione and Cristallini (2007), where an already curved proto-Andes converged during the Cenozoic into the Magallanes-Austral foreland basin to produce a thin-skinned fold and thrust belt, has been considered as a plausible scenario (Maffione et al. 2015).

Simple convergence of a rigid indenter cannot produce a radial strain field (Ghiglione and Cristallini 2007). A two-phase indentation mechanism, as already discussed, is inconsistent with both the pattern of shortening directions and the geological evidence that seems to indicate continuous deformation along both branches of the orogenic arc during the Cenozoic (Maffione et al. 2015).

Maffione et al. (2015) proposed that a radial strain field could be produced upon indentation of a curved rigid buttress if slip partitioning operated along preexisting faults oriented parallel to the margin of the indenter. Jurassic normal faults rooted in the basement of the South American continental margin played a key role in the evolution of the Magallanes-Austral foreland basin sedimentation and subsequent deformation (Menichetti et al. 2008; Likerman et al. 2013; Fosdick et al. 2011, 2014; Ghiglione et al. 2013). The occurrence of \sim N-S-oriented normal faults in the Southern Patagonian Andes and \sim E to NE oriented in the Fuegian Andes associated with the rifting of the Rocas Verdes basin has also been documented (Ghiglione et al. 2009, 2013; Fosdick et al. 2011; Likerman et al. 2013). Based on this evidence, Maffione et al. (2015) proposed that the preexisting Jurassic faults in the basement of the southernmost Andes controlled the Late Cretaceous to Cenozoic kinematic evolution and final geometry of the curved Magallanes fold and thrust belt (Fig. 5). Slip-partitioning mechanisms along these faulted blocks in the central belt allowed

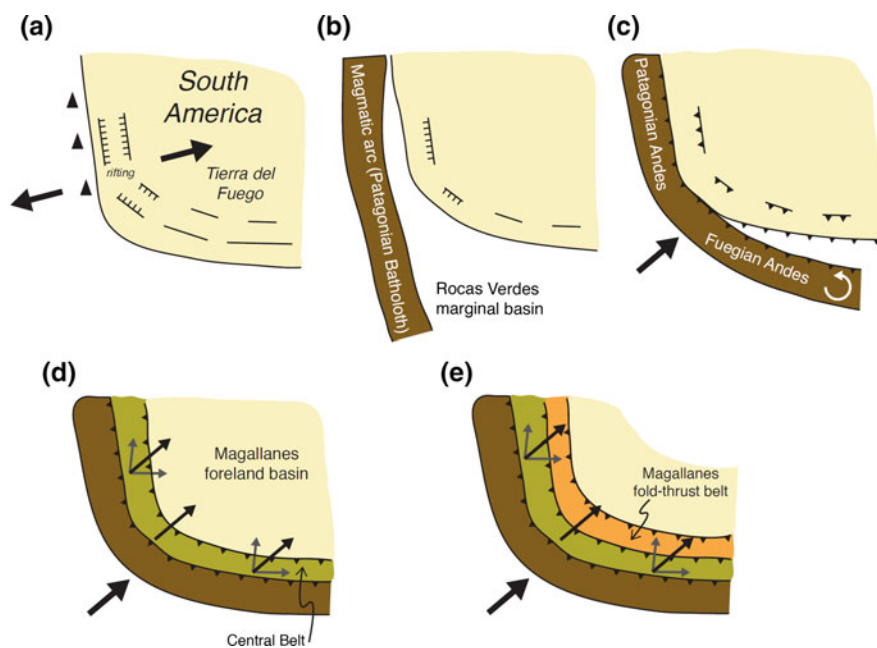


Fig. 5 Kinematic model for the evolution of the southernmost Andes from the Middle Jurassic to the Oligocene proposed by Maffione et al. (2015). *Thick black arrows* indicate the direction of the regional stress field. **a** *Black triangles* indicate active magmatism. **c** *Circular white arrow* indicates the regional vertical-axis rotation of the Fuegian Andes during the closure of the Rocas Verdes basin. **d, e** *Thin black arrows* indicate the displacement vectors of the basement-rooted faulted blocks within the central belt; *thin gray arrows* indicate the fault-parallel and fault-perpendicular components resulting from slip partitioning propagating into the Magallanes-Austral foreland basin and leading to the formation of the fold and thrust belt. Redrawn from Maffione et al. (2015). **a** Mid-Late Jurassic, **b** Late Jurassic, **c** Early Late Cretaceous, **d** Middle Late Cretaceous, **e** Paleocene–Oligocene

transference of fault-normal compression components into the Magallanes-Austral foreland (\sim N-ward and \sim E-ward contraction in the Fuegian and Patagonian Andes, respectively) throughout the Cenozoic, resulting in a radial strain field.

9 Conclusive Remarks

Since its first definition as Patagonian orocline by Carey (1958), the real nature and evolution of the regional-scale curvature of the southernmost Andes have been controversial. The debate revolved around the two conflicting hypotheses considering the curvature of the southernmost Andes either as a non-rotational (primary) arc, or a rotational arc (i.e., orocline or progressive arc). The curved shape of the Antarctic Peninsula and the growth during the Cenozoic of a new oceanic plate (Scotia plate) intervening between the South American and Antarctic plate were used as evidence at the basis of early tectonic models. With time, most of the early models resulted to be imprecise. Only with the acquisition of the first paleomagnetic data from the southernmost Andes, the debate on the nature of its curvature was resumed, continuing until today.

The mechanism proposed by Maffione et al. (2015) requires widespread sinistral and dextral strike-slip displacements on main thrusts from the internal domains of the Fuegian and Patagonian Andes, respectively. Further data identifying and quantifying such strike-slip tectonics in the southernmost Andes are, however, needed to fully test the proposed model.

Although more than 40 years of paleomagnetic investigation in the southernmost Andes has provided key constraints to define the timing, style, and kinematics of deformation in this region, their number and quality are still too low to allow detailed reconstructions. The available paleomagnetic data indicate that $\sim 90^\circ$ of CCW vertical-axis rotation affected the most internal structural domain of the Fuegian Andes (i.e., the outer part of the curvature) since ~ 90 Ma, $\sim 30^\circ$ of which occurred after ~ 72 Ma, and that rotations in the Magallanes fold and thrust belt (i.e., the inner part of the curvature) ended at ~ 50 Ma. Although these data are affected by uncertainties related to the age of magnetization, the absence of paleohorizontal control, and a poor stability of the magnetic remanence, an overall pattern of CCW rotations in the internal sectors of the belt appear evident, while rotations did not affect the Magallanes fold and thrust belt at least since the Early Eocene. These data suggest that the outer part of the curvature represents an orocline or a progressive arc (sensu Weil and Sussman 2004). Definition of precise timing and total amount of the bending awaits further investigations. On the other side, the absence of tectonic rotations in the Magallanes fold and thrust belt indicates that it developed in the Cenozoic as a primary arc (sensu Weil and Sussman 2004).

Based on the available paleomagnetic constraints and the most recent tectonic models, the broadly used term of 'Patagonian orocline' appears to be outdated and inappropriate. According to formal definitions (e.g., Weil and Sussman 2004), an orocline is a large-scale curved mountain belt formed upon bending of a previously

straight orogen. This definition, as demonstrated, may only apply to the outer side of the curvature of the southernmost Andes, being the inner side a primary arc. As recently proposed by several authors (Poblete et al. 2014; Maffione et al. 2015), the orogenic bend of the southernmost Andes is composed of two adjacent arcs: a rotational arc (orocline or progressive arc) and a non-rotational arc (primary arc) in the outer and inner part of the curvature, respectively. For this reason, Maffione et al. (2015) suggested that the old term ‘Patagonian orocline’ should be abandoned in favor of a more generic ‘Patagonian Arc’.

A broad consensus exists that invokes the closure of the Rocas Verdes marginal basin in the Late Cretaceous as the main mechanism of oroclinal bending of the internal sectors of the southernmost Andes. More uncertain is the evolution of the primary arc of the Magallanes fold and thrust belt. Proposed scenarios to explain the formation of the curved fold and thrust belt, in the context of a primary arc model, considered indentation of a curved rigid buttress (represented by the previously bent internal domains of the southernmost Andes) into the foreland sediments of the Magallanes-Austral basin. The presence of highly variable (radial pattern) shortening directions along the Magallanes fold and thrust belt (Maffione et al. 2015), uncommon in primary arcs, has been explained by the possible effect of slip partitioning along preexisting Jurassic faults at the South American margin, which could have enabled \sim N-ward contraction in the Fuegian Andes and \sim E-ward contraction in the Patagonian Andes. A slip-partitioning model in the southernmost Andes requires widespread strike-slip tectonics with dextral and sinistral kinematics in the Patagonian and Fuegian Andes, respectively. Future investigations are needed to test the occurrence of such tectonics and validate this model.

References

- Alvarez-Marrón J, McClay KR, Harambour S, Rojas L, Skyrmeta J (1993) Geometry and evolution of the frontal part of the Magallanes foreland thrust and fold belt (Vicuna-Area), Tierra del Fuego, Southern Chile. *Am Assoc Petr Geol Bull* 77:1904–1921
- Baraldo A, Rapalini A, Tassone A, Lippai H, Menichetti M, Lodolo E (2002) Estudio paleomagnético del intrusivo del cerro Hewhoepen, Tierra del Fuego, y sus implicancias tectónicas. XV Congreso Geológico Argentino (El Calafate) *Actas* 1:285–290
- Barker PF (2001) Scotia Sea regional tectonic evolution: implications for mantle flow and palaeocirculation. *Earth Sci Rev* 55:1–39
- Barker PF, Diekmann B, Escutia C (2007a) Onset of Cenozoic Antarctic glaciation. *Deep-Sea Res II* 54:2293–2307
- Barker PF, Filippelli GM, Florindo F, Martin EE, Scher HD (2007b) Onset and role of the Antarctic circumpolar current. *Deep-Sea Res II* 54:2388–2398
- Beck ME Jr, Burmester R, Cembrano J, Drake R, García A, Hervé F, Munizaga F (2000) Paleomagnetism of the North Patagonian Batholith, southern Chile. An exercise in shape analysis. *Tectonophysics* 326:185–202
- Biddle KT, Uliana MA, Mitchum RM, Fitzgerald MG, Wright RC (1986) The stratigraphy and structural evolution of the central and eastern Magallanes Basin, southern South America. In: Allen A, Homewood P (eds) *Foreland Basins* (vol 8). Blackwell Scientific Publications, London (Int Assoc Sediment Special Publication), pp 41–61

- Bruhn RL (1979) Rock structures formed during back-arc basin deformation in the Andes of Tierra del Fuego. *Geol Soc Am Bull* 90(11):998–1012
- Bruhn RL, Dalziel IWD (1977) Destruction of the Early Cretaceous marginal basin in the Andes of Tierra del Fuego. *Island Arcs, Deep Sea Trenches Back-Arc Basins* 395–405
- Bruhn RL, Stern CR, de Wit MJ (1978) Field and geochemical data bearing on the development of a mesozoic volcano-tectonic rift zone and back-arc basin in southernmost South America. *Earth Planet Sci Lett* 41:32–46
- Burns KL, Rickerd MJ, Belbin L, Chamalaun F (1980) Further palaeomagnetic confirmation of the magallanes orocline. *Tectonophysics* 63:75–90
- Calderón M, Fildani A, Hervé F, Fanning CM, Weislogel A, Cordani U (2007) Late Jurassic bimodal magmatism in the northern sea-floor remnant of the Rocas Verdes basin, Southern Patagonian Andes. *J Geol Soc Lond* 164:1011–1022
- Calderón M, Fosdick JC, Warren C, et al (2012) The low-grade Canal de las Montañas Shear Zone and its role in the tectonic emplacement of the Sarmiento Ophiolitic Complex and Late Cretaceous Patagonian Andes orogeny, Chile. *Tectonophysics* 524–525:165–185. doi: [10.1016/j.tecto.2011.12.034](https://doi.org/10.1016/j.tecto.2011.12.034)
- Cande SC, Leslie RB (1986) Late Cenozoic tectonics of the southern Chile Trench. *J Geophys Res-Sol EA* 91(B1):471–496
- Carey SW (1955) The orocline concept in geotectonics. *Proc R Soc Tasmania* 89:255–288
- Carey SW (1958) The tectonic approach to continental drift. *Continental drift: a symposium: Hobart. Geology Department, University of Tasmania, Tasmania*, pp 177–355
- Cifelli F, Mattei M, Rossetti F (2007) Tectonic evolution of arcuate mountain belts on top of a retreating subduction slab: the example of the Calabrian Arc. *J Geophys Res-Sol EA* 112(B9)
- Coutand I, Diraison M, Cobbold PR, Gapais D, Rossello EA, Miller M (1999) Structure and kinematics of a foothills transect, Lago Viedma, southern Andes (49°30'S). *J S Am Earth Sci* 12:1–15
- Cunningham WD (1993) Strike-slip faults in the southernmost Andes and the development of the Patagonian Orocline. *Tectonics* 12:169–186
- Cunningham WD (1994) Uplifted ophiolitic rocks on Isla Gordon, southernmost Chile: implications for the closure history of the Rocas Verdes marginal basin and the tectonic evolution of the Beagle Channel region. *J S Am Earth Sci* 7:135–147
- Cunningham WD (1995) Orogenesis at the southern tip of the Americas: the structural evolution of the Cordillera Darwin metamorphic complex, southernmost Chile. *Tectonophysics* 244:197–229
- Cunningham WD, Klepeis KYR, Gose WA, Dalziel IW (1991) The Patagonian Orocline: new paleomagnetic data from the Andean magmatic arc in Tierra del Fuego, Chile. *J Geophys Res-Sol EA* 96(B10):16061–16067
- Dalziel IWD (1981) Backarc extension in the southern Andes: a review and critical reappraisal. *Philos Trans R Soc Lond* 300:319–335
- Dalziel IWD, Elliot DH (1973) The Scotia arc and Antarctic margin. In: Nairn AEM, Stehli FG (eds) *The Ocean Basins and margins (vol 1). The South Atlantic* Plenum Press, New York, pp 171–245
- Dalziel IWD, Klingfield R, Lowrie W, Opdyke ND (1973) Paleomagnetic data from the southernmost Andes and the Antarctic Andes. In: Tarling DH, Runcom SK (eds) *Implications of continental drift to the earth sciences*. Academic Press, San Diego, pp 87–101
- Dalziel IWD, De Wit MF, Palmer KF (1974) Fossil marginal basin in the southern Andes. *Nature* 250:291–294
- Diraison M (1998) Evolution cénozoïque du Bassin de Magellan et tectonique des Andes Australes. *Mém Doc Géosciences-Rennes* 85:332
- Diraison M, Cobbold PR, Gapais D, Rossello EA, Le Corre C (2000) Cenozoic crustal thickening, wrenching and rifting in the foothills of the Southernmost Andes. *Tectonophysics* 316:91–119
- Eagles G (2016) Tectonic reconstructions of the Southernmost Andes and the Scotia Sea during the opening of the Drake Passage. In: Ghiglione MC (ed) *Geodynamic Evolution of the Southernmost Andes*. Springer Earth System Sciences, pp 75–108

- Eagles G, Livermore RA, Fairhead JD, Morris P (2005) Tectonic evolution of the west Scotia Sea. *J Geophys Res-Sol EA* 110:1–19
- Eldredge S, Bachtadse V, Van der Voo R (1985) Paleomagnetism and the orocline hypothesis. *Tectonophysics* 119:153–179
- Esteban F, Tassone A, Menichetti M, Rapalini AE, Remesal MB, Cerredo ME, Lippai H, Vilas JF (2011) Fabrica Magnética y Microestructuras a través de los Andes de Tierra del Fuego, Argentina. *Andean Geol* 38:64–81
- Fildani A, Hessler AM (2005) Stratigraphic record across a retroarc basin inversion: Rocas Verdes-Magallanes Basin, Patagonian Andes, Chile. *Geol Soc Am Bull* 117:1596–1614
- Fildani A, Cope TD, Graham SA, Wooden JL (2003) Initiation of the Magallanes foreland basin: Timing of the southernmost Patagonian Andes orogeny revised by detrital zircon provenance analysis. *Geology* 31:1081. doi: [10.1130/G20016.1](https://doi.org/10.1130/G20016.1)
- Fosdick JC, Romans BW, Fildani A, Bernhardt A, Calderón M, Graham SA (2011) Kinematic evolution of the Patagonian retroarc fold and thrust belt and Magallanes foreland basin, Chile and Argentina, 51°30'S. *Geol Soc Am Bull* 123:1679–1698
- Fosdick JC, Graham SA, Hilley GE (2014) Influence of attenuated lithosphere and sediment loading on flexure of the deep-water Magallanes retroarc foreland basin, Southern Andes. *Tectonics* 33:2505–2525. doi: [10.1002/2014TC003684](https://doi.org/10.1002/2014TC003684)
- Fosdick JC, Grove M, Hourigan JK, Calderón M (2013) Retroarc deformation and exhumation near the end of the Andes, southern Patagonia. *Earth Planet Sci Lett* 361:504–517. doi: [10.1016/j.epsl.2012.12.007](https://doi.org/10.1016/j.epsl.2012.12.007)
- Fosdick JC, Graham SA, Hilley GE (2015) Influence of attenuated lithosphere and sediment loading on flexure of the deep-water Magallanes retroarc foreland basin, Southern Andes. *Tectonics* 33:2505–2525
- Ghiglione MC (2002) Diques clásticos asociados a deformación transcurrente en depósitos sinorogénicos del Mioceno inferior de la Cuenca Austral. *Rev la Asoc Geol Argentina* 57:103–118
- Ghiglione MC, Cristallini EO (2007) Have the southernmost Andes been curved since Late Cretaceous times? An analog test for the Patagonian Orocline. *Geology* 35:13–16
- Ghiglione MC, Ramos VA (2005) Chronology of deformation in the southernmost Andes of Tierra del Fuego. *Tectonophysics* 405:25–46
- Ghiglione MC, Ramos VA, Cristallini EO (2002) Fuegian Andes foreland fold and thrust belt: structure and growth strata. *Rev Geol Chile* 29(1):17–41
- Ghiglione MC, Suarez F, Ambrosio A, Da Poian G, Cristallini EO, Pizzio MF, Reinoso RM (2009) Structure and evolution of the Austral basin fold–thrust belt, Southern Patagonian Andes. *Rev Asoc Geol Argentina* 65:215–226
- Ghiglione MC, Quinteros J, Yagupsky D, Bonillo-Martínez P, Hlebszevtich J, Ramos VA, Vergani G, Figueroa D, Quesada S, Zapata T (2010) Structure and tectonic history of the foreland basins of southernmost South America. *J S Am Earth Sci* 29:262–277
- Ghiglione MC, Navarrete-Rodríguez AT, González Guillot M, Bujaleski G (2013) The opening of the Magellan Strait and its geodynamic implications. *Terra Nova* 25(1):13–20
- Ghiglione MC, Sue C, Ramos ME, Tobal JE, Gallardo RE (2016a) The relation between Neogene Denudation of the southernmost Andes and sedimentation in the offshore Argentine and Malvinas basins during the opening of the Drake Passage. In: Ghiglione MC (ed) *Geodynamic Evolution of the Southernmost Andes*. Springer Earth System Sciences, pp 109–135
- Ghiglione MC, Ramos V, Cuitiño J, Barberón V (2016b) Growth of the Southern Patagonian Andes (46–53°S) and its relation with subduction processes. In: Folguera A, Naipauer M, Sagripanty L, Ghiglione MC, Orts D, Giambiagi LB (eds) *Growth of the Southern Andes*. Springer Earth System Sciences, Berlin, pp 201–240
- Guillot MG (2016) Magmatic evolution of the southernmost Andes and its relation with subduction processes. In: Ghiglione MC (ed) *Geodynamic Evolution of the Southernmost Andes*. Springer Earth System Sciences, pp 37–74
- González Guillot M, Escayola M, Acevedo R (2011) Calc-alkyline rear-arc magmatism in the Fuegian Andes: implications for the mid-Cretaceous tectonomagmatic evolution of southernmost South America. *J S Am Earth Sci* 31:1–16

- Grunow AM (1993) New paleomagnetic data from the Antarctic Peninsula and their tectonic implications. *J Geophys Res-Sol EA* 98(B8):13815–13833
- Halpern M, Rex DC (1972) Time of folding of the Yahgan Formation and age of the Tekenikyir beds, southern Chile, South America. *Geol Soc Am Bull* 83:1881–1886
- Hervé F, Nelson E, Kyrwasha K, Suárez M (1981) New isotopic ages and the timing of orogenic events in the Cordillera Darwin, southernmost Chilean Andes. *Earth Planet Sci Lett* 55(2):257–265
- Hervé M, Suárez M, Puig A (1984) The Patagonian Batholith south of Tierra del Fuego, Chile. Timing and tectonic implications. *J Geol Soc Lond* 141(5):909–917
- Hervé F, Pankhurst R, Fanning C, Calderón M, Yaxley G (2007) The South Patagonian Batholith: 150 my of granite magmatism on a plate margin. *Lithos* 97:373–394
- Hervé F, Calderón M, Faúndez V (2008) The metamorphic complexes of the Patagonian and Fuegian Andes. *Geologica Acta* 6:43–53
- Iglesia Llanos MP, Lanza R, Riccardi AC, Geuna S, Laurenzi MA, Ruffini R (2003) Palaeomagnetic study of the El Quemado complex and Marifil formation, Patagonian Jurassic igneous province, Argentina. *Geophys J Int* 154:599–617
- Kirschvink JL (1980) The least-squares line and plane and the analysis of palaeomagnetic data. *Geophys J* 62:699–718
- Klepeis KYR (1994) Relationship between uplift of the metamorphic core of the southernmost Andes and shortening in the Magallanes foreland fold and thrust belt, Tierra del Fuego, Chile. *Tectonics* 13:882–904
- Klepeis KYR, Austin JA (1997) Contrasting styles of superposed deformation in the southernmost Andes. *Tectonics* 16:755–776
- Klepeis K, Betkyr P, Clarke G, Fanning M, Hervé F, Rojas L, Mpodozis C, Thomson S (2010) Continental underthrusting and obduction during the Cretaceous closure of the Rocas Verdes rift basin, Cordillera Darwin, Patagonian Andes. *Tectonics* 29:TC3014
- Kohn MJ, Spear FS, Dalziel IWD (1993) Metamorphic P-T Paths from Cordillera Darwin, a Core Complex in Tierra del Fuego, Chile. *J Petrol* 34:519–542. doi: [10.1093/petrology/34.3.519](https://doi.org/10.1093/petrology/34.3.519)
- Kohn MJ, Spear FS, Harrison TM, Dalziel IWD (1995) 40Ar/39Ar geochronology and P-T-t paths from the Cordillera Darwin metamorphic complex, Tierra del Fuego, Chile. *J Metamorph Geol* 13:251–270
- Kraemer PE (1998) Structure of the Patagonian Andes: Regional balanced cross section at 50°S. *Argentina Int Geol Rev* 40:896–915
- Kraemer PE (2003) Orogenic shortening and the origin of the Patagonian orocline (56S). *J S Am Earth Sci* 15:731–748
- Kyrtz HR (1973) Contrasts in tectonic evolution of orogenic belts in the southwest Pacific. *J R Soc N Z* 3:333–362
- Lawver LA, Gahagan LM (2003) Evolution of Cenozoic seaways in the circum-Antarctic region. *Palaeogeog Palaeoclim Palaeoecol* 198:11–37
- Likerman L, Burlando JF, Cristallini EO, Ghiglione MC (2013) Along-strike structural variations in the Southern Patagonian Andes: insights from physical modeling. *Tectonophysics* 590:106–120
- Livemore RA, Nankivell AP, Eagles G, Morris P (2005) Paleogene opening of drake passage. *Earth Planet Sci Lett* 236:459–470
- Lodolo E, Coren F, Schreider AA, Ceccone G (1997) Geophysical evidence of a relict oceanic crust in the southwestern Scotia Sea. *Mar Geophys Res* 19:439–450
- Lodolo E, Menichetti M, Tassone A, Sterzai P (2002) Morphostructure of the central-eastern Tierra del Fuego Island from geological data and remote-sensing images. *EGS Stephan Mueller Spec Publ Ser* 2:1–16
- Lodolo E, Menichetti M, Bartole R, Ben-Avraham Z, Tassone A, Lippai H (2003) Magallanes-Fagnano continental transform fault (Tierra del Fuego, southernmost South America). *Tectonics* 22:1076
- Lodolo E, Donda F, Tassone A (2006) Western Scotia Sea margins: improved constraints on the opening of the Drake Passage. *J Geophys Res-Sol EA* 111(B6)
- Lowrie W, Hirt AM (1986) Paleomagnetism in arcuate mountain belts. In: Wezel FC (ed) *The origin of arcs, developments in geotectonics* (vol 21). Amsterdam, Elsevier, pp 141–158

- Maffione M, Speranza F, Faccenna C, Cascella A, Vignaroli G, Sagnotti L (2008) A synchronous Alpine and Corsica-Sardinia rotation. *J Geophys Res* 113(B3)
- Maffione M, Speranza F, Faccenna C (2009) Bending of the Bolivian orocline and growth of the central Andean plateau: paleomagnetic and structural constraints from the Eastern Cordillera (22–24°S, NW Argentina). *Tectonics* 28:TC002402
- Maffione M, Speranza F, Faccenna C, Rossello E (2010) Paleomagnetic evidence for a pre-early Eocene (~50 Ma) bending of the Patagonian orocline (Tierra del Fuego, Argentina): paleogeographic and tectonic implications. *Earth Planet Sci Lett* 289:273–286
- Maffione M, Speranza F, Cascella A, Longhitano SG, Chiarella D (2013) A ~125° post-early Serravallian counterclockwise rotation of the Gorgoglione formation (Southern Apennines, Italy): new constraints for the formation of the Calabrian arc. *Tectonophysics* 590:24–37
- Maffione M, Fernandez-Moreno C, Ghiglione M, Speranza F, van Hinsbergen DJJ, Lodolo E (2015) Constraints on deformation of the Southern Andes since the Cretaceous from anisotropy of magnetic susceptibility. *Tectonophysics* 665:236–250
- Maloney KT, Clarke GL, Klepeis KYR, Fanning CM, Wang W (2011) Crustal growth during back-arc closure: Cretaceous exhumation history of Cordillera Darwin, southern Patagonia. *J Metamorph Geol* 29(6):649–672
- Maloney KT, Clarke GL, Klepeis KYR, Quevedo L (2013) The Late Jurassic to present evolution of the Andean margin: drivers and the geological record. *Tectonics* 32:1049–1065
- Malumián N, Olivero EB (2006) The Cabo Domingo Group, Tierra del Fuego: biostratigraphy, paleoenvironments, and events of the marine Eocene-Miocene. *Rev Asoc Geol Argent* 61:139–160
- Malumián N, Panza JL, Parisi C, Nañez C, Caramés A, Torre E (2000) Hoja Geológica 5172-III-Yacimiento Río Turbio, provincia Santa Cruz, 1:250.000. Servicio Geológico Minero Argentino, Boletín 247: p 108
- Marshak S (1988) Kinematics of orocline and arc formation in thin-skinned orogens. *Tectonics* 7:73–86
- Marshak S (2004) Salients, recesses, arcs, oroclines, and syntaxes—a review of ideas concerning the formation of map-view curves in fold-thrust belts. *Thrust Tecton Hydrocarb Syst* 82:131–156
- McAtamney J, Klepeis K, Mehrrens C, Thomson S, Betkyr P, Rojas L, Snyder S (2011) Along-strike variability of back-arc basin collapse and the initiation of sedimentation in the Magallanes foreland basin, southernmost Andes (53–54.5°S). *Tectonics* 30(5):2010T. doi:10.1029/1107C002826
- Menichetti M, Lodolo E, Tassone A (2008) Structural geology of the Fuegian Andes and Magallanes fold thrust belt—Tierra del Fuego Island. *Geologica Acta* 6:19–42
- Morris A, Anderson MW, Robertson AHF (1998) Multiple tectonic rotations and transform tectonism in an intraoceanic suture zone, SW Cyprus. *Tectonophysics* 299:229–253
- Muttoni G, Argnani A, Kent DV, Abrahamsen N, Cibin U (1998) Paleomagnetic evidence for Neogene tectonic rotations in the northern Apennines, Italy. *Earth Planet Sci Lett* 154:25–40
- Nelson EP (1982) Posttectonic uplift of the Cordillera Darwin orogenic core complex: evidence for fission track geochronology and closing temperature time relationships. *J Geol Soc Lond* 139:755–761
- Olivero EB, Malumián N (1999) Eocene stratigraphy of Southeastern Tierra del Fuego Island, Argentina. *Am Assoc Petr Geol Bull* 83:295–313
- Olivero EB, Malumián N (2008) Mesozoic-Cenozoic stratigraphy of the Fuegian Andes, Argentina. *Geologica Acta* 6:5–18
- Olivero EB, Malumián N, Palamarczuk S (2003) Estratigrafía del Cretácico superior-Paleoceno del área de bahía Thetis, Andes Fueguinos, Argentina: acontecimientos tectónicos y paleobiológicos. *Rev Geol Chile* 30:245–263
- Pankhurst RJ, Riley TR, Fanning CM, Kelley SP (2000) Episodic silicic volcanism in Patagonia and the Antarctic Peninsula: chronology of magmatism associated with the break-up of Gondwana. *J Petrol* 41:605–625
- Parés JM, Van der Pluijm BA, Dinarès-Turell J (1999) Evolution of magnetic fabrics during incipient deformation of mudrocks (Pyrenees, northern Spain). *Tectonophysics* 307:1–14

- Poblete F, Arriagada C, Roperch P, Astudillo N, Hervé F, Kraus S, Le Roux JP (2011) Paleomagnetism and tectonics of the South Shetland Islands and the northern Antarctic Peninsula. *Earth Planet Sci Lett* 302:299–313
- Poblete F, Roperch P, Hervé F, Diraison M, Espinoza M, Arriagada C (2014) The curved Magallanes fold and thrust belt: tectonic insights from a paleomagnetic and anisotropy of magnetic susceptibility study. *Tectonics* 33:2526–2551
- Ramos VA (1989) Andean foothills structures in northern Magallanes basin. Argentina. *Am Assoc Petr Geol Bull* 73(7):887–903
- Ramos VA (2005) Seismic ridge subduction and topography: foreland deformation in the Patagonian Andes. *Tectonophysics* 399:73–86
- Ramos VA, Aleman A (2000) Tectonic evolution of the Andes Tectonic Evolution of South America. In: *Proceedings of XXXI International Geological Congress (Rio de Janeiro) Brazil*, pp 453–480
- Ramsay JG (1981) Tectonics of the Helvetic nappes. *Geol Soc Spec Publ* 9:293–309
- Rapalini AE (2007) A paleomagnetic analysis of the Patagonian orocline. *Geologica Acta* 5:287–294
- Rapalini AE, Hervé F, Ramos VA, Singer SE (2001) Paleomagnetic evidence for a very large counterclockwise rotation of the Madre de Dios Archipelago, Southern Chile. *Earth Planet Sci Lett* 184:471–487
- Rapalini AE, Calderón M, Hervé F, Cordani U, Singer S (2004) First Paleomagnetic Results on the Sarmiento Ophiolite, Southern Chile: implications for the Patagonian Orocline. *Bolletino di Geofisica Teorica ed Applicata* 45:246–249
- Rapalini AE, Lippai H, Tassone A, Cerredo ME (2005) An AMS and paleomagnetic study across the Andes in Tierra del Fuego. In: *VI international symposium on Andean geodynamics (Barcelona)*, extended abstracts, pp 596–599
- Rapalini AE, Peroni J, Luppo T, Tassone A, Cerredo ME, Federico E, Lippai H, Vilas JF (2015) Palaeomagnetism of Mesozoic magmatic bodies of the Fuegian Cordillera: implications for the formation of the Patagonian Orocline. *Geol Soc Spec Publ* 425:SP425–3
- Roperch P, Chauvin A, Calza F, Palacios C, Parraguez G, Pinto L, Goguitchaivilli A (1997) Paleomagnetismo de las rocas volcánicas del Jurásico tardío al Terciario temprano de la región de Aysén (Coyhaique-Cochrane). In: *VIII Congreso Geológico Chileno (Antofagasta) Universidad Católica del Norte, Actas 1*, pp 236–240
- Rossello EA (2005) Kinematics of the Andean sinistral wrenching along the Fagnano-Magallanes Fault Zone (Argentina-Chile Fuegian Foothills). In: *VI international symposium on Andean geodynamics (Barcelona)*, extended abstracts, pp 623–626
- Sagnotti L, Faccenna C, Funicello R, Mattei M (1994) Magnetic fabric and structural setting of Plio-Pleistocene clayey units in an extensional regime: the Tyrrhenian margin of central Italy. *J Struct Geol* 16:1243–1257
- Somoza R, Ghidella ME (2005) Convergence in the western margin of South America during the Cenozoic: subduction of Nazca, Farallon and Aluk plates. *Rev Asoc Geol Argentina* 60:797–809
- Somoza R, Ghidella ME (2012) Late Cretaceous to recent plate motions in western South America revisited. *Earth Planet Sci Lett* 331–332:152–163
- Speranza F, Sagnotti L, Mattei M (1997) Tectonics of the Umbria-Marche-Romagna Arc (central northern Apennines, Italy): new paleomagnetic constraints. *J Geophys Res-Sol EA* 102 (B2):3153–3166
- Stern CR, de Witt MJ (2003) Rocas Verdes ophiolites, southern South America: remnants of progressive stage of development of oceanic-type crust in a continental margin back-arc basin. *Geol Soc Spec Publ* 218:665–683
- Sue C, Ghiglione MC (2016) Wrenching tectonism in the southernmost Andes and the Scotia Sea constrained from fault kinematic and seismotectonic overviews. In: Ghiglione MC (ed) *Geodynamic Evolution of the Southernmost Andes*. Springer Earth System Sciences, pp 137–171
- Tarling DH, Hrouda F (1993) The magnetic anisotropy of rocks. Chapman, Hall, Lond, 217 pp

- Thomson SN, Herve F, Stockhert B (2001) The Mesozoic-Cenozoic denudation history of the Patagonian Andes (southern Chile) and its correlation to different subduction processes. *Tectonics* 20:693–711
- Torres Carbonell PJ, Olivero EB, Dimieri LV (2008) Structure and evolution of the Fuegian Andes foreland thrust-fold belt, Tierra del Fuego, Argentina: Paleogeographic implications. *J South Am Earth Sci* 25:417–439
- Torres Carbonell PJ, Dimieri LV, Martinioni DR (2013) Early foreland deformation of the Fuegian Andes (Argentina): constraints from the strain analysis of upper Cretaceous-Danian sedimentary rocks. *J Struct Geol* 48:14–32
- Van der Voo R (1990) The reliability of paleomagnetic data. *Tectonophysics* 184:1–9
- Van der Voo R (1993) Paleomagnetism of the Atlantic, Tethys and Iapetus oceans, 411 p
- Van der Voo R (2004) Paleomagnetism, oroclinal, and growth of the continental crust. *GSA Today* 14:4–9
- Van der Voo R, Channell JET (1980) Paleomagnetism in orogenic belts. *Rev Geophys Space Phys* 18:455–481
- Van der Voo R, Stamatakos JA, Parés JM (1997) Kinematic constraints on thrust-belt curvature from syndeformational magnetizations in the Lagos del Valle Syncline in the Cantabrian Arc, Spain. *J Geophys Res-Sol EA* 102(B5):10105–10119
- Weil AB, Sussman AJ (2004) Classifying curved orogens based on timing relationships between structural development and vertical-axis rotations. *Geol S Am S* 383:1–15
- Weil AB, Yonkee A, Sussman A (2010) Reconstructing the kinematic evolution of curved mountain belts: a paleomagnetic study of Triassic red beds from the Wyoming salient, Sevier thrust belt, USA. *Geol Soc Am Bull* 122:3–23
- Wilson TJ (1991) Transition from back-arc to foreland basin development in the southernmost Andes: stratigraphic record from the Ultima Esperanza District, Chile. *Geol Soc Am Bull* 103 (1):98–111
- Winslow MA (1981) Mechanisms for basement shortening in the Andean foreland fold belt of southern South America. *Geol Soc London, Spec Publ* 9:513–528. doi: [10.1144/GSL.SP.1981.009.01.46](https://doi.org/10.1144/GSL.SP.1981.009.01.46)
- Winslow MA (1982) The structural evolution of the Magallanes Basin and neotectonics in the southernmost Andes. *Antarctic Geoscience, III symposium on Antarctic geology and geophysics, Madison*, pp 143–154
- Yonkee A, Weil AB (2010) Quantifying vertical axis rotation in curved orogens: correlating multiple data sets with a refined weighted least squares strike test. *Tectonics* 29(3):TC2312
- Zachos J, Pagani H, Sloan L, Thomas E, Billups K (2001) Trends, rhythms, and aberrations in global climate 65 Ma to present. *Science* 292:686–693

Index

A

Accretionary complexes, 8, 14, 115
Active seismicity, 2
Adakitic magmatism, 55
Aftershock, 152
Alkali basalts, 89, 96
Analogue sandbox experiments, 191
Andean denudation, 113
Andean metamorphic complex, 9–11
Andean orogeny, 8, 43, 185, 189
Anisotropy of Magnetic Susceptibility (AMS), 185, 186, 191
Antarctica, 1, 2, 4, 76, 92, 96, 98, 100, 102, 115, 159, 161, 175
Antarctica–Nazca–South America triple junction, 116
Antarctic Circumpolar Current, 76, 86, 92, 128, 175
Antarctic Peninsula, 1–3, 10, 13, 14, 18, 25–27, 29, 40, 76, 78, 79, 88, 91, 98, 100, 102, 179, 184, 185, 193
Antarctic plate, 76, 83, 84, 98, 99, 155, 159, 161, 187, 193
Antarctic waters, 4, 110, 114
Apatite (U–Th)/He (AHe), 117
Aptian–Albian, 28, 78, 99, 103
Argentine basin, 4, 112, 119, 123–125, 127, 128
Argentine continental margin, 123, 126
Argentine continental shelf, 127
Asthenospheric slab window, 116
Asthenospheric window, 113, 121, 123, 127
Atlantic ocean, 76, 121, 154, 156, 176
Atlantic offshore basin, 110
Atlantic platform, 2, 113
Australia, 76
Austral Volcanic Zone (AVZ), 55

B

Bahía de la Lancha, 13
Barker/Aurora Bank, 85
Barros Arana basalts, 65
Barros Arana Formation, 52
Basement complexes, 10, 14
Basement domain, 113–118, 123, 128, 177
Beagle suite, 42–44, 48, 56, 57, 59, 61, 62
Beauvoir-La Paciencia Formations, 41
Bending, 41, 79, 94, 139, 151, 174, 178, 179, 190, 193
Bimodal magmatism, 22, 27
Bransfield basin, 159
Bransfield Strait, 77
Bruce Bank, 77, 88, 97, 101
Burdwood Bank, 77, 88, 90, 94, 97, 101, 117, 128
Burdwood transform fault, 94–96, 98

C

Calc-alkaline trench, 37
Cambrian, 15, 23, 25, 26
Canal Beagle, 22, 41–43, 48, 57, 110, 118, 144, 145, 154, 156, 182, 188
Canal Beagle fault zone, 143
Canal Bertrand Formation, 52
Canal de Hoces, 128
Canal de las Montañas Shear Zone (CMSZ), 24, 28
Cape Horn, 89
Capitán Aracena Complex (CAC), 19, 22
Carbajal valley fault zone, 143
Carboniferous, 13–16, 25, 27, 182
Carmen Silva Formation, 112, 123, 127
Centinela Formation, 119
Central Scotia Plate, 85, 90
Cerro Negro, 13

- Chenque, 119
 Chile ridge, 4, 116, 122
 Chile seismic ridge, 116
 Chon Aike, 10, 40, 90, 100, 101
 Chon Aike Silicic Large Igneous Province, 10
 Chonide orogeny, 27
 Chonos Metamorphic Complex (ChMC), 9, 16
 Continental extension, 27, 30, 95–97
 Continental rifting, 17
 Convergent margin, 27, 83
 Cooper Bay shear zone, 78
 Cordillera Darwin, 9, 22, 41, 42, 48, 57, 59, 114, 115, 118, 156, 175, 176
 Cordillera Darwin Metamorphic Complex (CDMC), 9, 14, 15, 25, 27, 28
 Cretaceous, 3, 4, 10, 17, 18, 22, 24, 28, 29, 38, 40, 41, 43, 44, 51, 53, 57, 59, 60, 63–66, 78, 79, 81, 83, 98, 99, 101, 103, 115, 126, 142, 145, 151, 175, 176, 180, 182, 183, 185, 186, 188–190, 192, 194
 Crustal extension, 27, 30, 97, 100
 Cumberland Bay Formation, 78, 101
 Curved belt, 5, 190
 Curved mountain, 5, 174, 178, 193
 Curved orogen, 41, 176, 178
- D**
 Darwin, Charles, 76
 Darwin suite, 42, 58, 63, 64
 Davis Bank, 77, 86, 88, 101
 Dawson Island, 142
 Deformation paths, 191
 Denaro Complex (DC), 15, 16
 Deseado Massif, 10, 13, 14, 25, 100
 Detrital U–Pb zircon, 8
 Detrital zircon, 11, 13, 15, 16, 19, 25–27, 52, 100, 177
 Devonian, 13–16, 25–27
 Diego de Almagro Metamorphic Complex (DAMC), 17–19, 24, 28
 Diego Ramirez Island, 18
 Diego Ramirez Metamorphic Complex (DRMC), 18
 Discovery Bank, 77, 94, 98
 Dove basins, 89, 97
 Drake Passage, 1–4, 76, 87, 92, 115, 117, 123, 127–129, 138, 142, 151, 174, 175, 179, 183, 184
 Duque de York Complex (DYC), 9, 15, 17, 24, 26, 27
- E**
 Earthquake, 5, 139, 141, 142, 152, 154–159, 161, 165, 166
 Eastern Andean Metamorphic Complex (EAMC), 9, 13–15, 17, 21, 25–27
 East Scotia Sea, 83, 86, 87
 El Chacay Formation, 119
 Elephant, 93
 El Quemado Complex, 115, 182
 Endurance collision zone, 92, 98
 Entremontense sea, 113, 123
 Estancia 25 de Mayo, 119
 Euler vector, 162
 Extra-Andean Patagonia, 4, 113, 114, 121, 123
- F**
 Fagnano fault, 5, 9, 22, 38, 42, 116, 117, 128, 138, 140, 142, 143, 152, 156, 177, 180
 Falkland Plateau, 97, 100, 101
 Falkland Trough, 77, 88
 Farallon/Nazca–Phoenix ridge, 65
 Farallon–Phoenix ridge, 177
 Faulting mechanisms, 159
 Fault kinematic, 2, 139, 145, 147, 148, 151, 165, 186, 191
 Fault mechanism, 139, 155, 158
 Fault slickenside, 146
 Fault slip data, 4, 147
 Fault system, 4, 128, 139, 143, 144, 146, 147, 151, 154, 175
 Fission-track, 117
 Fold and thrust belt, 28, 38, 41, 113–115, 117, 118, 122, 123, 144, 145, 147, 148, 150, 155, 159, 175, 177, 180, 183–194
 Foreland basin, 3, 4, 28, 142, 175–177, 190–192
 Fuegian Andes, 1, 5, 10, 14, 38, 56, 60, 65–67, 113–116, 118, 126–128, 142, 143, 145, 149, 150, 152, 154, 159, 175–177, 182–186, 188–190, 192–194
 Fuegian basement, 12
 Fuegian Batholith (FB), 41–46, 48, 55–57, 59, 61, 63, 65, 66, 114
 Fuegian orogeny, 8
 Fuegian Potassic Magmatism (FPM), 38, 45, 46, 48–53, 56, 57, 59–61, 63, 65
- G**
 Gabbroic assemblage, 43–45, 56
 Gaiman formations, 119
 Geochemistry, 4, 8, 23, 45, 51, 52, 54
 Geothermobarometry, 8, 17
 Glaciation, 76, 113, 114
 Gondwana, 8, 24–27, 40, 43, 98, 101, 114
 Gondwanaland, 15, 16
 Gondwanan, 3, 24, 100
 Gordon Island, 52

- Graham Land, 98
Greenschist facies, 14, 17, 23, 24, 114
- H**
Hardy Formation, 40, 41, 43, 45, 56, 62
- I**
Indenter, 165, 191, 192
Irigoyen basin, 110, 128
Isla de los Estados, 91, 142
Isla Diego de Almagro, 24
Isla Navarino, 22, 79
I-type granites, 43
- J**
Jane Basin, 85–87
Jeu-Jepén, 38, 44–46, 48, 49, 51, 60, 61
Jurassic, 3, 8, 10, 12, 14–18, 21, 24, 25, 27–29, 40–42, 56, 57, 63, 64, 66, 78, 100, 103, 114, 115, 155, 175, 176, 180, 182–184, 189, 192, 194
- K**
Kinematic databases, 4, 139
Kinematic evolution, 3, 5, 192
Kinematic reconstructions, 2, 3, 82, 116
Kranck pluton, 44, 49–51, 60
- L**
Ladrillero beds, 121
Lago Argentino, 110
Lago Belgrano, 110
Lago Buenos Aires, 110
Lago Deseado Fault, 143, 144
Lago Fagnano, 110, 128, 142, 144, 145, 147, 148, 150, 152, 154, 156, 157
Lago General Carrera unit, 13
Lago Posadas, 110, 118, 121
Lago San Martín, 110
Lago Viedma, 110
La Pera Formation, 52
Lu-Hf isotopic, 8
- M**
Maastrichtian, 98
Madre de Dios Accretionary Complex, 15
Madre de Dios Terrane (MDT), 9, 15
Magallanes–Austral basin, 3, 10, 12, 28, 110, 113, 115, 118, 119, 123, 126, 149, 150, 175, 177, 184, 194
Magallanes–Central Scotia plate boundary, 85, 90, 91
Magallanes–Fagnano fault system (MFF), 5, 38, 42, 116, 117, 128, 138–140, 142–146, 149–152, 154–159, 161, 162, 164, 165
Magallanes–Fagnano fault zone (MFFZ), 9
Magallanes fault, 143
Magallanes fold and thrust belt, 144, 147, 148, 150, 175, 177, 183–194
Magallanes strait, 110, 117, 128, 138, 142, 144, 149, 152, 155, 156
Magallanes Thrust and Fold Belt (MTFB), 9
Magmatic arc, 13, 16, 25, 28, 38, 40, 41, 43, 48, 63, 66, 114, 175, 176, 183, 189
Magmatic belt, 3, 8, 10, 14, 25, 27
Magmatic growth, 4
Magmatic suite, 4, 56
Magnetic fabric data, 5, 174
Main arc, 4, 38, 42, 43
Main Range Metamorphic Complex (MRMC), 9
Malvinas, 112, 127
Malvinas basin, 113, 114, 117, 119, 123, 126–128
Malvinas current, 127–129
Malvinas island, 139, 142
Malvinas trough, 113, 123, 128, 142
Map-view curvatures, 178
Marginal basin, 3, 10, 18, 25, 27, 28, 38, 41, 59, 63, 64, 66, 67, 79, 175, 176, 189
Marginal basin inversion, 40, 41, 64, 66
María Cristina beds, 121
Maurice Ewing Bank, 97
Mesozoic, 8–10, 14, 15, 19, 24, 38, 40, 42, 45, 78, 98, 142, 182, 185
Mesozoic metamorphic complexes, 3, 10
Metamorphic complex, 3, 8, 9, 11–19, 25, 30, 114
Metamorphic core complex, 15
Metamorphic pressure, 10
Metamorphic P–T conditions, 15
Metasedimentary complexes, 27
Metasedimentary rocks, 8, 11, 13, 15, 18, 21, 22, 26
Mid-Oceanic Ridge Basalts (MORB), 15, 23, 45, 51
Moat pluton, 44, 49–51, 60, 61
Monte León, 119
Monzonites of Navarino Island, 52
Mylonitic Belts, 10, 24
- N**
Navarino Island, 45, 46, 52, 56, 144, 154, 182
Nazca–Phoenix ridge, 66

- Nazca plate, 89, 116
 Non-rotational arc, 178, 179, 189, 194
 North-east Georgia Rise, 77, 85
 Northern Patagonia, 14
 North Patagonian Batholith, 41
 North Scotia Ridge (NSR), 76, 79, 83, 85, 86, 88, 90, 91, 94, 95, 100, 110, 116, 117, 120, 128, 138, 139, 141–144, 154, 159–161
- O**
 Oblique convergence, 41, 65, 165
 Oceanic-type seafloor, 8
 Offshore sedimentation, 2
 Omond Land, 98
 Ona Basin, 93
 Opening of the Drake Passage, 1–4, 92, 128, 138, 151, 174, 175, 179, 183, 184
 Ophiolitic complexes, 8, 10, 18, 20, 29, 78
 Ordovician, 13–16, 25–27
 Oroclinal bending, 4, 67, 78, 179, 182–185, 190, 191, 194
 Orocline, 2, 3, 5, 41, 65, 78, 79, 102, 139, 174, 178, 179, 183, 187, 189, 190, 193, 194
 Orogenic arc, 138, 139, 174, 178, 190, 191
 Orogenic curvature, 5, 174, 176, 182, 187, 191
 Orogenic growth, 2, 4, 113
- P**
 Pacific-Atlantic boundary, 154
 Pacific plate, 38, 63, 66, 76
 Pacific trench, 110, 114, 116, 127, 142, 161, 182
 Packsaddle Formation, 38, 41
 Packsaddle volcanics, 41, 43, 59
 Paleogeographic evolution, 10
 Paleomagnetic, 5, 100, 174, 178–180, 182–184, 187–190, 193
 Paleomagnetic constraints, 100, 179, 184, 187, 193
 Paleomagnetic directions, 180, 182–184, 188
 Paleomagnetism, 2, 178
 Paleozoic, 1–3, 9, 10, 14, 19, 21, 24–26, 28, 42, 78, 114, 175
 Patagonia, 1, 2, 4, 14, 21, 27, 28, 38, 40, 66, 100, 110, 113–115, 121–123, 126, 127, 138, 164
 Patagonian Andes, 27, 30, 38, 42, 99, 110, 115, 118, 159, 178, 186, 188, 193, 194
 Patagonian arc, 5, 190, 194
 Patagonian batholith, 2, 10, 41, 62, 114, 117, 118, 175, 176, 189
 Patagonian glaciations, 113
 Patagonian orocline, 2, 3, 5, 41, 139, 174, 179, 187, 190, 191, 193, 194
 Patagoniense, 112, 121
 Patagoniense transgression, 119
 Peninsula Hardy, 66, 183, 189
 Permian, 13–16, 22, 23, 25–27, 182
 Petrotectonic assemblages, 10
 Phoenix–Nazca plate boundary, 89
 Phoenix plate, 84, 177
 Pillow, 16, 20, 22, 23
 Pillow basalt, 15, 18, 20, 22, 23
 Pirie Bank, 77, 88, 94, 101
 Pirie Province, 90
 Plutonic complex, 14, 25
 Plutonic suite, 4, 55, 59
 Potassic, 38, 42, 48, 59, 60
 Potassic magmatism, 4, 38, 48, 59, 63, 64, 66
 Powell Basin, 88, 91, 95, 97
 Pre-Scotia times, 4
 Pressure–Temperature, 10
 Primary arc, 41, 174, 178, 187, 190, 191, 193, 194
 Progressive arc, 41, 174, 178, 189, 190, 193
 Protector Basin, 77, 87, 92, 95, 96
 Provenance areas, 8
 Provenance studies, 13
 Puerto Edén, 14
 Puerto Edén Igneous and Metamorphic Complex (PEIMC), 9, 17
 Pull-apart basin, 145, 157
 Punta Gruesa stage, 128
- R**
 Radial strain field, 186, 191, 193
 Rain shadow, 112
 Rear-arc, 4, 62
 Rear-arc suites, 44, 46, 56, 58, 59, 61, 62, 66
 Recent Cook deposits, 41
 Recent volcanism, 37
 Riedel, 145, 147–149, 155
 Rift, 8, 10, 18, 23, 25
 Rio Bueno thrusting, 177
 Río Chico high, 118, 126
 Río Guillermo, 118
 Río Lácteo Formation, 13
 Río Mayer Formation, 115
 Río Turbio, 110, 115, 177
 Rocas Verdes basin, 3, 8–10, 15, 20, 22–25, 28, 29, 40, 41, 52, 63, 67, 80, 100, 102, 175, 176, 192
 Rocas Verdes marginal basin, 2, 4, 8, 38, 40, 64, 66, 79, 176, 183, 185, 189, 190, 194
 Rocas Verdes ophiolites, 3, 19
 Rocas Verdes ophiolitic complexes, 18, 20
 Rodados Patagónicos, 113, 121, 123
 Rotational arc, 189, 194

S

- Sandebugten Formations, 79, 99–101
 Sandwich, 77, 86, 159
 Sandwich plate, 83, 85, 86
 San Pablo, 119, 157
 Santa Cruz Formation, 112, 113, 116, 121, 126
 San Vicente thrust, 177
 Sarmiento Complex (SC), 19–22, 24, 28
 Sarmiento Cordillera, 21
 Satellite pluton, 4, 40, 42, 46
 Scan Basin, 77, 85, 89, 91, 94
 Scotia Arc, 2
 Scotia Plate, 83, 85, 91, 116, 138, 139,
 141–143, 146, 151, 159, 161, 162, 174,
 184, 193
 Scotia Ridge, 100, 110, 117, 120, 128, 138,
 141, 142, 159, 161
 Scotia Sea, 1, 2, 4, 76–93, 95–99, 102, 103,
 110, 116, 121, 128, 140, 142, 152, 165, 175
 Scotia–South America plate boundary, 88, 128
 Seafloor-spreading, 79, 83, 84, 87, 90–93, 97,
 98
 Sediment dispersal, 3, 4
 Seismic, 82, 86, 112, 116, 119, 123–126, 129,
 139, 145, 154–158
 Seismicity, 139, 152, 154–156, 161
 Seismic risk, 139, 152
 Seismotectonic, 3, 152, 155, 158
 Seno Almirantazgo, 110, 128, 144, 147–149
 Seno Año Nuevo suite, 43–45, 56, 59, 65
 Seno Arcabuz Shear Zone (SASZ), 17, 18, 24
 Shackleton fracture zone, 84, 92, 141–143,
 154, 159–161
 Shag Rocks, 76, 86
 Shelf break, 113, 126
 Shortening, 28, 63, 64, 88, 96, 101, 114, 115,
 122, 128, 145, 147, 149–151, 164, 165,
 184–186, 190, 191, 194
 Shoshonites, 52, 56, 63
 Slab flattening, 38, 64–66
 Slab shallowing, 63
 S-like granitoids, 42, 56, 66
 Slip partitioning, 192
 South America, 1, 4, 8, 9, 18, 19, 26, 29, 30,
 38, 40–42, 66, 76, 79, 95, 96, 102, 115,
 116, 139, 141, 142, 146, 155, 159, 161,
 162, 174–176, 182, 187
 South America–Antarctica, 117
 South American–Antarctic Ridge, 86
 South American plate, 78, 83, 91, 95, 96, 98,
 99, 101, 116, 138, 142, 174, 176
 South America–Scotia continental plate
 boundary, 128
 South Atlantic, 79, 86, 98, 102, 128, 141, 176
 Southern Andean orogenic arc, 138
 Southern Atlantic margin, 114
 Southernmost Andes, 1–5, 19, 38, 40, 41, 59,
 65, 76, 110, 115, 126, 138, 139, 151, 154,
 155, 158–161, 165, 174–177, 179, 180,
 182–187, 188, 190–194
 Southern ocean, 1, 76, 139
 Southern Patagonia, 3, 4, 8, 10, 13, 14, 18,
 25–28, 58, 64, 138, 162
 Southern Patagonian Andes, 1, 10, 14, 18,
 24, 48, 59, 63, 65, 66, 78, 110, 113–118,
 121, 123, 161, 176, 177, 180, 185, 186,
 188, 192
 South Georgia, 4, 40, 76, 78–83, 86, 91, 94, 95,
 97, 99–103, 142
 South Orkney islands, 76, 78, 99
 South Orkney Microcontinent, 77, 79, 91,
 96–98
 South Patagonian Batholith (SPB), 17, 21, 28,
 40–42, 52, 58, 59, 65
 South Sandwich islands, 76
 South Sandwich subduction zone, 82, 98
 South Sandwich Trench, 77, 82, 85, 90, 91,
 94–96, 98
 South Scotia Ridge, 1, 2, 76, 83, 86, 88, 91, 97,
 159, 161
 South Shetland Islands, 76, 78, 84
 South Shetland Trench, 77
 Springhill, 115
 Staines Complex (SC), 9, 13
 Strain analysis, 164, 179
 Stress pattern, 4, 161, 165
 Strike-slip orocline model, 191
 Strike-slip tectonics, 174, 177, 182, 188, 193,
 194
 Subantarctic current, 127, 128
 Supra-subduction, 17, 27, 28, 30
 Supra-subduction zone, 10
 Synorogenic, 112, 115, 116
 Synorogenic sequences, 118
 Synrift, 21, 27, 115
- T**
- Tarlton Limestones (TL), 9, 15
 Tectonic reconstructions, 4, 188
 Tectonics, 80, 83, 87–89, 139, 152, 156, 158,
 175, 177, 182
 Terra Australis orogen, 2, 8
 Terror Rise, 77, 88, 92, 97, 98, 101
 Thermochronology, 8, 176
 Tholeiitic magmas, 23, 24
 Tierra del Fuego, 1, 4, 9, 10, 12, 38, 40, 44, 48,
 56, 58, 59, 62–66, 76, 78, 79, 81, 82, 88,
 91, 95–99, 102, 103, 110, 112–116, 119,

121, 123, 126–128, 138, 142, 144, 145,
149, 150, 152, 154, 161, 162, 164

Tierra del Fuego Igneous and Metamorphic
Complex (TFIMC), 12–15, 25, 26

Tobífera Formation, 21, 22, 25, 43

Tobífera/Lemaire, 115

Tortuga ophiolite, 21–23

Transform margin, 139

Trapecio Hill, 38, 53

Triassic, 13, 14, 16, 24, 27, 40, 114, 184

Trinity Peninsula Group (TPG), 27

Triple junction, 122, 138, 142

Turbiditic successions, 13, 15, 114

U

Última Esperanza, 115, 118

Ushuaia Peninsula Andesites (UPA), 38, 48,
53–56, 59, 61–63, 65

Ushuaia pluton, 44, 49, 50, 60, 61

V

Vertical-axis rotations, 174, 180, 188, 192, 193

Volcanic front, 4, 38, 57, 59, 60, 62, 63, 65, 66

Volcaniclastic sequences, 48

W

Weddell Sea, 40, 86, 98, 100, 184

West Antarctica large igneous, 40

Western Andes Metamorphic Complex, 114

West Scotia Ridge, 84–86, 88, 90–92

Widening of the arc, 4, 59, 66

Wrenching, 41, 145, 146, 149–151, 154

Y

Yahgán Formation, 19, 22, 41, 78–80

Z

Zapata Formation, 21

Zeballos Group, 112